LEABHARLANN CHOLÁISTE NA TRÍONÓIDE, BAILE ÁTHA CLIATH | TRINITY COLLEGE LIBRARY DUBLIN
Ollscoil Átha Cliath | The University of Dublin

Terms and Conditions of Use of Digitised Theses from Trinity College Library Dublin

Copyright statement

All material supplied by Trinity College Library is protected by copyright (under the Copyright and Related Rights Act, 2000 as amended) and other relevant Intellectual Property Rights. By accessing and using a Digitised Thesis from Trinity College Library you acknowledge that all Intellectual Property Rights in any Works supplied are the sole and exclusive property of the copyright and/or other IPR holder. Specific copyright holders may not be explicitly identified. Use of materials from other sources within a thesis should not be construed as a claim over them.

A non-exclusive, non-transferable licence is hereby granted to those using or reproducing, in whole or in part, the material for valid purposes, providing the copyright owners are acknowledged using the normal conventions. Where specific permission to use material is required, this is identified and such permission must be sought from the copyright holder or agency cited.

Liability statement

By using a Digitised Thesis, I accept that Trinity College Dublin bears no legal responsibility for the accuracy, legality or comprehensiveness of materials contained within the thesis, and that Trinity College Dublin accepts no liability for indirect, consequential, or incidental, damages or losses arising from use of the thesis for whatever reason. Information located in a thesis may be subject to specific use constraints, details of which may not be explicitly described. It is the responsibility of potential and actual users to be aware of such constraints and to abide by them. By making use of material from a digitised thesis, you accept these copyright and disclaimer provisions. Where it is brought to the attention of Trinity College Library that there may be a breach of copyright or other restraint, it is the policy to withdraw or take down access to a thesis while the issue is being resolved.

Access Agreement

By using a Digitised Thesis from Trinity College Library you are bound by the following Terms & Conditions. Please read them carefully.

I have read and I understand the following statement: All material supplied via a Digitised Thesis from Trinity College Library is protected by copyright and other intellectual property rights, and duplication or sale of all or part of any of a thesis is not permitted, except that material may be duplicated by you for your research use or for educational purposes in electronic or print form providing the copyright owners are acknowledged using the normal conventions. You must obtain permission for any other use. Electronic or print copies may not be offered, whether for sale or otherwise to anyone. This copy has been supplied on the understanding that it is copyright material and that no quotation from the thesis may be published without proper acknowledgement.

The Weakly Coupled Chiral Schwinger Model On A Finite Lattice

by

Carlos Pinto

M.Sc.

A thesis submitted to
the University of Dublin
for the degree of Ph.D.

School of Mathematics
University of Dublin
Trinity College

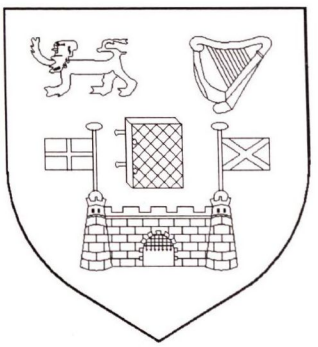

October, 1999.

Declaration

This thesis has not been submitted as an exercise for a degree at any other university. Except where otherwise stated, the work presented herein has been carried out by the author alone. The Library of Trinity College, Dublin may lend or copy this thesis upon request. The copyright belongs jointly to the University of Dublin and Carlos Pinto

Signature of author ..... Carlos Pinto .....

Carlos Pinto

October, 1999

Abstract

The primary aim of this work is the development of a perturbative analysis of the phase structure of the lattice Schwinger model. A novel method for implementing this analysis is presented.

It is shown analytically that the photon propagators which appear in the solution can be specified without ambiguity, provided special boundary conditions are implemented on the lattice.

A detailed numerical study is carried out to confirm this analytical work.

The results of the perturbative calculation indicate the absence of a phase transition in the weakly coupled Schwinger model, contrary to the findings, based on numerical studies, of other groups.

Acknowledgements

I would like to thank my supervisor, Dr James Sexton for his invaluable guidance during all stages of this work.
My thanks also to Dr Ralph Kenna with whom I worked closely and who was always available for help and advice.
This work would not have been possible without the support of the system staff of the Mathematics Department, David Malone, Ian Dowse, Dermot Frost and Eoin Lawless.
I would like to thank my fellow graduate students, particularly Alfredo Iorio for many illuminating discussions on physics and Fabian Sievers for, among other things, making available to me his expertise in TEX.
I express my appreciation for the financial support I received from Dublin Corporation and for the forbearance of my employers, Hitachi Dublin Laboratory during the final phases of this work.
I thank my family, and particularly my parents for their encouragement and last but by no means least, Jillian Coffey for her unfailing support through the hard times.

Table of Contents

1. Introduction

The beginner ... should not be discouraged if ... he finds that he does not have the prerequisites for reading the prerequisites.
– P. Halmos

1. Background

The successful description of the fundamental structure of matter remains one of the primary aims of physics. The most promising approach to this goal at the present time is provided by relativistic quantum field theories.

The earliest theories of this type were introduced shortly after the development of quantum mechanics by, amongst others, Dirac, Born, Jordan, Pauli and Heisenberg. This work was motivated by the need to achieve a description for the electromagnetic field that was consistent with both special relativity and the new quantum mechanics.

Following twenty years of development by many physicists, the theory of quantum electrodynamics reached its finished form in the work of Feynman, Schwinger, Tomonaga and Dyson. It remains the most successful and accurate theory in physics to the present day.

Quantum electrodynamics cannot be solved exactly; indeed very few exact solutions are known in quantum field theory as a whole. It owes its success, rather, to the fact that the coupling constant associated with the electromagnetic field is small ($\alpha \approx 1/137$). As a consequence, the perturbative expansion of the theory in powers of the coupling constant yields highly accurate approximate solutions.

The techniques that had proved so effective in the case of quantum electrodynamics were also applied to the other fundamental interactions. A quantum field theory of the strong interaction, quantum chromodynamics, (QCD) was developed in the 1970s. QCD describes the interactions between quarks and gluons and has the curious property of *asymptotic freedom*; the quarks interact weakly at short distances with the strength of the interaction growing with separation. As a consequence, the high energy (short distance) features of QCD can be analysed with conventional perturbation theory; however this approach fails in the low energy regime. Perturbative QCD cannot therefore be used, for example, to calculate hadron masses or to investigate the confinement of quarks. These phenomena are fundamentally non–perturbative.

The most promising current approach to these non–perturbative problems is a formulation proposed by Wilson, in which spacetime is discretised into a set of finitely spaced points (a *lattice*). Such a model is in many ways analogous to spin systems in statistical mechanics. Lattice field theories possess two important advantages as far as non–perturbative studies are concerned. Firstly, they admit *strong coupling* approximations, which cannot be realised in a continuum theory. Secondly, the discrete nature of the lattice means that lattice theories lend themselves to numerical investigation. Indeed the potential of this numerical approach is limited only by the power of present day computer technology. Numerical studies in lattice field theory are today the principal tool in theoretical hadron physics. They are currently able to predict low lying hadron masses to an accuracy of a few percent.

The lattice approach is not without its disadvantages, however. On the one hand, the transcription of continuum fields onto the lattice presents technical problems, most notoriously so in the case of fermions, where a doubling of the fermionic degrees of freedom in the lattice formulation appears unavoidable. The most natural cure for this problem is to add an extra (Wilson) term to the lattice fermion action; this term however raises additional difficulties of its own.

The opposite transition, from the lattice to the physical continuum theory presents its own difficulties; indeed, only under very special conditions does a lattice theory have a meaningful physical continuum limit. The determination of these conditions is in general a highly non–trivial problem.

The complexity of full QCD renders many of these problems intractable. Some insight may be gained, however, by a study of simpler 'toy' theories and a variety of such theories have been investigated. One of the most important is the Schwinger model which describes the interaction of photons and electrons in $1+1$ dimensions. Although this model might seem grossly unphysical, it actually shares some interesting features with QCD, not the least of which is confinement of charge. Moreover, the massless version is exactly solvable in the continuum and is therefore a useful testbed for the development of numerical methods involving dynamical fermions.

A crucial feature of any lattice field theory is its phase structure, since it is only at the critical points in the parameter space of the theory that a continuum limit may be attained. The phase diagram of the Schwinger model has not been fully determined. There is considerable current interest in this problem, since it is believed that the phase structure is likely to be similar in some respects to that of QCD.

It is known that the Schwinger model possesses critical points in both the strong and the weak coupling limits; some numerical results have also been obtained at intermediate values. The primary aim of this thesis is to complement these numerical approaches with an ana-

lytical investigation of the phase structure of the Schwinger model.

Our approach will be as follows. The critical behaviour of the theory is governed by the behaviour of the zeroes of the partition function as the lattice size goes to infinity. The locations of these zeroes must therefore be determined, (for fixed coupling) as a function of lattice size. These locations cannot be determined exactly; therefore a perturbative scheme in the coupling strength is implemented. The analysis will therefore be restricted to the weak coupling regime.

The perturbative expansion yields terms which are functions of expectation values over the photon field. It is well known that such expectation values are potentially ill–defined; for example the photon propagator exhibits an infra–red divergence at weak coupling in Feynman gauge.

A second objective of this work is therefore to develop a scheme for the unambiguous specification of such expectation values. We will trace the origins of the problem to the vacuum degeneracy exhibited by the photon field on a finite lattice, and demonstrate that this degeneracy can be removed by a suitable choice of boundary conditions.

The gauge of choice in perturbative lattice calculations is Feynman gauge; however the propagator cannot be determined exactly in this gauge and it is necessary to use a weak coupling approximation.

The third objective of the thesis is to determine expectation values exactly, in order to investigate their behaviour under different choices of boundary condition. We find exact expressions for quite general classes of expectation values in axial gauge and show, in particular, that the expectation value $\langle {\phi_i}^2 \rangle$ of relevance to the main perturbative calculation is actually independent of both coupling and lattice size when the usual periodic boundary conditions are imposed. This means that axial gauge with periodic boundary conditions cannot be used for the perturbative calculation. On the other hand $\langle {\phi_i}^2 \rangle$ acquires the proper functional dependence when the proposed new boundary conditions are employed.

The fourth objective of the thesis is to investigate the behaviour of the expectation values numerically. We find that Monte Carlo simulations reproduce the analytic results obtained in axial gauge as well as in Feynman gauge with the proposed new boundary conditions. We would expect unusual numerical behaviour in the case of the Feynman propagator with periodic boundary conditions in view of the infra–red divergence associated with this object and indeed we find enormously long decorrelation times. We present evidence that suggests that the simulation in this case is not ergodic.

With these results in hand an unambiguous weak coupling expansion can be implemented for the Schwinger model on a finite lattice. The lowest zeroes of the partition function are located to first order. Their scaling behaviour indicates the absence of a phase transition in

the weak coupling regime. This analytic result contradicts the findings of recent numerical findings based on finite size scaling.

2. Outline Of The Thesis

The thesis is structured in the following way.

Chapters 2, 3 and 4 consist mainly of an overview of field theory in the lattice setting.

Chapter 2 begins with a brief review of the path integral approach to quantum field theory. The concept of the lattice as a regulator of the continuum theory is then introduced and some technicalities associated with lattice calculations are discussed. The next part of Chapter 2 describes how useful physical information can be extracted from the lattice and demonstrates that such calculations are only valid at the points of phase transition of the lattice theory. The Chapter concludes with a discussion of the method of Lee and Yang for determining the location of such a phase transition from an investigation of the zeroes of the partition function.

Gauge fields are introduced in Chapter 3. The discussion is restricted to U(1) fields in two dimensions since it is fields of this type that appear in the Schwinger model. The Wilson action is introduced and the lattice versions of gauge invariance and gauge fixing are discussed.

The final part of Chapter 3 addresses the problem of implementing a weak coupling approximation scheme for the pure gauge field. The vacuum degeneracy of the gauge field on a finite lattice with periodic boundary conditions is explicitly demonstrated. The new idea of imposing *zero* boundary conditions is introduced. It is shown that such a procedure eliminates the vacuum degeneracy and permits an unambiguous weak coupling approximation to be implemented.

Chapter 4 concerns itself with fermion fields. After a brief review of the theory of linear operators, the continuum fermion field is discretised and the lattice fermion propagator is computed. It is shown that naive discretisation leads to the well–known fermion doubling effect and that this doubling can be removed by the addition of a momentum dependent mass term (Wilson term) to the action.

Following these three, mostly introductory, Chapters, the Schwinger model is introduced in Chapter 5. The motivation for the work to be described in subsequent Chapters and its relevance to analogous problems in QCD is discussed. The continuum Schwinger model is introduced and the corresponding lattice action derived. Previous work on the phase structure of the lattice Schwinger model is reviewed.

The analytical determination of the phase structure of the Schwinger model described in this thesis is based on an expansion of the partition function around the free fermion field. Chapter 6 therefore concerns itself with an analysis of the free field problem. The two–dimensional and four–dimensional cases are analogous and are treated in parallel. Although the thesis is concerned primarily with the Schwinger model, the results of this Chapter show that, as far the fermion field is concerned, similar methods can (in principle at least) be applied to four–dimensional QED.

The first important result of this Chapter is that the fermion matrix, although not hermitian, *does* belong to the more general class of normal matrices. Standard perturbative techniques can therefore be applied to the free fermion operator. The eigenvalues and eigenvectors of the operator are obtained and are shown to be highly degenerate. This degeneracy considerably complicates the perturbative expansion of the operator. The Chapter closes with an analytic determination, via an investigation of the zeroes of the partition function, of the phase structure of the free fermion theory.

The proposed weak coupling expansion requires the calculation of gauge–dependent pure gauge expectation values. This presents a serious obstacle to the calculation since such objects depend on both the gauge and the boundary conditions. The unambiguous definition of the object $\langle {\phi_i}^2 \rangle$ which is required for first–order perturbation theory presents particular difficulties. The next four Chapters in the thesis are devoted to a careful investigation, both analytical and numerical, of such expectation values.

The major part Chapter 7 is devoted to the analytical evaluation of both gauge–invariant and gauge–dependent expectation values. General expressions for a wide class of expectation values on a finite lattice in axial gauge are derived. The quantity $\langle {\phi_i}^2 \rangle$ is shown to be ill–defined in both axial gauge (where it is constant) and in the weak coupling approximation in Feynman gauge (where it is divergent) as long as periodic boundary conditions are imposed. The imposition of zero boundary conditions results results in well-defined expressions in both gauges.

The numerical confirmation of these analytical results forms the major content of Chapters 8, 9 and 10. Chapter 8 introduces the basic technique of Monte Carlo integration and discusses the statistical analysis of the results. The technique is then applied to the calculation of the plaquette expectation value. The statistical fluctuations and finite size errors occurring in a calculation of this type are demonstrated explicitly by comparing the results with the analytic value for the expectation value of the plaquette on an infinite lattice.

Chapter 9 focuses on calculations in axial gauge. The additional problems associated with numerical calculations in a fixed gauge are discussed in general terms and then demonstrated explicitly. The expectation value of $\langle {\phi_i}^2 \rangle$ is calculated with both periodic and zero boundary

conditions and found to agree with the predicted values in both cases.

The case of Feynman gauge is considered in Chapter 10. The value of $\langle {\phi_i}^2 \rangle$ is predicted to diverge in this gauge when periodic boundary conditions are imposed. This divergence manifests itself as a non–ergodicity in the numerical simulation. The value of $\langle {\phi_i}^2 \rangle$ obtained when zero boundary conditions are imposed is in agreement with the theoretical prediction.

The first part of Chapter 11 is concerned with the implementation of the weak coupling expansion in the Schwinger model. Both additive and multiplicative expansions are presented. Although neither expansion on its own suffices to identify the zeroes of the partition function, it is shown that the two expansions taken together *do* suffice to determine these zeroes.

The second part of Chapter 11 consists of an analysis of the first order shifts in the lowest zeroes. It is shown that the behaviour of these zeroes indicates the absence of the expected phase transition.

2. The Lattice

Suit the action to the word, the word to the action; with this special observance, that you o'er step not the modesty of nature: for anything so overdone is from the purpose of playing, whose end, both at the first and now, was and is to hold, as 'twere, the mirror up to nature.

– Hamlet

This Chapter consists of a review of the lattice formulation of field theory. The path integral approach to field theory is described and the lattice introduced as a regulator of the continuum theory. Difference operators and Fourier transforms are defined on the lattice. The problem of extracting physically meaningful information from the lattice is discussed. It is argued that such information can only be extracted when the lattice theory is at one of its critical points and a method for determining such critical points is introduced.

3. Path Integrals

In this section we will briefly review some basic elements of field theory in the continuum. The path integral approach as developed by Feynman (1948) will be used throughout.

Quantum field theory is concerned with the study of dynamical systems of quantised fields. It is essentially a generalisation of quantum mechanics which is consistent with special relativity, in contrast to the original formulation of quantum mechanics which treated the dynamics of particles and was fundamentally non-relativistic in nature.

The most natural and intuitive approach to quantum mechanics is the *path integral.* The method can be generalised in a straightforward way to the quantisation of fields and has several attractive formal features, not the least of which is manifest Lorentz invariance. Details of the path integral approach can be found in many texts; see, for example, Rivers (1987) and Roepstorff (1994).

From our point of view the greatest virtue of the path integral approach is that it lends itself to a discretised formulation from which numerical results can be obtained.

Consider a spacetime field $\phi(x)$. A particular choice for the function ϕ corresponds to a *configuration* of the field. The path integral method assigns a weight e^{iS} to each such configuration. The *expectation value* of a function of the field is then the value of the function averaged over all the weighted configurations, thus

$$\langle\, F(\phi(x))\,\rangle = \frac{\int\limits_{all\ configs} F(\phi(x))\, e^{iS}}{\int\limits_{all\ configs} e^{iS}}$$

which we will write

$$\langle F(\phi(x)) \rangle = \frac{\int [D\phi]\, F(\phi(x))\, e^{iS}}{\int [D\phi]\, e^{iS}} \tag{2.1}$$

The weight function characterises the particular field theory being considered. The quantity S occurring in this weight function is the *action* of the classical theory

$$S = \int d^4x \mathcal{L}(\phi)$$

where $\mathcal{L}(\phi)$, the classical Lagrangian density, is required as an input to the theory. The ingredients of the weight function are thus entirely classical—field quantisation enters through the definition of the integration measure $[D\phi]$.

The expectation value (2.1) is an example of a functional integral (or path integral), the integral running over all possible functions, or configurations, $\phi(x)$.

A fundamental quantity in the theory is the two-point *correlation function*

$$\langle \phi(x_1)\phi(x_2) \rangle = \frac{\int [D\phi]\, \phi(x_1)\, \phi(x_2)\, e^{iS}}{\int [D\phi]\, e^{iS}}$$

Higher order correlation functions are defined similarly

$$\langle \phi(x_1) \dots \phi(x_n) \rangle = \frac{\int [D\phi]\, \phi(x_1) \dots \phi(x_n)\, e^{iS}}{\int [D\phi]\, e^{iS}} \tag{2.2}$$

The entire content of the theory resides in the weight function e^{iS} and the integration measure $[D\phi]$. All information relating to *local* properties, such as scattering amplitudes and decay rates, is contained in the correlation functions (2.2), which connect particular points in spacetime.

The *global* structure of the theory, on the other hand, is determined by the physical parameters contained in the Lagrangian and by the measure. The fundamental object describing this global structure is the *partition function*, which is obtained by integrating out the fields using the prescribed measure

$$Z(\alpha_1 \dots \alpha_n) = \int [D\phi]\, e^{iS} \tag{2.3}$$

where the α's are the physical parameters of the theory.

The mathematical problem therefore reduces to the evaluation of the functional integrals of the type (2.3) and (2.2). This is by no means a trivial matter—indeed, the integrals as we have so far presented them are not even properly defined. In the first place, the weight factor is complex and strongly oscillating. Secondly we have not yet given a definition of the integration measure. Lastly there is no guarantee that the integrals even converge.

These issues will be addressed in the following two sections; for the moment let us simply define the two actions we will be considering.

The action describing free fermions is given by

$$S_F = \int \overline{\psi} \left(i\gamma^\mu \partial_\mu - m \right) \psi \, d^4x \tag{2.4}$$

where ψ and $\overline{\psi}$ are Grassman variables and the γ^μ are defined by the anti-commutation relation

$$\{\gamma^\mu \, , \, \gamma^\nu\} = 2g^{\mu\nu}$$

The action associated with the electromagnetic field is

$$S_G = -\frac{1}{4} \int F_{\mu\nu} F^{\mu\nu} \, d^4x \tag{2.5}$$

where the field strength tensor $F_{\mu\nu}$ is given in terms of the vector potential by

$$F_{\mu\nu} = \partial_\mu A_\nu - \partial_\nu A_\mu$$

The full action describing fermions interacting with photons is

$$S_{QED} = \int \overline{\psi} \left(i\gamma^\mu D_\mu - m \right) \psi - \frac{1}{4} F_{\mu\nu} F^{\mu\nu} \, d^4x \tag{2.6}$$

where the *gauge covariant derivative* D_μ is defined by

$$D_\mu = \partial_\mu + igA_\mu$$

the parameter g being the fermionic charge, or *coupling constant* associated with the theory. The fermion-photon theory is therefore parametrised by two physical constants, the mass m and the charge g.

We will not discuss here the details of QED in the continuum, but will simply list the main steps in the analysis. Detailed accounts of QED can be found in standard works; see for example Peskin and Schroeder (1995) and Kaku (1993)

The two-point correlation functions (or *propagators*) associated with the free theories (2.4) and (2.5) can be computed explicitly. Correlation functions for the interacting theory are then calculated via a perturbation expansion in powers of the coupling constant; individual terms in this series may be visualised in terms of the well-known *Feynman diagrams.* The higher order terms in the perturbation series are formally divergent, due to the presence of interactions at arbitrarily small separation (or, equivalently, at arbitrarily large momentum). These *ultraviolet divergences* are controlled by imposing some sort of regulator on the theory; in effect a device to arbitrarily cut off the high momentum contributions to the divergent integrals. At the end of the calculation the regulator is removed while simultaneously rescaling the parameters of the theory so as to keep the results finite (*renormalisation*).

The theory of perturbative QED in the continuum actually produces results in excellent agreement with experiment and is well established and understood. It therefore provides a useful standard against which to explore the limiting behaviour of lattice formulations of field theory.

4. Field Theory in Euclidean Space

In this section we will begin the process of giving meaning to the path integral (2.1). In particular, we address the problem of the complex, strongly oscillating weight function e^{iS}, which, as we will see, takes on a more tractable form if we treat time as a pure imaginary coordinate.

Before proceeding further let us review some features of Minkowski space where time is treated as a real variable. The properties of Minkowski space are encoded in its *metric*, which we will represent (in four dimensions) by

$$g^{\mu\nu} = \begin{pmatrix} 1 & 0 & 0 & 0 \\ 0 & -1 & 0 & 0 \\ 0 & 0 & -1 & 0 \\ 0 & 0 & 0 & -1 \end{pmatrix} = g_{\mu\nu}$$

with an analogous form in two dimensions.

The inner product is given by

$$\begin{aligned} x^\mu x_\mu &= g^{\mu\nu} x_\nu x_\mu \\ &= t^2 - {x_1}^2 - {x_2}^2 - {x_3}^2 \end{aligned} \tag{2.7}$$

where the *contravariant* vector x^μ is given by

$$x^\mu = (t,\, x_1,\, x_2,\, x_3) \tag{2.8}$$

and the *covariant* vector by

$$x_\mu = (t,\, -x_1,\, -x_2,\, -x_3) \tag{2.9}$$

The covariant and contravariant derivatives are defined by

$$\partial_\mu = \frac{\partial}{\partial x^\mu} \qquad \partial^\mu = \frac{\partial}{\partial x_\mu} \tag{2.10}$$

and the Laplacian by

$$\partial^\mu \partial_\mu = \partial_\mu \partial^\mu = \frac{\partial^2}{\partial t^2} - \nabla^2 \tag{2.11}$$

Next we change time to an imaginary variable

$$t = -ix_0 \qquad x_0 \in \mathbf{R} \tag{2.12}$$

In order to find the fermion Lagrangian in the new coordinates it is convenient to consider first the Klein-Gordon equation. This is given in Minkowski space by

$$(\partial^\mu \partial_\mu + m^2)\psi = 0$$

Substituting from (2.14) gives the Euclidean form

$$(\partial_\mu \partial_\mu - m^2)\psi = 0 \tag{2.15}$$

The Dirac equation may be written

$$(\gamma_\mu \partial_\mu + m)\psi = 0 \tag{2.16}$$

where the γ_μ are now *Euclidean* gamma matrices. Their algebra is determined by the requirement that solutions to the Euclidean Dirac equation satisfy the Euclidean Klein-Gordon equation (2.15).

$$\begin{aligned}
&(\gamma_\mu \partial_\mu + m)\psi = 0 \\
&\qquad \Rightarrow (\gamma_\mu \partial_\mu + m)(\gamma_\mu \partial_\mu + m)\psi = 0 \\
&\qquad \Rightarrow (\gamma_\mu \gamma_\nu \partial_\mu \partial_\nu + 2m\gamma_\mu \partial_\mu + m^2)\psi = 0 \\
&\qquad \Rightarrow (\gamma_\mu \gamma_\nu \partial_\mu \partial_\nu - m^2)\psi = 0 \\
&\qquad \Rightarrow \{\frac{1}{2}(\gamma_\mu \gamma_\nu + \gamma_\nu \gamma_\mu)\partial_\mu \partial_\nu - m^2\}\psi = 0
\end{aligned}$$

This satisfies the Euclidean Klein-Gordon equation provided

$$\gamma_\mu \gamma_\nu + \gamma_\nu \gamma_\mu = 2\delta_{\mu\nu} \tag{2.17}$$

The Lagrangian density that generates the Euclidean field equation (2.16) and its adjoint is given by

$$\mathcal{L} = \overline{\psi}(\gamma_\mu \partial_\mu + m)\psi \tag{2.18}$$

so that the pure fermionic path integral in Euclidean space is

$$\langle F(\psi, \overline{\psi}) \rangle_F = \frac{\int [D\psi \overline{\psi}]\, F(\psi, \overline{\psi})\, e^{-\int \overline{\psi}(\gamma_\mu \partial_\mu + m)\psi \, d^4 x}}{\int [D\psi \overline{\psi}]\, e^{-\int \overline{\psi}(\gamma_\mu \partial_\mu + m)\psi \, d^4 x}}$$

It will occasionally be useful to have an explicit representation of the Euclidean gamma matrices. We will use the following form in two dimensions

$$\gamma_0 = \begin{pmatrix} 0 & 1 \\ 1 & 0 \end{pmatrix} \qquad \gamma_1 = \begin{pmatrix} 0 & -i \\ i & 0 \end{pmatrix}$$

while in four dimensions we will use

$$\gamma_0 = \begin{pmatrix} 1 & 0 & 0 & 0 \\ 0 & 1 & 0 & 0 \\ 0 & 0 & -1 & 0 \\ 0 & 0 & 0 & -1 \end{pmatrix} \qquad \gamma_1 = \begin{pmatrix} 0 & 0 & 0 & 1 \\ 0 & 0 & 1 & 0 \\ 0 & 1 & 0 & 0 \\ 1 & 0 & 0 & 0 \end{pmatrix}$$

$$\gamma_2 = \begin{pmatrix} 0 & 0 & 0 & -i \\ 0 & 0 & i & 0 \\ 0 & -i & 0 & 0 \\ i & 0 & 0 & 0 \end{pmatrix} \qquad \gamma_3 = \begin{pmatrix} 0 & 0 & 1 & 0 \\ 0 & 0 & 0 & -1 \\ 1 & 0 & 0 & 0 \\ 0 & -1 & 0 & 0 \end{pmatrix}$$

5. The Lattice Regulator

The transition to Euclidean space has converted the weight function from an oscillating phase factor to a real exponential factor—to this extent the path integral is somewhat better defined

$$\langle F(\phi(x)) \rangle = \frac{\int [D\phi]\, F(\phi(x))\, e^{-S}}{\int [D\phi]\, e^{iS}} \tag{2.19}$$

We have yet to give meaning to the measure $[D\phi]$, however. Let us sidestep this problem for the moment by changing the structure on which the theory is defined. Working, for concreteness, in four dimensions, let us replace the the continuous Euclidean space $\mathbf{R}^4$ by a finite lattice $\mathbf{Z}_N^4$ with N lattice sites along each axis. (We will usually assume for simplicity of notation that the lattice has the same number of sites along each axis, although this restriction is not necessary.)

Objects in the continuum theory can be translated to the lattice setting without difficulty; functions on $\mathbf{R}^4$ are now defined only at the lattice points, which are finite in number. The lattice analogues of standard operators and transforms are discussed in Sections (6) and (7). The important point in the present context is that the Euclidean path integral (2.19) immediately acquires an unambiguous meaning. A field configuration on the lattice is specified by the field values at a *finite* number of points; therefore all configurations can be counted by integrating over all possible field values at each lattice point

$$[D\phi] = \prod_{i=1}^{N^4} d\phi_i \tag{2.20}$$

The path integral thus reduces to an ordinary multi-dimensional integral.

It should be stressed that the lattice theory is not simply a discretisation of the continuum theory. In the first place, the underlying structure is finite rather than infinite in extent.

Secondly, any continuous symmetries associated with the underlying Euclidean space are lost in the lattice formulation. Indeed the lattice theory as we have so far introduced it is not a physical theory at all in the sense that no physical dimension has so far been introduced and all quantities are dimensionless. The relationship between the lattice and continuum theories will be discussed in Section (8).

6. Discretisation

In this section we will discuss the technicalities involved with working on a discrete lattice and establish definitions of lattice operators and transforms. The lattice spacing a will be included explicitly for later convenience; for the present it is simply a dimensionless constant equal to unity.

Consider a d dimensional hypercubic lattice with N sites along each axis, containing N^d sites. Each site is represented by its position vector $\underline{n}$, relative to the basis $\{\underline{\mu}_\mu\,,\ \mu = 0 \ldots (d-1)\}$ The coordinate system is defined symmetrically so that the site coordinates n_μ are integers lying in the range

$$-\frac{N}{2} \leq n_\mu < \frac{N}{2}$$

There is some freedom in the choice of a discretised derivative; we shall have occasion to use three different operators.

The action of the *symmetric* difference operator on a lattice function $f(\underline{n})$ is given by

$$\partial_\mu f(\underline{n}) = \frac{f(\underline{n}+\underline{\mu}) - f(\underline{n}-\underline{\mu})}{2a} \tag{2.21}$$

The *left* and *right* difference operators are defined by

$$\partial^L_\mu f(\underline{n}) = \frac{f(\underline{n}) - f(\underline{n}-\underline{\mu})}{a}$$

$$\partial^R_\mu f(\underline{n}) = \frac{f(\underline{n}+\underline{\mu}) - f(\underline{n})}{a}$$

We will also require a lattice Laplacian, given in terms of the left and right derivatives by

$$\nabla^2 f(\underline{n}) = \partial^L_\mu \partial^R_\mu f(\underline{n}) = \partial^R_\mu \partial^L_\mu f(\underline{n}) = \frac{\sum_\mu f(\underline{n}+\underline{\mu}) + f(\underline{n}-\underline{\mu}) - 2f(\underline{n})}{a^2}$$

If the lattice is periodic, the left and right derivatives satisfy the following important identities

$$\begin{aligned} \sum_{\underline{n}} \left(\partial^R_\mu f(\underline{n})\right)\ g(\underline{n}) &= -\sum_{\underline{n}} f(\underline{n})\ \left(\partial^L_\mu g(\underline{n})\right) \\ \sum_{\underline{n}} \left(\partial^L_\mu f(\underline{n})\right)\ g(\underline{n}) &= -\sum_{\underline{n}} f(\underline{n})\ \left(\partial^R_\mu g(\underline{n})\right) \end{aligned} \tag{2.22}$$

These follow since

$$\sum_{\underline{n}} \left(\partial_\mu^R f(\underline{n})\right)\ g(\underline{n}) = \sum_{\underline{n}} \{f(\underline{n}+\underline{\mu}) - f(\underline{n})\}\ g(\underline{n})$$
$$= \sum_{\underline{n}} f(\underline{n}+\underline{\mu})\ g(\underline{n}) - \sum_{\underline{n}} f(\underline{n})\ g(\underline{n})$$

Since the lattice is periodic the summation variable in the first term may be shifted from $\underline{n}$ to $\underline{m} = \underline{n} + \underline{\mu}$ giving

$$\sum_{\underline{n}} \left(\partial_\mu^R f(\underline{n})\right)\ g(\underline{n}) = \sum_{\underline{m}} f(\underline{m})\ g(\underline{m}-\underline{\mu}) - \sum_{\underline{n}} f(\underline{n})\ g(\underline{n})$$
$$= \sum_{\underline{n}} f(\underline{n})\ g(\underline{n}-\underline{\mu}) - f(\underline{n})\ g(\underline{n})$$
$$= -\sum_{\underline{n}} f(\underline{n})\ \left(\partial_\mu^L g(\underline{n})\right)$$

and similarly for the left derivative.

7. Fourier Transforms on the Lattice

In this section we will develop a definition of the Fourier transform of a function defined on a finite, discrete lattice. We work on a d-dimensional hypercubical lattice with N sites along each axis.The sites are labelled by coordinates n_μ:

$$\frac{-N}{2} \leq n_\mu < \frac{N}{2}$$

Let us also introduce the *dual lattice*. The coordinates of points on this dual lattice are labelled by real numbers q_μ:

$$q_\mu = \frac{2\pi p_\mu}{Na} \tag{2.23}$$

where the values of p_μ are determined by the boundary conditions. It is convenient also to introduce the parameter k_μ by

$$k_\mu = aq_\mu = \frac{2\pi p_\mu}{N} \tag{2.24}$$

Consider now any function $f(\underline{n})$ defined on the lattice sites $\underline{n}$. The value of $f(\underline{n})$ at each site is arbitrary; the function therefore has N^d independent degrees of freedom and may be expanded in terms of N^d basis functions, $\mathbf{e}_{\underline{p}}(\underline{n})$. These basis functions must satisfy the orthogonality condition

$$\sum_{all\ sites} \mathbf{e}_{\underline{p}}(\underline{n})\ \mathbf{e}_{\underline{p}'}(\underline{n}) \propto \delta_{\underline{p}\underline{p}'} \tag{2.25}$$

We will use as our basis functions the discrete version of the standard Fourier basis:

$$\mathbf{e}_{\underline{p}}(\underline{n}) = e^{\frac{2\pi i}{N}\underline{p}.\underline{n}} = e^{i\underline{k}.\underline{n}} \quad ; \quad -\frac{N}{2} \leq p_\mu < \frac{N}{2} \tag{2.26}$$

Let us now impose *periodic* boundary conditions on the lattice; that is, we require every lattice function to satisfy

$$f(n_\mu - N) = f(n_\mu) = f(n_\mu + N) \qquad \forall \mu$$

In particular, the basis functions $\mathbf{e}_{\underline{p}}(\underline{n})$ must be periodic. Therefore

$$e^{\frac{2\pi i}{N}p_\mu (n_\mu - N)} = e^{\frac{2\pi i}{N}p_\mu n_\mu} = e^{\frac{2\pi i}{N}p_\mu (n_\mu + N)}$$
$$\Rightarrow e^{2\pi i p_\mu} = 1 = e^{-2\pi i p_\mu}$$

which in turn requires that the p_μ be integer–valued.

It will occasionally be necessary (for example, in the case of fermions) to impose *anti–periodic* boundary conditions along one or more axes of the lattice. These anti–periodic functions are defined by

$$f(n_\mu - N) = -f(n_\mu) = f(n_\mu + N)$$

and the basis functions which generate them satisfy

$$e^{\frac{2\pi i}{N}p_\mu (n_\mu - N)} = -e^{\frac{2\pi i}{N}p_\mu n_\mu} = e^{\frac{2\pi i}{N}p_\mu (n_\mu + N)}$$
$$\Rightarrow e^{2\pi i p_\mu} = -1 = e^{-2\pi i p_\mu}$$

In the case of anti–periodic functions, therefore, the p_μ take on half–integer values.

The basis functions with p_μ integer or half–integer can easily be shown to satisfy the orthogonality relation (2.25). In one dimension, the sum

$$S_p = \sum_{n=\frac{-N}{2}}^{\frac{N}{2}-1} e^{\frac{2\pi i}{N}(p-p')n}$$

is a geometric progression of N terms with first term $e^{\pi i(p-p')}$ and common ratio $e^{\frac{2\pi i}{N}(p-p')}$. The sum is therefore

$$S_p = e^{\pi i(p-p')}\frac{1 - e^{2\pi i(p-p')}}{1 - e^{\frac{2\pi i}{N}(p-p')}} = 0 \qquad \left(e^{\frac{2\pi i}{N}(p-p')} \neq 1\right)$$
$$= N \qquad \left(e^{\frac{2\pi i}{N}(p-p')} = 1\right)$$

The sum is therefore only non-zero if

$$p - p' = mN \qquad (m = 0 \pm 1, \pm 2 \ldots)$$

According to (2.26), the integers p satisfy

$$-\frac{N}{2} \leq p_\mu < \frac{N}{2}$$

The only allowed value of m is therefore zero, leading to the required orthogonality relation:

$$\sum_{n=\frac{-N}{2}}^{\frac{N}{2}-1} e^{\frac{2\pi i}{N}(p-p')n} = N\delta_{pp'}$$

This result generalises straightforwardly to d dimensions

$$\sum_{n=\frac{-N}{2}}^{\frac{N}{2}-1} e^{\frac{2\pi i}{N}(\underline{p}-\underline{p}')\cdot\underline{n}} = N^d\delta_{\underline{p}\underline{p}'} \qquad \sum_{p=\frac{-N}{2}}^{\frac{N}{2}-1} e^{\frac{2\pi i}{N}(\underline{n}-\underline{n}')\cdot\underline{p}} = N^d\delta_{\underline{n}\underline{n}'}$$

or

$$\sum_{n=\frac{-N}{2}}^{\frac{N}{2}-1} e^{i(\underline{k}-\underline{k}')\cdot\underline{n}} = N^d\delta_{\underline{k}\underline{k}'} \qquad \sum_{p=\frac{-N}{2}}^{\frac{N}{2}-1} e^{i(\underline{n}-\underline{n}')\cdot\underline{k}} = N^d\delta_{\underline{n}\underline{n}'}$$

An arbitrary lattice function $f(\underline{n})$ may therefore be expanded

$$f(\underline{n}) = \frac{1}{N^d}\sum_{\underline{k}} f(\underline{k})\, e^{i\underline{k}.\underline{n}} \tag{2.27}$$

where the expansion coefficients $f(\underline{k})$ may be regarded as a discrete function defined on the dual lattice. To obtain the back transform, note that

$$\begin{aligned}
&\frac{1}{N^d}\sum_{\underline{k}} f(\underline{k}) \sum_{\underline{n}} e^{i(\underline{k}-\underline{k}')\cdot\underline{n}} = \sum_{\underline{n}} f(\underline{n}) e^{-i\underline{k}'\cdot\underline{n}} \\
&\Rightarrow \frac{1}{N^d}\sum_{\underline{k}} f(\underline{k}) N^d \delta_{\underline{k}\underline{k}'} = \sum_{\underline{n}} f(\underline{n}) e^{-i\underline{k}'\cdot\underline{n}} \\
&\Rightarrow f(\underline{k}') = \sum_{\underline{n}} f(\underline{n})\, e^{-i\underline{k}'\cdot\underline{n}}
\end{aligned} \tag{2.28}$$

The real numbers q_μ are usually referred to as momenta, by analogy with the continuum theory. They form a discrete set lying in the range

$$\frac{-\pi}{a} \leq q_\mu < \frac{\pi}{a}$$

As the lattice spacing a tends to zero, this range increases to infinity. On the other hand, the *number* of elements in the set $\{q_\mu\}$ increases with N so that in the thermodynamic limit the momenta become continuous.

Let us now restrict the set of allowable functions $f(\underline{n})$ to those satisfying

$$f(-N/2) = 0 \tag{2.29}$$

That is, we restrict $f(n_\mu)$ to zero on the boundary of the lattice. These functions form a proper subspace of the full space of periodic functions, generated by the basis vectors

$$\mathbf{e}_{p_\mu}(n_\mu) - \mathbf{e}_{-p_\mu}(n_\mu) = e^{\frac{2\pi i}{N} p_\mu n_\mu} - e^{-\frac{2\pi i}{N} p_\mu n_\mu} \qquad (p_\mu \neq 0, -N/2)$$

One additional basis vector satisfying the zero boundary condition may be constructed from a linear combination of the zero and $-N/2$ momentum modes:

$$(-1)^n \mathbf{e}_{-N/2}(n_\mu) - \mathbf{e}_0(n_\mu) = (-1)^{-N/2} e^{\pi i n_\mu} - 1$$

The coefficients in the Fourier expansion of such functions therefore satisfy

$$\begin{aligned} f(p_\mu) &= -f(-p_\mu) \qquad (p_\mu \neq 0, -N/2) \\ f(0) &= -(-1)^{N/2} f(-N/2) \end{aligned} \tag{2.30}$$

This is the corresponding boundary condition on the dual lattice.
Consider now a two–dimensional periodic lattice, with zero boundary conditions imposed along both axes. In particular, we have

$$f(-N/2,\, -N/2) = 0$$

Using (2.27) we obtain

$$\sum_{\underline{p}} f(\underline{p})\, e^{-i\,(\sum_\mu p_\mu)\,\pi} = f(\underline{-N/2}) = 0$$

which gives

$$f(\underline{0}) = -\sum_{\underline{p} \neq \underline{0}} (-1)^{(\sum_\mu p_\mu)}\, f(\underline{p})$$

The zero momentum mode is therefore independent of $\underline{n}$, a fact which will be crucial in deriving an unambiguous expression for the gauge field propagator.
With these boundary conditions, the Fourier transform (2.27) may be written

$$f(\underline{n}) = \frac{1}{N^d} \sum_{\underline{p} \neq \underline{0}} f(\underline{p})\, (e^{i\underline{p}.\underline{n}} - (-1)^{(\sum_\mu p_\mu)}) \tag{2.31}$$

8. Physics From The Lattice

The lattice theory has so far been considered as a construct in itself, without any reference to the underlying physics that we are ultimately trying to represent. The objects of interest, physical observables, are encoded in the expectation values of the continuum theory.

$$\langle O(\phi(x))\rangle = \frac{\int [D\phi]\, O(\phi(x))\, e^{-S}}{\int [D\phi]\, e^{-S}} \quad ; \quad x \in \mathbf{R}^d \tag{2.32}$$

The expectation values that are numerically computable, on the other hand, are defined on a finite discrete lattice with lattice spacing a:

$$\langle O(\phi(q))\rangle = \frac{\int \prod_{i=1}^{N^d} O(\phi(q))\, e^{-S(a)} d\phi_i}{\int \prod_{i=1}^{N^d} e^{-S(a)} d\phi_i} \quad ; \quad q \in \mathbf{Z}^d \tag{2.33}$$

The aim is to derive unambiguous values for the continuum expectation values (2.32) from their lattice versions (2.33).

The naive approach is to compute the value of the required observable $\langle O(a)\rangle$ from (2.33) for successively smaller values of a and then to remove the regulator by attempting to extrapolate to $a = 0$. There is no *a priori* reason why this expectation value should tend to a finite value in the limit of zero lattice spacing—indeed, we would expect the opposite in general, since the regulator has been removed without any renormalisation of the bare parameters of the theory (in this case, the mass m and the coupling g). Moreover, the existence of a finite limit for a single observable does not guarantee the existence of a continuum limit for the theory; for this, we require that *all* observables have finite values in the limit of vanishing lattice spacing.

A continuum limit, if it exists at all, will exist only for certain special values of the bare parameters—the so-called *ultra violet fixed points* of the theory. The problem is therefore to identify these fixed points.

This is actually quite a subtle question; we will give here only a heuristic argument to justify our conclusions.

Let us start with a finite d-dimensional lattice L_Z, embedded in $\mathbf{Z}^d$. There is no notion of lattice spacing and all quantities are dimensionless. It is on this lattice, L_Z, that numerical calculations are actually performed.

Consider now a second lattice, L_R endowed with a fixed finite lattice spacing a_0 and embedded in $a_0\mathbf{Z}^d$, a subset of $\mathbf{R}^d$. We will allow the parameters of the L_R theory to depend on the lattice spacing, which is the only dimensionful quantity; consequently any quantity Q in the L_R world must have dimension L^q where q is some rational number. In particular, masses must have dimension L^{-1} in order that they take on their proper dimension M^1 when the

physical constants $\hbar$ and c are eventually introduced. The two point correlation function between two sites on L_R can be shown to decay exponentially with the distance between the sites according to

$$\langle \phi(\underline{r}_2)\, \phi(\underline{r}_1) \rangle \propto e^{-|\underline{r}_2 - \underline{r}_1| M_{LR}(a_0, m(a_0), g(a_0))} \tag{2.34}$$

where M_{LR} is the physical mass of the lightest particle in the L_R theory. By analogy with the corresponding expression in statistical mechanics we define the physical correlation length:

$$\xi_R(a_0) = \frac{1}{M_{LR}(a_0, m(a_0), g(a_0))}$$

Next, let us consider a series of theories $L_R(a)$ indexed by the lattice spacing a. Each such theory is associated with different values of the bare parameters $m(a)$ and $g(a)$. If the generic L_R theory admits of a continuum limit the functional dependence of m and g on the lattice spacing must be such that the lightest mass $M_{LR}(a)$ tends to its (finite) continuum physical value M_C as the lattice spacing goes to zero. Therefore

$$\lim_{a \to 0} \xi_R(a) = \xi_R(0) = \xi_C \tag{2.35}$$

In other words, the correlation length tends to its finite continuum value. As a consequence, as a goes to zero the correlation length extends over an increasing number of sites.
Let us translate this result back to the dimensionless lattice L_Z. The correlation functions on L_Z are given by (cf (2.34))

$$\langle \phi(\underline{m})\, \phi(\underline{n}) \rangle \propto e^{-|\underline{m} - \underline{n}| M_{LZ}}$$

and we define the dimensionless correlation number by

$$\xi_Z = \frac{1}{M_{LZ}(m, g)}$$

This number represents the *number* of sites over which correlations extend, in contrast to ξ_R which represents the physical *length* over which they extend; the *convergence* of ξ_R as the lattice spacing tends to zero is therefore reflected on L_Z by a *divergence* of ξ_Z.
In other words, the existence of a continuum limit for the L_R theory requires a divergence of the correlation number in the L_Z theory.This implies that the L_Z parameters must be chosen so that the L_Z theory is at one of its points of second (or higher) order phase transition. Note, however, that although this conditon is necessary, there is no guarantee that it is sufficient.
We now encounter a technical difficulty, in that an infinite correlation number ξ_Z cannot be realised on a finite lattice; that is, as long as the lattice dimension N is finite the L_Z

theory cannot exhibit the required phase transition. It is therefore necessary to take the thermodynamic (large volume) limit before an approach to the continuum is attempted. The presents obvious difficulties from the point of view of numerical computations.
Let us list the steps required to extract the values of physical observables from the lattice:

1. Define a finite dimensionless lattice L_Z. Expectation values may be explicitly computed on this lattice using standard techniques.
2. Construct the phase diagram of the theory; that is, identify the parameter values which give rise to critical points in the infinite volume limit.
3. Identify the fixed points on the phase diagram which lead to a continuum limit.
4. Compute the required expectation values on the finite lattice using the appropriate values for the bare parameters. If these values lead to singularities in the action (as one would expect, in general, since we are effectively computing in the continuum limit), then use neighbouring values and attempt to extrapolate to the required values.
5. Repeat the computation on successively larger lattices and attempt to extrapolate to the thermodynamic limit.
6. The end result of this process is a number representing the physical continuum value of the required observable. The final step is to scale and dimension this number by reference to some experimentally known quantity. Alternatively, the ratio of two observables (for example, the mass ratio of two particles) may be computed.

Note that the lattice spacing never appears explicitly in the entire lattice calculation.

9. Phase Transitions

In this section we will review the basic theory of phase transitions and introduce a technique for determining critical points from the zeroes of the partition function.
A phase transition, from the point of view of statistical mechanics, occurs at a point in the parameter space where the partition function ceases to be analytic. Such points are characterised by discontinuities in the derivatives of the *thermodynamic potentials*, for example the *free energy*

$$F = -kT \log Z$$

An nth order phase transition corresponds to a discontinuity in the nth derivative. All second and higher order phase transitions are classified as *continuous* transitions; continuous phase transitions are associated with a divergent correlation length and are therefore of particular interest in the context of lattice field theory.

The idea that the location of a phase transition could be determined by an investigation of the zeroes of the partition function was first introduced by Lee and Yang (1952) and further developed by Fisher (1968). An elementary discussion can be found in ter Haar (1995).

Let us briefly review the main idea.

Suppose we are interested in the value of some (real, positive) physical parameter y at which a phase transition takes place. Consider the partition function Z as a function of y. We will show later that, for the partition functions and parameters of interest, this function can be written as a finite polynomial in y.

$$Z = \sum_{i=1}^{M} a_i y^i \tag{2.36}$$

where M is the number of lattice sites and the coefficients a_i are all non-negative.

Next we define the lattice analogue of the free energy per site at constant temperature

$$f(y) = \frac{\log Z(y)}{M}$$

where it is understood that M is finite. In view of (2.36), $f(y)$ is clearly an analytic function of y except at the zeroes of Z. Moreover, since the coefficients in (2.36) are all positive there can be no zero for any real positive value of y. Therefore $f(y)$ is analytic for all real positive y. As a consequence there can be no discontinuity in any of its derivatives on the real positive y axis and therefore no phase transition.

Let us next consider the limit of infinite M. We define

$$F(y) = \lim_{M\to\infty} f(y)$$

It was shown by Lee and Yang (1952) that this limit is well–defined; that is, $F(y)$ exists for all real positive y. Moreover $f(y)$ converges uniformly to $F(y)$ for all real y as M tends to infinity. It follows that F(y) is also analytic everywhere except at the zeroes of Z.

Now consider a a small but finite region R free of zeroes and containing a point r on the real positive y axis. If, as M tends to infinity R continues to be free of zeros then $F(y)$ is analytic throughout R. If, on the other hand, no such region R can be found (in other words, if the zeroes approach r arbitrarily closely) then $F(y)$ cannot be analytic at r and must therefore possess a discontinuous derivative at some order. A phase transition therefore occurs as the physical parameter y passes through the value r.

To summarise, the points of phase transition of a lattice theory (with respect to some particular physical parameter such as the mass) may be determined in the following way. First express the partition function as a polynomial in the relevant parameter on a finite lattice. Next determine the distribution of zeroes of this polynomial. Finally, analyse the change in this distribution as the lattice size tends to infinity and locate those points (if any) on the real axis on which the zeroes converge.

3. Abelian Gauge Fields In Two Dimensions

In the beginning God created the heaven and the earth
And the earth was without form, and void, and darkness was upon the face of the deep
And the Spirit of God moved upon the face of the waters
And God said, Let there be light and there was light
– Genesis

The first half of this Chapter consists of a review of U(1) gauge fields on a plane lattice. The gauge invariant lattice action due to Wilson is introduced and the concept of gauge invariance in the lattice context is discussed. It is shown that it is not necessary to fix the gauge in order to compute the expectation value of a gauge–invariant object; however gauge–fixing is mandatory if one is to obtain a non–zero value for the expectation value of a gauge–dependent object.The second half of the Chapter is concerned with the weak coupling approximation for the pure gauge field. It is shown that the vacuum state is degenerate if periodic boundary conditions are applied, but that a unique vacuum is obtained if zero boundary conditions are applied.

10. The Wilson Action

In this chapter and the next we review gauge and matter fields in their lattice formulation. A more detailed discussion of these issues is to be found in several standard works; see for example, Creutz (1983), Montvay and Munster (1994), Rothe (1997) and Callaway (1985). Gauge fields may be placed on the lattice in a way which preserves exact gauge invariance, (Wilson, 1974). We will consider here the case of Abelian fields—more precisely U(1) fields; the discussion can easily be generalised to the non–Abelian case.
The pure gauge action in the continuum is given by

$$S_G = \frac{1}{4}\int F_{\mu\nu}F_{\mu\nu}\ d^4x$$

where the field strength tensor $F_{\mu\nu}$ is defined in terms of the vector potential by

$$F_{\mu\nu} = \partial_\mu A_\nu - \partial_\nu A_\mu$$

Let us define *link variables* on the lattice to be elements of U(1) with the form

$$U_\mu(\underline{n}) = e^{i\phi_\mu(\underline{n})} = e^{igaA_\mu(\underline{n})}$$

where g is a coupling constant, a is the lattice spacing and $A_\mu(\underline{n})$ is the value of the μth component of the vector potential at the lattice site n. The angular variable $\phi_\mu(\underline{n})$ is understood to be restricted to the range

$$-\pi < \phi_\mu(\underline{n}) \leq \pi$$

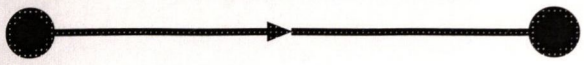

A link variable may be thought of as connecting adjacent sites on the lattice; thus $U_\mu(\underline{n})$ connects the site $\underline{n}$ with the site $(\underline{n}+\underline{\mu})$.
Furthermore, we have

$$U_{-\mu}(\underline{n}) = e^{igaA_{-\mu}(\underline{n})} = e^{-igaA_\mu(\underline{n})} = U_\mu^{-1}(\underline{n}) = U_\mu^\dagger(\underline{n})$$

Thus $U_\mu^\dagger(\underline{n})$ has the opposite orientation to $U_\mu(\underline{n})$.
These link variables represent the gauge fields on the lattice. The aim is to construct from them a gauge–invariant action which reduces to the continuum action as the lattice spacing a approaches zero. The simplest such action is the plaquette action due to Wilson. This is defined in terms of the elementary *plaquette* or square, $U_p(\underline{n}, \underline{\mu},\ \nu > \mu)$. (Figure (3.1)).

$$U_p(\underline{n}, \underline{\mu},\ \nu > \mu) = U_\mu(\underline{n})U_\nu(\underline{n}+\underline{\mu})U_\mu^\dagger(\underline{n}+\underline{\nu})U_\nu^\dagger(\underline{n})$$

The restriction $\nu > \mu$ ensures that each plaquette occurs with only one orientation.

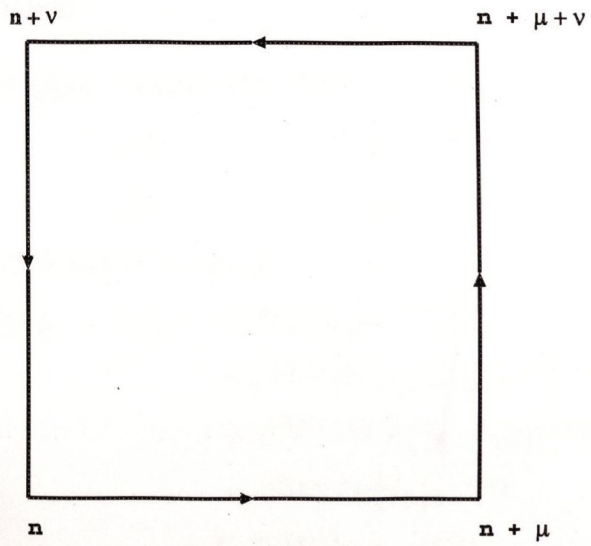

Figure 3.1: The elementary plaquette

In terms of the continuum fields A_μ the plaquette becomes

$$\begin{aligned} U_p(\underline{n}, \underline{\mu},\ \nu > \mu) &= e^{igaA_\mu(\underline{n})} e^{igaA_\nu(\underline{n}+\underline{\mu})} e^{-igaA_\mu(\underline{n}+\underline{\nu})} e^{-igaA_\nu(\underline{n})} \\ &= \exp\, iga((A_\nu(\underline{n}+\underline{\mu}) - A_\nu(\underline{n})) - (A_\mu(\underline{n}+\underline{\nu}) - A_\mu(\underline{n}))) \\ &= \exp\, iga^2 \left(\frac{A_\nu(\underline{n}+\underline{\mu}) - A_\nu(\underline{n})}{a} - \frac{A_\mu(\underline{n}+\underline{\nu}) - A_\mu(\underline{n})}{a} \right) \end{aligned}$$

For small a the plaquette is given approximately by

$$U_p(\underline{n}, \underline{\mu},\ \nu > \mu) \approx \exp\, iga^2(\partial_\mu A_\nu - \partial_\nu A_\mu) = \exp\, iga^2 F_{\mu\nu} = e^{ia^2\phi_p}$$

where $\phi_p = gF_{\mu\nu}$.

Consider now the action

$$S_G = \frac{1}{g^2} \sum_p \sum_{\mu,\nu,\nu>\mu} \text{Re}\ (1 - U_p) = \frac{1}{2g^2} \sum_p \sum_{\mu,\nu} (1 - \cos a^2\phi_p) \tag{3.1}$$

Expanding the cosine and retaining the leading term in a gives

$$S_G = \frac{1}{2g^2} \sum_p \sum_{\mu,\nu} \frac{a^4 {\phi_p}^2}{2} = \frac{1}{4} \sum_p a^4 F_{\mu\nu} F_{\mu\nu}$$

As a tends to zero we have

$$\lim_{a\to 0} \sum_p a^4 = \int d^4x$$

yielding the correct continuum limit

$$\lim_{a\to 0} S_G = \frac{1}{4} \int F_{\mu\nu} F_{\mu\nu}\ d^4x$$

11. Gauge Invariance

The elementary plaquette $U_p(\underline{n})$ is invariant under the transformation

$$\begin{aligned} U_\mu(\underline{n}) &\longrightarrow e^{if(\underline{n})} U_\mu(\underline{n}) e^{-if(\underline{n}+\underline{\mu})} \\ U_\mu^\dagger(\underline{n}) &\longrightarrow e^{if(\underline{n}+\underline{\mu})} U_\mu^\dagger(\underline{n}) e^{-if(\underline{n})} \end{aligned} \tag{3.2}$$

where $f(\underline{n})$ is an arbitrary function of the lattice site:

$$\begin{aligned} {U'}_p(\underline{n}, \underline{\mu},\ \nu > \mu) &= e^{if(\underline{n})} U_\mu(\underline{n}) e^{-if(\underline{n}+\underline{\mu})} \\ &\quad \times e^{if(\underline{n}+\underline{\mu})} U_\nu(\underline{n}+\underline{\mu}) e^{-if(\underline{n}+\underline{\mu}+\underline{\nu})} \\ &\quad \times e^{if(\underline{n}+\underline{\nu}+\underline{\mu})} U_\mu^\dagger(\underline{n}+\underline{\nu}) e^{-if(\underline{n}+\underline{\nu})} \\ &\quad \times e^{if(\underline{n}+\underline{\nu})} U_\nu^\dagger(\underline{n}) e^{-if(\underline{n})} \\ &= U_\mu(\underline{n}) U_\nu(\underline{n}+\underline{\mu}) U_\mu^\dagger(\underline{n}+\underline{\nu}) U_\nu^\dagger(\underline{n}) \\ &= U_p(\underline{n}, \underline{\mu},\ \nu > \mu) \end{aligned} \tag{3.3}$$

Transformations of this type are *local gauge transformations* and the elementary plaquette is said to be *gauge invariant.*

The transformation (3.2) can be written

$$e^{iagA_\mu(\underline{n})} \longrightarrow e^{iag\left(A_\mu(\underline{n})-\left(\frac{1}{g}\right)\frac{f(\underline{n}+\underline{\mu})-f(\underline{n})}{a}\right)}$$

In other words the effect of the gauge transformation is to add the discrete analogue of an arbitrary divergence to the vector potential. In the limit of small a the lattice gauge transformation goes over to the usual continuum gauge transform

$$A_\mu(\underline{x}) \longrightarrow A_\mu(\underline{x}) + \partial_\mu f(\underline{x})$$

apart from an overall factor of $1/g$. This factor can be absorbed into the definition of $f(\underline{n})$ as long as g is finite; that is, the gauge function $f(\underline{x})$ is the continuum limit of the function $(1/g)f(\underline{n})$, except at $g = 0$ (weak coupling limit) and $g = \infty$ (strong coupling limit).

It is clear from the construction (3.3) that the product of link variables around *any* closed loop is gauge invariant. Moreover, functions of such products are also gauge invariant:

$$f(U'_{loop}) = f(U_{loop})$$

In particular, the action S_G proposed in the previous section is gauge invariant.

Let us now assign some arbitrary value $U_\mu(\underline{n})$ to each link on the lattice. Such a set of link variables is termed a *field configuration.* Quantisation of the system requires the calculation of expectation values over all possible configurations and for this purpose a measure $[dU]$ on the space of configurations must be established. The appropriate measure for the group U(1) is well known (Cornwell, 1984):

$$[dU] = \int_\pi^\pi \prod_{\mu,\underline{n}} \frac{d\phi_\mu(\underline{n})}{2\pi} \tag{3.4}$$

where

$$U_\mu(\underline{n}) = e^{i\phi_\mu(\underline{n})} \in \mathrm{U}(1) \quad \text{and} \quad -\pi < \phi_\mu(\underline{n}) \leq \pi$$

Each angular variable $\phi_\mu(\underline{n})$ undergoes a phase shift under a gauge transformation:

$$\phi_\mu(\underline{n}) \longrightarrow \phi_\mu(\underline{n}) + f(\underline{n}) - f(\underline{n}+\underline{\mu}) = \phi'_\mu(\underline{n})$$

The gauge function $f(\underline{n})$ is independent of $\phi_\mu(\underline{n})$, so that we have in addition:

$$d\phi_\mu(\underline{n}) = d\phi'_\mu(\underline{n})$$

$$\int_{\pi}^{\pi} d\phi_\mu(\underline{n}) \longrightarrow \int_{\pi+f(\underline{n})-f(\underline{n}+\underline{\mu})}^{\pi+f(\underline{n})-f(\underline{n}+\underline{\mu})} d\phi'_\mu(\underline{n}) = \int_{\pi}^{\pi} d\phi_\mu(\underline{n})$$

It follows that the measure $[dU]$ is invariant under gauge transformations. Since the action is also invariant, the expectation value of a gauge–independent function, or 'observable', $\mathcal{O}$ is itself gauge–independent.

$$\langle \mathcal{O} \rangle = \frac{\int [dU]\, \mathcal{O}\, e^{-S}}{\int [dU]\, e^{-S}} \tag{3.5}$$

It is clear that redundant degrees of freedom exist in this integral since each configuration may be replaced by an arbitrary gauge transform of itself without altering the integrand or the measure. The integral runs over all configurations, and consequently over all gauge transforms of each 'distinct' configuration. It is therefore enhanced by a factor equal to the volume of the group of gauge transforms. This effect occurs also in the continuum gauge theory where the volume of the group is infinite. It is usually dealt with there by *fixing the gauge*; that is, by adjusting the action so that the integral picks out precisely one representative from each distinct family of gauge transforms. Gauge fixing is not necessary in the lattice theory, however, since the volume of the group of gauge transforms is finite—actually unity with the normalisation in (3.4).

This can be demonstrated explicitly by removing the gauge degrees of freedom and showing that the integral is unchanged. Let us first write the gauge transform (3.2) in the form

$$U_\mu(\underline{n}) \longrightarrow \Lambda(\underline{n}) U_\mu(\underline{n}) \Lambda^\dagger(\underline{n}+\underline{\mu})$$

The gauge freedom associated with the link $U_\mu(\underline{n}) = e^{i\phi_\mu(\underline{n})}$ can be removed by defining $\Lambda(\underline{n})$ and $\Lambda^\dagger(\underline{n}+\underline{\mu})$ so that

$$\Lambda(\underline{n}) U_\mu(\underline{n}) \Lambda^\dagger(\underline{n}+\underline{\mu}) = 1$$

In other words $\Lambda(\underline{n})$ and $\Lambda^\dagger(\underline{n}+\underline{\mu})$ are assigned a dependence on $\underline{n}$ that exactly cancels that of $U_\mu(\underline{n})$.

Let us next choose $\Lambda^\dagger(\underline{n}+\underline{\mu}+\underline{\nu})$ so that

$$\Lambda^\dagger(\underline{n}+\underline{\mu}) U_\nu(\underline{n}+\underline{\mu}) \Lambda^\dagger(\underline{n}+\underline{\mu}+\underline{\nu}) = 1$$

This process can be continued, fixing an arbitrary number of link variables to unity, subject only to the condition that no set of fixed links forms a closed loop. (The last object in a closed loop is $\Lambda^\dagger(\underline{n})$ which cannot be chosen arbitrarily since $\Lambda(\underline{n})$ has already been fixed.) When all links that can be fixed have been fixed (the so–called maximal tree), all the redundant degrees of freedom have been removed from the integrand in (3.5) and the gauge is said to be fixed.

Let us now suppose that k links have been fixed (not necessarily a maximal tree) by an appropriate gauge transformation leaving m free links. The integral (3.5) becomes

$$\langle \mathcal{O}(U'_m) \rangle = \frac{\int [dU'_m][dU'_k]\, \mathcal{O}(U'_m)\, e^{-S(U'_m)}}{\int [dU'_m][dU'_k]\, e^{-S(U'_m)}}$$

Now $\mathcal{O}$, S and $[dU]$ are all gauge invariant, thus

$$\mathcal{O}(U'_m) = \mathcal{O}$$
$$S(U'_m) = S$$
$$[dU'_m][dU'_k] = [dU]$$

Moreover the normalisation adopted in (3.4) means that

$$\int [dU'_k] = \int_{-\pi}^{\pi} \prod_k \frac{d\phi'_k}{2\pi} = 1$$

so that

$$\frac{\int [dU'_m]\, \mathcal{O}(U'_m)\, e^{-S(U'_m)}}{\int [dU'_m][dU'_k]\, e^{-S(U'_m)}} = \frac{\int [dU]\, \mathcal{O}\, e^{-S}}{\int [dU]\, e^{-S}}$$

and the expectation value (3.5) is unaltered.

$$\langle \mathcal{O}(U'_m) \rangle = \langle \mathcal{O} \rangle$$

It follows that the gauge degrees of freedom contribute nothing to the integral and no gauge–fixing is required to calculate the expectation value of a gauge invariant object.

Having established the basic idea of gauge invariance, let us introduce a more convenient notation. Denote a set of links $U_\mu(\underline{n})$ making up a configuration by U_c. A function of these links is a function of the configuration:

$$g(U_\mu(\underline{n})) = g(U_c)$$

A gauge transform on a configuration shifts each link by an arbitrary phase :

$$U_c \longrightarrow U_c e^{i\theta_c(\underline{n},\mu)}$$

Each 'distinct' configuration is represented by a family of gauge transforms;

$$U_c = \{\, U_c\, e^{i\theta_c(\underline{n},\mu)} \quad : \quad -\pi < \theta_c(\underline{n},\mu) \leq \pi \,\}$$

With this notation the weighted integral of a function over all configurations can be broken up explicitly into an integral over distinct configurations and an integral over gauge transforms

$$\int [dU]\, g(U_c) e^{-S_c} = \int_c \int_{-\pi}^{\pi} g(U_c\, e^{i\theta_c(\underline{n},\mu)})\, \exp\left(-S_c\, e^{i\theta_c(\underline{n},\mu)}\right) \frac{d\theta_c}{2\pi}$$

Since the action S_c is invariant under gauge transforms this can be written

$$\int [dU]\, g(U_c) e^{-S_c} = \int_c e^{-S_c} \int_{-\pi}^{\pi} g(U_c\, e^{i\theta_c(\underline{n},\mu)})\, \frac{d\theta_c}{2\pi} \tag{3.6}$$

If the function g is also gauge independent, this reduces further to

$$\int [dU]\, g(U_c) e^{-S_c} = \int_c g(U_c) e^{-S_c} \int_{-\pi}^{\pi} \frac{d\theta_c}{2\pi} = \int_c g(U_c) e^{-S_c}$$

the integral over gauge transformations just contributing a factor of unity as before.

It is worth noting in passing that a constant function $g = k$ is independent of the link variables, reducing (3.6) to

$$\int [dU]\, g(U_c) e^{-S_c} = k \int_c e^{-S_c}$$

If g depends on the gauge, the change of variable $x = e^{i\theta_c}$ gives

$$\int [dU]\, g(U_c) e^{-S_c} = \int_c e^{-S_c} \int_{e^{i\pi}}^{e^{-i\pi}} ig(U_c x)\, \frac{dx}{2\pi x} = 0$$

The expectation value of a gauge dependent function is therefore annihilated in the process of integrating over all gauges and it is mandatory to remove at least some of the gauge degrees of freedom if we wish to obtain non–zero values for such objects. Two gauges which are in common use on the lattice will be introduced in the following sections.

12. Axial Gauge

This is implemented by fixing all timelike link variables to unity. The links fixed in this way do not quite form a maximal tree on an infinite lattice, since additional spacelike links can be fixed without forming a closed loop.

Some care is required in setting axial gauge on a periodic finite lattice since each string of timelike links then forms a closed loop. It is therefore necessary to leave at least one timelike link in each string unfixed.

13. Feynman Gauge

It is also possible to fix the gauge by modifying the action, as is done in the continuum. The modified action is given by

$$S'_G = \frac{1}{2g^2} \sum_p \sum_{\mu,\nu} (1 - \cos a^2 \phi_{\mu,\nu}(p)) + \frac{1}{2\alpha} \sum_p \sum_{\mu} (\Delta^L_\mu \phi_\mu(p))^2$$

where Δ_μ^L, the *left lattice derivative* is defined by

$$\Delta_\mu^L f(x) = \frac{f(x) - f(x-\mu)}{a}$$

and α is an arbitrary parameter. Lorentz gauge is therefore a family of gauges corresponding to different choices of α. Of particular interest is the case $\alpha = 1$, the *Feynman* gauge.

14. Weak Coupling

Our eventual goal will be to determine the phase structure of the lattice Schwinger model in the weak coupling regime. In this section we will discuss some important issues associated with the implementation of a weak coupling approximation.

Let us consider some generic "pure gauge" expectation value:

$$\langle O \rangle = \frac{\int O e^{-S_G}}{\int e^{-S_G}}$$

We wish to find an approximate form of $\langle O \rangle$ valid at weak coupling, that is to say at large β. This expectation value is weighted by the exponential of the negative of the pure gauge action, which is given by

$$S_G = \beta \sum_{p,\mu,\nu} (1 - \cos \phi_p(\mu,\nu))$$

$$\phi_p(\mu,\nu) = \phi_\mu(\underline{p}) + \phi_\nu(\underline{p} + \underline{\mu}) - \phi_\mu(\underline{p} + \underline{\nu}) - \phi_\nu(\underline{p})$$

Here, the angular link variables are given by

$$\phi_\mu(\underline{p}) = g a A_\mu(\underline{p})$$

At first sight it might appear that for large β (small g), $\phi_\mu(\underline{p})$ is small and that one can therefore expand the partition function in powers of ϕ. This is incorrect; in order to preserve the group structure of the theory it is essential that the ϕ's are allowed to take all values in the interval $[-\pi\ ,\ \pi]$. It is, instead, the continuum field $A_\mu(\underline{p})$ which scales with g:

$$\frac{-\pi}{ga} < A_\mu(\underline{p}) \leq \frac{\pi}{ga}$$

We will show, however, that under certain conditions it *is* permissible to restrict attention to small values of the angular variables.

Firstly, we note that for large β, the partition function is largely determined by those configurations which satisfy

$$\sum_p \sum_{\mu,\nu} (1 - \cos \phi_p(\mu,\nu)) \approx 0$$

where Δ_μ^L, the *left lattice derivative* is defined by

$$\Delta_\mu^L f(x) = \frac{f(x) - f(x-\mu)}{a}$$

and α is an arbitrary parameter. Lorentz gauge is therefore a family of gauges corresponding to different choices of α. Of particular interest is the case $\alpha = 1$, the *Feynman* gauge.

14. Weak Coupling

Our eventual goal will be to determine the phase structure of the lattice Schwinger model in the weak coupling regime. In this section we will discuss some important issues associated with the implementation of a weak coupling approximation.

Let us consider some generic "pure gauge" expectation value:

$$\langle O \rangle = \frac{\int O e^{-S_G}}{\int e^{-S_G}}$$

We wish to find an approximate form of $\langle O \rangle$ valid at weak coupling, that is to say at large β. This expectation value is weighted by the exponential of the negative of the pure gauge action, which is given by

$$S_G = \beta \sum_{p,\mu,\nu} (1 - \cos \phi_p(\mu,\nu))$$

$$\phi_p(\mu,\nu) = \phi_\mu(\underline{p}) + \phi_\nu(\underline{p} + \underline{\mu}) - \phi_\mu(\underline{p} + \underline{\nu}) - \phi_\nu(\underline{p})$$

Here, the angular link variables are given by

$$\phi_\mu(\underline{p}) = gaA_\mu(\underline{p})$$

At first sight it might appear that for large β (small g), $\phi_\mu(\underline{p})$ is small and that one can therefore expand the partition function in powers of ϕ. This is incorrect; in order to preserve the group structure of the theory it is essential that the ϕ's are allowed to take all values in the interval $[-\pi\ ,\ \pi]$. It is, instead, the continuum field $A_\mu(\underline{p})$ which scales with g:

$$\frac{-\pi}{ga} < A_\mu(\underline{p}) \leq \frac{\pi}{ga}$$

We will show, however, that under certain conditions it *is* permissible to restrict attention to small values of the angular variables.

Firstly, we note that for large β, the partition function is largely determined by those configurations which satisfy

$$\sum_p \sum_{\mu,\nu} (1 - \cos \phi_p(\mu,\nu)) \approx 0$$

Each term in the sum over p is non-negative; therefore, for sufficiently large β, the only configurations we need consider are those for which

$$\sum_{\mu,\nu} 1 - \cos\phi_p(\mu,\nu) \approx 0 \quad \forall p \tag{3.7}$$

which implies

$$\phi_p(\mu,\nu) \approx 0 \quad \forall p \quad (-\pi < \phi_p(\mu,\nu) \leq \pi)$$

That is to say, the links associated with each plaquette P satisfy

$$(\phi_{\underline{\mu}}(\underline{p}) + \phi_{\underline{\nu}}(\underline{p}+\underline{\mu}))) - (\phi_{\underline{\mu}}(\underline{p}+\underline{\nu}) - \phi_{\underline{\nu}}(\underline{p})) \approx 0 \tag{3.8}$$

This condition is clearly satisfied if the value of each individual link $\phi_{\underline{\mu}}(\underline{p})$ is small; each link variable $U_{\underline{\mu}}(\underline{p})$ is then close to the identity. Let us denote the class of configurations in this category by C_0.

If all configurations satisfying (3.8) belonged to C_0, we would be justified (for sufficiently small coupling) in restricting attention to small values of the angular variables, the so–called *saddle point* approximation.

Unfortunately, there is also a large class of configurations satisfying (3.8) in which the individual links are *not* small; we will denote this class by C_L. The existence of these configurations means that a saddle–point approximation cannot be applied, since certain configurations with large values of the angular variables will contribute significantly to the integral and cannot therefore be neglected.

It is sometimes said that each member of C_L is gauge equivalent to a member of C_0 and that the 'bad' configurations in C_L can be eliminated by fixing the gauge.This assumption holds on an *infinite* lattice, as we will now show.

Consider some arbitrary member of C_L. Each plaquette U_p, in this configuration can be written in the form

$$U_p = e^{i\phi_1}\, e^{i\phi_2}\, e^{-i\phi_3}\, e^{-i\phi_4}$$

where

$$\begin{aligned}
\phi_1 &= \phi_{\underline{\mu}}(\underline{p}) \\
\phi_2 &= \phi_{\underline{\nu}}(\underline{p}+\underline{\mu}) \\
\phi_3 &= \phi_{\underline{\mu}}(\underline{p}+\underline{\nu}) \\
\phi_4 &= \phi_{\underline{\nu}}(\underline{p})
\end{aligned}$$

Since every plaquette satisfies (3.8) we have

$$U_p \approx 1 \quad = 1 + \delta_p \quad ; \quad |\delta_p| \ll 1 \quad \forall p$$

We seek a gauge transformation such that

$$\begin{aligned} U'_p = U_p &= e^{i\theta_1}\, e^{i\theta_2}\, e^{-i\theta_3}\, e^{-i\theta_4} \\ &= 1 + \delta_p \quad ; \quad |\delta_p| \ll 1 \quad \forall p \end{aligned} \tag{3.9}$$

and

$$\theta_i(p) = \epsilon_i(p) \quad ; \quad |\epsilon_i(p)| \ll 1 \quad \forall i, p \tag{3.10}$$

Let us now choose a particular plaquette and apply a general gauge transformation (3.2) to it:

$$\begin{aligned} U_p &= e^{i\phi_1}\, e^{i\phi_2}\, e^{-i\phi_3}\, e^{-i\phi_4} \\ &\longrightarrow e^{i\theta_1}\, e^{i\theta_2}\, e^{-i\theta_3}\, e^{-i\theta_4} \end{aligned}$$

where

$$\begin{aligned} e^{i\theta_1} &= e^{if(\underline{p})}\, e^{i\phi_1}\, e^{-if(\underline{p}+\underline{\mu})} \\ e^{i\theta_2} &= e^{if(\underline{p}+\underline{\mu})}\, e^{i\phi_2}\, e^{-if(\underline{p}+\underline{\mu}+\underline{\nu})} \\ e^{i\theta_3} &= e^{if(\underline{p}+\underline{\mu}+\underline{\nu})}\, e^{i\phi_3}\, e^{-if(\underline{p}+\underline{\nu})} \\ e^{i\theta_4} &= e^{if(\underline{p}+\underline{\nu})}\, e^{i\phi_4}\, e^{-f(\underline{p})} \end{aligned}$$

Let $f(\underline{p})$ be arbitrary and define $f(\underline{p}+\underline{\mu})$ so that $\theta_1 = \epsilon_1$. Similarly, define $f(\underline{p}+\underline{\mu}+\underline{\nu})$ so that $\theta_2 = \epsilon_2$ and $f(\underline{p}+\underline{\nu})$ so that $\theta_3 = \epsilon_3$.

Now

$$U'_p = U_p \longrightarrow e^{i\epsilon_1} e^{i\epsilon_2} e^{i\epsilon_3} e^{i\theta_4} = 1 + \delta_p$$

and hence

$$\begin{aligned} e^{i\theta_4} &= (1+\delta_p) e^{-i\epsilon_1} e^{-i\epsilon_2} e^{-i\epsilon 3} \\ &= (1+\delta)(1+O(\epsilon)) \end{aligned}$$

since $|\epsilon_i| \ll 1$. Therefore we may write $\theta_4 = \epsilon_4$ with $|\epsilon_4| \ll 1$.

It is important to note that the transformation of this first plaquette is not completely specified because of the arbitrariness of $f(\underline{p})$.

Having thus transformed the first plaquette we move to an adjacent plaquette and repeat the procedure with the two remaining free sites. Notice that there is no phase freedom associated with the second or subsequent plaquettes.

Proceeding in this way we define a gauge transform on the whole configuration to produce a new configuration satisfying the conditions (3.9) and (3.10). For each plaquette in the interior of the lattice there is sufficient freedom to force three of the four links to be small; the fourth link is then guaranteed small by gauge invariance.

15. Vacuum Degeneracy on a Finite Lattice

In the absence of boundary plaquettes (ie on an infinite lattice) this procedure suffices to eliminate all configurations in C_L. In particular, the action then has a unique minimum corresponding to all links equal to the identity.

On a finite lattice, however, the boundary plaquettes are additionally constrained by the boundary conditions and the gauge fixing procedure outlined above cannot be implemented. The situation is illustrated in (3.2) for a 3×3 lattice satisfying periodic boundary conditions.

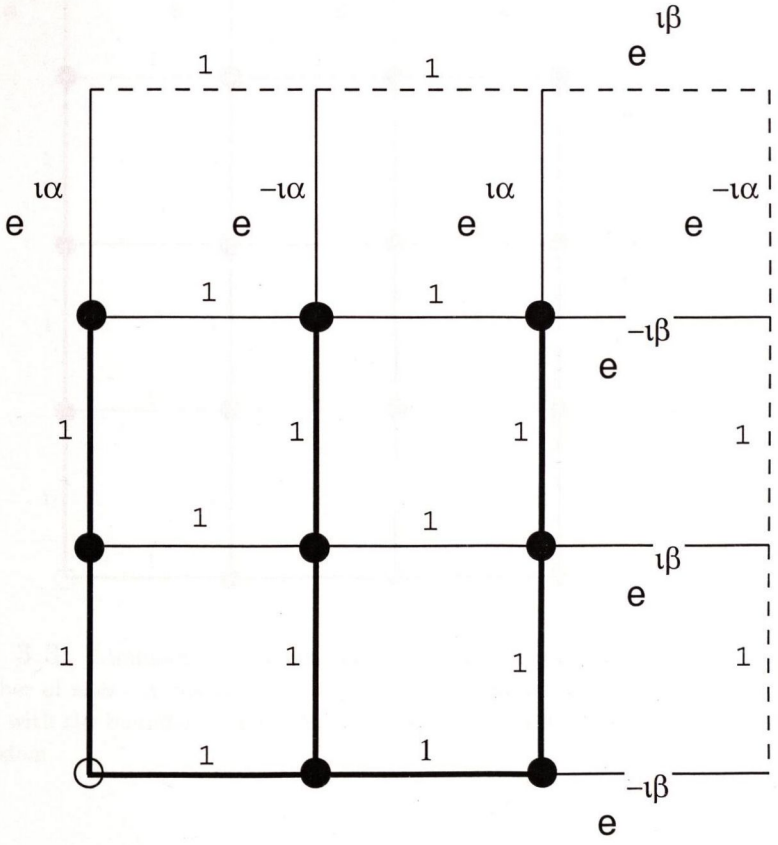

Figure 3.2: Minimum energy configurations on a gauge fixed finite lattice with an odd number of sites. Bold lines indicate fixed links, dotted lines indicate the periodic boundary. Black circles denote the sites whose gauge freedom has been removed. The whites circle is the single remaining free site associated with the overall global gauge freedom. Four minimum energy configurations are consistent with the boundary conditions.

Periodicity requires only that

$$e^{i\alpha} = e^{-i\alpha} \quad ; \quad e^{i\beta} = e^{-i\beta}$$

which is satisfied for $\alpha = 0, \pi$, $\beta = 0, \pi$. There are therefore four distinct minimum energy configurations, three of which are associated with large values of the angular variables ($\sim \pi$).

These large values are confined to boundary plaquettes; for large lattices their significance lies not in their numerical value but rather in the fact that their *existence* introduces a new class of significant configurations into the integral.

The situation is even worse in the case of lattices with an even number of sites along each axis, as illustrated in (3.3).

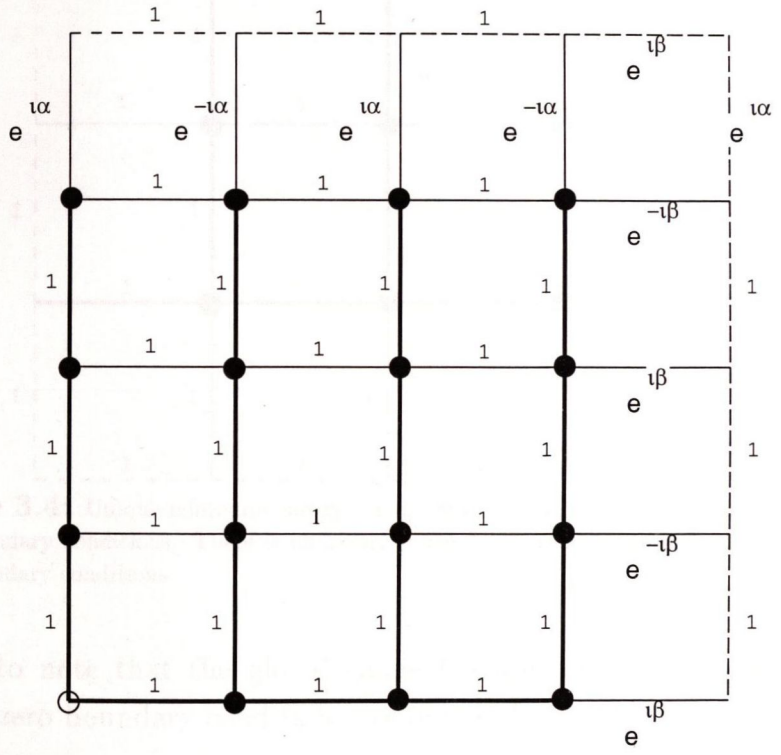

Figure 3.3: Minimum energy configurations on a gauge fixed finite lattice with an even number of sites. A continuous double infinity of minimum energy configurations are consistent with the boundary conditions. As with the odd lattice, there is an overall global gauge freedom.

In this case, the boundary condition imposes no restriction on the parameters α and β and there is a continuous double infinity of minimum energy configurations.

In both the even and odd cases the gauge fixing is defined only up to an arbitrary phase, or global gauge transform.

The difficulty clearly lies in the fact that periodic boundary conditions are insufficiently restrictive; an unambiguous saddle point approximation requires the imposition of a *zero boundary condition* on the lattice. The angular variables are constrained to zero on the boundary. The existence of this fixed boundary then allows all plaquettes to be treated as interior plaquettes and fixing the gauge then defines a unique minimum of the action, just as in the case of an infinite lattice.The scheme is illustrated in (3.4)

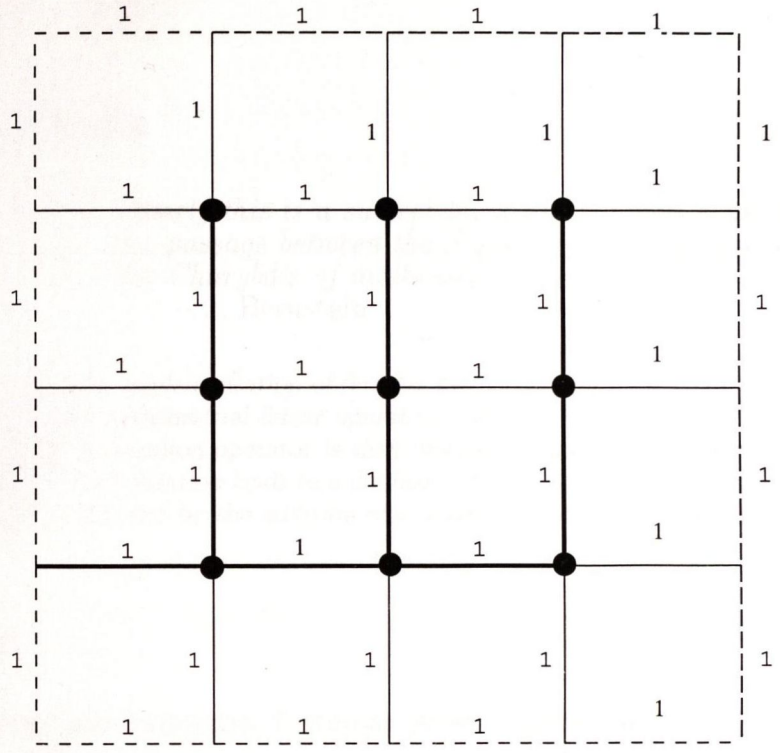

Figure 3.4: Unique minimum energy configurations on a gauge fixed finite lattice with zero boundary conditions. There is no global gauge freedom on a gauge fixed lattice with zero boundary conditions.

It is interesting to note that the global gauge freedom associated with periodic lattices disappears when zero boundary conditions are imposed.

4. Matter Fields

Clearly this is a subject in which common sense will have to guide the passage between the Scylla of mathematical Talmudism and the Charybdis of mathematical nonsense
– J. Bernstein

In this Chapter we review the implementation of fermion fields on the lattice.The Dirac operator appears in the lattice setting as a finite dimensional linear operator; therefore we begin with a brief discussion of the theory of such operators.The fermion operator is then discretised and the free propagator calculated. It is shown that the process of discretisation leads to a doubling of the number of fermions in each dimension and that this doubling can be removed by the addition of a momentum dependent mass term to the action.

16. Overview

Most forms of matter are fermionic. Fermions present special problems on the lattice; most particularly, the transcription to the lattice setting results inevitably in a doubling of the number of fermions in each dimension. Although this doubling might be tolerable in the free case, it cannot be accepted when one is dealing with an interacting theory and the unwanted fermions can be pair–produced.

Two principal methods have been proposed to deal with the doubling problem. Kogut and Susskind (1975) suggested that the fermion field components be distributed over the lattice sites so that only a single component was assigned to each site. The fermion multiplicity is reduced, in four dimensions, from sixteen to four; the remaining fermions are then interpreted as physical flavours.

Wilson (1975) proposed modifying the lattice fermion action so as to eliminate the extra fermions. This modification disappears in the continuum limit.This is the approach we will follow.

Although the Wilson approach is more straightforward to implement it suffers from a serious drawback; the extra Wilson term in the action destroys the chiral symmetry which the action would otherwise possess at zero fermion mass and therefore complicates lattice investigations of massless physics.

We should mention in passing another peculiarity of fermions on a finite lattice; it proves in most cases more convenient to use anti–periodic boundary conditions in the time direction, and we will follow this practice. For a further discussion of this point, see Montvay and Munster (1994).

17. Linear Operators

We will see in the following sections that the fermionic operator takes the form of a finite dimensional linear operator. Before proceeding, therefore, we will briefly review elementary properties of linear operators and establish basic definitions and notation.

Suppose V is a finite dimensional vector space with $v, w \in V$. We will define a linear operator as a mapping from V to itself, satisfying

$$T(av + bw) = aT(v) + bT(w)$$

where a and b are scalars. Note that the complete specification of the operator requires that both the action of the operator and the vector space on which it acts be defined.

It follows immediately that

$$T(0) = 0$$

Furthermore, if T and S are linear operators and k is a scalar, then kT, $T + S$ and TS are also linear operators. We can therefore construct polynomials in T which are themselves linear operators

$$p(T) = a_0 + a_1 T + a_2 T^2 + \cdots + a_n T^n$$

and indeed, T and S satisfy the usual algebraic rules:

$$\begin{aligned} S(T + T') &= ST + ST' \\ (S + S')T &= ST + S'T \\ k(ST) &= (kS)T = S(kT) \\ (ST)T' &= S(TT') \end{aligned}$$

The *identity* operator I maps every vector in V to itself and is clearly linear; an operator T is said to be *invertible* if there exists an operator T^{-1} such that

$$TT^{-1} = T^{-1}T = I$$

Note that this commutative property does *not* hold for linear operators in general.

It can be shown that every linear operator on an n-dimensional vector space can be represented by an n-square matrix if the action of the operator is defined by the usual matrix-vector multiplication rule; conversely every such matrix determines a linear operator. In particular, the fermion matrix M determines a linear operator on some vector space.

The operator algebra outlined above translates directly to the algebra of n-square matrices, the definition of invertibility corresponding to the usual definition of invertibility for matrices.

The matrix representation of an operator is not unique, but must be specified relative to some particular basis of the vector space. It can be shown that two matrices P and Q

represent the same operator if and only if they can be transformed into each other by a similarity transform:

$$P = R^{-1}QR \quad ; \quad Q = RPR^{-1}$$

In particular, if P represents a linear operator T and there exists a transformation matrix D such that $D^{-1}PD$ is diagonal, then T is said to be diagonalisable. If such a transformation matrix does not exist then T cannot be diagonalised. It will be essential for our purposes to have a criterion for determining whether a given operator is diagonalisable. Before discussing this point further, it is convenient to introduce some more terminology.

Consider an operator T on a space V and suppose that T satisfies

$$Tv = \lambda v \tag{4.1}$$

where λ is a scalar and v is a non-zero vector in V. Then v is said to be an *eigenvector* of T belonging to the *eigenvalue* λ. Indeed the set of vectors satisfying (4.1) forms a subspace of V, which we will call the *eigenspace* associated with the eigenvalue λ. The entire set of all possible eigenvalues and eigenvectors will be termed the *eigensystem.* The same terminology goes over unchanged to the matrix representation, A, of T.

Note that if ψ is an eigenvector of A with eigenvalue λ and B is a similarity transform of A

$$B = RAR^{-1}$$

then $R\psi$ is an eigenvector of B with the *same* eigenvalue λ. All matrix representations of an operator therefore have the same set of eigenvalues—the eigenvalues of the operator they collectively represent. This set will usually be referred to as the *spectrum* of the operator.

Two useful scalar invariants may be constructed from the spectrum of an operator. We will define the *trace* of an operator T to be the sum of its eigenvalues

$$\mathrm{tr}T = \sum_i \lambda_i$$

and the *determinant* of T to be the product of eigenvalues

$$\det T = \prod_i \lambda_i$$

The trace and determinant of any matrix representation of T are defined similarly.

The *characteristic polynomial* of an n-square matrix A is defined by

$$p(A) = \det(A - \lambda I)$$

which is a polynomial of degree n in λ. The roots of the characteristic polynomial are precisely the eigenvalues of A. A root occurring with multiplicity p corresponds to an eigenvalue

of *algebraic multiplicity p*. The *geometric multiplicity* of an eigenvalue is the maximum number of linearly independent eigenvectors associated with it. An eigenvalue is *semisimple* if its algebraic and geometric multiplicities are equal; otherwise it is said to be *defective*.

Let us now introduce some rather standard matrix terminology. The transpose conjugate of a matrix A is termed its *adjoint* and denoted $A^\dagger$. The transpose conjugate (or *dual*) of a vector v is similarly denoted $v^\dagger$. The following identities apply:

$$(AB)^\dagger = B^\dagger A^\dagger \quad ; \quad (Av)^\dagger = v^\dagger A^\dagger \tag{4.2}$$

An alternative notation for vectors, which we will sometimes use, denotes a vector v by $|v\rangle$ and its dual, $v^\dagger$, by $\langle v|$. The eigenvectors of a matrix will usually be designated ψ or χ, general vectors by Ψ or α or β.

A number of special matrices will occur repeatedly in the sequel. Their definitions and a brief review of their properties are given below.

A *hermitian* matrix A is defined as a matrix satisfying

$$A = A^\dagger$$

An *antihermitian* matrix satisfies

$$A = -A^\dagger$$

A matrix U is *unitary* if

$$U^{-1} = U^\dagger$$

and a *unitary transformation* on a matrix M is defined by

$$M' = UMU^{-1} = UMU^\dagger$$

The unitary transforms thus constitute a subset of the similarity transforms.

A *normal* matrix N satisfies

$$N^\dagger N = NN^\dagger$$

Hermitian matrices possess a number of useful attributes. In particular, their eigenvalues are real, since for any eigenvector ψ

$$\psi^\dagger A\psi = \psi^\dagger(A\psi) = \lambda\psi^\dagger\psi$$

and also

$$\psi^\dagger A\psi = (\psi^\dagger A^\dagger)\psi = \lambda^*\psi^\dagger\psi$$

Hence $\lambda = \lambda^*$ and λ is real.

If, in addition, the eigenvalues are all strictly positive, the matrix is termed *positive definite*.

Hermitian matrices are a special case of normal matrices (that is, matrices that commute with their adjoint).

We are now in a position to state the fundamental results of this section—that is, to give necessary and sufficient conditions for a matrix to be diagonalisable. We begin with a useful preliminary result:

1. **Non-zero eigenvectors belonging to distinct eigenvalues are linearly independent.**

Next, a special result for normal matrices:

2. **A normal matrix can always be diagonalised by a unitary transformation. In particular, hermitian matrices can be so diagonalised.**
3. **If a matrix can be diagonalised by a unitary transformation it is necessarily normal.**

and finally two, equivalent, general criteria for diagonalisability:

4. **An n-square matrix is diagonalisable if and only if it possesses n linearly independent eigenvectors.**
5. **An n-square matrix is diagonalisable if and only if all its eigenvalues are semisimple.**

It follows from (4) that a matrix which is diagonalisable on a vector space V possesses n independent eigenvectors, ψ_i, sufficient to span V. Any vector in V can therefore be written as a linear combination of eigenvectors:

$$\Psi = \sum_{i=1}^{n} c_i \psi_i \tag{4.3}$$

18. Discretisation

In this section we discuss the discretisation of the fermion operator, defined in the Euclidean continuum (cf (2.18) by

$$\mathcal{D} = \gamma_\mu \partial_\mu + m \tag{4.4}$$

The first step in the process of placing fermions on the lattice is to discretise the field derivatives $\partial_\mu \psi$. We use the symmetric derivative (2.21); that is

$$\partial_\mu \psi_{\underline{m}} \longrightarrow \frac{\psi_{(\underline{m}+\underline{\mu})} - \psi_{(\underline{m}-\underline{\mu})}}{2a} \tag{4.5}$$

It is this use of the symmetric derivative that gives rise to the doubling problem, by effectively doubling the lattice spacing. This difficulty could be avoided by the use of a simple left or right derivative, Unfortunately, detailed analysis has shown that such a procedure would render the theory non–renormalisable. Further details are given in Sadooghi and Rothe (1996).

The lattice action is

$$\begin{aligned} S &= a^d \bar{\psi}_{\underline{m}} \left\{ \frac{\gamma_\mu(\psi_{\underline{m}+\underline{\mu}} - \psi_{\underline{m}-\underline{\mu}})}{2a} + m\psi_{\underline{m}} \right\} \\ &= \bar{\psi}_{\underline{m}} M_{\underline{m}\,\underline{n}} \psi_{\underline{n}} \end{aligned} \tag{4.6}$$

where the lattice Dirac operator in position space is defined to be

$$M_{\underline{m}\,\underline{n}} = a^d \left\{ \frac{\gamma_\mu(\delta_{\underline{n},(\underline{m}+\underline{\mu})} - \delta_{\underline{n},(\underline{m}-\underline{\mu})})}{2a} + m\delta_{\underline{m}\,\underline{n}} \right\} \tag{4.7}$$

19. The Propagator

The free lattice fermion propagator is

$$S_{\underline{m}\,\underline{n}} = M^{-1}_{\underline{m}\,\underline{n}} \tag{4.8}$$

This inversion is most conveniently carried out in momentum space, where the operator is diagonal.

A consistent definition of the fermion fields in momentum space requires some care. The general lattice Fourier transform is defined by (2.27) and (2.28)

$$\psi_{\underline{k}} = F_{\underline{k}\,\underline{n}} \psi_{\underline{n}} \qquad \psi_{\underline{n}} = F^{-1}{}_{\underline{n}\,\underline{k}} \psi_{\underline{k}} \tag{4.9}$$

The corresponding conjugate fields, on the other hand, are related by

$$\bar{\psi}_{\underline{k}} = \overline{F_{\underline{k}\,\underline{n}} \psi_{\underline{n}}} = N^4 \bar{\psi}_{\underline{n}} F^{-1}{}_{\underline{n}\,\underline{k}} \qquad \bar{\psi}_{\underline{n}} = \overline{F^{-1}{}_{\underline{n}\,\underline{k}} \psi_{\underline{k}}} = \bar{\psi}_{\underline{k}} F_{\underline{k}\,\underline{n}} \tag{4.10}$$

Note that the conjugate fields are *not* Fourier transforms of each other; the definition (2.27) gives

$$\tilde{\bar{\psi}}_{\underline{n}} = \bar{\psi}_{-\underline{k}} \qquad \tilde{\bar{\psi}}_{\underline{k}} = \bar{\psi}_{-\underline{n}} \tag{4.11}$$

Substituting for $\bar{\psi}_{\underline{m}}$ and $\psi_{\underline{m}}$ in the action (4.6) we find

$$\begin{aligned} S &= a^d \sum_{\underline{m},\underline{k},\underline{k}'} \left[\left\{ \frac{\bar{\psi}_{\underline{k}'}}{N^d} e^{i\underline{k}'.\underline{m}} \right\} \right. \\ &\qquad \left. \times \left\{ m \frac{\psi_{\underline{k}}}{N^d} e^{-i\underline{k}.\underline{n}} + \sum_\mu \frac{\gamma_\mu}{2a} \left(\frac{\psi_{\underline{k}}}{N^d} e^{-i\underline{k}.(\underline{m}+\underline{\mu})} - \frac{\psi_{\underline{k}}}{N^d} e^{-i\underline{k}.(\underline{m}-\underline{\mu})} \right) \right\} \right] \\ &= \frac{a^d}{N^{2d}} \sum_{\underline{m},\underline{k},\underline{k}'} \bar{\psi}_{\underline{k}'} \left\{ m + \sum_\mu \frac{\gamma_\mu}{2a} \left(e^{-ik_\mu} - e^{ik_\mu} \right) \right\} \psi_{\underline{k}} e^{i(\underline{k}'-\underline{k}).\underline{m}} \\ &= \frac{a^d}{N^d} \sum_{\underline{k},\underline{k}'} \bar{\psi}_{\underline{k}'} \left\{ m + \sum_\mu \frac{-i\gamma_\mu}{a} \sin ak_\mu \right\} \psi_{\underline{k}} \delta_{\underline{k}'\underline{k}} \\ &= \frac{a^d}{N^d} \sum_{\underline{k},\underline{k}'} \bar{\psi}_{\underline{k}'} \tilde{M}_{\underline{k}'\underline{k}} \psi_{\underline{k}} \end{aligned} \tag{4.12}$$

where the operator

$$\tilde{M}_{\underline{k}'\underline{k}} = \left\{ m + \sum_\mu \frac{-i\gamma_\mu}{a} \sin ak_\mu \right\} \delta_{\underline{k}'\underline{k}} \tag{4.13}$$

is diagonal.

Substituting for $\psi_{\underline{k}}$ and $\bar{\psi}_{\underline{k}'}$ yields

$$\begin{aligned} S &= \frac{a^d}{N^d} \left\{ N^d \bar{\psi}_{\underline{m}} F_{\underline{m}\,\underline{k}'} \right\} \tilde{M}_{\underline{k}'\underline{k}} \left\{ F_{\underline{k}\,\underline{n}} \bar{\psi}_{\underline{n}} \right\} \\ &= \bar{\psi}_{\underline{m}} \left\{ a^d {F^{-1}}_{\underline{m}\,\underline{k}'} \tilde{M}_{\underline{k}'\underline{k}} F_{\underline{k}\,\underline{n}} \right\} \psi_{\underline{n}} \end{aligned} \tag{4.14}$$

Comparing this with (4.6) we see that

$$M_{\underline{m}\,\underline{n}} = a^d {F^{-1}}_{\underline{m}\,\underline{k}'} M_{\underline{k}'\underline{k}} F_{\underline{k}\,\underline{n}} \tag{4.15}$$

We can write down the inverse by observing that

$$M_{\underline{m}\,\underline{n}} A_{\underline{n}\,\underline{p}} = \delta_{\underline{m}\,\underline{p}}$$

where

$$A_{\underline{n}\,\underline{p}} = {M^{-1}}_{\underline{n}\,\underline{p}} = \frac{1}{a^d} {F^{-1}}_{\underline{n}\,\underline{j}'} \tilde{M}^{-1}_{\underline{j}'\underline{j}} F_{\underline{j}\,\underline{p}} \tag{4.16}$$

or

$$
\begin{aligned}
M^{-1}{}_{\underline{m}\,\underline{n}} &= \frac{1}{a^d} F^{-1}{}_{\underline{m}\,\underline{k}'} \tilde{M}^{-1}_{\underline{k}'\,\underline{k}} F_{\underline{k}\,\underline{n}} \\
&= \frac{1}{a^d} \sum_{\underline{k}'\,\underline{k}} \left\{ \frac{1}{N^d} e^{-i\underline{k}'.\underline{m}} \right\} \left\{ m + \sum_{\mu} \frac{-i\gamma_\mu}{a} \sin ak_\mu \right\}^{-1} \delta_{\underline{k}\,\underline{k}'} \left\{ e^{i\underline{k}.\underline{n}} \right\} \\
&= \frac{1}{a^d N^d} \sum_{k_\mu = -\frac{N}{2}+1}^{k_\mu = N/2} e^{i\underline{k}.(\underline{n}-\underline{m})} \left\{ m + \sum_{\mu} \frac{-i\gamma_\mu}{a} \sin ak_\mu \right\}^{-1} \\
&= \frac{1}{a^d N^d} \sum_{k_\mu = \frac{N}{2}-1}^{k_\mu = -N/2} e^{-i\underline{k}.(\underline{n}-\underline{m})} \left\{ m + \sum_{\mu} \frac{i\gamma_\mu}{a} \sin ak_\mu \right\}^{-1}
\end{aligned}
\tag{4.17}
$$

This is the discretised free fermion propagator on a lattice of finite size with finite lattice spacing.

In the thermodynamic limit ($N \to \infty$), the momenta $q_\mu = k_\mu/a$ (cf (2.24) become continuous and the discrete sum over k_μ goes over to the corresponding integral over q_μ

$$
\frac{1}{N^4} \sum_{k_\mu = N/2-1}^{-N/2} \to \frac{1}{(2\pi)^4} \int_{-\pi/a}^{\pi/a} d^4q \tag{4.18}
$$

The position space propagator is then

$$
S_{\underline{m}\,\underline{n}} = \frac{1}{(2\pi)^4} \int_{-\pi/a}^{\pi/a} e^{-i\underline{q}.(\underline{n}-\underline{m})a} \left\{ m + \sum_{\mu} \frac{i\gamma_\mu}{a} \sin aq_\mu \right\}^{-1} d^4q \tag{4.19}
$$

20. Fermion Doubling

Let us next investigate the continuum limit of the lattice propagator.

The Dirac propagator in the continuum is given by

$$
S(\underline{x}) = \frac{1}{(2\pi)^4} \int_{-\infty}^{\infty} e^{-i\underline{q}.\underline{x}} \left\{ m + i\gamma_\mu q_\mu \right\}^{-1} d^4q \tag{4.20}
$$

The integrand tends to zero for large $\underline{q}$ so that high-momentum contributions to the integral are suppressed.

The continuum limit of (4.19) is extracted by setting $\underline{x} = (\underline{n} - \underline{m})a$ and allowing $a \to 0$.We obtain

$$
\begin{aligned}
\lim_{a\to 0} S(\underline{m}\,\underline{n}) &\longrightarrow \frac{1}{(2\pi)^4} \int_{-\infty}^{\infty} e^{-i\underline{q}.\underline{x}} \left\{ m + i\gamma_\mu q_\mu \right\}^{-1} d^4q \qquad (q_\mu \ll \frac{\pi}{a}) \\
\lim_{a\to 0} S(\underline{m}\,\underline{n}) &\longrightarrow \frac{1}{(2\pi)^4} \int_{-\infty}^{\infty} e^{-i\underline{q}.\underline{x}} \left\{ m \right\}^{-1} d^4q \qquad (q_\mu \to \frac{\pi}{a})
\end{aligned}
\tag{4.21}
$$

The continuum limit in this form exhibits the correct behaviour in the low momentum region but fails to provide the required suppression of the integrand at high momenta; in fact the second integral in (4.21) is indeterminate as it stands.

We can find an explicit form for the continuum limit by rewriting (4.19)

$$S_{\underline{m}\,\underline{n}} = \frac{1}{(2\pi)^4}\int_{-\pi/a}^{\pi/a} A\ d^3q \int_{-\pi/a}^{\pi/a} dq_0\ e^{-iq_0.(n_0-m_0)a}\left\{m + B + \sum_\mu \frac{i\gamma_\mu}{a}\sin aq_0\right\}^{-1}$$

where

$$A = e^{-i\sum_{j=1}^3 q_j.(n_j-m_j)a} \qquad B = \sum_{j=1}^{3}\frac{i\gamma_j}{a}\sin aq_j$$

The bad high and low energy limits on the q_0 integral can be removed by defining a new momentum variable

$$\tilde{q_0} = q_0 - \pi/a$$

This gives

$$\begin{aligned} S_{\underline{m}\,\underline{n}} = \frac{1}{(2\pi)^4}\int_{-\pi/a}^{\pi/a} A\ d^3q \\ \times \Bigg\{ \int_{-\pi/2a}^{\pi/2a} dq_0\ e^{-iq_0.(n_0-m_0)a}\left\{m + B + \frac{i\gamma_0}{a}\sin aq_0\right\}^{-1} \\ + (-1)^{(n_0-m_0)}\int_{-\pi/2a}^{0} d\tilde{q_0}\ e^{-i\tilde{q_0}.(n_0-m_0)a}\left\{m + B - \frac{i\gamma_0}{a}\sin a\tilde{q_0}\right\}^{-1} \\ + (-1)^{(n_0-m_0)}\int_{-2\pi/a}^{-3\pi/2a} d\tilde{q_0}\ e^{-i\tilde{q_0}.(n_0-m_0)a}\left\{m + B - \frac{i\gamma_0}{a}\sin a\tilde{q_0}\right\}^{-1}\Bigg\} \end{aligned}$$

The second integral on $\tilde{q_0}$ is equivalent to

$$(-1)^{(n_0-m_0)}\int_{0}^{\pi/2a} d\tilde{q_0}\ e^{-i\tilde{q_0}.(n_0-m_0)a}\left\{m + B - \frac{i\gamma_0}{a}\sin a\tilde{q_0}\right\}^{-1}$$

since the integrand is periodic with period 2π.

Assuming, for concreteness, that $(n_0 - m_0)$ is even, we obtain

$$\begin{aligned} S_{\underline{m}\,\underline{n}} = \frac{1}{(2\pi)^4}\int_{-\pi/a}^{\pi/a} A\ d^3q \\ \times \Bigg\{ \int_{-\pi/2a}^{\pi/2a} dq_0\ e^{-iq_0.(n_0-m_0)a}\left\{m + B + \frac{i\gamma_0}{a}\sin aq_0\right\}^{-1} \\ + \int_{-\pi/2a}^{\pi/2a} d\tilde{q_0}\ e^{-i\tilde{q_0}.(n_0-m_0)a}\left\{m + B + \frac{i\tilde{\gamma_0}}{a}\sin a\tilde{q_0}\right\}^{-1}\Bigg\} \end{aligned}$$

where

$$\tilde{\gamma_0} = -\gamma_0$$

Note that the set $\{\gamma_\mu\}$ satisfies (2.17) and constitutes an acceptable representation of the γ_μ in (4.4). We can in fact change the sign of any or all the γ_μ and still get a representation since the only non-zero terms in (2.17) are of the form $\gamma_\mu\gamma_\mu$.

The zeroth component of (4.19) has been split into the zeroth components of *two* propagators associated with the two independent momentum variables q_0 and $\tilde{q_0}$. Each momentum variable is linked to a different representation of the gamma matrices.

Repeating this procedure with the remaining components leads to more doublings, giving

$$S_{\underline{m}\,\underline{n}} = \sum_R \frac{1}{(2\pi)^4} \int_{-\pi/2a}^{\pi/2a} e^{-i\underline{q}^R.(\underline{n}-\underline{m})a} \left\{ m + \sum_\mu \frac{i\gamma_\mu{}^R}{a} \sin aq^R{}_\mu \right\}^{-1} d^4q^R \tag{4.22}$$

The index R labels the 2^d independent momenta $\underline{q}^R$ and the 2^d corresponding gamma representations

$$\gamma^R = \{\pm\gamma_0, \pm\gamma_1, \pm\gamma_2, \pm\gamma_3\}$$

Each term in (4.22) has the continuum limit

$$\begin{aligned} &\lim_{a\to 0} S^R(\underline{m}\,\underline{n}) \longrightarrow \frac{1}{(2\pi)^4} \int_{-\infty}^{\infty} e^{-i\underline{q}^R.\underline{x}} \left\{ m + i\gamma_\mu{}^R q^R{}_\mu \right\}^{-1} d^4q^R \qquad (q^R{}_\mu \ll \frac{\pi}{2a}) \\ &\lim_{a\to 0} S^R(\underline{m}\,\underline{n}) \longrightarrow 0 \qquad\qquad (q^R{}_\mu \to \frac{\pi}{2a}) \end{aligned} \tag{4.23}$$

This limit has the correct behaviour for both high and low momenta.

We conclude that the correct continuum limit of (4.19) is not one but 2^d independent continuum propagators.

21. Wilson Fermions

This degeneracy in the fermion spectrum can be removed by adding an extra term to (4.13)

$$\tilde{M}'_{\underline{k}'\underline{k}} = \left\{ m + \sum_\mu \frac{-i\gamma_\mu}{a} \sin ak_\mu + \sum_\mu \frac{1}{a}(1 - \cos ak_\mu) \right\} \delta_{\underline{k}'\underline{k}} \tag{4.24}$$

The lattice propagator (4.19) becomes

$$S'(\underline{m}\,\underline{n}) = \frac{1}{(2\pi)^4} \int_{-\pi/a}^{\pi/a} e^{-i\underline{q}.(\underline{n}-\underline{m})} \left\{ m + \sum_\mu \frac{i\gamma_\mu}{a} \sin aq_\mu + \sum_\mu \frac{1}{a}(1 - \cos aq_\mu) \right\}^{-1} d^4q \tag{4.25}$$

The new term, which acts like a momentum-dependent mass, vanishes for small $\underline{q}$ but provides the required suppression of the integrand in the high momentum limit. Note also that the Wilson term vanishes in the limit of zero lattice spacing.

We can use (4.15) to find the modified Dirac operator in coordinate space

$$\begin{aligned} M'_{\underline{m}\,\underline{n}} &= a^d \sum_{\underline{k},\underline{k}'} \left\{ \frac{1}{N^d} e^{-i\underline{k}'.\underline{m}/N} \right\} \left\{ m + \sum_\mu \frac{-i\gamma_\mu}{a} \sin ak_\mu + \sum_\mu \frac{1}{a}(1-\cos ak_\mu) \right\} \delta_{\underline{k}'\underline{k}} \left\{ e^{i\underline{k}.\underline{n}/N} \right\} \\ &= \frac{a^d}{N^d} \sum_{\underline{k}} \left\{ e^{i\underline{k}.(\underline{n}-\underline{m}/N} \right\} \left\{ \left(m + \frac{d}{a} \right) \sum_\mu \left\{ \frac{\gamma_\mu}{2a} \left(e^{-ik_\mu} - e^{ik_\mu} \right) - \frac{1}{2a} \left(e^{ik_\mu} + e^{-ik_\mu} \right) \right\} \right\} \\ &= a^d \left(m + \frac{d}{a} \right) \delta_{\underline{m}\,\underline{n}} + a^d \left\{ \frac{\gamma_\mu}{2a} \left(\delta_{\underline{n},(\underline{m}+\underline{\mu})} - \delta_{\underline{n},(\underline{m}-\underline{\mu})} \right) - \frac{1}{2a} \left(\delta_{\underline{n},(\underline{m}-\underline{\mu})} + \delta_{\underline{n},(\underline{m}+\underline{\mu})} \right) \right\} \\ &= \left(ma^d + da^{d-1} \right) \delta_{\underline{m}\,\underline{n}} + \frac{a^{d-1}}{2} \left\{ (\gamma_\mu - 1)\delta_{\underline{n},(\underline{m}+\underline{\mu})} - (\gamma_\mu + 1)\delta_{\underline{n},(\underline{m}-\underline{\mu})} \right\} \end{aligned} \tag{4.26}$$

or

$$M'_{\underline{m}\,\underline{n}} = \left(ma^d + da^{d-1} \right) \delta_{\underline{m}\,\underline{n}} - \frac{a^{d-1}}{2} \left\{ (1-\gamma_\mu)\delta_{\underline{n},(\underline{m}+\underline{\mu})} + (1+\gamma_\mu)\delta_{\underline{n},(\underline{m}-\underline{\mu})} \right\} \tag{4.27}$$

This can be cast into a more convenient form by redefining the fermion fields.

Our modified lattice action is

$$\begin{aligned} S' &= \bar{\psi}_{\underline{m}} M'_{\underline{m}\,\underline{n}} \psi_{\underline{n}} \\ &= \bar{\psi}_{\underline{m}} \left\{ (ma^d + da^{d-1})\psi_{\underline{m}} - \frac{a^{d-1}}{2} \left\{ (1-\gamma_\mu)\psi_{\underline{m}+\underline{\mu}} + (1+\gamma_\mu)\psi_{\underline{m}-\underline{\mu}} \right\} \right\} \end{aligned} \tag{4.28}$$

We define a rescaled fermion field by

$$\begin{aligned} \bar{\psi}'_{\underline{m}} &= (ma^d + da^{d-1})^{1/2} \bar{\psi}_{\underline{m}} \\ \psi'_{\underline{m}} &= (ma^d + da^{d-1})^{1/2} \psi_{\underline{m}} \end{aligned} \tag{4.29}$$

The action is now

$$\begin{aligned} S' &= \bar{\psi}'_{\underline{m}} \left\{ \psi'_{\underline{m}} - \frac{1}{2(ma+d)} \left\{ (1-\gamma_\mu)\psi'_{\underline{m}+\underline{\mu}} + (1+\gamma_\mu)\psi'_{\underline{m}-\underline{\mu}} \right\} \right\} \\ &= \bar{\psi}'_{\underline{m}} M''_{\underline{m}\,\underline{n}} \psi'_{\underline{n}} \end{aligned} \tag{4.30}$$

where

$$M''_{\underline{m}\,\underline{n}} = \delta_{\underline{m}\,\underline{n}} - \kappa \left\{ (1-\gamma_\mu)\delta_{\underline{n},(\underline{m}+\underline{\mu})} + (1+\gamma_\mu)\delta_{\underline{n},(\underline{m}-\underline{\mu})} \right\} \tag{4.31}$$

and

$$\kappa = \frac{1}{2(ma+d)} \to \frac{1}{2d} \qquad \text{as} \qquad a \to 0 \tag{4.32}$$

5. The Schwinger Model

Everything should be made as simple as possible but not simpler
– A. Einstein

Having introduced the lattice and discussed the lattice implementation of fermionic and gauge fields, we turn in this Chapter to the main object of interest in this thesis—the Schwinger model. The reasons for the widespread interest in this model are discussed in the first section.The Schwinger model in the continuum is then introduced and its lattice equivalent developed. Previous work on the phase diagram of the model is briefly reviewed.

22. Chiral Symmetry And Massless Physics

In the preceding chapters, we developed the lattice formulation of quantum field theory and implemented fermion fields and gauge fields on the lattice. Next, we turn our attention to an interacting theory; QED_2, which describes the interaction of electrons and photons in two dimensions.

This investigation of QED_2 is motivated by the striking resemblances which it bears to QCD in four dimensions. Before introducing lattice QED_2, therefore, let us consider some of the relevant features of QCD. The issues discussed here are also reviewed by Peskin and Schroeder (1995) and Aoki (1989).

Consider QCD restricted to the up and down quarks. These are the lightest of the quarks and may be approximated as massless. If this approximation is made the QCD action is invariant under chiral transformations; this symmetry of the action should lead to an associated (approximate) conservation law of the strong interaction. There is however no obvious candidate for such a law. It was suggested by Nambu and Jona–Lasinio in 1961 that chiral symmetry might be spontaneously broken in the strong interactions.

A consequence of such a spontaneously broken symmetry is the appearance of a massless particle (Goldstone, 1961); the breaking of the symmetry is signalled by a non–zero expectation value for the *chiral condensate*:

$$\langle \bar{\psi}\psi \rangle \neq 0$$

The spontaneous breakdown of chiral symmetry in QCD actually corresponds to the breakdown of four continuous symmetries; therefore one would expect four Goldstone bosons. In fact, since the up and down quarks are not truly massless, these bosons should have a small

mass. The observed masses of the three pion states are consistent with those expected for the Goldstone bosons but there is no obvious candidate for the fourth boson. While several theoretical suggestions have been advanced to account for this lack, the issue remains unresolved and indeed the spontaneous breakdown of chiral symmetry itself has not been conclusively established in the case of QCD.

These questions are non–perturbative in nature and are the appropriate domain of lattice QCD. A fundamental problem arises, however, in the application to massless physics of lattice theory with Wilson fermions. The Wilson term itself breaks chiral symmetry even when the fermion mass is zero. Although this term goes to zero in the continuum limit, it is necessary to tune the mass parameter κ to ensure that this limit actually corresponds to zero "true mass" physics; the dependence of κ on the true mass is not known *a priori.*

The problem then, is to determine the set of critical points in the parameter space of the theory which give rise to zero mass physics, the "line of massless physics". The existence of such a line for all values of the coupling has not been established.

Quantum electrodynamics in two dimensions possesses many of the properties expected in QCD and has been the object of intense study since it provides a simpler environment in which to gain an insight into QCD. It is to this model that we turn in the next section.

23. Continuum Theory

The Schwinger model, describing the interaction of electrons and photons in two dimensions was first introduced by Schwinger in 1962. It has served as an invaluable laboratory for quantum field theorists ever since.

The action for the single flavour Schwinger model with massive fermions is given in the continuum by

$$S(\bar{\psi}, \psi, A_\mu) = \int d^2x \left(\frac{1}{4} {F_{\mu\nu}}^2(x) - \bar{\psi}(x) \left(m + \gamma^\mu \partial_\mu + ie\gamma_\mu A^\mu \right) \psi(x) \right)$$

This model is exactly solvable in the case $m = 0$ (see, for example, Zinn–Justin (1993) for a discussion of Schwinger's original work).

The massless Schwinger model bears some remarkable resemblances to QCD in four dimensions. Charges are confined, a property also expected in QCD. The model also exhibits *charge screening*, that is to say, the absence of long-range forces. The mass spectrum consists of neutral massive non–interacting bosons.

Perhaps most importantly from the present point of view, the massless Schwinger model is known to exhibit spontaneous breakdown of chiral symmetry although there is no associated Goldstone boson in two dimensions.

The model has not been exactly solved for fermions with non–zero mass; it is expected, however, that the main features of the massless theory are preserved, at least for fermions of small mass.

24. The Lattice Schwinger Model

Let us now implement the Schwinger model on the lattice. The simplest approach, as in the continuum case, is to impose the requirement of local gauge invariance on the fermion field. The free fermion action is given by (4.30)

$$S_F = \bar{\psi}_{\underline{m}} \left\{ \psi_{\underline{m}} - \kappa \left\{ (1-\gamma_\mu)\psi_{\underline{m}+\underline{\mu}} + (1+\gamma_\mu)\psi_{\underline{m}-\underline{\mu}} \right\} \right\} \tag{5.1}$$

This action exhibits a global invariance under a constant phase shift of the fields:

$$\psi_{\underline{n}} \longrightarrow e^{i\Lambda}\psi_{\underline{n}} \qquad ; \qquad \bar{\psi}_{\underline{n}} \longrightarrow \bar{\psi}_{\underline{n}} e^{-i\Lambda}$$

The pure gauge action is, from (3.1)

$$S_G = \frac{1}{g^2} \sum_p \sum_{\mu,\nu,\nu>\mu} \mathrm{Re}\,(1-U_p) = \frac{1}{2g^2} \sum_p \sum_{\mu,\nu} (1-\cos a^2\phi_p)$$

As discussed in Section (11), this action possesses a stronger, local invariance under the transformation

$$\begin{aligned} U_\mu(\underline{n}) &\longrightarrow e^{if(\underline{n})} U_\mu(\underline{n}) e^{-if(\underline{n}+\underline{\mu})} \\ U^\dagger{}_\mu(\underline{n}) &\longrightarrow e^{if(\underline{n}+\underline{\mu})} U^\dagger{}_\mu(\underline{n}) e^{-if(\underline{n})} \end{aligned} \tag{5.2}$$

The full QED action is determined by promoting the global invariance of the fermion action to a local gauge invariance; that is, the action should be invariant under the set of transformations

$$\begin{aligned} \psi_{\underline{n}} &\longrightarrow e^{if(\underline{n})}\psi_{\underline{n}} \\ \bar{\psi}_{\underline{n}} &\longrightarrow \bar{\psi}_{\underline{n}} e^{-if(\underline{n})} \\ U_\mu(\underline{n}) &\longrightarrow e^{if(\underline{n})} U_\mu(\underline{n}) e^{-if(\underline{n}+\underline{\mu})} \\ U^\dagger{}_\mu(\underline{n}) &\longrightarrow e^{if(\underline{n}+\underline{\mu})} U^\dagger{}_\mu(\underline{n}) e^{-if(\underline{n})} \end{aligned}$$

The pure gauge action and the mass term in the fermion action automatically satisfy local gauge invariance, but the fermion derivative term requires modification. We require, in fact, the lattice equivalent of the continuum gauge-covariant derivative. The necessary modification is easily seen to be

$$\begin{aligned} \delta_{\underline{n}(\underline{m}+\underline{\mu})} &\longrightarrow U_{\underline{\mu}}(\underline{m})\, \delta_{\underline{n}(\underline{m}+\underline{\mu})} \\ \delta_{\underline{n}(\underline{m}-\underline{\mu})} &\longrightarrow U^\dagger{}_{\underline{\nu}}(\underline{m}-\underline{\mu})\, \delta_{\underline{n}(\underline{m}-\underline{\mu})} \end{aligned}$$

The gauge invariant QED action is then given by

$$S_{QED} = S_{FG} + S_G \tag{5.3}$$

where

$$S_{FG} = \bar{\psi}_{\underline{m}} \left\{ \delta_{\underline{nm}} - \kappa \left\{ (1-\gamma_\mu)\, U_{\underline{\mu}}(\underline{m})\, \delta_{\underline{n}(\underline{m}+\underline{\mu})} + (1+\gamma_\mu)\, U^\dagger{}_{\underline{\mu}}(\underline{m}-\underline{\mu})\, \delta_{\underline{n}(\underline{m}-\underline{\mu})} \right\} \right\} \psi_{\underline{n}}$$

and

$$S_G = \frac{1}{2g^2} \sum_p \sum_{\mu,\nu} \mathrm{Re}\,(1 - U_p)$$

25. Current Status Of The Phase Diagram

The phase diagram of the lattice Schwinger model has been the subject of considerable interest in recent years, since the general belief is that the phase structure of the Schwinger model is likely to resemble that of QCD.

Although the phase diagram has not been fully determined, some partial results have been obtained.

The Schwinger action contains two parameters, the coupling parameter g and the mass parameter m, conventionally represented by the inverse coupling squared β and the hopping parameter κ respectively.

Attention has been focused principally on the location of the chiral phase transition; the line representing massless physics in the (β, κ) plane.

It is known (Gausterer and Lang 1995) that there exists a critical point in the strong coupling limit ($\beta \to 0$) as well as at $(\infty, \frac{1}{4})$. The question is whether there is a critical line corresponding to finite values of β and κ connecting these points.

It was argued, on the basis of numerical evidence, that the critical line did not in fact exist (Gausterer, Lang and Salmhofer, 1992); however the same group have since found evidence for critical points at finite values of β. (Gausterer and Lang, 1994, Hip, Lang and Teppner, 1998). These results were based on the finite size scaling of Lee–Yang zeroes and chiral susceptibility and suggest a critical exponent $\nu \approx 1$.

A second group (Azcoiti et al, 1996) have used similar techniques on larger lattices. They have located the critical line in roughly the same region, but find a critical exponent $\nu \approx 2/3$.

The present situation then is that there is general consensus as to the existence and approximate location of the critical line, but uncertainty as to the nature of the transition.

It should be borne in mind, however that both of the recent major studies have been based on numerical investigations combined with finite size scaling.

We propose to adopt an alternative, analytical approach in this work.

6. The Fermion Matrix

Gentlemen: there's lots of room left in Hilbert space!
– S. Maclane

In this Chapter we begin our analysis of the phase diagram of the Schwinger model by considering the free fermion field. It is shown that the fermion matrix, although not hermitian, is a normal matrix; therefore standard perturbation theory techniques may be applied to it. The eigenvalues and eigenvectors of the free operator are obtained and are shown to exhibit a high degree of degeneracy. It will therefore be necessary to apply the perturbative techniques appropriate to a degenerate operator when the full Schwinger model is considered. It is shown that analogous results hold in the four–dimensional case; consequently the same perturbative technique can, in principle, be applied to four–dimensional QED. The zeroes of the free fermion partition function are calculated explicitly and the phase structure of the free fermion field analysed. It is around this solution that the Schwinger model partition function will be expanded.

26. Structure of the Fermion Operator

The fermion operator on the lattice was obtained in the form of a matrix in Section (21). In order for the operator to be fully determined it is also necessary to specify the vector space on which it acts. In this section we will examine the structure of the fermion matrix more closely and define an appropriate vector space.

The fermion matrix is given by

$$M_{\underline{nm}} = \delta_{\underline{nm}} - \kappa \left\{ (1-\gamma_\mu)\delta_{\underline{n},(\underline{m}+\underline{\mu})} + (1+\gamma_\mu)\delta_{\underline{n},(\underline{m}-\underline{\mu})} \right\} \tag{6.1}$$

We will assume for concreteness that the lattice is two dimensional—the argument is identical for the four dimensional case. The fermion matrix then has $\underline{m} = N^2$ entries in each row, each entry consisting of a sub-matrix of dimension 2, which we will call a *spin block*. The overall dimension of the matrix is therefore $2N^2$. Each row of the matrix contains a spin block for each lattice site and similarly for each column. A general entry M_{ij} in the matrix therefore contains a spin block linking lattice site i with lattice site j.

The fermion matrix thus has a rather complex structure, containing a (constant) mass term and derivative term which act on the spacetime vector space (indexed by the spatial indices $\underline{m}, \underline{n}$) as well as a spin-related term which acts on the inner 'spin space' associated with each lattice site. This spin space is indexed by the gamma matrix indices, which have been suppressed in (6.1).

Let us now consider the vector space V on which the fermion operator acts. This is a product of the N^2 dimensional space acted on by the derivative operator and the two dimensional space acted on by the spin operator. That is to say, a vector in V will have the form ωv, ω being a two component spin vector and v an N^2 component spacetime, or *site space*, vector. It is to be understood that ω is acted on by the spin operators only, while v is acted on by the mass and derivative operators.The order in which ω and v are written is immaterial, thus

$$|\omega v\rangle = |v\omega\rangle$$

and

$$\langle \omega v|\omega' v'\rangle = \langle \omega|\omega'\rangle\langle v|v'\rangle$$

A set of N^2 independent vectors is required to span the site space; a convenient set is the set of *plane waves*

$$\psi_{\underline{n}}(\underline{k}) = e^{i\underline{k}.\underline{n}}$$

each independent wave being characterised by a different value of the parameter $\underline{k}$. In the physical continuum theory $\underline{k}$ corresponds, of course, to the momentum and we shall continue to refer to it as such in the lattice context.

Two independent two-component vectors are required to span the spin space associated with each independent plane wave; we shall write these as $U(\alpha, \underline{k}), \alpha = 0, 1$, each *basis* now being parameterised by $\underline{k}$.

A basis $\{e\}$ for V is then given by the set of $2N^2$ independent vectors of the form

$$e_{\underline{n}}(\alpha, \underline{k}) = U(\alpha, \underline{k})\ \psi_{\underline{n}}(\underline{k})$$

In the general case of a d dimensional lattice, dN^d independent vectors are required, with the spin space being spanned by d independent d-component vectors and $\underline{k}$ running over N^d values.

Having defined our vector space and constructed a basis for it, let us next examine the structure of the fermion matrix more closely.

The fermion action is local in nature, the derivative term linking neighbouring sites only. As a consequence, most spin blocks in the matrix are zero. Furthermore, for realistic lattices, the dimension of the matrix will be large. For example a four dimensional lattice with eight sites per side will be represented by a matrix of dimension $4 \times 8^4 = 16384$. From a computational point of view, the fermion matrix is a member of the class of *large sparse* matrices.

The free fermion matrix is unfortunately not hermitian and it will be convenient at this point to define some related operators with nicer symmetry properties. Let us write

$$M = 1 - kA$$

where

$$A = (1 - \gamma_\mu)\delta_{\underline{n},(\underline{m}+\underline{\mu})} + (1 + \gamma_\mu)\delta_{\underline{n},(\underline{m}-\underline{\mu})} \tag{6.2}$$

Now the gamma matrices in the representation exhibited in Section (4) are hermitian, thus

$$\gamma_\mu = {\gamma_\mu}^\dagger$$

Let us define an additional matrix, γ_5, by

$$\gamma_5 = \prod_\mu \gamma_\mu \tag{6.3}$$

The following properties follow immediately from (6.3) and the definition of the gamma matrices (2.17).

$$\begin{aligned}
{\gamma_\mu}^2 &= 1 \\
\gamma_\mu\gamma_\nu &= -\gamma_\nu\gamma_\mu \\
{\gamma_5}^2 &= 1 \\
\gamma_5 &= -{\gamma_5}^\dagger \\
\gamma_5\gamma_\mu &= -\gamma_\mu\gamma_5 \\
\gamma_5(1 + \gamma_\mu) &= (1 - \gamma_\mu)\gamma_5 \\
\gamma_5(1 - \gamma_\mu) &= (1 + \gamma_\mu)\gamma_5
\end{aligned} \tag{6.4}$$

Next, note that

$${\delta_{\underline{n}(\underline{m}+\underline{\mu})}}^\dagger = \delta_{\underline{m}(\underline{n}+\underline{\mu})} = \delta_{\underline{n}(\underline{m}-\underline{\mu})}$$

and similarly

$${\delta_{\underline{n}(\underline{m}-\underline{\mu})}}^\dagger = \delta_{\underline{n}(\underline{m}+\underline{\mu})}$$

In addition, the spin and derivative operators act on different objects—the spin operator on the d component spin vector and the derivative operator on the N^d component site space vector. The order in which the operators are written is therefore immaterial:

$$\begin{aligned}
(1 - \gamma_\mu)\delta_{\underline{n},(\underline{m}+\underline{\mu})} &= \delta_{\underline{n},(\underline{m}+\underline{\mu})}(1 - \gamma_\mu) \\
(1 + \gamma_\mu)\delta_{\underline{n},(\underline{m}-\underline{\mu})} &= \delta_{\underline{n},(\underline{m}-\underline{\mu})}(1 + \gamma_\mu)
\end{aligned}$$

The adjoint of (6.2) can therefore be written

$${A_{\underline{n}\underline{m}}}^\dagger = (1 - \gamma_\mu)\delta_{\underline{n},(\underline{m}-\underline{\mu})} + (1 + \gamma_\mu)\delta_{\underline{n},(\underline{m}+\underline{\mu})}$$

and using the last two identities in (6.4) gives

$$\begin{aligned}
A^\dagger &= \gamma_5 A \gamma_5 \\
A &= \gamma_5 A^\dagger \gamma_5
\end{aligned}$$

Therefore A, and hence M, is not hermitian. The operator $\gamma_5 A$ *is* hermitian, however, since

$$\gamma_5 A = (\gamma_5)^2 A^\dagger \gamma_5 = A^\dagger \gamma_5 = (\gamma_5 A)^\dagger$$

It follows that $\gamma_5 M = \gamma_5(1 - kA)$ is hermitian, with real eigenvalues.Moreover

$$M^\dagger M = (\gamma_5 M \gamma_5) M = (\gamma_5 M)^2$$

If λ is a (real) eigenvalue of $\gamma_5 M$ then λ^2 is an eigenvalue of $M^\dagger M$, which is therefore positive definite.

Although A is not hermitian, it does belong to the more general class of normal matrices—that is, it commutes with its adjoint. We will show this by direct calculation.

Let us write

$$A = P_{\underline{nm}} + Q_{\underline{nm}} \quad ; \quad A^\dagger = R_{\underline{mp}} + S_{\underline{mp}}$$

where

$$P_{\underline{nm}} = \sum_\mu (1 - \gamma_\mu)\delta_{\underline{n}(\underline{m}+\underline{\mu})}$$

$$Q_{\underline{nm}} = \sum_\mu (1 + \gamma_\mu)\delta_{\underline{n}(\underline{m}-\underline{\mu})}$$

$$R_{\underline{mp}} = \sum_\nu (1 - \gamma_\nu)\delta_{\underline{m}(\underline{p}-\underline{\nu})}$$

$$S_{\underline{mp}} = \sum_\nu (1 + \gamma_\nu)\delta_{\underline{m}(\underline{p}+\underline{\nu})}$$

We then have

$$[A\,,\, A^\dagger] = C_1 + C_2 + C_3 + C_4$$

where

$$\begin{aligned} C_1 &= [P\,,\, R] \\ C_2 &= [P\,,\, S] \\ C_3 &= [Q\,,\, R] \\ C_4 &= [Q\,,\, S] \end{aligned} \tag{6.5}$$

Next note that

$$\begin{aligned} \delta_{\underline{n}(\underline{m}+\underline{\mu})}\delta_{\underline{m}(\underline{p}-\underline{\nu})} &= \delta_{\underline{n}(\underline{p}+\underline{\mu}-\underline{\nu})} \\ \delta_{\underline{n}(\underline{m}+\underline{\mu})}\delta_{\underline{m}(\underline{p}+\underline{\nu})} &= \delta_{\underline{n}(\underline{p}+\underline{\mu}+\underline{\nu})} \\ \delta_{\underline{n}(\underline{m}-\underline{\mu})}\delta_{\underline{m}(\underline{p}+\underline{\nu})} &= \delta_{\underline{n}(\underline{p}-\underline{\mu}+\underline{\nu})} \\ \delta_{\underline{n}(\underline{m}-\underline{\mu})}\delta_{\underline{m}(\underline{p}-\underline{\nu})} &= \delta_{\underline{n}(\underline{p}-\underline{\mu}-\underline{\nu})} \end{aligned}$$

and also

$$\begin{aligned} (1 - \gamma_\mu)(1 - \gamma_\nu) - (1 - \gamma_\nu)(1 - \gamma_\mu) &= [\gamma_\mu\,,\, \gamma_\nu] \\ (1 - \gamma_\mu)(1 + \gamma_\nu) - (1 + \gamma_\nu)(1 - \gamma_\mu) &= [\gamma_\nu\,,\, \gamma_\mu] \\ (1 + \gamma_\mu)(1 - \gamma_\nu) - (1 - \gamma_\nu)(1 + \gamma_\mu) &= [\gamma_\nu\,,\, \gamma_\mu] \\ (1 + \gamma_\mu)(1 + \gamma_\nu) - (1 + \gamma_\nu)(1 + \gamma_\mu) &= [\gamma_\mu\,,\, \gamma_\nu] \end{aligned}$$

The commutators (6.5) may therefore be written

$$\begin{aligned}
C_1 &= \sum_{\mu\nu} [\gamma_\mu\,,\,\gamma_\nu]\,\delta_{\underline{n}(\underline{p}+\underline{\mu}-\underline{\nu})} \\
&= \frac{1}{2}\sum_{\mu\nu}\Big([\gamma_\mu\,,\,\gamma_\nu]\,\delta_{\underline{n}(\underline{p}+\underline{\mu}-\underline{\nu})} + [\gamma_\nu\,,\,\gamma_\mu]\delta_{\underline{n}(\underline{p}+\underline{\nu}-\underline{\mu})}\Big) \\
C_2 &= \sum_{\mu\nu} [\gamma_\nu\,,\,\gamma_\mu]\,\delta_{\underline{n}(\underline{p}+\underline{\mu}+\underline{\nu})} \\
&= \frac{1}{2}\sum_{\mu\nu}\Big([\gamma_\nu\,,\,\gamma_\mu]\,\delta_{\underline{n}(\underline{p}+\underline{\mu}+\underline{\nu})} + [\gamma_\mu\,,\,\gamma_\nu]\delta_{\underline{n}(\underline{p}+\underline{\nu}+\underline{\mu})}\Big) = 0 \\
C_3 &= \sum_{\mu\nu} [\gamma_\nu\,,\,\gamma_\mu]\,\delta_{\underline{n}(\underline{p}-\underline{\mu}-\underline{\nu})} \\
&= \frac{1}{2}\sum_{\mu\nu}\Big([\gamma_\nu\,,\,\gamma_\mu]\,\delta_{\underline{n}(\underline{p}+\underline{\mu}-\underline{\nu})} + [\gamma_\mu\,,\,\gamma_\nu]\delta_{\underline{n}(\underline{p}-\underline{\nu}-\underline{\mu})}\Big) = 0 \\
C_4 &= \sum_{\mu\nu} [\gamma_\mu\,,\,\gamma_\nu]\,\delta_{\underline{n}(\underline{p}-\underline{\mu}+\underline{\nu})} \\
&= \frac{1}{2}\sum_{\mu\nu}\Big([\gamma_\mu\,,\,\gamma_\nu]\,\delta_{\underline{n}(\underline{p}-\underline{\mu}+\underline{\nu})} + [\gamma_\nu\,,\,\gamma_\mu]\delta_{\underline{n}(\underline{p}-\underline{\nu}+\underline{\mu})}\Big)
\end{aligned}$$

Finally, we have

$$C_1 + C_4 = 0$$

so that

$$[A, A^\dagger] = 0$$

and A is indeed normal.

It follows that M is also a normal matrix and commutes with $M^\dagger$. It can therefore be diagonalised by a unitary transformation. Furthermore all its eigenvalues must be semisimple, with their algebraic and geometric multiplicities being equal.

A further consequence of the normality of M is that γ_5 and $M^\dagger M$ commute, since

$$\begin{aligned}
\gamma_5 M^\dagger M - M^\dagger M\gamma_5 &= \gamma_5 M^\dagger M - (\gamma_5 M\gamma_5)M\gamma_5 \\
&= \gamma_5 M^\dagger M - \gamma_5 M(\gamma_5 M\gamma_5) \\
&= \gamma_5(M^\dagger M - MM^\dagger) = 0
\end{aligned}$$

It will be convenient to summarise our conclusions about the structure of the fermion operator at this point.

1. The fermion matrix is a large sparse matrix of dimension dN^d, It represents a linear operator acting on a dN^d dimensional vector space which is the product of a d dimensional spin space and an N^d dimensional site space.

2. The fermion matrix is not hermitian, but is normal.
3. Two related hermitian operators may be defined; the operators $\gamma_5 M$ and $M^\dagger M$—the latter is, in addition, positive definite.
4. As a consequence of the normality of M, it is guaranteed to be diagonalisable.
5. The eigenvalues of M are semisimple.
6. The following commutation relations apply

$$[M^\dagger, M] = 0 \quad ; \quad [\gamma_5, M^\dagger M] = 0$$

27. The Eigensystem

In this section we find explicit expressions for the eigenvalues and eigenvectors of the operator $M_{\underline{mn}}$, its adjoint $M^\dagger_{\underline{mn}}$ and some related operators.
The matrix M can be written

$$M = 1 - \kappa A$$

where 1 is the identity matrix $\delta_{\underline{mn}}$, κ is the hopping parameter and A is given by

$$A_{\underline{mn}} = \sum_\mu \left\{ (1 - \gamma_\mu)\, \delta_{\underline{m},\underline{n}+\underline{\mu}} + (1 + \gamma_\mu)\, \delta_{\underline{m},\underline{n}-\underline{\mu}} \right\}$$

If $\psi_{\underline{n}}(\alpha, \underline{k})$ is an eigenvector of $A_{\underline{mn}}$ with eigenvalue $a(\alpha, \underline{k})$, it is also an eigenvector of $M_{\underline{mn}}$, with eigenvalue $\lambda_{\underline{n}} = 1 - \kappa\, a(\alpha, \underline{k})$.
Consider now a vector of the form

$$\psi_{\underline{n}}(\alpha, \underline{k}) = U(\alpha, \underline{k}) e^{i\underline{k}.\underline{n}}$$

belonging to the space acted on by $A_{\underline{mn}}$.
Here $U(\alpha, \underline{k})$ is a d-component basis vector of the inner spin space and $e^{i\underline{k}.\underline{n}}$ is a plane wave vector with $\underline{n} = N^d$ components. There are thus $d\underline{k} = dN^d$ independent vectors $\psi_{\underline{n}}(\alpha, \underline{k})$ which span the space of $A_{\underline{mn}}$.
The eigenvalues $a(\alpha, \underline{k})$ associated with these eigenvectors may be determined from the relation

$$A_{\underline{mn}} \psi_{\underline{n}}(\alpha, \underline{k}) = a(\alpha, \underline{k})\, \psi_{\underline{m}}(\alpha, \underline{k}) \tag{6.6}$$

which gives

$$\begin{aligned}
&\sum_{\mu} \left\{(1-\gamma_\mu)\,\delta_{\underline{m},\underline{n}+\underline{\mu}} + (1+\gamma_\mu)\,\delta_{\underline{m},\underline{n}-\underline{\mu}}\right\} U(\alpha,\underline{k}) e^{i\underline{k}.\underline{n}} \\
&= \sum_{\mu} \left\{(1-\gamma_\mu)\, e^{i\underline{k}.(\underline{m}-\underline{\mu})} + (1+\gamma_\mu)\, e^{i\underline{k}.(\underline{m}+\underline{\mu})}\right\} U(\alpha,\underline{k}) \\
&= \sum_{\mu} \left\{(e^{ik_\mu} + e^{-ik_\mu}) + \gamma_\mu (e^{ik_\mu} - e^{-ik_\mu})\right\} U(\alpha,\underline{k}) e^{i\underline{k}.\underline{m}} \\
&= \sum_{\mu} (2\cos k_\mu + 2i\gamma_\mu \sin k_\mu)\, U(\alpha,\underline{k}) e^{i\underline{k}.\underline{m}} \\
&= a(\alpha,\underline{k})\, \psi_{\underline{m}}(\alpha,\underline{k})
\end{aligned}$$

We thus obtain a homogeneous system of d equations:

$$KU(\alpha,\underline{k}) = 0 \tag{6.7}$$

where

$$K = \sum_{\mu} (\cos k_\mu) - \frac{a(\alpha,\underline{k})}{2} + \sum_{\mu} (i\gamma_\mu \sin k_\mu) \tag{6.8}$$

The required eigenvalues $a(\alpha,\underline{k})$ can be determined by observing that the system (6.7) has a non–trivial solution if and only if $\det K = 0$. This implies that $\det KK' = \det K \det K' = 0$ for any arbitrary matrix K'. Let us define

$$K' = -\sum_{\nu} (\cos k_\nu) + \frac{a(\alpha,\underline{k})}{2} + \sum_{\nu} (i\gamma_\nu \sin k_\nu)$$

This gives

$$KK' = -\sum_{\mu} (\sin^2 k_\mu) - \left(\sum_{\mu} (\cos k_\mu) - \frac{a(\alpha,\underline{k})}{2}\right)^2$$

which is diagonal, with determinant zero provided:

$$\sum_{\mu} (\sin^2 k_\mu) + \left(\sum_{\mu} (\cos k_\mu) - \frac{a(\alpha,\underline{k})}{2}\right)^2 = 0$$

so that

$$a(\alpha,\underline{k}) = 2\sum_{\mu} (\cos k_\mu) \pm 2i \left(\sum_{\mu} \sin^2 k_\mu\right)^{\frac{1}{2}} \tag{6.9}$$

Indeed, when this condition is satisfied, we have

$$KK' = 0$$

Now the spin eigenvectors $U_\alpha(\underline{k})$ of $A_{\underline{mn}}$ satisfy (6.7) so that every column of K' is in fact an eigenvector.

It is convenient to simplify notation at this point. Let us write:

$$P = \sum_{\mu} (\cos k_\mu) \qquad Q = \left(\sum_{\mu} \sin^2 k_\mu \right)^{\frac{1}{2}} \qquad R = \left(\sum_{\mu} \gamma_\mu \sin k_\mu \right) \tag{6.10}$$

The eigenvalues are then given by

$$a(\alpha, \underline{k}) = 2(P \pm iQ) \tag{6.11}$$

and the matrix K' by

$$K' = i(R \pm Q) \tag{6.12}$$

and the columns of $R+Q$ and $R-Q$ are eigenvectors.
In two dimensions the gamma matrices may be represented as

$$\gamma_0 = \begin{pmatrix} 0 & 1 \\ 1 & 0 \end{pmatrix} \qquad \gamma_1 = \begin{pmatrix} 0 & -i \\ i & 0 \end{pmatrix}$$

and $Q^2 = SS^*$, where $S = \sin k_0 + i \sin k_1$. The matrix $R+Q$ then takes the form

$$R + Q = \begin{pmatrix} Q & S^* \\ S & Q \end{pmatrix}$$

The eigenvectors represented by the columns of this matrix are not independent; indeed, we have

$$Q \begin{pmatrix} Q \\ S \end{pmatrix} = S \begin{pmatrix} S^* \\ Q \end{pmatrix}$$

A second independent eigenvector may be derived from $R-Q$:

$$R - Q = \begin{pmatrix} -Q & S^* \\ S & -Q \end{pmatrix}$$

where the columns are related by

$$-Q \begin{pmatrix} -Q \\ S \end{pmatrix} = S \begin{pmatrix} S^* \\ -Q \end{pmatrix}$$

Taking the first column of $R+Q$ and the last column $R-Q$, two independent normalised eigenvectors are :

$$U(0, \underline{k}) = \frac{1}{\sqrt{2Q^2}} \begin{pmatrix} Q \\ S \end{pmatrix} \qquad U(1, \underline{k}) = \frac{1}{\sqrt{2Q^2}} \begin{pmatrix} S^* \\ -Q \end{pmatrix}$$

These vectors are actually orthonormal:

$$\langle U(\alpha, \underline{k}) | U(\beta, \underline{k}) \rangle = \delta_{\alpha\beta}$$

These two independent eigenvectors suffice to span the spin space of $A_{\underline{mn}}$ in two dimensions. The spin eigenvectors in four dimensions may be obtained similarly. The gamma matrices in our representation are:

$$\gamma_0 = \begin{pmatrix} 1 & 0 & 0 & 0 \\ 0 & 1 & 0 & 0 \\ 0 & 0 & -1 & 0 \\ 0 & 0 & 0 & -1 \end{pmatrix} \qquad \gamma_1 = \begin{pmatrix} 0 & 0 & 0 & 1 \\ 0 & 0 & 1 & 0 \\ 0 & 1 & 0 & 0 \\ 1 & 0 & 0 & 0 \end{pmatrix}$$

$$\gamma_2 = \begin{pmatrix} 0 & 0 & 0 & -i \\ 0 & 0 & i & 0 \\ 0 & -i & 0 & 0 \\ i & 0 & 0 & 0 \end{pmatrix} \qquad \gamma_3 = \begin{pmatrix} 0 & 0 & 1 & 0 \\ 0 & 0 & 0 & -1 \\ 1 & 0 & 0 & 0 \\ 0 & -1 & 0 & 0 \end{pmatrix}$$

Let us define

$$T = \sin k_1 + i \sin k_2 \qquad X = \sin k_0 \qquad W = \sin k_3$$

Then

$$W^2 + TT^* = (Q + X)(Q - X)$$

and the matrix $R + Q$ is given by

$$R + Q = \begin{pmatrix} (Q+X) & 0 & W & T^* \\ 0 & (Q+X) & T & -W \\ W & T^* & (Q-X) & 0 \\ T & -W & 0 & (Q-X) \end{pmatrix}$$

The last two columns are linear combinations of the first two, since

$$W \begin{pmatrix} (Q+X) \\ 0 \\ W \\ T \end{pmatrix} + T \begin{pmatrix} 0 \\ (Q+X) \\ T^* \\ -W \end{pmatrix} = (Q+X) \begin{pmatrix} W \\ T \\ (Q-X) \\ 0 \end{pmatrix}$$

and

$$T^* \begin{pmatrix} (Q+X) \\ 0 \\ W \\ T \end{pmatrix} - W \begin{pmatrix} 0 \\ (Q+X) \\ T^* \\ -W \end{pmatrix} = (Q+X) \begin{pmatrix} T^* \\ -W \\ 0 \\ (Q-X) \end{pmatrix}$$

The two remaining independent eigenvectors may be obtained from the matrix $R - Q$

$$R - Q = \begin{pmatrix} (-Q+X) & 0 & W & T^* \\ 0 & (-Q+X) & T & -W \\ W & T^* & (-Q-X) & 0 \\ T & -W & 0 & (-Q-X) \end{pmatrix}$$

As before, only two of the four columns are linearly independent:

$$W \begin{pmatrix} (-Q+X) \\ 0 \\ W \\ T \end{pmatrix} + T \begin{pmatrix} 0 \\ (-Q+X) \\ T^* \\ -W \end{pmatrix} = (-Q+X) \begin{pmatrix} W \\ T \\ (-Q-X) \\ 0 \end{pmatrix}$$

and

$$T^* \begin{pmatrix} (-Q+X) \\ 0 \\ W \\ T \end{pmatrix} - W \begin{pmatrix} 0 \\ (-Q+X) \\ T^* \\ -W \end{pmatrix} = (-Q+X) \begin{pmatrix} T^* \\ -W \\ 0 \\ (-Q-X) \end{pmatrix}$$

Let us select the first two columns from $R+Q$ and the last two columns from $R-Q$ as our independent spin vectors. These four vectors each have magnitude

$$((Q+X)^2 + W^2 + TT^*)^{\frac{1}{2}} = \sqrt{2Q(Q+X)}$$

so that the four normalised spin eigenvectors are

$$U(0,\underline{k}) = \frac{1}{\sqrt{2Q(Q+X)}} \begin{pmatrix} (Q+X) \\ 0 \\ W \\ T \end{pmatrix} \quad ; \quad U(1,\underline{k}) = \frac{1}{\sqrt{2Q(Q+X)}} \begin{pmatrix} 0 \\ (Q+X) \\ T^* \\ -W \end{pmatrix}$$

$$U(2,\underline{k}) = \frac{1}{\sqrt{2Q(Q+X)}} \begin{pmatrix} W \\ T \\ -(Q+X) \\ 0 \end{pmatrix} \quad ; \quad U(3,\underline{k}) = \frac{1}{\sqrt{2Q(Q+X)}} \begin{pmatrix} T^* \\ -W \\ 0 \\ -(Q+X) \end{pmatrix}$$

Next, consider the adjoint operator

$$A^\dagger_{\underline{m}\underline{n}} = \sum_\mu \left\{ (1-\gamma_\mu)\, \delta_{\underline{m},\underline{n}-\underline{\mu}} + (1+\gamma_\mu)\, \delta_{\underline{m},\underline{n}+\underline{\mu}} \right\}$$

It is not *a priori* clear that this operator shares the same eigenspace as $A_{\underline{m},\underline{n}}$; we will show that this is indeed the case by explicit calculation.

The eigenvalues of $A^\dagger$ may be computed as before—we assume eigenvectors of the form

$$\chi_{\underline{n}}(\alpha,\underline{k}) = V(\alpha,\underline{k}) e^{i\underline{k}.\underline{n}}$$

and solve

$$A^\dagger_{\underline{m}\underline{n}} \chi_{\underline{n}}(\alpha,\underline{k}) = b(\alpha,\underline{k})\, \chi_{\underline{m}}(\alpha,\underline{k})$$

This time we find

$$\begin{aligned}
&\sum_\mu \left\{ (1-\gamma_\mu)\, \delta_{\underline{m},\underline{n}-\underline{\mu}} + (1+\gamma_\mu)\, \delta_{\underline{m},\underline{n}+\underline{\mu}} \right\} V(\alpha,\underline{k}) e^{i\underline{k}.\underline{n}} \\
&\quad = \sum_\mu \left\{ (1-\gamma_\mu)\, e^{i\underline{k}.(\underline{m}+\underline{\mu})} + (1+\gamma_\mu)\, e^{i\underline{k}.(\underline{m}-\underline{\mu})} \right\} V(\alpha,\underline{k}) \\
&\quad = \sum_\mu \left\{ (e^{ik_\mu} + e^{-ik_\mu}) - \gamma_\mu (e^{ik_\mu} - e^{-ik_\mu}) \right\} V(\alpha,\underline{k}) e^{i\underline{k}.\underline{m}} \\
&\quad = \sum_\mu (2\cos k_\mu - 2i\gamma_\mu \sin k_\mu)\, V(\alpha,\underline{k}) e^{i\underline{k}.\underline{m}} \\
&\quad = b(\alpha,\underline{k})\, \chi_{\underline{m}}(\alpha,\underline{k})
\end{aligned}$$

As before, the homogeneous system

$$KV(\alpha, \underline{k}) = 0$$

must be solved, but now

$$K = \sum_{\mu}(\cos k_\mu) - \frac{b(\alpha, \underline{k})}{2} - \sum_{\mu}(i\gamma_\mu \sin k_\mu)$$

This time we define

$$K' = -\sum_{\nu}(\cos k_\nu) + \frac{b(\alpha, \underline{k})}{2} - \sum_{\nu}(i\gamma_\nu \sin k_\nu)$$

This gives

$$KK' = -\sum_{\mu}(\sin^2 k_\mu) - \left(\sum_{\mu}(\cos k_\mu) - \frac{a(\alpha, \underline{k})}{2}\right)^2$$

exactly as before.The eigenvalues of $A^\dagger$ are therefore given by

$$b(\alpha, \underline{k}) = 2\sum_{\mu}(\cos k_\mu) \pm 2i\left(\sum_{\mu}\sin^2 k_\mu\right)^{\frac{1}{2}}$$

and are the same as those of A. In terms of our simplified notation (6.10), the eigenvalues are

$$b(\alpha, \underline{k}) = 2(P \pm iQ)$$

and the matrix K' is

$$K' = i(-R \pm Q)$$

The columns of $-R+Q$ and $-R-Q$ are therefore eigenvectors of $A^\dagger$. These matrices are given explicitly in two dimensions by

$$-R+Q = \begin{pmatrix} Q & -S^* \\ -S & Q \end{pmatrix} \quad ; \quad -R-Q = \begin{pmatrix} -Q & -S^* \\ -S & -Q \end{pmatrix}$$

As before, the first and second columns of each matrix are proportional:

$$Q\begin{pmatrix} Q \\ -S \end{pmatrix} = -S\begin{pmatrix} -S^* \\ Q \end{pmatrix} \quad ; \quad -Q\begin{pmatrix} -Q \\ -S \end{pmatrix} = -S\begin{pmatrix} -S^* \\ -Q \end{pmatrix}$$

This time we select the second column of $-R+Q$ and the first column $-R-Q$ to obtain two independent normalised spin eigenvectors of $A^\dagger$

$$V(0, \underline{k}) = \frac{1}{\sqrt{2Q^2}}\begin{pmatrix} -S^* \\ Q \end{pmatrix} \quad ; \quad V(1, \underline{k}) = \frac{1}{\sqrt{2Q^2}}\begin{pmatrix} -Q \\ -S \end{pmatrix}$$

After the trivial redefinition

$$V(0,\underline{k}) \longrightarrow -V(0,\underline{k}) \quad ; \quad V(1,\underline{k}) \longrightarrow -V(1,\underline{k})$$

the eigenvectors of $A^\dagger$ and A coincide:

$$V(0,\underline{k}) = U(1,\underline{k})$$
$$V(1,\underline{k}) = U(0,\underline{k})$$

A similar result holds in four dimensions. The matrix $-R+Q$ is

$$-R+Q = \begin{pmatrix} (Q-X) & 0 & -W & -T^* \\ 0 & (Q-X) & -T & W \\ -W & -T^* & (Q+X) & 0 \\ -T & W & 0 & (Q+X) \end{pmatrix}$$

while $-R-Q$ is given by

$$-R-Q = \begin{pmatrix} (-Q-X) & 0 & -W & -T^* \\ 0 & (-Q-X) & -T & W \\ -W & -T^* & (-Q+X) & 0 \\ -T & W & 0 & (-Q+X) \end{pmatrix}$$

Selecting the last two columns from $-R+Q$ and the first two from $-R-Q$ and changing the sign as above yields

$$V(0,\underline{k}) = U(2,\underline{k})$$
$$V(1,\underline{k}) = U(3,\underline{k})$$
$$V(2,\underline{k}) = U(0,\underline{k})$$
$$V(3,\underline{k}) = U(1,\underline{k})$$

Note that although $A^\dagger$ and A have the same eigenvectors these do *not* in general correspond to the same eigenvalues. In fact if we set

$$\lambda(0,\underline{k}) = 2(P+iQ) = \lambda(\underline{k})$$
$$\lambda(1,\underline{k}) = 2(P-iQ) = \lambda^*(\underline{k})$$

and

$$\psi(0,\underline{k}) = U(0,\underline{k})e^{i(\underline{k}.\underline{n})}$$
$$\psi(1,\underline{k}) = U(1,\underline{k})e^{i(\underline{k}.\underline{n})}$$
$$\psi(2,\underline{k}) = U(2,\underline{k})e^{i(\underline{k}.\underline{n})}$$
$$\psi(3,\underline{k}) = U(3,\underline{k})e^{i(\underline{k}.\underline{n})}$$

we find, in two dimensions

$$A\psi(0,\underline{k}) = \lambda(\underline{k})\psi(0,\underline{k})$$
$$A\psi(1,\underline{k}) = \lambda^*(\underline{k})\psi(1,\underline{k})$$

$$A^\dagger\psi(0,\underline{k}) = \lambda^*(\underline{k})\psi(0,\underline{k})$$
$$A^\dagger\psi(1,\underline{k}) = \lambda(\underline{k})\psi(1,\underline{k})$$

while in four dimensions

$$\begin{aligned} A\psi(0,\underline{k}) &= \lambda(\underline{k})\psi(0,\underline{k}) \\ A\psi(1,\underline{k}) &= \lambda(\underline{k})\psi(1,\underline{k}) \\ A\psi(2,\underline{k}) &= \lambda^*(\underline{k})\psi(2,\underline{k}) \\ A\psi(3,\underline{k}) &= \lambda^*(\underline{k})\psi(3,\underline{k}) \end{aligned}$$

$$\begin{aligned} A^\dagger\psi(0,\underline{k}) &= \lambda^*(\underline{k})\psi(0,\underline{k}) \\ A^\dagger\psi(1,\underline{k}) &= \lambda^*(\underline{k})\psi(1,\underline{k}) \\ A^\dagger\psi(2,\underline{k}) &= \lambda(\underline{k})\psi(2,\underline{k}) \\ A^\dagger\psi(3,\underline{k}) &= \lambda(\underline{k})\psi(3,\underline{k}) \end{aligned}$$

With a complete set of eigenvectors and eigenvalues of A and $A^\dagger$ in hand, it is now straightforward to write down the corresponding objects for the full fermion operators.

Let $\psi(\alpha,\underline{k})$ be any eigenvector of A and $A^\dagger$ with eigenvalue $\lambda(\underline{k})$ on A and eigenvalue $\lambda^*(\underline{k})$ on $A^\dagger$. Then

$$\begin{aligned} A\psi &= \lambda\psi = 2(P \pm iQ)\psi \\ A^\dagger\psi &= \lambda^*\psi \\ M\psi &= (1-\kappa\lambda)\psi = \lambda_M\psi \\ M^\dagger\psi &= (1-\kappa\lambda^*)\psi = \lambda_{M^\dagger}\psi \\ M^\dagger M\psi &= (1-\kappa(\lambda^*+\lambda)+\kappa^2\lambda^*\lambda)\psi = \lambda_{M^\dagger M}\psi \\ MM^\dagger\psi &= (1-\kappa(\lambda+\lambda^*)+\kappa^2\lambda\lambda^*)\psi = \lambda_{MM^\dagger}\psi \end{aligned} \tag{6.13}$$

The operators A, $A^\dagger$, M, $M^\dagger$, $M^\dagger M$ and $MM^\dagger$ all have the same eigenvectors; the corresponding eigenvalues for each operator are given by (6.13). Furthermore, the eigenvectors (though not the eigenvalues) are independent of the value of the hopping parameter κ.

28. Properties of the Eigensystem

In this section we will explore the structure of the free fermion eigenspace, focusing particularly on those properties which bear on the perturbative analysis to be discussed later—namely commutation relations, zero modes and degeneracies.

We note first that the free fermion operator has all the properties anticipated in Section (26). It is certainly diagonalisable, by construction. Its eigenvalues are semisimple with algebraic and geometric multiplicity $d/2$ per momentum mode. Moreover, the fact that the fermion operator and its adjoint share the same eigenspace, L, has the consequence that that M and

$M^\dagger$ commute. This follows from the fact that any vector in L can be written as a linear combination of eigenvectors:

$$\Psi = \sum_i c_i \psi_i$$

Now letting $\lambda_M = \lambda$, we have from (6.13)

$$M\psi_i = \lambda_i \psi_i \Rightarrow M^\dagger \psi_i = \lambda_i^* \psi_i$$

and therefore

$$(MM^\dagger - M^\dagger M)\Psi = \sum_i c_i(\lambda_i \lambda_i^* - \lambda_i^* \lambda_i)\psi_i = 0$$

for *any* choice Ψ in L. It follows that

$$MM^\dagger - M^\dagger M = 0$$

A second consequence is that if a vector ψ is a right eigenvector of M, it is also a left eigenvector, since

$$M|\psi\rangle = \lambda|\psi\rangle \quad \Rightarrow \quad M^\dagger \psi = \lambda^*|\psi\rangle \quad \Rightarrow \quad \langle\psi|M = \langle\psi|\lambda$$

with a similar result for $M^\dagger$.

This property, which follows automatically from hermiticity, does *not* hold in general for non-hermitian matrices such as M. It is, however, essential if a perturbation expansion around the free fermion field is to be attempted.

The fermion operator exhibits a high degree of degeneracy, since its eigenvalues depend only on the magnitudes of the momentum components k_μ and not on their ordering or their sign. A general eigenvalue of M is given by

$$\lambda_M(\pm, \underline{k}) = 1 - 2\kappa(P \pm iQ) = 1 - 2\kappa \left(\sum_\mu (\cos k_\mu) \pm i \left(\sum_\mu \sin^2 k_\mu \right)^{\frac{1}{2}} \right) \tag{6.14}$$

In the worst two-dimensional case, with periodic boundary conditions in both dimensions and k_0 and k_1 non-zero and distinct the following set of momentum vectors are all associated with the same eigenvalue:

$$\begin{array}{ll} (k_0, k_1) & (k_1, k_0) \\ (-k_0, k_1) & (k_1, -k_0) \\ (k_0, -k_1) & (-k_1, k_0) \\ (-k_0, -k_1) & (-k_1, -k_0) \end{array}$$

This eightfold degeneracy is the maximum possible in two dimensions. If antiperiodic boundary conditions are imposed, as is customary, in the time direction, the maximum degeneracy is reduced to four.

The situation is much worse in four dimensions, where there are four components of momentum to be permuted by position and sign, giving rise to a 384-fold degeneracy in the momenta. There is, in the four-dimensional case, an additional spin degeneracy since the spin eigenvectors $U(0, \underline{k})$ and $U(1, \underline{k})$ share the same eigenvalue, as do the vectors $U(2, \underline{k})$ and $U(3, \underline{k})$. The total degeneracy factor in the general case, where all momentum components are non-zero and distinct, is therefore 768.

Note that this momentum degeneracy does not affect the semisimple nature of the eigensystem, since different momentum modes are still associated with distinct eigenvectors. If the moment degeneracy is η, then the algebraic and geometric multiplcities are each $\eta d/2$.

The high level of degeneracy in the fermion operator presents a serious obstacle to any attempt to construct a perturbative expansion.

Let us next consider the eigenvalues of M themselves, which are given explicitly by (6.14) and are plotted in Figures (6.1) and (6.2)

Although complex in general, they occur in conjugate pairs. As a consequence, the determinant of M, which is simply the product over all eigenvalues, is always real, as is the determinant of $M^\dagger$.

The fact that corresponding eigenvalues of M and $M^\dagger$ are complex conjugates means, of course, that the eigenvalues of the product operators $MM^\dagger$ and $M^\dagger M$ are real and corresponding eigenvalues are equal.

The maximum and minimum eigenvalues of M follow from (6.14):

$$\lambda_{max} = 1 + 2d\kappa \quad ; \quad \lambda_{min} = 1 - 2d\kappa$$

The minimum eigenvalue, which occurs at $\underline{k} = 0$, is of particular interest; it approaches zero as κ approaches $1/2d$—that is, as $a \to 0$, if the mass is held fixed. That is to say, M becomes increasingly ill-conditioned as the naive continuum limit is approached, the determinant goes to zero in this limit and the matrix is no longer invertible.

Although the zero momentum eigenvalue remains well-behaved at zero momentum (for finite lattice spacing), a difficulty arises with the zero-momentum eigenvectors. Indeed, at zero momentum we have

$$Q = S = T = W = X = 0$$

so that all eigenvectors are zero. There is no linearly independent eigenvector associated with the zero mode, so that a degree of freedom is missing.

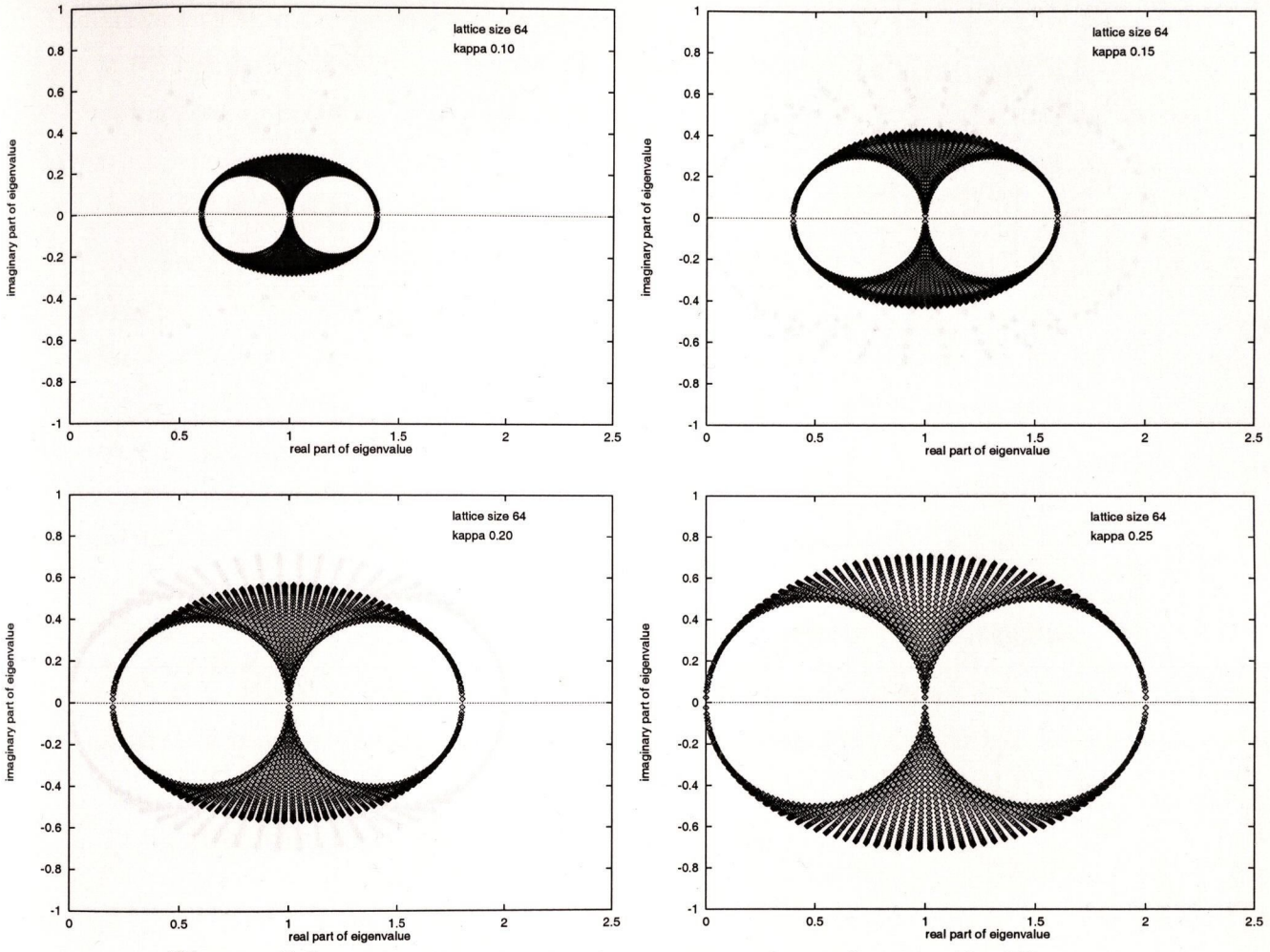

Figure 6.1: : Eigenvalues of the free fermion operator in two dimensions for different values of the hopping parameter. Note that a zero eigenvalue appears at the critical value $\kappa = 0.25$; the fermion operator becomes singular.

A closer inspection shows that the problem arises because all the terms Q, S, T, W, X which occur in the expression for the eigenvectors are purely kinetic—there is no mass term. The mass term, P, has been eliminated from the eigenvectors via (6.8), (6.11) and (6.12) as a direct consequence of the fact that all eigenvalues of the operator are non-zero (except in the continuum limit).

It is instructive to compare this with the physical (ie, continuum, Minkowski space) case, where we solve the Dirac equation

$$(i\gamma^\mu \partial_\mu - m)\psi = 0$$

This is in effect a restricted version of (6.6), where we solve for the particular eigenvalue $\lambda = 0$. The requirement that λ be zero leads to the well-known mass-shell condition

$$\omega^2 = \underline{k}^2 + m^2 \tag{6.15}$$

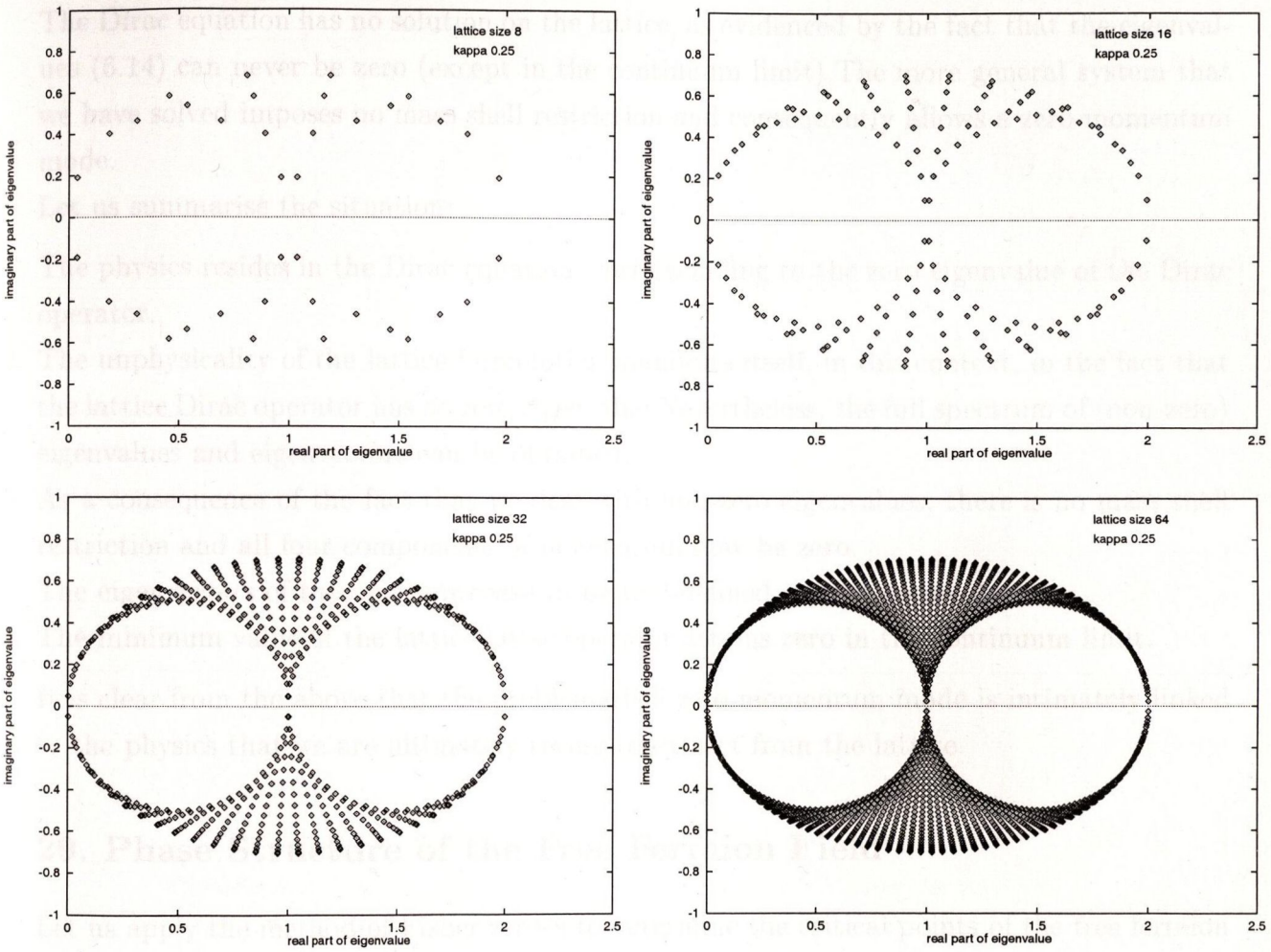

Figure 6.2: : Eigenvalues of the free fermion operator in two dimensions at the critical value of the hopping parameter. The distribution of eigenvalues is shown for several different lattice sizes. The eigenvalues are confined to a fixed region, but their density increases with increasing lattice size.

The eigenvectors associated with this zero eigenvalue may be derived by methods similar to those used in the previous section. In four dimensions the spin eigenvectors take the form

$$U(0,\underline{k}) = \frac{1}{\sqrt{2\omega(\omega+m)}} \begin{pmatrix} \omega+m \\ 0 \\ k_z \\ k_x+ik_y \end{pmatrix} \quad ; \quad U(1,\underline{k}) = \frac{1}{\sqrt{2\omega(\omega+m)}} \begin{pmatrix} 0 \\ \omega+m \\ k_x-ik_y \\ -k_z \end{pmatrix}$$

$$U(2,\underline{k}) = \frac{1}{\sqrt{2\omega(\omega+m)}} \begin{pmatrix} k_z \\ k_x+ik_y \\ \omega+m \\ 0 \end{pmatrix} \quad ; \quad U(3,\underline{k}) = \frac{1}{\sqrt{2\omega(\omega+m)}} \begin{pmatrix} k_x-ik_y \\ -k_z \\ 0 \\ \omega+m \end{pmatrix}$$

so that a mass term is present. The mass shell condition (6.15) now excludes the possibility that all four components of momentum are zero.

The Dirac equation has no solution on the lattice, as evidenced by the fact that the eigenvalues (6.14) can never be zero (except in the continuum limit).The more general system that we have solved imposes no mass shell restriction and consequently allows a zero momentum mode.

Let us summarise the situation:

1. The physics resides in the Dirac equation, corresponding to the zero eigenvalue of the Dirac operator.
2. The unphysicality of the lattice formulation manifests itself, in this context, in the fact that the lattice Dirac operator has no zero eigenvalue.Nevertheless, the full spectrum of (non-zero) eigenvalues and eigenvectors can be obtained.
3. As a consequence of the fact that we deal with non-zero eigenvalues, there is no mass shell restriction and all four components of momentum may be zero.
4. The eigen*vectors* of the operator cease to be well-defined at zero momentum.
5. The minimum value of the lattice Dirac operator attains zero in the continuum limit.

It is clear from the above that the problematical zero momentum mode is intimately linked to the physics that we are ultimately trying to extract from the lattice.

29. Phase Structure of the Free Fermion Field

Let us apply the method of Fisher zeroes to determine the critical points of the free fermion lattice theory in two dimensions.

The free fermion partition function is given by

$$Z_F = \det M = \prod_i \lambda_i$$

where the dimensionless fermion operator M is given by (6.1) and the eigenvalues λ_i by (6.14). A zero of the partition function function occurs when any eigenvalue is zero, thus we require

$$1 - 2\kappa \left(\sum_\mu \cos k_\mu \pm i \left(\sum_\mu \sin^2 k_\mu \right)^{\frac{1}{2}} \right) = 0$$

which occurs for values of κ satisfying

$$2\kappa = \frac{\sum_\mu \cos k_\mu \pm i \left(\sum_\mu \sin^2 k_\mu \right)^{\frac{1}{2}}}{\left(\sum_\mu \cos k_\mu \right)^2 + \left(\sum_\mu \sin^2 k_\mu \right)} \tag{6.16}$$

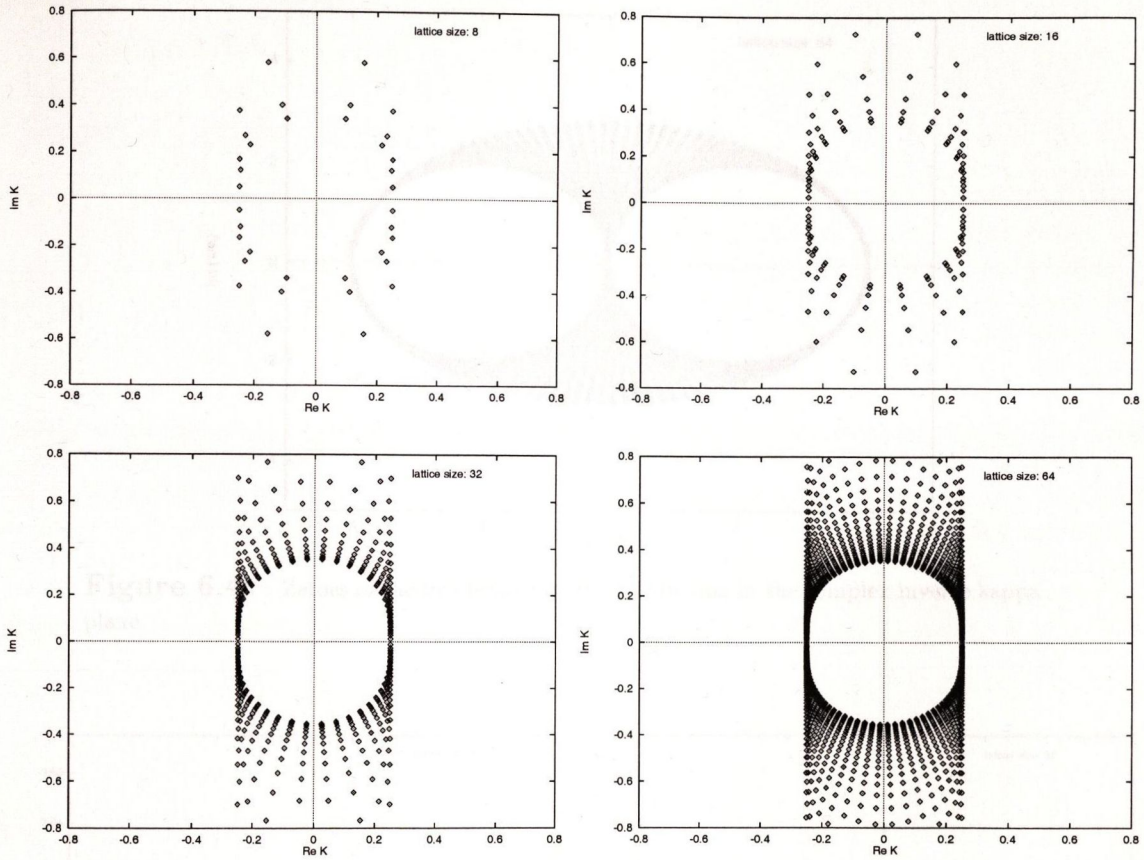

Figure 6.3: : Zeroes of the free fermion partition function in the complex kappa plane

The development of this system of zeroes with increasing lattice size is shown in Figure (6.3). It is apparent from the figure that the real axis is pinched at the two critical points $\kappa = \pm\frac{1}{4}$. There are in fact two additional critical points at $\kappa = \pm\infty$. These appear explicitly as a pinching of the real axis at the origin when the zeroes are plotted in the inverse κ plane as in Figure (6.4).

The existence of a phase transition requires an accumulation of zeroes in the neighbourhood of the critical point as the lattice size increases. This process is demonstrated in Figure (6.5) for the critical point $\kappa_c = \frac{1}{4}$.

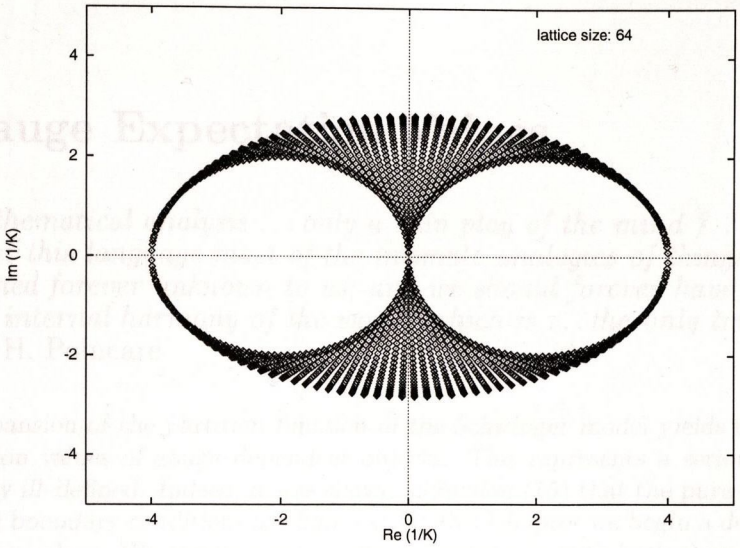

Figure 6.4: : Zeroes of the free fermion partition function in the complex inverse kappa plane

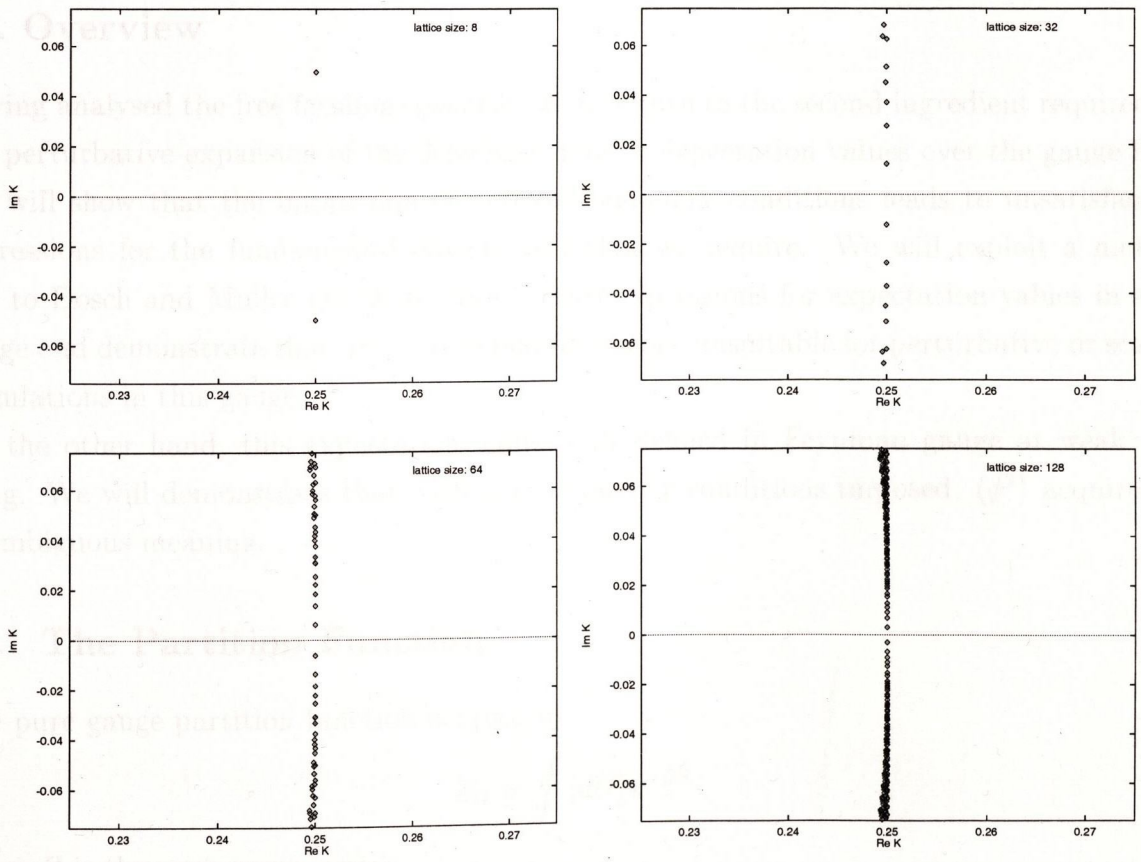

Figure 6.5: : Accumulation of zeroes at the critical point

7. Pure Gauge Expectation Values

Is mathematical analysis ... only a vain play of the mind ? ... Far from it; without this language most of the intimate analogies of things would have remained forever unknown to us; and we should forever have been ignorant of the internal harmony of the world, which is ... the only true objective reality.
– H. Poincare

The perturbative expansion of the partition function of the Schwinger model yields expressions containing pure gauge expectation values of gauge–dependent objects. This represents a serious obstacle since such objects are potentially ill–defined. Indeed, it was shown in Section (15) that the pure gauge vacuum state is degenerate if periodic boundary conditions are imposed. In this Chapter we begin a detailed investigation of pure gauge expectation values. We obtain exact results in axial gauge with both periodic and zero boundary conditions and similar results in Feynman gauge in the weak coupling regime. We show in particular that the object $\langle {\phi_i}^2 \rangle$ *is well–defined in Feynman gauge if zero boundary conditions are imposed.*

30. Overview

Having analysed the free fermion operator, we now turn to the second ingredient required for the perturbative expansion of the Schwinger model; expectation values over the gauge field. We will show that the imposition of periodic boundary conditions leads to unsatisfactory expressions for the fundamental object, $\langle \phi^2 \rangle$ that we require. We will exploit a method due to Dosch and Muller (1979) to obtain *exact* expressions for expectation values in axial gauge and demonstrate that $\langle \phi^2 \rangle$ is constant and hence unsuitable for perturbative or scaling calculations in this gauge.
On the other hand, this expectation value is ill–defined in Feynman gauge at weak coupling. We will demonstrate that with zero boundary conditions imposed, $\langle \phi^2 \rangle$ acquires an unambiguous meaning.

31. The Partition Function

The pure gauge partition function is given by

$$Z_G = \int [dU]\, e^{-\beta S}$$

where S is the pure gauge action

$$S = \sum_p \mathrm{Re}(1 - U_p)$$

and U_p is the product of gauge variables around an elementary plaquette.

$$U_p = e^{iag(A_{\underline{\mu}}(\underline{n})+A_{\underline{\nu}}(\underline{n}+\underline{\mu})-A_{\underline{\mu}}(\underline{n}+\underline{\nu})-A_{\underline{\nu}}(\underline{n}))} = e^{iag\phi_p}$$

We will set ag equal to unity for the moment and rewrite

$$S = \sum_p 1 - \text{Re } e^{i\phi_p} = \sum_p 1 - \cos\phi_p$$

The invariant integration measure for U(1) over a lattice L is given by

$$\int [dU] = \int_{-\pi}^{\pi} \prod_{\phi_i \in L} \left(\frac{d\phi_i}{2\pi}\right)$$

Putting everything together, the partition function becomes

$$Z_G = e^{-\beta|L|} \int_{-\pi}^{\pi} \prod_{\phi_i \in L} \left(\frac{d\phi_i}{2\pi}\right) \prod_p e^{\beta \cos\phi_p(\phi_i)}$$

Each factor in the integrand may be expanded in a Fourier series

$$e^{\beta\cos\phi_p} = \sum_{r=-\infty}^{\infty} a_r(\beta)\, e^{ir\phi_p} \tag{7.1}$$

The coefficients a_r may be determined by considering the generating function for the modified Bessel functions

$$e^{\left(\frac{x}{2}\right)\left(t+\frac{1}{t}\right)} = \sum_{r=-\infty}^{\infty} I_r(x)\, t^r$$

Setting $t = e^{i\phi}$ gives

$$e^{x\cos\phi} = \sum_{r=-\infty}^{\infty} I_r(x)\, e^{ir\phi} \tag{7.2}$$

and comparing (7.1) and (7.2) we identify a_r with $I_r(\beta)$, the modified Bessel function of order r.

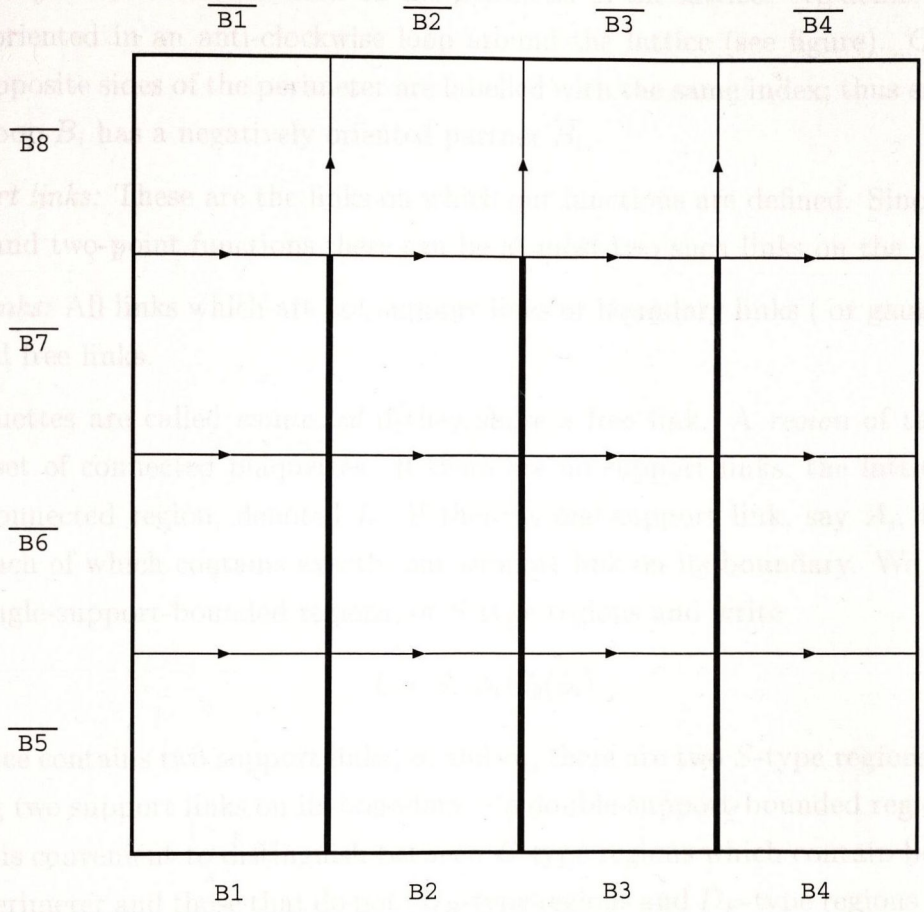

Figure 7.1: Finite lattice in axial gauge. The thick vertical lines are the gauge fixed links. No boundary conditions are imposed.

32. Axial Gauge

The discussion so far has been completely general; no gauge has been fixed and the lattice L is not necessarily finite. We now consider a finite lattice in axial gauge. The lattice is shown in Figure (7.1), which also serves to establish notation. Note that the fixed timelike links do not form a maximal set; additional spacelike links can still be fixed. In the infinite volume limit, of course, axial gauge does constitute a complete gauge fixing.

We will rewrite the partition function using the expansion (7.1) and distinguishing now between boundary and inner links.

$$Z_G = e^{-\beta|L|} \int_{-\pi}^{\pi} \prod_{n=1}^{2N} \left(\frac{dB_n}{2\pi}\right) \left(\frac{d\overline{B_n}}{2\pi}\right) \prod_{\phi_i \in L} \left(\frac{d\phi_i}{2\pi}\right) \prod_{p} \sum_{r=-\infty}^{\infty} I_r(\beta)\, e^{ir\phi_p(\phi_i, B_n, \overline{B_n})}$$

Before proceeding to evaluate the integrals it is helpful to introduce some terminology.

We identify three types of link (apart from fixed links):

(1) *Boundary links:* These are links on the perimeter of the lattice. We define these so that they are oriented in an anti-clockwise loop around the lattice (see figure). Corresponding links on opposite sides of the perimeter are labelled with the same index; thus each positively oriented loop B_i has a negatively oriented partner $\overline{B_i}$.

(2) *Support links:* These are the links on which our functions are defined. Since we consider only one and two-point functions there can be at most two such links on the lattice.

(3) *Free links:* All links which are not support links or boundary links (or gauge-fixed links) are termed free links.

Two plaquettes are called *connected* if they share a free link. A *region* of the lattice is a maximal set of connected plaquettes. If there are no support links, the lattice as a whole forms a connected region, denoted L. If there is one support link, say A_i, there are two regions, each of which contains exactly one support link on its boundary. We will call such regions single-support-bounded regions, or S-type regions and write

$$L = S_1(\phi_i)S_2(\phi_i)$$

If the lattice contains two support links, ϕ_i and ϕ_j, there are two S-type regions and a region containing two support links on its boundary— a double-support-bounded region, or D-type region. It is convenient to distinguish between D-type regions which contain boundary links on their perimeter and those that do not (D_B-type regions and D_F-type regions respectively). With two support links on the lattice we write

$$L = S_1(\phi_i)D_B(\phi_i,\phi_j)S_2(\phi_J)$$

or

$$L = S_1(\phi_i)D_F(\phi_i,\phi_j)S_2(\phi_J)$$

Next we write down an expression for the integral over a single free link

$$\int_{-\pi}^{\pi}\left(\frac{d\phi_k}{2\pi}\right)\left\{\sum_{r=-\infty}^{\infty} I_r(\beta)e^{ir(\phi_k+\phi_p)}\sum_{r'=-\infty}^{\infty} I_{r'}(\beta)e^{ir'(-\phi_k+\phi_{p'})}\right\} = \sum_{rr'} I_r(\beta)e^{ir\phi_p}I_{r'}(\beta)e^{ir'\phi_{p'}}\delta_{rr'}$$
$$= \sum_r I_r^2(\beta)e^{ir(\phi_p+\phi_{p'})}$$

Here p and p' are the two plaquettes containing ϕ_i while ϕ_p and ϕ'_p are the sums of the remaining links around p and p' respectively.
Integrating all the free links in a region R gives

$$\int_{-\pi}^{\pi}\prod_{\phi_k\in R}\left(\frac{d\phi_k}{2\pi}\right)R = \sum_r {I_r}^n(\beta)e^{irL_{loop}}$$

where n is the number of plaquettes in R and L_{loop} is the sum of links around the perimeter of R, taken anticlockwise. These links consist of boundary links, support links and fixed links (which are set to zero). Let α be the set of positive boundary links and $\overline{\alpha}$ the set of negative boundary links on the perimeter of R.

Define

$$B_\alpha = \sum_{m\in\alpha} B_m$$

$$\overline{B}_{\overline{\alpha}} = \sum_{n\in\overline{\alpha}} \overline{B_n}$$

Let ϕ_s be the sum of support links on the perimeter of R. With this notation we can write

$$e^{irL_{loop}} = e^{ir(B_\alpha+\overline{B}_{\overline{\alpha}})}e^{ir\phi_s}$$

Setting $R = L$ gives

$$\begin{aligned}\int_{-\pi}^{\pi} \prod_{\phi_k\in L}\left(\frac{d\phi_k}{2\pi}\right) L &= \sum_r {I_r}^{|L|}(\beta)e^{ir(B_\alpha+\overline{B}_{\overline{\alpha}})} \\ &= {I_0}^{|L|}\left\{1+\sum_{r\neq 0} {g_r}^{|L|}(\beta)e^{ir\sum_{m=1}^{2N}(B_m+\overline{B}_m)}\right\}\end{aligned}$$

where

$$g_r(\beta) = \frac{I_r(\beta)}{I_0(\beta)}$$

If R is an S-type region we find

$$\int_{-\pi}^{\pi} \prod_{\phi_k\in S^\pm}\left(\frac{d\phi_k}{2\pi}\right) S^\pm = {I_0}^{|S^\pm|}\left\{1+\sum_{r\neq 0} {g_r}^{|S^\pm|}(\beta)e^{ir(B_\alpha+\overline{B}_{\overline{\alpha}})}e^{\pm ir\phi_i}\right\}$$

The negative sign arises if the support link ϕ_i has negative orientation on the perimeter of S.

Setting $R = D_F$ gives

$$\int_{-\pi}^{\pi} \prod_{\phi_k\in D_F}\left(\frac{d\phi_k}{2\pi}\right) D_F = {I_0}^{|D_F|}\left\{1+\sum_{r\neq 0} {g_r}^{|D_F|}(\beta)e^{ir(\phi_i-\phi_j)}\right\}$$

Note that the boundary links do not appear in this expression. Moreover the support links ϕ_i and ϕ_j necessarily occur with opposite signs.

Setting $R = D_B$ gives

$$\int_{-\pi}^{\pi} \prod_{\phi_k\in {D_B}^\pm}\left(\frac{d\phi_k}{2\pi}\right) {D_B}^\pm = {I_0}^{|{D_B}^\pm|}\left\{1+\sum_{r\neq 0} {g_r}^{|{D_B}^\pm|}\beta)e^{ir(B_\alpha+\overline{B_{\overline{\alpha}}})}e^{ir(\phi_i\pm\phi_j)}\right\}$$

The negative sign corresponds to negative orientation of ϕ_j. (We can without loss of generality assume that ϕ_i is positively oriented since our gauge-fixing ensures that no region can have both support links negatively oriented.)
With these preliminaries out of the way we can write down directly the integrals we require

$$Z_G = e^{-\beta|L|} I_0{}^{|L|} \int_{-\pi}^{\pi} \prod_{n=1}^{2N} \left(\frac{dB_n}{2\pi}\right)\left(\frac{d\overline{B_n}}{2\pi}\right) \left\{1 + \sum_{r\neq 0} g_r{}^{|L|}(\beta) e^{ir\left(\sum_{n=1}^{2N} B_n + \overline{B}_n\right)}\right\} \tag{7.3}$$

$$\begin{aligned}\langle f(\phi_i)\rangle = \frac{e^{-\beta|L|} I_0{}^{|L|}}{Z_G} \int_{-\pi}^{\pi} \prod_{n=1}^{2N} \left(\frac{dB_n}{2\pi}\right)\left(\frac{d\overline{B_n}}{2\pi}\right)\left(\frac{d\phi_i}{2\pi}\right) f(\phi_i) \\ \times \left\{1 + \sum_{r\neq 0} g_r{}^{|S_1|}(\beta) e^{ir(B_\alpha + \overline{B_{\bar{\alpha}}})} e^{-ir\phi_i}\right\} \\ \times \left\{1 + \sum_{r'\neq 0} g_{r'}{}^{|S_2|}(\beta) e^{ir'(B_{\alpha'} + \overline{B_{\bar{\alpha}'}})} e^{ir'\phi_i}\right\}\end{aligned} \tag{7.4}$$

$$\begin{aligned}\langle f(\phi_i) g(\phi_j)\rangle_B^{\pm} = \frac{e^{-\beta|L|} I_0{}^{|L|}}{Z_G} \int_{-\pi}^{\pi} \prod_{n=1}^{2N} \left(\frac{dB_n}{2\pi}\right)\left(\frac{d\overline{B_n}}{2\pi}\right)\left(\frac{d\phi_i}{2\pi}\right)\left(\frac{d\phi_j}{2\pi}\right) f(\phi_i) g(\phi_j) \\ \times \left\{1 + \sum_{r\neq 0} g_r{}^{|S_1|}(\beta) e^{ir(B_\alpha + \overline{B_{\bar{\alpha}}})} e^{-ir\phi_i}\right\} \\ \times \left\{1 + \sum_{r'\neq 0} g_{r'}{}^{|D_B|}(\beta) e^{ir'(B_{\alpha'} + \overline{B_{\bar{\alpha}'}})} e^{ir'(\phi_i \pm \phi_j)}\right\} \\ \times \left\{1 + \sum_{r''\neq 0} g_{r''}{}^{|S_2|}(\beta) e^{ir''(B_{\alpha''} + \overline{B_{\bar{\alpha}''}})} e^{\mp ir''\phi_j}\right\}\end{aligned} \tag{7.5}$$

$$\begin{aligned}\langle f(\phi_i) g(\phi_j)\rangle_F = \frac{e^{-\beta|L|} I_0{}^{|L|}}{Z_G} \int_{-\pi}^{\pi} \prod_{n=1}^{2N} \left(\frac{dB_n}{2\pi}\right)\left(\frac{d\overline{B_n}}{2\pi}\right)\left(\frac{d\phi_i}{2\pi}\right)\left(\frac{d\phi_j}{2\pi}\right) f(\phi_i) g(\phi_j) \\ \times \left\{1 + \sum_{r\neq 0} g_r{}^{|S_1|}(\beta) e^{ir(B_\alpha + \overline{B_{\bar{\alpha}}})} e^{-ir\phi_i}\right\} \\ \times \left\{1 + \sum_{r'\neq 0} g_{r'}{}^{|D_F|}(\beta) e^{ir'(\phi_i - \phi_j)}\right\} \\ \times \left\{1 + \sum_{r''\neq 0} g_{r''}{}^{|S_2|}(\beta) e^{ir''(B_{\alpha''} + \overline{B_{\bar{\alpha}''}})} e^{ir''\phi_j}\right\}\end{aligned} \tag{7.6}$$

Note that we cannot yet carry out the integrals over the boundary links since B_n and $\overline{B_n}$ are not in general free variables but are constrained by the boundary conditions which have yet to be specified.

33. Infinite Volume Limit

In taking the infinite volume limit we will assume that both the lattice size and the distance between a support link and the boundary grow to infinity. This implies

$$|L| \longrightarrow \infty \qquad |S| \longrightarrow \infty \qquad |D_B| \longrightarrow \infty$$

although D_F in general will remain finite.

Also note that

$$|g_r(\beta)e^{ir\Lambda}| < 1 \qquad \forall \Lambda \in \Re, \qquad r \neq 0$$

We will assume for the moment that

$$\lim_{n\to\infty} \sum_{r\neq 0} g_r^n(\beta)e^{ir\Lambda} = 0$$

The infinite volume limits we require are then

$$\lim_{|L|\to\infty} Z_G = e^{-\beta|L|}{I_0}^{|L|} \int_{-\pi}^{\pi} \prod_{n=1}^{2N} \left(\frac{dB_n}{2\pi}\right)\left(\frac{d\overline{B_n}}{2\pi}\right)$$

$$= e^{-\beta|L|}{I_0}^{|L|}$$

$$\lim_{|L|,|S_1|,|S_2|\to\infty} \langle f(\phi_i)\rangle = \frac{e^{-\beta|L|}{I_0}^{|L|}}{Z_G} \int_{-\pi}^{\pi} \prod_{n=1}^{2N} \left(\frac{dB_n}{2\pi}\right)\left(\frac{d\overline{B_n}}{2\pi}\right)\left(\frac{d\phi_i}{2\pi}\right) f(\phi_i) \tag{7.7}$$

$$= \int_{-\pi}^{\pi} \left(\frac{d\phi_i}{2\pi}\right) f(\phi_i)$$

$$\lim_{|L|,|S_1|,|S_2||D_B|\to\infty} \langle f(\phi_i)g(\phi_j)\rangle_B^{\pm} = \frac{e^{-\beta|L|}{I_0}^{|L|}}{Z_G} \int_{-\pi}^{\pi} \prod_{n=1}^{2N} \left(\frac{dB_n}{2\pi}\right)\left(\frac{d\overline{B_n}}{2\pi}\right) \times \int_{-\pi}^{\pi} \left(\frac{d\phi_i}{2\pi}\right)\left(\frac{d\phi_j}{2\pi}\right) f(\phi_i)g((\phi_j)$$

$$= \int_{-\pi}^{\pi} \left(\frac{d\phi_i}{2\pi}\right)\left(\frac{d\phi_j}{2\pi}\right) f(\phi_i)g(\phi_j)$$

$$\lim_{|L|\to\infty} \langle f(\phi_i)g(\phi_j)\rangle_F = \frac{e^{-\beta|L|}{I_0}^{|L|}}{Z_G} \int_{-\pi}^{\pi} \prod_{n=1}^{2N} \left(\frac{dB_n}{2\pi}\right)\left(\frac{d\overline{B_n}}{2\pi}\right)\left(\frac{d\phi_i}{2\pi}\right)\left(\frac{d\phi_j}{2\pi}\right) f(\phi_i)g(\phi_j) \times \left\{1 + \sum_{r'\neq 0} {g_{r'}}^{|D_F|}(\beta)e^{ir'(\phi_i-\phi_j)}\right\}$$

$$= \int_{-\pi}^{\pi} \left(\frac{d\phi_i}{2\pi}\right)\left(\frac{d\phi_j}{2\pi}\right) f(\phi_i)g(\phi_j)\left\{1 + \sum_{r'\neq 0} {g_{r'}}^{|D_F|}(\beta)e^{ir'(\phi_i-\phi_j)}\right\}$$

All three types of expectation value are therefore independent of the boundary conditions in the infinite volume limit.

34. Boundary Conditions

The integrals over the boundary links must now be eliminated. In view of the result obtained in the previous section, we are free to specify any boundary conditions; let us first select unrestricted periodic boundary conditions. This implies

$$\overline{B_n} = -B_n$$

Before proceeding further it will be convenient to modify our notation. A region R which contains boundary links may contain both a link B_n and its negatively oriented partner $\overline{B_n}$. Such pairs cancel under the assumption of periodic boundary conditions, leaving a set of unmatched links which we will denote by u. We therefore write

$$B_\alpha + \overline{B_\alpha} = (\pm B)_u$$

The set u may or may not be empty; if it is not, we will extract one link and write

$$(\pm B)_u = (\pm B)_v (\pm B_m)$$

In the case of the partition function the boundary is the whole lattice and there are no unmatched links; the general expression (7.3) therefore reduces to

$$\begin{aligned} Z_G &= e^{-\beta|L|} I_0{}^{|L|} \int_{-\pi}^{\pi} \prod_{n=1}^{2N} \left(\frac{dB_n}{2\pi}\right) \left(\frac{d\overline{B_n}}{2\pi}\right) \left\{1 + \sum_{r\neq 0} g_r{}^{|L|}(\beta)\right\} \\ &= e^{-\beta|L|} I_0{}^{|L|} \left\{1 + \sum_{r\neq 0} g_r{}^{|L|}(\beta)\right\} \end{aligned} \tag{7.8}$$

Next we note that an S-type region must contain at least one unmatched link - the boundary link in the same column (row) as its spacelike (timelike) support link. The one-point function (7.4) may therefore be written

$$\begin{aligned} \langle f(\phi_i)\rangle = \frac{e^{-\beta|L|} I_0{}^{|L|}}{Z_G} &\int_{-\pi}^{\pi} \prod_{n\in v} \left(\frac{dB_n}{2\pi}\right) \left(\frac{d\phi_i}{2\pi}\right) f(\phi_i) \\ \times \int_{-\pi}^{\pi} \left(\frac{dB_m}{2\pi}\right) &\left\{1 + \sum_{r\neq 0} g_r{}^{|S_1|}(\beta) e^{irB_v} e^{-ir\phi_i} e^{irB_m} + \sum_{r'\neq 0} g_{r'}{}^{|S_2|}(\beta) e^{-ir'B_v} e^{ir'\phi_i} e^{-ir'B_m} \right. \\ &\left. + \sum_{r\neq 0}\sum_{r'\neq 0} g_r{}^{|S_1|}(\beta) g_{r'}{}^{|S_2|}(\beta) e^{i(r-r')B_v} e^{i(r'-r)\phi_i} e^{i(r-r')B_m}\right\} \end{aligned}$$

Integrating over B_m yields

$$\begin{aligned}\langle f(\phi_i)\rangle &= \frac{e^{-\beta|L|}I_0{}^{|L|}}{Z_G}\int_{-\pi}^{\pi}\prod_{n\in v}\left(\frac{dB_n}{2\pi}\right)\left(\frac{d\phi_i}{2\pi}\right)f(\phi_i)\\ &\times\Bigg\{1+\sum_{r\neq 0}g_r{}^{|S_1|}(\beta)e^{irB_v}e^{-ir\phi_i}\delta_{r0}+\sum_{r'\neq 0}g_{r'}{}^{|S_2|}(\beta)e^{-ir'B_v}e^{ir'\phi_i}\delta_{r'0}\\ &\quad+\sum_{r\neq 0}\sum_{r'\neq 0}g_r{}^{|S_1|}(\beta)g_{r'}{}^{|S_2|}(\beta)e^{i(r-r')B_v}e^{i(r'-r)\phi_i}\delta_{rr'}\Bigg\}\\ &= \frac{e^{-\beta|L|}I_0{}^{|L|}}{Z_G}\int_{-\pi}^{\pi}\left(\frac{d\phi_i}{2\pi}\right)f(\phi_i)\Bigg\{1+\sum_{r\neq 0}g_r{}^{|L|}(\beta)\Bigg\}\\ &= \int_{-\pi}^{\pi}\left(\frac{d\phi_i}{2\pi}\right)f(\phi_i)\end{aligned}\tag{7.9}$$

This is identical to the infinite volume limit (7.7). We conclude that one point functions are independent of lattice size under periodic boundary conditions.

Turning next to the two-point function $\langle f(\phi_i)g(\phi_j)\rangle_F$, each S-type region again has an unmatched link, while the D_F-type region contains no boundary links. As before we expand (7.6) and integrate term by term over the unmatched link B_m. The linear terms yield

$$\int_{-\pi}^{\pi}\left(\frac{dB_m}{2\pi}\right)=1$$

$$\int_{-\pi}^{\pi}\left(\frac{dB_m}{2\pi}\right)\sum_{r\neq 0}g_r{}^{|S_1|}(\beta)e^{irB_v}e^{-ir\phi_i}e^{irB_m}=\sum_{r\neq 0}g_r{}^{|S_1|}(\beta)e^{irB_v}e^{-ir\phi_i}\delta_{r0}=0$$

$$\int_{-\pi}^{\pi}\left(\frac{dB_m}{2\pi}\right)\sum_{r'\neq 0}g_{r'}{}^{|D_F|}(\beta)e^{ir'(\phi_i-\phi_j)}=\sum_{r'\neq 0}g_{r'}{}^{|D_F|}(\beta)e^{ir'(\phi_i-\phi_j)}$$

$$\int_{-\pi}^{\pi}\left(\frac{dB_m}{2\pi}\right)\sum_{r''\neq 0}g_r''{}^{|S_2|}(\beta)e^{-ir''B_v}e^{ir''\phi_j}e^{-ir''B_m}=\sum_{r\neq 0}g_r''{}^{|S_2|}(\beta)e^{-ir''B_v}e^{ir''\phi_j}\delta_{r''0}=0$$

The quadratic terms give

$$\begin{aligned}&\int_{-\pi}^{\pi}\left(\frac{dB_m}{2\pi}\right)\sum_{r'\neq 0}\sum_{r\neq 0}g_r'{}^{|D_F|}(\beta)g_r{}^{|S_1|}(\beta)e^{irB_v}e^{i(r'-r)\phi_i}e^{-ir'\phi_j}e^{irB_m}\\ &\quad=\sum_{r'\neq 0}\sum_{r\neq 0}g_r'{}^{|D_F|}(\beta)g_r{}^{|S_1|}(\beta)e^{irB_v}e^{i(r'-r)\phi_i}e^{-ir'\phi_j}\delta_{r0}=0\end{aligned}$$

$$\int_{-\pi}^{\pi}\left(\frac{dB_m}{2\pi}\right)\sum_{r\neq 0}\sum_{r''\neq 0} g_r{}^{|S_1|}(\beta)g_r''{}^{|S_2|}(\beta)e^{i(r-r'')B_v}e^{-ir\phi_i}e^{ir''\phi_j}e^{i(r-r'')B_m}$$
$$=\sum_{r\neq 0}\sum_{r''\neq 0} g_r{}^{|S_1|}(\beta)g_r''{}^{|S_2|}(\beta)e^{i(r-r'')B_v}e^{-ir\phi_i}e^{ir''\phi_j}\delta_{rr''}$$
$$=\sum_{r\neq 0} g_r{}^{(|S_1|+|S_2|)}(\beta)e^{-ir(\phi_i-\phi_j)}$$

$$\int_{-\pi}^{\pi}\left(\frac{dB_m}{2\pi}\right)\sum_{r'\neq 0}\sum_{r''\neq 0} g_r'{}^{|D_F|}(\beta)g_r''{}^{|S_2|}(\beta)e^{ir''B_v}e^{i(r''-r')\phi_j}e^{ir'\phi_i}e^{ir''B_m}$$
$$=\sum_{r'\neq 0}\sum_{r''\neq 0} g_r'{}^{|D_F|}(\beta)g_r''{}^{|S_2|}(\beta)e^{ir''B_v}e^{i(r''-r')\phi_j}e^{ir'\phi_i}\delta_{r''0}=0$$

The cubic term gives

$$\int_{-\pi}^{\pi}\left(\frac{dB_m}{2\pi}\right)\sum_{r\neq 0}\sum_{r'\neq 0}\sum_{r''\neq 0} g_r{}^{|S_1|}(\beta)g_r'{}^{|D_F|}(\beta)g_r''{}^{|S_2|}(\beta)e^{i(r-r'')B_v}e^{i(r'-r)\phi_i}e^{i(r''-r')\phi_j}e^{i(r-r'')B_m}$$
$$=\sum_{r\neq 0}\sum_{r'\neq 0}\sum_{r''\neq 0} g_r{}^{|S_1|}(\beta)g_r'{}^{|D_F|}(\beta)g_r''{}^{|S_2|}(\beta)e^{i(r-r'')B_v}e^{i(r'-r)\phi_i}e^{i(r''-r')\phi_j}\delta_{rr''}$$
$$=\sum_{r\neq 0}\sum_{r'\neq 0} g_r{}^{|S_1|+|S_2|}(\beta)g_r'{}^{|D_F|}(\beta)e^{i(r'-r)(\phi_i-\phi_j)}$$

All surviving terms are independent of the remaining unmatched boundary links B_v, yielding the final result

$$\begin{aligned}\langle f(\phi_i)g(\phi_j)\rangle_F = \frac{e^{-\beta|L|}I_0{}^{|L|}}{Z_G}\int_{-\pi}^{\pi}\left(\frac{d\phi_i}{2\pi}\right)\left(\frac{d\phi_j}{2\pi}\right)f(\phi_i)g(\phi_j)\\ \times\Bigg\{1+\sum_{r\neq 0} g_r{}^{|D_F|}(\beta)e^{ir(\phi_i-\phi_j)}\\ +\sum_{r\neq 0} g_r{}^{(|S_1|+|S_2|)}(\beta)e^{-ir(\phi_i-\phi_j)}\\ +\sum_{r\neq 0}\sum_{r'\neq 0} g_r{}^{|S_1|+|S_2|}(\beta)g_{r'}{}^{|D_F|}(\beta)e^{i(r'-r)(\phi_i-\phi_j)}\Bigg\}\end{aligned}\tag{7.10}$$

Lastly we consider the two-point function $\langle f(\phi_i)g(\phi_j)\rangle_B$. Let us denote the sum of unmatched links in the S-type regions by B_u and $B_{u''}$, and the sum of unmatched links in the D_B-type region by $B_{u'}$. There are three distinct cases to consider:

(1) $B_u = B_vB_m$; $B_{u'}=0$; $B_{u''}=(-B_v)(-B_m)$

This situation arises when both support links are timelike (TT case)

(2) $B_u = B_v(B_m)$; $B_{u'}=B_{v'}(-B_m)(\pm B_n)$; $B_{u''}=B_{v''}(\mp B_n)$

This occurs when one support link is timelike and the other is spacelike. (TS case)

(3) $B_u = B_v B_m; \qquad B_{u'} = B_{v'}(\pm B_n); \qquad B_{u''} = B_{v''}(-B_m)(\mp B_n)$

Here both support links are spacelike (SS case)

The TT case is identical to the calculation of $\langle f(\phi_i)g(\phi_j)\rangle_F$; note that ϕ_j can only occur with negative orientation on the perimeter of D_B.

$$\begin{aligned}\langle f(\phi_i)g(\phi_j)\rangle_{TT} = \frac{e^{-\beta|L|}I_0{}^{|L|}}{Z_G}\int_{-\pi}^{\pi}\left(\frac{d\phi_i}{2\pi}\right)\left(\frac{d\phi_j}{2\pi}\right)f(\phi_i)g(\phi_j)\\ \times\Bigg\{1+\sum_{r'\neq 0} g_{r'}{}^{|D_B|}(\beta)e^{ir'(\phi_i-\phi_j)}\\ +\sum_{r\neq 0} g_r{}^{(|S_1|+|S_2|)}(\beta)e^{-ir(\phi_i-\phi_j)}\\ +\sum_{r\neq 0}\sum_{r'\neq 0} g_r{}^{|S_1|+|S_2|}(\beta)g_{r'}{}^{|D_B|}(\beta)e^{i(r'-r)(\phi_i-\phi_j)}\Bigg\}\end{aligned} \tag{7.11}$$

Next we deal with the TS case; note that

$B_{u'} = B_{v'}(-B_m)(+B_n) \iff \phi_j$ is negatively oriented on the perimeter of D_B

$B_{u'} = B_{v'}(-B_m)(-B_n) \iff \phi_j$ is positively oriented on the perimeter of D_B

Proceeding as before we expand (7.5) and integrate term by term. This time the linear term is unity. The first quadratic term gives

$$\int_{-\pi}^{\pi}\left(\frac{dB_n}{2\pi}\right)\left(\frac{dB_m}{2\pi}\right)\sum_{r'\neq 0}\sum_{r\neq 0} g_{r'}{}^{|D_B|}(\beta)g_r{}^{|S_1|}(\beta)e^{irB_v}e^{ir'B'_v}e^{-ir\phi_i}e^{ir'(\phi_i\pm\phi_j)}e^{i(r'-r)B_m}e^{\mp ir'B_n}$$

$$=\int_{-\pi}^{\pi}\left(\frac{dB_m}{2\pi}\right)\sum_{r'\neq 0}\sum_{r\neq 0} g_{r'}{}^{|D_B|}(\beta)g_r{}^{|S_1|}(\beta)e^{irB_v}e^{ir'B_{v'}}e^{-ir\phi_i}e^{ir'(\phi_i\pm\phi_j)}e^{i(r'-r)B_m}\delta_{r'0}=0$$

The other quadratic terms similarly give zero.

The cubic term is

$$\int_{-\pi}^{\pi}\left(\frac{dB_m}{2\pi}\right)\left(\frac{dB_n}{2\pi}\right)\sum_{r\neq 0}\sum_{r'\neq 0}\sum_{r''\neq 0} g_r{}^{|S_1|}(\beta)g_{r'}{}^{|D_B|}(\beta)g_{r''}{}^{|S_2|}(\beta)$$
$$\times e^{irB_v}e^{ir'B_{v'}}e^{ir''B_{v''}}e^{-ir\phi_i}e^{ir'(\phi_i\mp\phi_j)}e^{\pm ir''\phi_j}e^{i(r-r')B_m}e^{\pm(r'-r'')B_n}$$

$$=\int_{-\pi}^{\pi}\left(\frac{dB_m}{2\pi}\right)\sum_{r\neq 0}\sum_{r'\neq 0} g_r{}^{|S_1|}(\beta)g_{r'}{}^{|D_B|+|S_2|}(\beta)e^{irB_v}e^{ir'(B_{v'}+B_{v''}}e^{-ir\phi_i}e^{ir'(\phi_i}e^{i(r-r')B_m}$$

$$=\sum_{r\neq 0} g_r{}^{|S_1|+|D_B|+|S_2|}(\beta)e^{ir(B_v+B_{v'}+B_{v''})}=\sum_{r\neq 0} g_r{}^{|L|}(\beta)$$

Overall we obtain

$$\begin{aligned}\langle f(\phi_i)g(\phi_j)\rangle_{TS} &= \frac{e^{-\beta|L|}I_0{}^{|L|}}{Z_G}\int_{-\pi}^{\pi}\left(\frac{d\phi_i}{2\pi}\right)\left(\frac{d\phi_j}{2\pi}\right)f(\phi_i)g(\phi_j)\left\{1+\sum_{r\neq 0}g_r{}^{|L|}(\beta)\right\} \\ &= \int_{-\pi}^{\pi}\left(\frac{d\phi_i}{2\pi}\right)\left(\frac{d\phi_j}{2\pi}\right)f(\phi_i)g(\phi_j)\end{aligned} \tag{7.12}$$

This is the same as the infinite volume expression for $\langle f(\phi_i)g(\phi_j)\rangle_B^{\pm}$ so that this class of expectation values is independent of lattice size.

The SS calculation is almost the same (with the minor modification that ϕ_j is always negatively oriented on the perimeter of D_B) and gives exactly the same result

$$\langle f(\phi_i)g(\phi_j)\rangle_{SS} = \int_{-\pi}^{\pi}\left(\frac{d\phi_i}{2\pi}\right)\left(\frac{d\phi_j}{2\pi}\right)f(\phi_i)g(\phi_j) \tag{7.13}$$

We note in passing that these expressions all coincide in the infinite volume limit with the results obtained in the previous section

35. Some Useful Expectation Values

The results obtained above can be used to calculate some standard expectation values explicitly for a *finite* lattice with periodic boundary conditions in axial gauge. Let us first consider functions of a single link variable.From (7.9) we have

$$\langle f(\phi_i)\rangle = \int_{-\pi}^{\pi}\left(\frac{d\phi_i}{2\pi}\right)f(\phi_i)$$

which yields immediately the following results:

$$\begin{aligned}\langle U_i\rangle = \left\langle U_i^{\dagger}\right\rangle &= 0 \\ \langle\phi_i\rangle &= 0 \\ \langle\phi_i^2\rangle &= \frac{\pi^2}{3}\end{aligned} \tag{7.14}$$

These expectation values are independent of lattice size.

Turning next to functions of two link variables we have from (7.6), (7.11), (7.12) and (7.13)

$$\langle f(\phi_i)g(\phi_j)\rangle_{SS} = \langle f(\phi_i)g(\phi_j)\rangle_{TS} = \int_{-\pi}^{\pi}\left(\frac{d\phi_i}{2\pi}\right)\left(\frac{d\phi_j}{2\pi}\right)f(\phi_i)g(\phi_j)$$

$$\langle f(\phi_i)g(\phi_j)\rangle_F = \langle f(\phi_i)g(\phi_j)\rangle_{TT} = \frac{e^{-\beta|L|}{I_0}^{|L|}}{Z_G}\int_{-\pi}^{\pi}\left(\frac{d\phi_i}{2\pi}\right)\left(\frac{d\phi_j}{2\pi}\right) f(\phi_i)g(\phi_j)$$
$$\times\left\{1+\sum_{r\neq 0} {g_r}^{|D_F|}(\beta)e^{ir(\phi_i-\phi_j)}\right.$$
$$+\sum_{r\neq 0} {g_r}^{(|S_1|+|S_2|)}(\beta)e^{-ir(\phi_i-\phi_j)}$$
$$\left.+\sum_{r\neq 0}\sum_{r'\neq 0} {g_r}^{|S_1|+|S_2|}(\beta){g_{r'}}^{|D_F|}(\beta)e^{i(r'-r)(\phi_i-\phi_j)}\right\}$$

Expectation values of the type $\langle f(\phi_i)g(\phi_j)\rangle_{TT}$, $\langle f(\phi_i)g(\phi_j)\rangle_{SS}$, $\langle f(\phi_i)g(\phi_j)\rangle_{TS}$, relate to functions defined on links at the boundary of the lattice; although they can be computed from the expressions above, it is links of the type $\langle f(\phi_i)g(\phi_j)\rangle_{FF}$ that are of real interest.
Let us first calculate the expectation value of the product of two link variables

$$\left\langle U_i U_j^\dagger\right\rangle_F = \frac{e^{-\beta|L|}{I_0}^{|L|}}{Z_G}\left\{\int_{-\pi}^{\pi}\left(\frac{d\phi_i}{2\pi}\right)\left(\frac{d\phi_j}{2\pi}\right)e^{i\phi_i}e^{-i\phi_j}\right.$$
$$+\int_{-\pi}^{\pi}\left(\frac{d\phi_i}{2\pi}\right)\left(\frac{d\phi_j}{2\pi}\right)\sum_{r\neq 0} {g_r}^{|D_F|}(\beta)e^{i(r+1)\phi_i}e^{-i(r+1)\phi_j}$$
$$+\int_{-\pi}^{\pi}\left(\frac{d\phi_i}{2\pi}\right)\left(\frac{d\phi_j}{2\pi}\right)\sum_{r\neq 0} {g_r}^{(|S_1|+|S_2|)}(\beta)e^{-i(r-1)\phi_i}e^{i(r-1)\phi_j}$$
$$\left.+\int_{-\pi}^{\pi}\left(\frac{d\phi_i}{2\pi}\right)\left(\frac{d\phi_j}{2\pi}\right)\sum_{r\neq 0}\sum_{r'\neq 0} {g_r}^{|S_1|+|S_2|}(\beta){g_{r'}}^{|D_F|}(\beta)e^{i(r'-r+1)(\phi_i-\phi_j)}\right\}$$

$$= \frac{e^{-\beta|L|}{I_0}^{|L|}}{Z_G}\left\{0+{g_{-1}}^{|D_F|}(\beta)+{g_1}^{(|S_1|+|S_2|)}(\beta)+\sum_{r\neq 0}\sum_{(r-1)\neq -1,0} {g_r}^{|S_1|+|S_2|}(\beta){g_{(r-1)}}^{|D_F|}(\beta)\right\}$$

$$= \frac{\left\{{g_1}^{|D_F|}(\beta)+{g_1}^{(|S_1|+|S_2|)}(\beta)+\sum_{r\neq 0}\sum_{(r-1)\neq -1,0} {g_r}^{|S_1|+|S_2|}(\beta){g_{(r-1)}}^{|D_F|}(\beta)\right\}}{\left\{1+\sum_{r\neq 0}{g_r}^{|L|}(\beta)\right\}} \tag{7.15}$$

where we have used (7.8) and the fact that ${g_{-1}}^{|D_F|} = {g_1}^{|D_F|}$.
The first term in (7.15) dominates for large lattices so that we have

$$\left\langle U_i U_j^\dagger\right\rangle_F \approx {g_1}^{|D_F|}(\beta) \qquad (\,|L|\gg|D_F|\,)$$

Of particular interest is the case $D_F = 1$. This quantity is numerically equal to the invariant plaquette in axial gauge giving

$$\langle U_p\rangle_F \approx g_1(\beta) \qquad (\,|L|\gg 1\,) \tag{7.16}$$

which is gauge invariant.
A similar calculation gives

$$\langle U_i U_j \rangle_F = \left\langle U_i^\dagger U_j^\dagger \right\rangle_F = 0$$

With these in hand, we have directly

$$\langle (U_i - 1)(U_j - 1) \rangle_F = \left\langle (U_i^\dagger - 1)(U_j^\dagger - 1) \right\rangle_F = 1$$

$$\left\langle (U_i^\dagger - 1)(U_j - 1) \right\rangle_F = \left\langle (U_i - 1)(U_j^\dagger - 1) \right\rangle_F = 1 + g_1{}^{|D_F|}(\beta)$$

36. Axial Gauge with Zero Boundary Conditions

In this section we will compute the finite lattice expectation values for the plaquette and the square of a spacelike link in axial gauge with zero boundary conditions.
The general expression we require to compute the plaquette is given by (7.6)

$$\begin{aligned} \langle f(\phi_i) g(\phi_j) \rangle_F = \frac{e^{-\beta|L|} I_0{}^{|L|}}{Z_G} \int_{-\pi}^{\pi} \prod_{n=1}^{2N} \left(\frac{dB_n}{2\pi} \right) \left(\frac{d\overline{B_n}}{2\pi} \right) \left(\frac{d\phi_i}{2\pi} \right) \left(\frac{d\phi_j}{2\pi} \right) f(\phi_i) g(\phi_j) \\ \times \left\{ 1 + \sum_{r \neq 0} g_r{}^{|S_1|}(\beta) e^{ir(B_\alpha + \overline{B_{\bar{\alpha}}})} e^{-ir\phi_i} \right\} \\ \times \left\{ 1 + \sum_{r' \neq 0} g_{r'}{}^{|D_F|}(\beta) e^{ir'(\phi_i - \phi_j)} \right\} \\ \times \left\{ 1 + \sum_{r'' \neq 0} g_{r''}{}^{|S_2|}(\beta) e^{ir''(B_{\alpha''} + \overline{B_{\bar{\alpha}''}})} e^{ir''\phi_j} \right\} \end{aligned} \tag{7.17}$$

Setting

$$B_\alpha = \overline{B_{\bar{\alpha}}} = 0$$

and carrying out the boundary integrals yields

$$\begin{aligned} \langle f(\phi_i) g(\phi_j) \rangle_F = \frac{1}{1 + \sum_{r \neq 0} g_r(\beta)^{|L|}} \int_{-\pi}^{\pi} \left(\frac{d\phi_i}{2\pi} \right) \left(\frac{d\phi_j}{2\pi} \right) f(\phi_i) g(\phi_j) \\ \times \left\{ 1 + \sum_{r \neq 0} g_r{}^{|S_1|}(\beta) e^{-ir\phi_i} \right\} \\ \times \left\{ 1 + \sum_{r' \neq 0} g_{r'}{}^{|D_F|}(\beta) e^{ir'(\phi_i - \phi_j)} \right\} \\ \times \left\{ 1 + \sum_{r'' \neq 0} g_{r''}{}^{|S_2|}(\beta) e^{ir''\phi_j} \right\} \end{aligned} \tag{7.18}$$

This expression yields the plaquette if we set

$$f(\phi_i) = e^{i\phi_i}$$
$$g(\phi_j) = e^{-i\phi_j}$$
$$|D_F| = 1$$

Carrying out the integrations as before, we obtain

$$\langle U_p \rangle = \frac{g_1(\beta) + g_1^{|L|-1}}{1 + \sum_{r\neq 0} g_r(\beta)^{|L|}}$$

For large lattices, this reduces as expected to the same infinite volume limit as the plaquette calculated under periodic boundary conditions.

$$\lim_{|L|\to\infty} \langle U_p \rangle = g_1(\beta) \tag{7.19}$$

Next, we turn to the expectation value of the square of a link. According to (7.4), this is given, for arbitrary boundary conditions, by

$$\begin{aligned}\langle {\phi_i}^2 \rangle = \frac{e^{-\beta|L|} {I_0}^{|L|}}{Z_G} \int_{-\pi}^{\pi} \prod_{n=1}^{2N} \left(\frac{dB_n}{2\pi}\right)\left(\frac{d\overline{B_n}}{2\pi}\right)\left(\frac{d\phi_i}{2\pi}\right) {\phi_i}^2 \\ \times \left\{1 + \sum_{r\neq 0} {g_r}^{|S_1|}(\beta) e^{ir(B_\alpha + \overline{B_\alpha})} e^{-ir\phi_i}\right\} \\ \times \left\{1 + \sum_{r'\neq 0} {g_{r'}}^{|S_2|}(\beta) e^{ir'(B_{\alpha'} + \overline{B_{\alpha'}})} e^{ir'\phi_i}\right\}\end{aligned} \tag{7.20}$$

This reduces, in the case of zero boundary conditions, to

$$\begin{aligned}\langle {\phi_i}^2 \rangle = \frac{1}{1 + \sum_{r\neq 0} g_r(\beta)^{|L|}} \int_{-\pi}^{\pi} \left(\frac{d\phi_i}{2\pi}\right) {\phi_i}^2 \\ \times \left\{1 + \sum_{r\neq 0} {g_r}^{|S_1|}(\beta) e^{-ir\phi_i}\right\} \\ \times \left\{1 + \sum_{r'\neq 0} {g_{r'}}^{|S_2|}(\beta) e^{ir'\phi_i}\right\}\end{aligned}$$

Integrating this expression gives

$$\begin{aligned}\langle {\phi_i}^2 \rangle = \frac{\pi^2}{3} + \lim_{K\to\infty} \frac{4}{1 + 2\sum_{r=1}^{K} g_r(\beta)^{|L|}} \cdot \left\{\sum_{r=1}^{K} \frac{(-1)^r}{r^2} \left({g_r}^{|S_1|}(\beta) + {g_r}^{|S_2|}(\beta)\right)\right\} \\ + \lim_{K\to\infty} \frac{2}{1 + 2\sum_{r=1}^{K} g_r(\beta)^{|L|}} \left\{\sum_{\substack{r'=-K \\ r'\neq 0, r}}^{K} \sum_{\substack{r=-K \\ r\neq 0}}^{K} \frac{(-1)^{(r'-r)}}{(r'-r)^2} {g_r}^{|S_1|}(\beta) {g_r}^{|S_2|}(\beta)\right\}\end{aligned} \tag{7.21}$$

37. The Action In Feynman Gauge

The bare gauge action is given by

$$S_{bare} = \frac{1}{2g^2} \sum_{\underline{n}} \sum_{\mu,\nu} (1 - \cos \theta_{\mu\nu}(\underline{n})) \tag{7.22}$$

where $\theta_{\mu\nu}(\underline{n})$ is defined by

$$\theta_{\mu\nu}(\underline{n}) = \left(\partial^R_\nu \phi_\mu(\underline{n}) - \partial^R_\mu \phi_\nu(\underline{n})\right) \tag{7.23}$$

and the $\phi_\mu(\underline{n})$ are the usual angular field variables. The gauge is fixed by introducing an additional term into the action

$$S_{gf} = \frac{1}{2g^2} \sum_{\underline{n}} \left(\partial^L_\mu \phi_\mu(\underline{n})\right)^2$$

Let us also add a (gauge–dependent) mass term for reasons that will become apparent

$$S_m = \frac{1}{2g^2} \sum_{\underline{n}} \phi_\mu(\underline{n})\, m^2\, \phi_\mu(\underline{n}) \tag{7.24}$$

The full action is then the sum of these three components

$$S = S_{bare} + S_{gf} + S_m \tag{7.25}$$

38. Weak Coupling Expansion

The aim is to find an approximate expression for the propagator $\langle \phi_\mu(\underline{n}),\, \phi_\nu(\underline{m}) \rangle$

$$\langle \phi_\mu(\underline{n})\, \phi_\nu(\underline{m}) \rangle \frac{= \int [dU]\, \phi_\mu(\underline{n})\, \phi_\nu(\underline{m})\, e^{-S}}{\int [dU]\, e^{-S}}$$

If the coupling constant g is small, the weight factor e^{-S} will tend to suppress all contributions to the integral except those for which

$$\sum_{\underline{n}} \sum_{\mu,\nu} (1 - \cos \theta_{\mu\nu}(\underline{n})) \approx 0 \tag{7.26}$$

Note that

$$(1 - \cos \theta_{\mu\nu}(\underline{n})) \geq 0$$

so that (7.26) will be valid if

$$\theta_{\mu\nu}(\underline{n}) \approx 0 \quad \forall \underline{n}, \mu, \nu$$

Therefore, the cosine in (7.22) may be expanded to give an approximate version of the action, valid for weak coupling. Expanding as far as terms quadratic in the fields yields an approximate expression for the bare action

$$S_{bare} \approx \frac{1}{2g^2} \sum_{\underline{n}} \frac{1}{2} \theta_{\mu\nu}(\underline{n}) \theta_{\mu\nu}(\underline{n})$$

From the definition (7.23) we have

$$\sum_{\underline{n}} \theta_{\mu\nu}(\underline{n}) \theta_{\mu\nu}(\underline{n}) = \sum_{\underline{n}} 2 \left(\partial^R_\mu \phi_\nu(\underline{n})\right)^2 - 2 \left(\partial^R_\mu \phi_\nu(\underline{n})\right) \left(\partial^R_\nu \phi_\mu(\underline{n})\right)$$

This can be reduced to a more convenient form by making use of the identities (2.22).

$$\begin{aligned} \sum_{\underline{n}} \theta_{\mu\nu}(\underline{n})\, \theta_{\mu\nu}(\underline{n}) &= -\sum_{\underline{n}} 2\, \phi_\nu(\underline{n})\, \partial^L_\mu \partial^R_\mu \phi_\nu(\underline{n}) - 2\, \phi_\nu(\underline{n})\, \partial^L_\mu \partial^R_\nu \phi_\mu(\underline{n}) \\ &= -2 \sum_{\underline{n}} \phi_\nu(\underline{n}) \left(\delta_{\mu\nu}\, \nabla^2 - \partial^L_\mu\, \partial^R_\nu\right) \phi_\mu(\underline{n}) \end{aligned}$$

Thus the bare action can be written

$$S_{bare} = -\frac{1}{2g^2} \sum_{\underline{n}} \phi_\nu(\underline{n}) \left(\delta_{\mu\nu}\, \nabla^2 - \partial^L_\mu\, \partial^R_\nu\right) \phi_\mu(\underline{n})$$

Turning next to the gauge term, we have

$$\begin{aligned} S_g &= \frac{1}{2g^2} \sum_{\underline{n}} \partial^L_\nu \phi_\nu(\underline{n})\, \partial^L_\mu \phi_\mu(\underline{n}) \\ &= \frac{-1}{2g^2} \sum_{\underline{n}} \phi_\nu(\underline{n})\, \partial^R_\nu \partial^L_\mu \phi_\mu(\underline{n}) \end{aligned}$$

Lastly, the mass term gives

$$S_m = \frac{1}{2g^2} \sum_{\underline{n}} \phi_\nu(\underline{n}) \delta_{\mu\nu} m^2 \phi_\mu(\underline{n})$$

The full action is therefore (up to terms quadratic in the fields)

$$\begin{aligned} S &\approx -\sum_{\underline{n}} \phi_\nu(\underline{n}) \left(\frac{1}{2g^2} (\delta_{\mu\nu} \left(\nabla^2 - m^2\right))\right) \phi_\mu(\underline{n}) \\ &= -\sum_{\underline{n},\underline{m}} \phi_\nu(\underline{n}) \left(\frac{1}{2g^2} \delta_{\underline{n}\underline{m}} (\delta_{\mu\nu} \left(\nabla^2 - m^2\right))\right) \phi_\mu(\underline{m}) \qquad (7.27) \\ &= -\sum_{\underline{n},\underline{m}} \phi_\nu(\underline{n})\, M_{\mu\nu}(\underline{n}, \underline{m}) \phi_\mu(\underline{m}) \end{aligned}$$

The propagator we require is then given by

$$\langle \phi_\nu(\underline{n}) \, , \, \phi_\mu(\underline{m}) \rangle = M^{-1}_{\mu\nu}(\underline{n}, \underline{m})$$

The operator M is most easily inverted in momentum space where it is diagonal. Let us therefore rewrite (7.27), inserting the Fourier transforms of $\phi_\nu(\underline{n})$ and $\phi_\mu(\underline{m})$

$$S(\underline{k}, \underline{k}') = \frac{-1}{N^4} \sum_{\underline{k},\underline{k}'} \sum_{\underline{n},\underline{m}} \phi_\nu(\underline{k}) e^{-i\underline{k}.\underline{n}} \left(\frac{1}{2g^2} \delta_{\underline{n}\underline{m}} (\delta_{\mu\nu} (\nabla^2 - m^2)) \right) \phi_\mu(\underline{k}') e^{-i\underline{k}'.\underline{m}}$$

Carrying out the sum over $\underline{m}$ yields

$$S(\underline{k}, \underline{k}') = \frac{-1}{N^4} \sum_{\underline{k},\underline{k}'} \sum_{\underline{n},\underline{m}} \phi_\nu(\underline{k}) e^{-i\underline{k}.\underline{n}} \phi_\mu(\underline{k}') \left(\frac{1}{2g^2} \delta_{\mu\nu} (\nabla^2 - m^2)) \right) e^{-i\underline{k}'.\underline{n}}$$

Now

$$\begin{aligned} \nabla^2 e^{-i\underline{k}'.\underline{n}} &= e^{-\underline{k}'.\underline{n}} \left(\sum_\alpha e^{ik'_\alpha} + e^{-ik'_\alpha} - 2 \right) = e^{-i\underline{k}'.\underline{n}} \left(2 \sum_\alpha \cos k'_\alpha - 1 \right) \\ &= e^{-i\underline{k}'.\underline{n}} \left(2 \sum_\alpha (2 \cos^2 \frac{k'_\alpha}{2} - 1) - 1 \right) = e^{-i\underline{k}'.\underline{n}} \left(-4 \sum_\alpha \sin^2 \frac{k'_\alpha}{2} \right) \end{aligned}$$

The action thus reduces to

$$S(\underline{k}, \underline{k}') = \frac{1}{N^4} \sum_{\underline{k},\underline{k}'} \sum_{\underline{n}} \phi_\nu(\underline{k}) e^{-i(\underline{k}+\underline{k}').\underline{n}} \left(\frac{1}{2g^2} \delta_{\mu\nu} \right) \left(4 \sum_\alpha \sin^2 \frac{k'_\alpha}{2} + m^2 \right) \phi_\mu(\underline{k}')$$

Summing over the remaining site index gives

$$S(\underline{k}, \underline{k}') = \frac{1}{N^2} \sum_{\underline{k},\underline{k}'} \phi_\nu(\underline{k}) \delta_{\underline{k},-\underline{k}'} \left(\frac{1}{2g^2} \delta_{\mu\nu} \right) \left(4 \sum_\alpha \sin^2 \frac{k'_\alpha}{2} + m^2 \right) \phi_\mu(\underline{k}')$$

Lastly we sum over $\underline{k}'$ to give the final result

$$\begin{aligned} S(\underline{k}) &= \sum_{\underline{k}} \phi_\nu(\underline{k}) \left(\frac{1}{2g^2 N^2} \delta_{\mu\nu} \right) \left(4 \sum_\alpha \sin^2 \frac{k_\alpha}{2} + m^2 \right) \phi_\mu(-\underline{k}) \\ &= \sum_{\underline{k}} \phi_\nu(\underline{k}) M_{\mu\nu}(\underline{k}) \phi_\mu(-\underline{k}) \end{aligned} \tag{7.28}$$

The momentum space propagator $M^{-1}_{\mu\nu}(\underline{k})$ is then given by

$$\langle \phi_\nu(\underline{k}) \phi_\mu(-\underline{k}) \rangle = \frac{2g^2 N^2 \delta_{\mu\nu}}{4 \sum_\alpha \sin^2 \frac{k_\alpha}{2} + m^2} \tag{7.29}$$

That is, we have

$$M_{\mu\alpha}(\underline{k})\, M^{-1}_{\alpha\nu}(\underline{k}) = \delta_{\mu\nu}$$

The position space representation of the propagator can now be found by inserting the Fourier transforms of $\phi_\nu(\underline{k})$ and $\phi_\mu(-\underline{k})$ into (7.28).

$$\begin{aligned} S &= \sum_{\underline{m},\underline{n}} \phi_\nu(\underline{m}) \sum_{\underline{k}} M_{\mu\nu}(\underline{k})\, e^{\underline{k}.(\underline{m}-\underline{n})} \phi_\mu(\underline{n}) \\ &= \sum_{\underline{m},\underline{n}} \phi_\nu(\underline{m}) M_{\mu\nu}(\underline{m},\underline{n}) \phi_\mu(\underline{n}) \end{aligned}$$

The propagator is then given by

$$\langle \phi_\nu(\underline{m}) \phi_\mu(\underline{n}) \rangle = M^{-1}_{\mu\nu}(\underline{m},\underline{n}) = \left(\sum_{\underline{k}} M_{\mu\nu}(\underline{k})\, e^{\underline{k}.(\underline{m}-\underline{n})} \right)^{-1}$$

This inverse can be written down explicitly:

$$A_{\alpha\nu}(\underline{n},\underline{p}) = \frac{1}{N^4} \sum_{\underline{j}} M^{-1}_{\alpha\mu}(\underline{j}) e^{-i\underline{j}.(\underline{p}-\underline{m})}$$

as can be verified by direct multiplication

$$\begin{aligned} M^{-1}_{\nu\alpha}(\underline{m},\underline{n})\, A_{\alpha\mu}(\underline{n},\underline{p}) &= \frac{1}{N^4} \sum_{\underline{n}} \sum_{\underline{j},\underline{k}} M_{\nu\alpha}(\underline{k})\, M^{-1}_{\alpha\mu}(\underline{j}) e^{i\underline{k}.\underline{m}} e^{-i\underline{j}.\underline{p}} ei(\underline{k}-\underline{j}).\underline{n} \\ &= \frac{1}{N^2} \sum_{\underline{j},\underline{k}} M_{\nu\alpha}(\underline{k})\, M^{-1}_{\alpha\mu}(\underline{j}) e^{i\underline{k}.\underline{m}} e^{-i\underline{j}.\underline{p}} \delta_{\underline{j}\underline{k}} \\ &= \frac{1}{N^2} \sum_{\underline{k}} M_{\nu\alpha}(\underline{k})\, M^{-1}_{\alpha\mu}(\underline{k}) e^{i\underline{k}.(\underline{m}-\underline{p})} \\ &= M_{\nu\alpha}(\underline{k})\, M^{-1}_{\alpha\mu}(\underline{k}) \delta_{\underline{m}\underline{p}} \\ &= \delta_{\mu\nu} \delta_{\underline{m}\underline{p}} \end{aligned}$$

The final result for the propagator in position space at weak coupling is

$$\langle \phi_\nu(\underline{m}) \phi_\mu(\underline{n}) \rangle = \frac{2g^2}{N^2} \sum_{\underline{k}} \frac{\delta_{\mu\nu}\, e^{-i\underline{k}.(\underline{m}-\underline{n})}}{4 \sum_\alpha \sin^2 \frac{k_\alpha}{2} + m^2}$$

In particular, if $\mu = \nu$ and $\underline{m} = \underline{n}$ we obtain

$$\langle \phi^2_\nu(\underline{n}) \rangle = \frac{2g^2}{N^2} \sum_{\underline{k}} \frac{1}{4 \sum_\alpha \sin^2 \frac{k_\alpha}{2} + m^2}$$

The reason for adding the mass term (7.24) to the action is now clear—it serves to suppress the the infra–red divergence at $\underline{k} = 0$.

§39. The Feynman Propagator with Zero Boundary Conditions

39. The Feynman Propagator with Zero Boundary Conditions

The infra-red divergence in the Feynman propagator can be removed by imposing zero boundary conditions on the lattice.
The action (without the mass term) is given in position space by (7.27)

$$S \approx -\sum_{\underline{n},\underline{m}} \phi_\nu(\underline{n}) \left(\frac{1}{2g^2}\, \delta_{\underline{n}\underline{m}}\, \delta_{\mu\nu}\, \nabla^2 \right) \phi_\mu(\underline{m})$$

As before, the operator is inverted by transforming to momentum space. Using the Fourier transform (2.31), appropriate for zero boundary conditions, we obtain

$$\begin{aligned} S(\underline{p},\underline{p}') = \frac{-1}{N^4} \sum_{\underline{p},\underline{p}' \neq \underline{0}} \sum_{\underline{n},\underline{m}} & \phi_\nu(\underline{p}) \left(e^{-i\underline{p}.\underline{n}} - (-1)^{(\sum_\alpha p_\alpha)} \right) \\ & \times \left(\frac{1}{2g^2}\, \delta_{\underline{n}\underline{m}}\, \delta_{\mu\nu}\, \nabla^2 \right) \\ & \times \phi_\mu(\underline{p}') \left(e^{-i\underline{p}'.\underline{m}} - (-1)^{(\sum_\beta p_\beta')} \right) \end{aligned}$$

$$\begin{aligned} = \frac{-1}{N^4} \sum_{\underline{p},\underline{p}' \neq \underline{0}} \sum_{\underline{n}} & \phi_\nu(\underline{p}) \left(e^{-i\underline{p}.\underline{n}} - (-1)^{(\sum_\alpha p_\alpha)} \right) \\ & \times \left(\frac{1}{2g^2}\, \delta_{\mu\nu} \right) \\ & \times \phi_\mu(\underline{p}') e^{-i\underline{p}'.\underline{n}} \left(-4 \sum_\lambda \sin^2 \frac{k'_\lambda}{2} \right) \end{aligned}$$

$$\begin{aligned} = \frac{-1}{N^2} \sum_{\underline{p},\underline{p}' \neq \underline{0}} & \phi_\nu(\underline{p}) \left(\delta_{\underline{p},-\underline{p}'} - (-1)^{(\sum_\alpha p_\alpha)} \delta_{\underline{p}',\underline{0}} \right) \\ & \times \left(\frac{1}{2g^2}\, \delta_{\mu\nu} \right) \phi_\mu(\underline{p}') \left(-4 \sum_\lambda \sin^2 \frac{k'_\lambda}{2} \right) \end{aligned}$$

$$= \sum_{\underline{p} \neq \underline{0}} \phi_\nu(\underline{p}) \left(\frac{1}{2g^2 N^2}\, \delta_{\mu\nu} \right) \left(4 \sum_\lambda \sin^2 \frac{k'_\lambda}{2} \right) \phi_\mu(\underline{p}')$$

This is identical to the result obtained under the assumption of unrestricted periodic boundary conditions, except that the zero momentum mode is now explicitly excluded and no mass term is necessary.

8. Numerical Evaluation of Expectation Values

God made the integers, all else is the work of man.
– L. Kronecker

In this Chapter we commence the numerical investigation of pure gauge expectation values. The technique of Monte Carlo integration is introduced and the statistical analysis of the results is dicussed. As a test case we evaluate the expectation value of the plaquette. We demonstrate the agreement between the numerical results and the analytical prediction in the infinite volume limit and display explicitly the deviations arising from finite size effects.

40. Monte Carlo Integration

The expectation values obtained in the previous Chapter can also be found by approximate numerical evaluation. This serves as a check on the calculation and also as a validation of the numerical algorithm, which can then be used to evaluate gauge dependent quantities in other gauges.

The problem, then, is to obtain a numerical approximation to integrals of the type

$$\langle \mathcal{O} \rangle = \frac{\int_{configs} \mathcal{O}(U_c) e^{-\beta S(U_c)}}{\int_{configs} e^{-\beta S(U_c)}} \tag{8.1}$$

In principle, all that is necessary is to generate a random set v of configurations large enough to be representative of the whole space of configurations and to evaluate the expectation value on this subset:

$$\langle \mathcal{O} \rangle \approx \frac{\sum_v \mathcal{O}(U_c) e^{-\beta S(U_c)}}{\sum_v e^{-\beta S(U_c)}} \tag{8.2}$$

There are two practical difficulties with this *simple sampling* approach. Firstly, the integrand in (8.1) is a function of a large number of link variables. Indeed, on a two–dimensional lattice of size N the dimension of the space of configurations is $2N^2$. Secondly, the integral is not distributed uniformly throughout the configuration space but is strongly peaked around configurations close to the minimum of the action. Most configurations therefore contribute a negligible amount to the sum in (8.2).

For both these reasons, the number of configurations required to make v representative of the whole space is impracticably large. The naive simple sampling approach is therefore

inadequate and it is necessary to employ some variety of *importance sampling*; that is, to select a set of configurations w which reflect the Boltzmann weighting in (8.2).

To be more specific, suppose that the sample set w contains n_i configurations with action S_i and n_j configurations with action S_j. Then the set w should have the property that

$$\frac{n_i}{n_j} = \frac{e^{-\beta S_i}}{e^{-\beta S_j}} \tag{8.3}$$

If this condition is satisfied the required expectation value is given simply by

$$\langle \mathcal{O} \rangle \approx \frac{1}{|w|} \sum_{w} \mathcal{O}(U_c) \tag{8.4}$$

A simple algorithm for generating the set w is to start with some arbitrary configuration and generate each successive configuration C_{m+1} in w from the preceding one C_m according to the following rule:

1. Generate C_{m+1} from C_m by making a random change.
2. If $S_{m+1} < S_m$ add C_{m+1} to w.
3. If $S_{m+1} > S_m$, generate a random number p between 0 and 1. If $p < e^{-\beta(S_{m+1}-S_m)}$ add C_{m+1} to w. Otherwise discard C_{m+1}.

It is straightforward to show that the set of configurations generated in this way satisfies the condition (8.3). Consider two values of the action S_i and S_j such that $S_i < S_j$. Let the probability of moving from a configuration C_i with action S_i to a configuration C_j with action S_j be P_{ij}. The probability of the reverse transition is then P_{ji} and the corresponding transition rates are R_{ij} and R_{ji} respectively. Let the number of configurations with action S_i be N_i. Then

$$R_{ij} = N_i P_{ij}; \quad R_{ji} = N_j P_{ji}; \quad \text{(no summation implied)}$$

Now in equilibrium, $R_{ij} = R_{ji}$. In addition, the proposed algorithm ensures that

$$P_{ij} = e^{-\beta(S_j - S_i)}; \quad P_{ji} = 1;$$

Hence

$$N_i e^{-\beta(S_j - S_i)} = N_j \quad \Longrightarrow \quad \frac{N_i}{N_j} = \frac{e^{-\beta S_i}}{e^{-\beta S_j}}$$

as required.

Some comments on practicalities are in order here. In the first place Step 1 of the algorithm calls for a 'random change' to the current configuration. This may take the form of a change to a single link, some subset of links, or indeed every link in the lattice. In making this

change it is essential to ensure that the corresponding change in the action is not excessively large, or higher action configurations will almost never be accepted in Step 3. It is therefore usual to restrict the update to a single link at a time and to restrict the maximum possible change in this link to some fixed value or *step size.*

On the other hand a step size which is set too low will result in a very slow evolution of the system. The time to reach equilibrium will be correspondingly increased and a large number of configurations will be required to explore the whole configuration space. Even worse, the system may become trapped in a metastable equilibrium, near some local minimum of the action, from which it is unable to escape.

The optimum step size depends on the parameters of the simulation—in this case the operator being investigated and the value of β. There is no general prescription for determining this optimum and therefore no alternative to tuning by trial and error until a 'satisfactory' outcome is achieved. In practice an 'accept/reject' ratio of about 0.7 is usually acceptable.

The algorithm places no restriction on the initial configuration and therefore implicitly assumes that equilibrium can be reached from any starting configuration. It can be shown (see, for example, Montvay and Munster 1994) that this assumption is valid provided that the system is ergodic—that is, that any configuration can be reached from any other configuration in a finite number of steps. This question of ergodicity is quite subtle and it will be assumed here that ergodicity is satisfied for practical purposes if the step size is sufficiently small and the number of configurations in the sample sufficiently large. Of course the choice of the initial configuration will affect the time taken to reach equilibrium.

The approach to equilibrium is not a major factor in the type of simulation being considered here, the number of non–equilibrium configurations generally being very small compared with the total number of configurations in the sample.

A final point concerns the statistical independence of the configurations in the sample set w. Each configuration is generated from the preceding one and, in general, lies 'close' to it in the sense that the actions associated with the two configurations differ by a relatively small amount. The set of configurations forms a *Markov chain* with configurations close together in the chain exhibiting a positive statistical correlation. These correlations must be taken into account when performing any statistical analysis on w.

41. Statistics

With an appropriate sample w of configurations in hand, one may proceed to measure the mean value of any operator on the sample set, according to (8.4). This *sample mean* $\overline{\mathcal{O}}$ provides an approximation to the true expectation value $\langle \mathcal{O} \rangle$. Let us suppose for the moment

that all configurations in the sample are independent. The *sample variance* is defined by

$$\text{Var } \mathcal{O} = \frac{1}{N}\sum_{i=1}^{N}(\mathcal{O}_i - \overline{\mathcal{O}})^2 = \overline{(\mathcal{O} - \overline{\mathcal{O}})^2}$$

Here $N = |w|$, the number of configurations in w.
The set w is of course only one out of an infinite number of possible sets, each with its own sample mean and variance. These means are normally distributed around $\langle\mathcal{O}\rangle$ with variance

$$\text{Var } \overline{\mathcal{O}} = \frac{1}{(N-1)}\,\overline{(\mathcal{O} - \overline{\mathcal{O}})^2} \tag{8.5}$$

The *standard deviation in the mean* is defined as

$$\epsilon_m = \sqrt{\text{Var } \overline{\mathcal{O}}} \tag{8.6}$$

This quantity serves as an estimate of the error associated with the measurement of $\langle\mathcal{O}\rangle$. It is valid provided the configurations in w are independent or *uncorrelated.* As we have seen, however, w is actually a Markov chain, with neighbouring configurations having a significant interdependence or *autocorrelation.* The variance as computed from (8.5) will underestimate the error on such a set.
The degree of autocorrelation between configurations is measured by the *sample autocorrelation coefficient*

$$C_L = \frac{1}{\text{Var } \mathcal{O}}\sum_{i=1}^{N-L}(\mathcal{O}_i - \overline{\mathcal{O}})(\mathcal{O}_{i+L} - \overline{\mathcal{O}})$$

which is an estimator of the correlation between configurations separated by a distance or *lag* L in the Markov chain. It is normalised so that

$$\begin{aligned} C_L = 1 &\implies \text{complete correlation} \\ C_L = 0 &\implies \text{no correlation} \\ C_L = -1 &\implies \text{complete anticorrelation} \end{aligned}$$

It is possible to derive a corrected version of the error estimator (8.5) which takes the effect of autocorrelations into account. If, however, large sample sets can be generated at low computational cost, it is preferable to simply select a subset of widely separated configurations for analysis.
In other words, if $C_L \approx 0$ for some value $L = L_0$, one simply selects a subset of the sample consisting of configurations separated by a lag L_0 and so forms a new, uncorrelated sample set. This is the approach that will be adopted in the following sections.

42. The Plaquette Without Gauge Fixing

In this section we will apply the techniques outlined in the preceding two sections to the computation of the value of the elementary plaquette for different values of β.

In some ways the whole process—generation of a configuration set and evaluation of the average plaquette—is completely straightforward, and it is therefore tempting to simply compute this quantity and compare it with the analytic value. This, however, yields no useful information so far as the computation of *unknown* quantities is concerned.

The purpose of this exercise is rather to illustrate with a concrete example some of the issues which arise with Monte Carlo calculations of this type and to determine the optimum parameters to use in subsequent computations.

An analytic expression for the value of an interior plaquette on a finite lattice follows from (7.15):

$$P_I = \frac{1}{\left\{1 + \sum_{r\neq 0} {g_r}^{|L|}(\beta)\right\}} \left\{ g_1(\beta) + {g_1}^{(|L|-1)}(\beta) + \sum_{r\neq 0} \sum_{(r-1)\neq -1,0} {g_r}^{|L|-1}(\beta) g_{(r-1)}(\beta) \right\} \tag{8.7}$$

where $|L|$ is the number of plaquettes in the lattice and

$$g_r(\beta) = \frac{I_r(\beta)}{I_0(\beta)}$$
$$|g_r(\beta)| < 1 \quad \forall r \neq 0\,;\, \beta > 0$$

Note that $\beta = 0$ constitutes a special case. Although simulations can be carried out at this value of β they are not especially useful in the context of a general analysis of the simulation algorithm for arbitrary β (for example, the accept/reject ratio is always 1). We will not therefore consider this case in the rest of the analysis.

The first step in conducting a numerical experiment of this type is to generate a set of configurations to analyse. Such a set may be constructed according to the prescription in Section (40). The action we require is the pure gauge action, given by

$$S = \sum_p 1 - \cos\theta_p \tag{8.8}$$

The update of a single link will only alter the values of the two plaquettes which share this link as a common boundary—θ_1 and θ_2, say. Under an update these plaquettes go to θ_1' and θ_2' respectively. The difference between the new action and the old action is

$$\Delta S = S' - S = (\cos\theta_1 + \cos\theta_2) - (\cos\theta_1' + \cos\theta_2')$$

According to the algorithm this change is accepted unconditionally if $\Delta S < 0$ and accepted with probability $e^{-\beta\Delta S}$ otherwise. Each new configuration is then generated from the previous one by sweeping through all the links in the lattice and attempting to update each one.

A separate set of configurations were generated in this way for each of the following numerical experiments. The usual starting configuration was one in which all links were set to unity, corresponding to a value of zero for the action (cold start) although randomised starting configurations (hot starts) are also considered below.

With a set of configurations in hand, the value of the quantity of interest (in this case the plaquette) can be computed and the accuracy of the calculation statistically analysed.

The effective sample size can be considerably increased by computing the *average* plaquette value over the lattice; that is, we will actually calculate

$$\langle P \rangle = \frac{1}{|L|} \sum_{i=0}^{|L|} P_i$$

Let us now consider in turn the factors which may affect the accuracy of the calculation and the reliability of the error estimate. In the following numerical experiments the Monte Carlo step is adjusted to make the accept/reject ratio about 0.7, unless otherwise stated. The step sizes required for different values of β are given in Figure (8.17)

β	step size	accept/reject
0.5	5.00	0.719
2.5	0.80	0.699
5.0	0.50	0.712
7.5	0.43	0.694
10.0	0.35	0.708
12.5	0.31	0.710
15.0	0.28	0.712
17.5	0.26	0.710
20.0	0.25	0.703

Figure 8.1: Monte Carlo steps and accept/reject ratios for different values of β

The most obvious consideration is the sample size. This is the size of the set w of configurations generated for the statistical analysis. In general only a subset of these configurations will be used in the analysis. The first z configurations generated before equilibrium has

been reached will be discarded, and a certain proportion of intermediate configurations will also be dropped to ensure that the remaining configurations are statistically independent. A small sample size will *ipso facto* yield a less accurate estimate. However it also has a further, less obvious disadvantage—the behaviour of the autocorrelation as a function of lag becomes less smooth. This effect is illustrated in Figure (8.2).

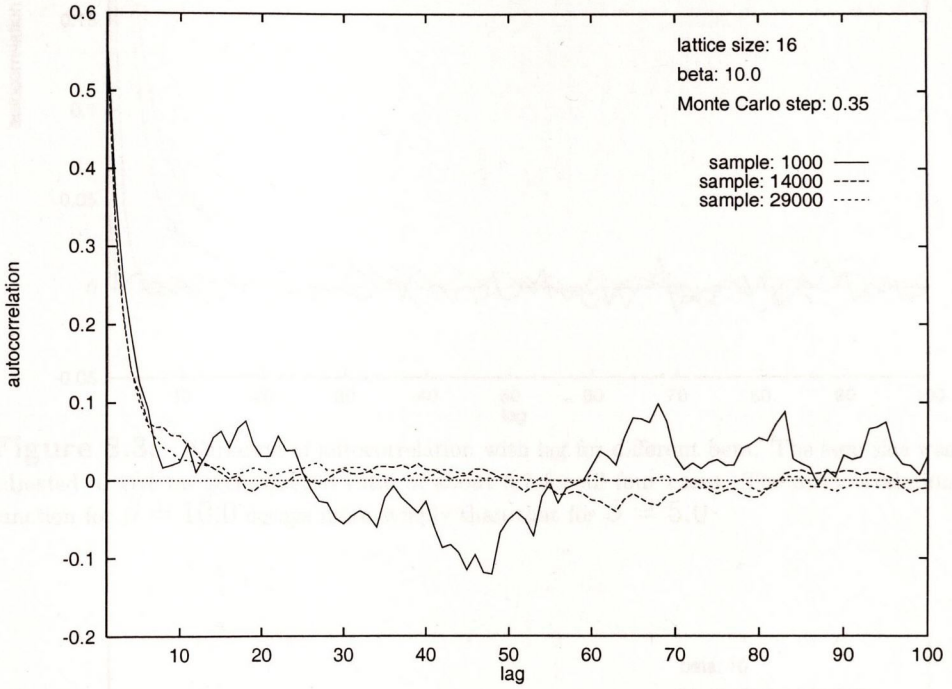

Figure 8.2: : Variation of autocorrelation with lag for different sample sizes. The first 1000 configurations have been dropped from the initial set $\mathcal{W}$ in each case.

A total sample size of 30,000 configurations (29,000 after the removal of the first 1000 configurations) gives adequate decorrelation behaviour and was used as a baseline in the following experiments except where otherwise stated.

Next, let us consider the effect of the value of β on the autocorrelation function. If the accept/reject ratio is to be kept constant, the step size must increase with decreasing β; the system therefore evolves more rapidly and configurations in the Markov chain should therefore decorrelate more rapidly. In other words we expect the autocorrelation function to decay more rapidly with decreasing β. The results of such an experiment are plotted in Figure (8.3). The expected behaviour is observed from $\beta = 0.5$ up to $\beta = 5.0$. The autocorrelation function for $\beta = 10.0$, however, decays *more* steeply than that for $\beta = 5.0$. The reasons for this behaviour are not clear.

The behaviour of the autocorrelation function with lattice size is shown in Figure (8.4). A slow increase in decay rate is observed as the lattice size increases.

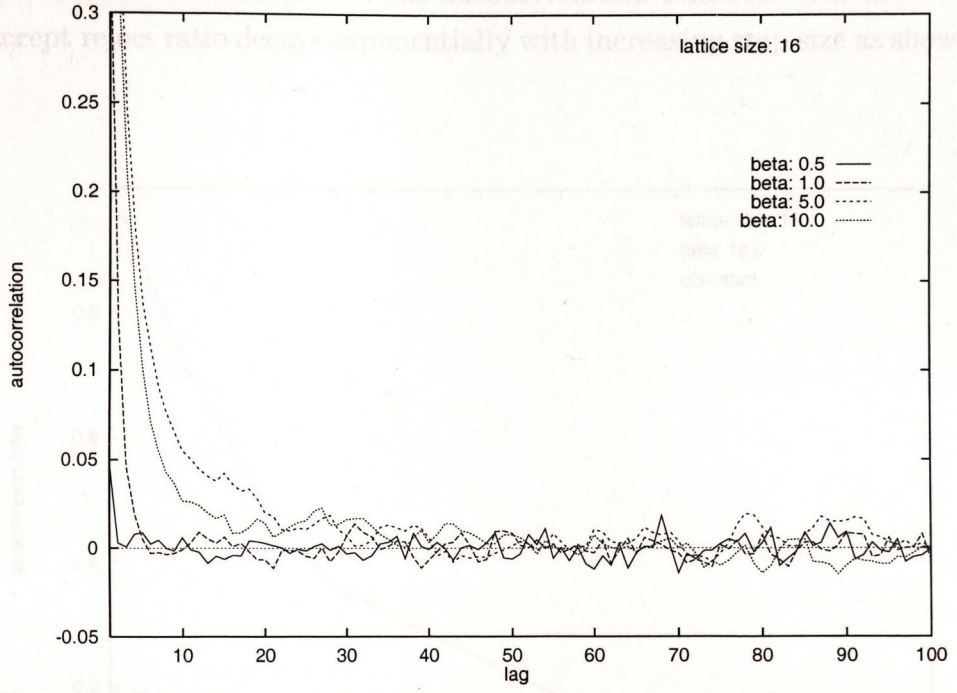

Figure 8.3: : Variation of autocorrelation with lag for different beta. The step size was adjusted to give an accept/reject ratio of about 0.7 for all four cases. The autocorrelation function for $\beta = 10.0$ decays more steeply than that for $\beta = 5.0$

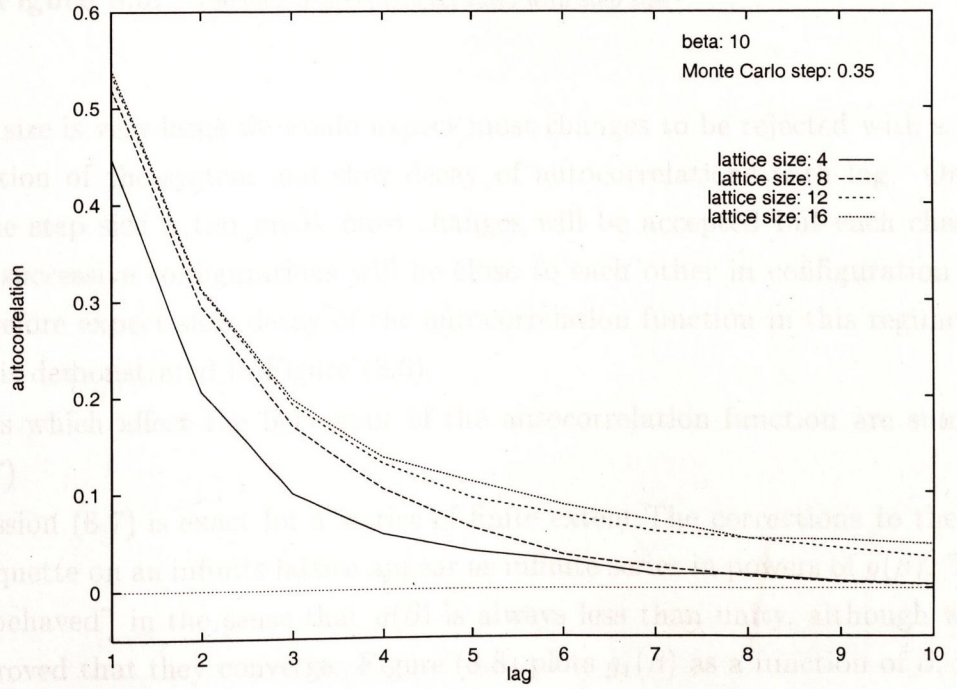

Figure 8.4: : Variation of autocorrelation with lag for different lattice sizes. A sample of 30,000 configurations was used in each case.

Let us next consider the behaviour of the autocorrelation function with Monte Carlo step size. The accept reject ratio decays exponentially with increasing step size as shown in Figure (8.6).

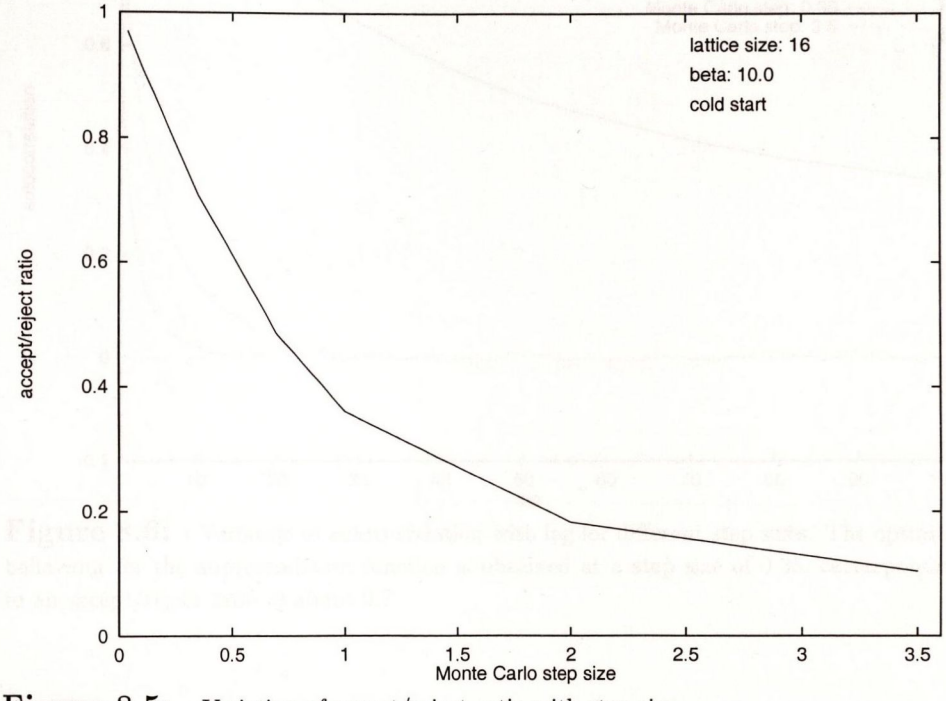

Figure 8.5: : Variation of accept/reject ratio with step size

If the step size is very large we would expect most changes to be rejected with a consequent slow evolution of the system and slow decay of autocorrelations with lag. On the other hand, if the step size is too small, most changes will be accepted but each change will be small and successive configurations will lie close to each other in configuration space. We would therefore expect slow decay of the autocorrelation function in this regime also. This behaviour is demonstrated in Figure (8.6).

The factors which affect the behaviour of the autocorrelation function are summarised in Figure (8.7)

The expression (8.7) is exact for a lattice of finite extent.The corrections to the expression for the plaquette on an infinite lattice appear as infinite series in powers of $g(\beta)$. These series are "well behaved" in the sense that $g(\beta)$ is always less than unity, although we have not formally proved that they converge. Figure (8.8) plots $g_1(\beta)$ as a function of β; we see that $g(\beta)$ decreases with β and may therefore expect the correction terms to disappear as $\beta \to 0$. Equation (8.7) also implies that the correction terms disappear as the lattice size tends to infinity, giving the usual infinite volume limit for the plaquette:

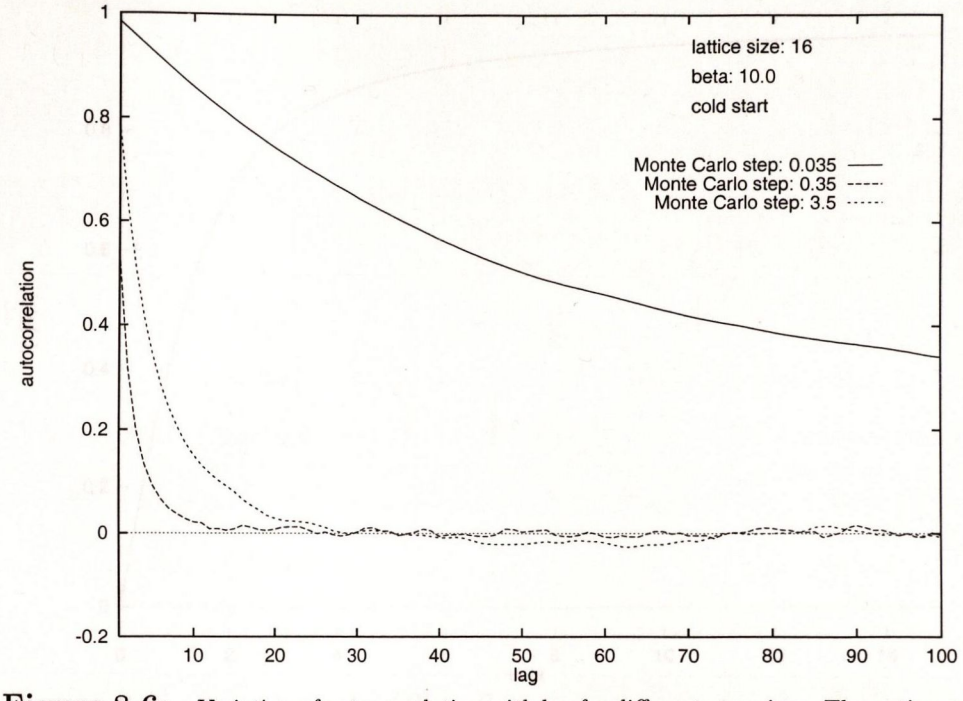

Figure 8.6: : Variation of autocorrelation with lag for different step sizes. The optimum behaviour for the autocorrelation function is obtained at a step size of 0.35, corresponding to an accept/reject ratio of about 0.7

Parameter	Decay rate	Smoothness
Sample size	Unaffected	Improves with increasing sample size
β	Best at intermediate values	Unaffected
Lattice size	Increases slowly with lattice size	Unaffected
Monte Carlo step	Best at values giving an accept/reject ratio of about 0.7	Unaffected

Figure 8.7: Behaviour of the autocorrelation function as different parameters are varied.

$$\lim_{N\to\infty} P_I = g_1(\beta)$$

It should be noted also that (8.7) applies to plaquettes in the *interior* of the lattice. On the other hand, all calculations so far have averaged over *all* the plaquettes in the lattice. In the absence of an exact expression for the boundary plaquettes it is not *a priori* clear how big an inaccuracy is thus introduced.

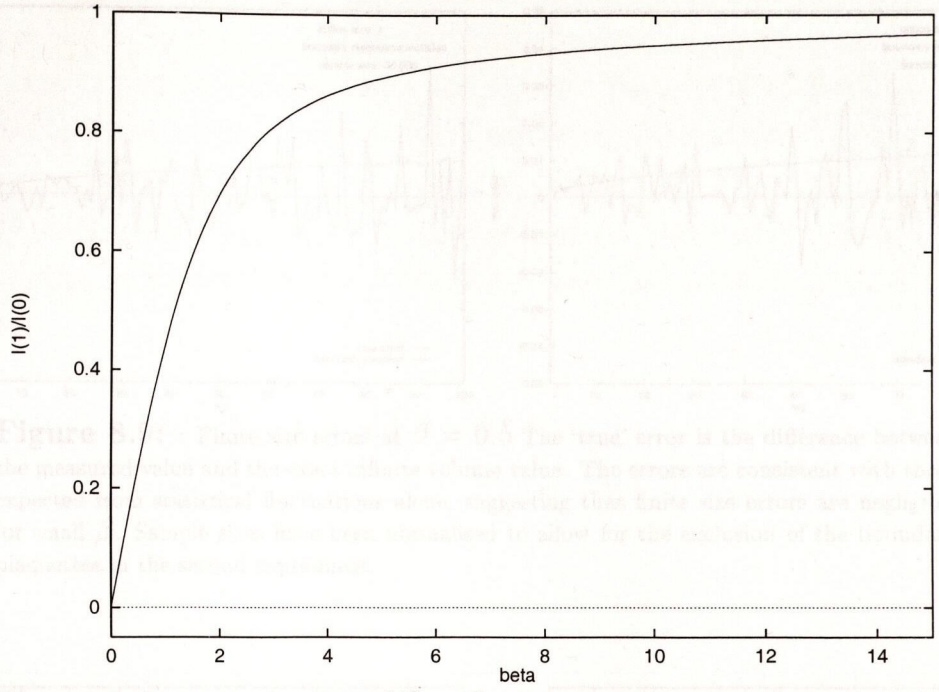

Figure 8.8: : Dependence of $g_1(\beta)$ on β

Figure (8.9) compares the measured difference between the computed value and the infinite volume analytic value with the predicted errors from statistical fluctuations. The computation was carried out on a 4×4 lattice with $\beta = 0.5$. The boundary plaquettes were included in the average in the first experiment and excluded in the second. In both cases the measured errors are consistent with those predicted from statistical fluctuations alone. This suggests firstly that finite size errors are negligible, even for very small lattices, provided β is small. Secondly, the results indicate that the boundary plaquette values do not differ significantly from those of the inner plaquettes at small β; indeed, on a 4×4 lattice there are eight boundary plaquettes and only one inner plaquette so that we are effectively measuring the mean value of the boundary plaquettes.

A different picture emerges when the experiment is repeated for large β. The first two diagrams in Figure (8.10) are the equivalent of those in Figure (8.9) with $\beta = 10.0$. The measured errors significantly exceed those predicted on the basis of statistical fluctuations alone. It is notable that the results are essentially the same irrespective of whether or not the boundary plaquettes are included, suggesting that the boundary plaquettes do not differ significantly in value from the interior plaquettes irrespective of the value of β. Nevertheless, this result may not continue to hold for expectation values other than that of the plaquette. Boundary links will therefore be excluded from subsequent computations unless otherwise stated.

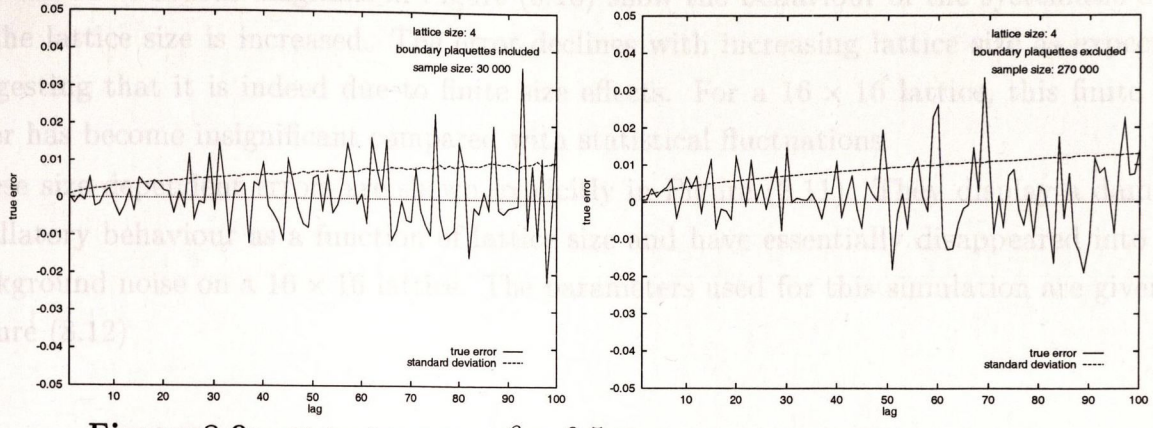

Figure 8.9: : Finite size errors at $\beta = 0.5$ The 'true' error is the difference between the measured value and the exact infinite volume value. The errors are consistent with those expected from statistical fluctuations alone, suggesting that finite size errors are negligible for small β. Sample sizes have been normalised to allow for the exclusion of the boundary plaquettes in the second experiment

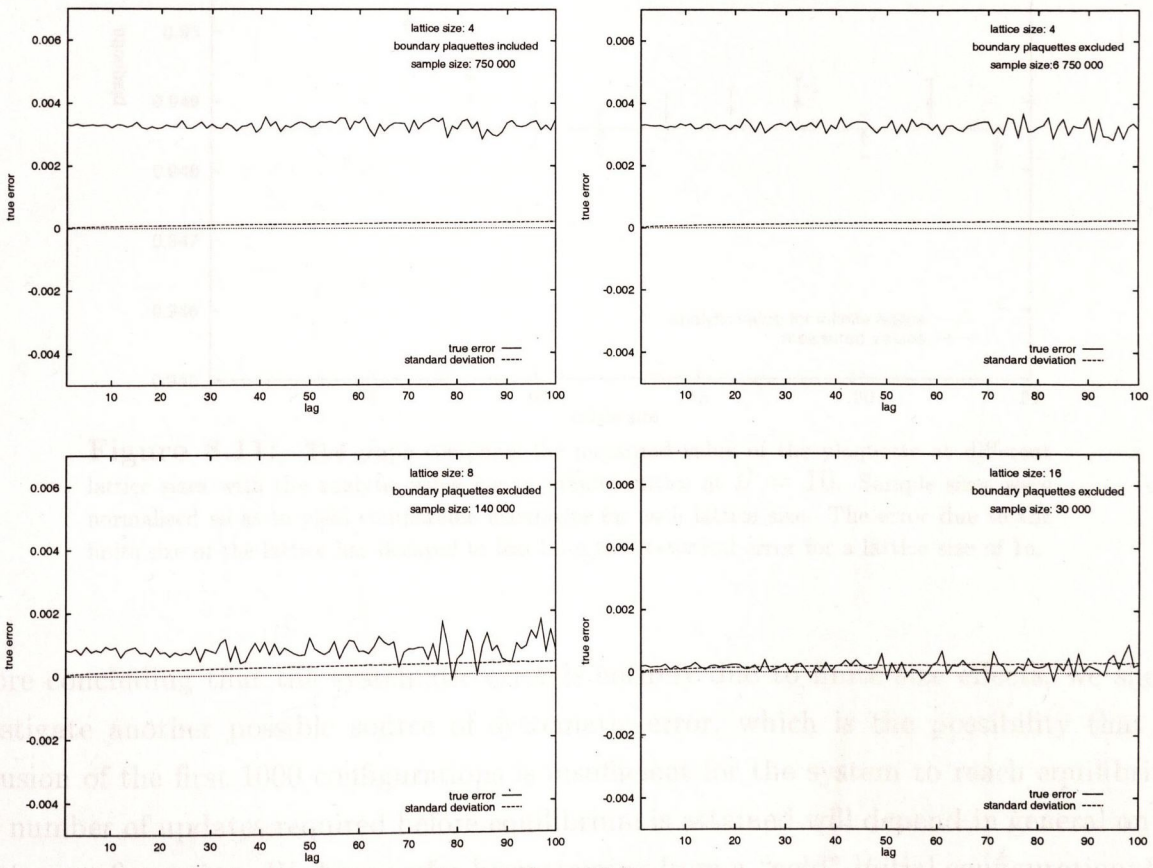

Figure 8.10: : Finite size errors at $\beta = 10.0$ A significant systematic error appears at this value of β. The error decreases with increasing lattice size. Sample sizes have been normalised to give the same scale on each diagram

The third and fourth diagrams in Figure (8.10) show the behaviour of the systematic error as the lattice size is increased. The error declines with increasing lattice size as expected, suggesting that it is indeed due to finite size effects. For a 16×16 lattice, this finite size error has become insignificant compared with statistical fluctuations.

These size dependent errors are shown explicitly in Figure (8.11). They display a damped oscillatory behaviour as a function of lattice size and have essentially disappeared into the background noise on a 16×16 lattice. The parameters used for this simulation are given in Figure (8.12)

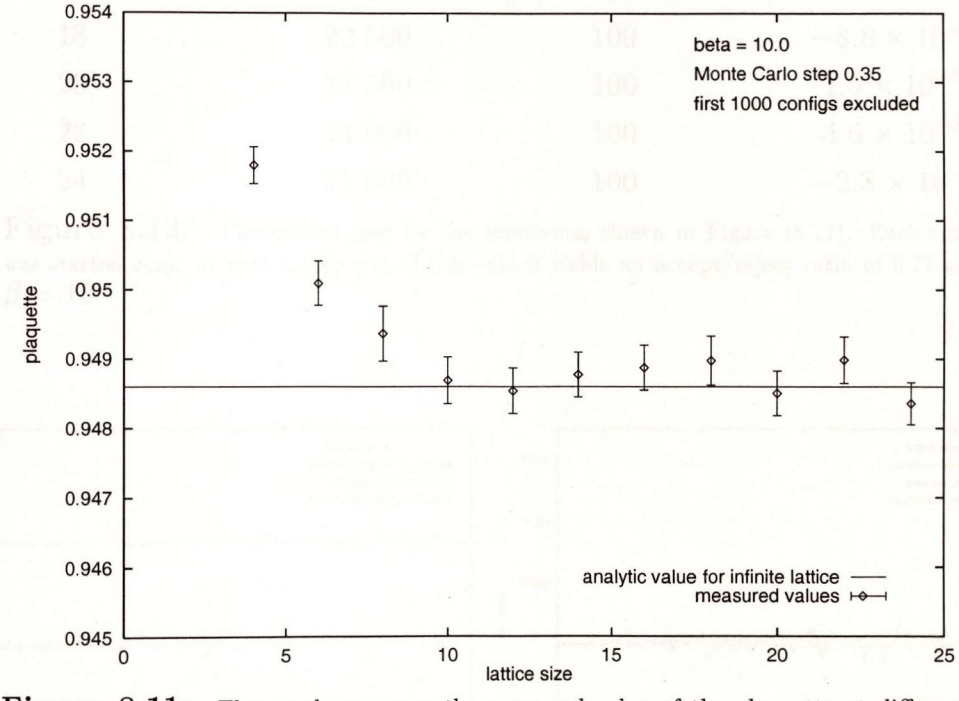

Figure 8.11: :The graph compares the measured value of the plaquette at different lattice sizes with the analytic value for an infinite lattice at $\beta = 10$. Sample sizes were normalised so as to yield comparable accuracies for each lattice size. The error due to the finite size of the lattice has decayed to less than the statistical error for a lattice size of 16.

Before concluding that the systematic error is entirely due to finite size effects, we should investigate another possible source of systematic error, which is the possibility that the exclusion of the first 1000 configurations is insufficient for the system to reach equilibrium. The number of updates required before equilibrium is attained will depend in general on the starting configuration. We have so far been starting from a "cold" initial configuration; that is one in which all links are set to zero.

Figure (8.13) repeats the first and last diagrams of Figure(8.10) with a larger set of initial configurations excluded. The results are unchanged, suggesting that 1000 updates are

lattice size	sample size	lag	autocorrelation
4	6 750 000	100	4.1×10^{-4}
6	550 000	100	1.7×10^{-3}
8	140 000	100	1.7×10^{-3}
10	100 000	100	-3.0×10^{-3}
12	62 000	100	-3.7×10^{-3}
14	42 000	100	-1.5×10^{-6}
16	30 000	100	7.6×10^{-3}
18	22 500	100	-8.8×10^{-3}
20	17 500	100	1.5×10^{-3}
22	14 000	100	4.6×10^{-3}
24	11 500	100	-2.3×10^{-2}

Figure 8.12: Parameters used for the simulation shown in Figure (8.11). Each run was started cold. at with a step size of 0.35 which yields an accept/reject ratio of 0.71 at $\beta = 10$

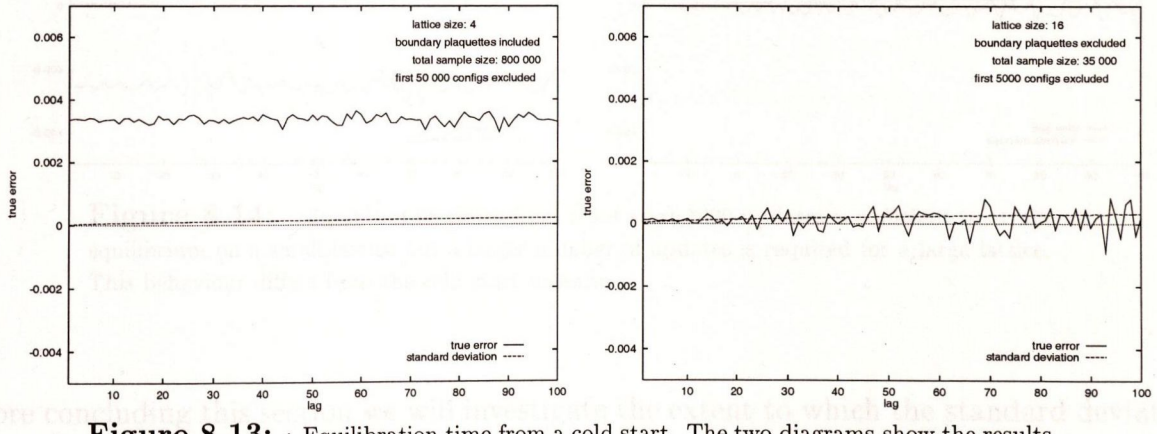

Figure 8.13: : Equilibration time from a cold start. The two diagrams show the results of repeating the first and fourth experiments in Figure (8.10) with a larger number of initial configurations excluded. The results are the same.

sufficient for the system to equilibrate from a cold start.

The same is *not* true for a "hot" start, in which the initial links are assigned random values. Comparison of Figure (8.14) with Figure (8.10) shows that identical results are obtained on a 4×4 lattice, irrespective of the initial configuration, if the first 1000 configurations are excluded. For the larger 16×16 lattice, however, an additional systematic error appears if the system is started hot, which is not present if it is started cold. This additional error

disappears if the number of initial configurations discarded is increased. We conclude that equilibration is significantly slowed down when starting from a hot initial configuration on a large lattice.

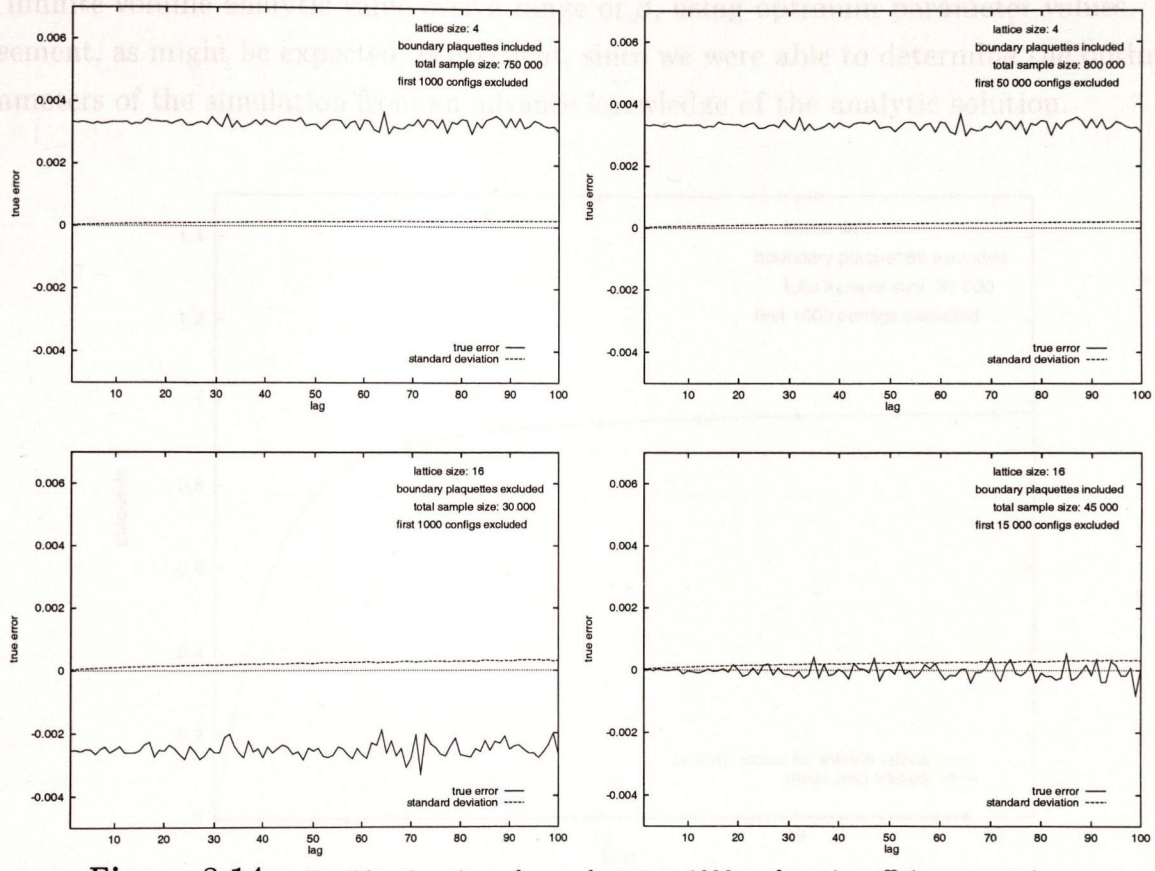

Figure 8.14: : Equilibration times from a hot start 1000 updates is sufficient to attain equilibrium on a small lattice but a larger number of updates is required for a large lattice. This behaviour differs from the cold start scenario.

Before concluding this section we will investigate the extent to which the standard deviation as defined in (8.6) provides a good estimate of the errors due to statistical fluctuations.In general, the standard deviation will underestimate the error as long as the autocorrelation function is significantly greater than zero, but should prove a good estimator when the correlation between successive configurations is small. Figure (8.15) compares the predicted errors with the measured errors; the step size has been set at a non–optimal value so that the autocorrelation function decays slowly.

The first point to note is that a systematic correlation error appears when the lag value is small. This error actually depends on the starting point of the simulation; it is positive if the system is started cold and negative if it is started hot.

Secondly, the standard deviation does underestimate the error for small lag values, as expected; moreover, in both hot and cold cases the standard deviation becomes a more accurate estimator as the autocorrelation function decreases.

Lastly, in Figure (8.16), we compare the measured value of the average plaquette against the infinite volume analytic value over a range of β, using optimum parameter values. The agreement, as might be expected, is excellent, since we were able to determine the optimum parameters of the simulation from an advance knowledge of the analytic solution.

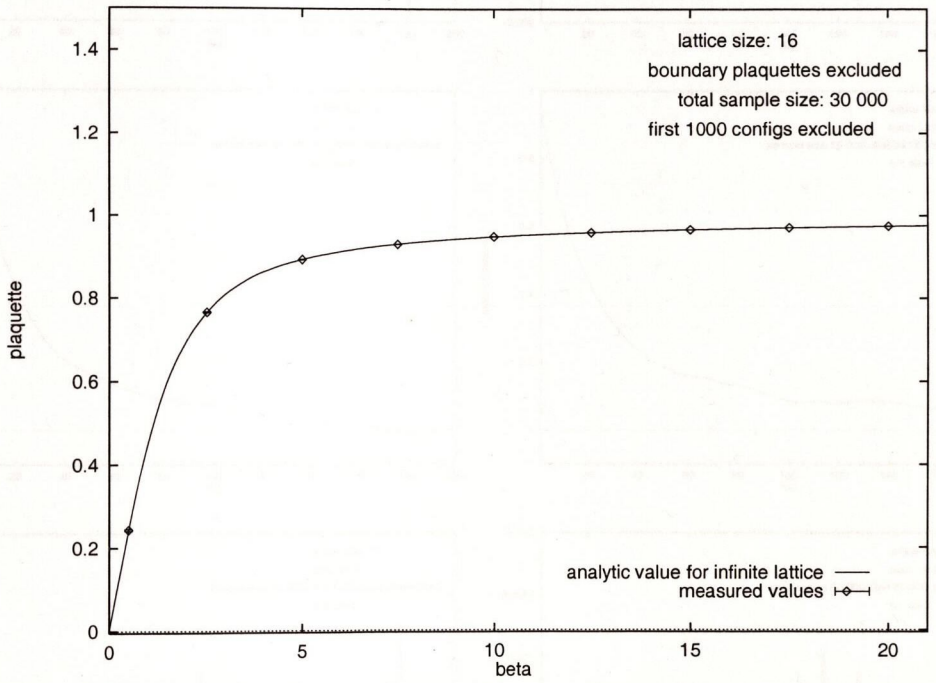

Figure 8.16: : Comparison of numerical and analytic results for the average plaquette value at different β. All simulations were started cold. The Monte Carlo step was chosen to make the accept/reject ratio approximately 0.7 at each value of β. The lag value chosen was 50 in each case; the corresponding values of the autocorrelation function are given in Figure (8.17)

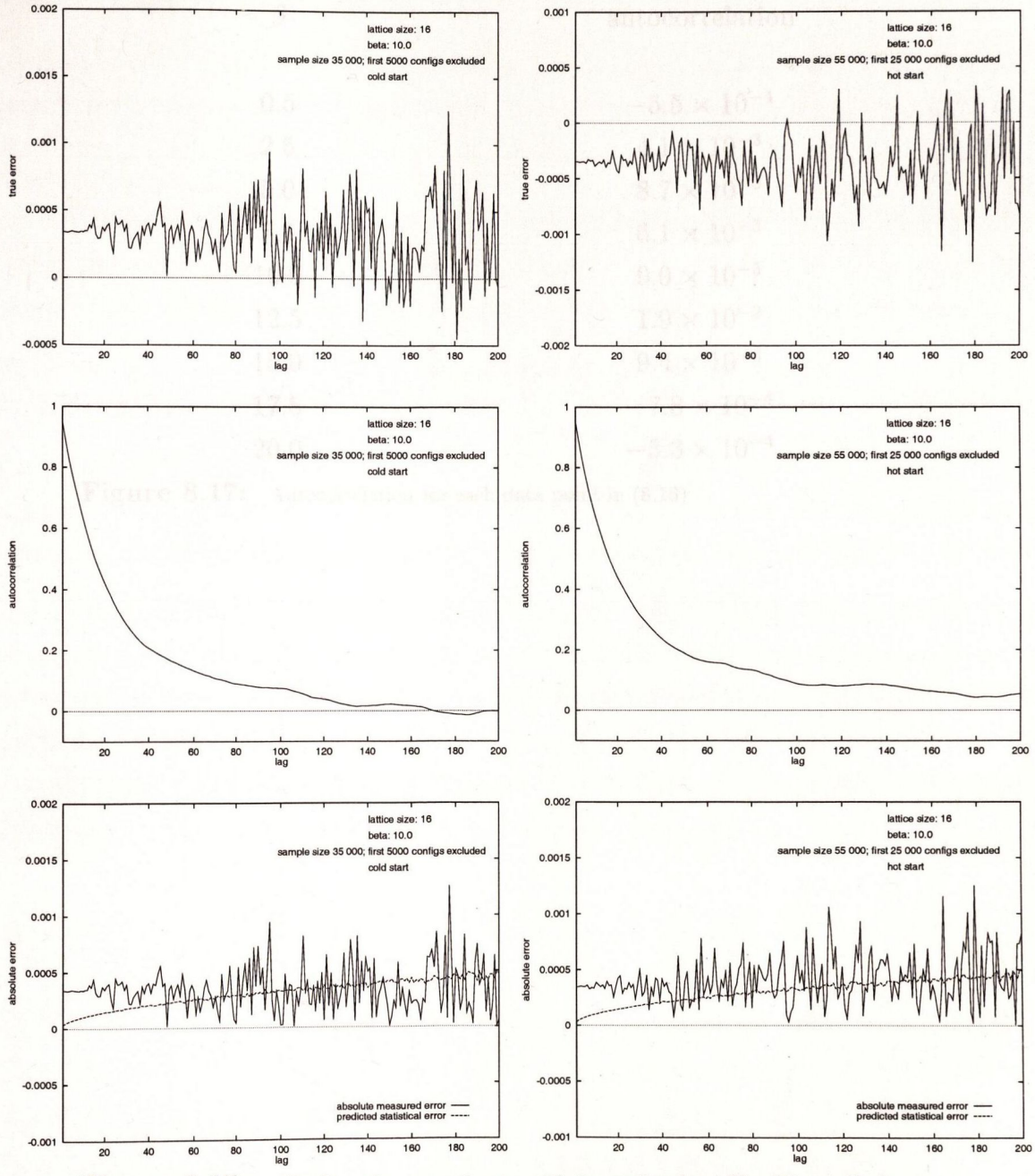

Figure 8.15: : Quality of error estimate with increasing lag. The Monte Carlo step was set at 0.07 for each experiment, to obtain a slow decay of the correlation function. The accept/reject ratio for this step size is 0.94 at $\beta = 10$. The top two diagrams show the measured errors for both hot and cold starts; the two diagrams immediately below plot the corresponding autocorrelation functions. The lowest pair of diagrams compare the absolute measured errors with the standard deviation, which measures statistical errors. The standard deviation becomes an accurate predictor of the error as the autocorrelation function decays to zero.

β	autocorrelation
0.5	-5.5×10^{-4}
2.5	4.1×10^{-3}
5.0	8.7×10^{-3}
7.5	6.1×10^{-3}
10.0	9.0×10^{-3}
12.5	1.9×10^{-2}
15.0	9.4×10^{-3}
17.5	-7.8×10^{-4}
20.0	-3.3×10^{-4}

Figure 8.17: Autocorrelation for each data point in (8.16)

43. Conclusions

In general, of course, the result of a simulation is not known in advance. The numerical experiments performed in this section, however, provide us with a basis for assessing the quality of the numerical solution. A number of conclusions can be drawn from these experiments.

1 Boundary links should be excluded from the calculation since they will not, in general, yield the same answers for the quantity being calculated.

2 A sample large enough to yield a smooth autocorrelation function should be used.

3 The Monte Carlo step size should be adjusted to give the optimum decay rate for the autocorrelation function.

4 On the basis of the plaquette computation, finite size effects appear to be negligible on a 16×16 lattice. A lattice of this size should therefore be used as a baseline for subsequent experiments, although all results should be checked by repeating them on a larger lattice.

5 The cold start simulations appear to equilibrate more quickly than the hot starts on large lattices and should therefore be used as a baseline. However the calculation should be repeated with a larger number of initial configurations discarded to ensure that equilibrium has in fact been reached.

6 The computation should be produce the same result when the simulation is started hot; this provides a useful consistency check on the whole calculation.

9. The Propagator in Axial Gauge

"Would you tell me please, which way I ought to go from here ?"
"That depends a good deal on where you want to get to."
"I don't much care where—"
"Then it doesn't matter which way you go."
– Alice in Wonderland

In this Chapter we compute the value of the plaquette and of $\langle {\phi_i}^2 \rangle$ in axial gauge. After a discussion of the issues involved in fixing the gauge in a numerical simulation, the simulations are performed with both periodic and zero boundary conditions. Agreement with the analytical prediction is demonstrated in both cases.

44. Computing in a Fixed Gauge

In this section we will investigate the numerical behaviour of a gauge dependent quantity in finite axial gauge. An analytic result for the expectation value of the square of a spacelike link (SSL) on a finite lattice in finite axial gauge was obtained in Section ((35)):

$$\langle \phi_i^2 \rangle = \frac{\pi^2}{3}$$

This is a special case of the pure gauge propagator $\langle \phi_i \phi_j \rangle$ and is clearly gauge dependent since any link can be set to an arbitrary constant value by an appropriate gauge fixing. As before, we will actually calculate the expectation value of the mean of all SSLs on the lattice:

$$\langle \overline{\phi_i^2} \rangle = \frac{\pi^2}{3} \tag{9.1}$$

Before proceeding with the analysis, some preliminary remarks are in order.
Firstly, working in axial gauge is computationally more expensive since half the links are fixed. We would therefore naively expect that the sample size should be doubled in order to achieve comparable accuracy with a similar calculation without gauge fixing. In other words we might compare working in axial gauge with working on a lattice half the size without gauge fixing. This analogy is misleading, however, since the fixed links do not disappear from the gauge fixed action, and continue to affect the expectation values we are trying to calculate. From a numerical point of view, fixing axial gauge means always rejecting updates for the gauge fixed links. This means, in effect, that the 'true' accept/reject ratio can never

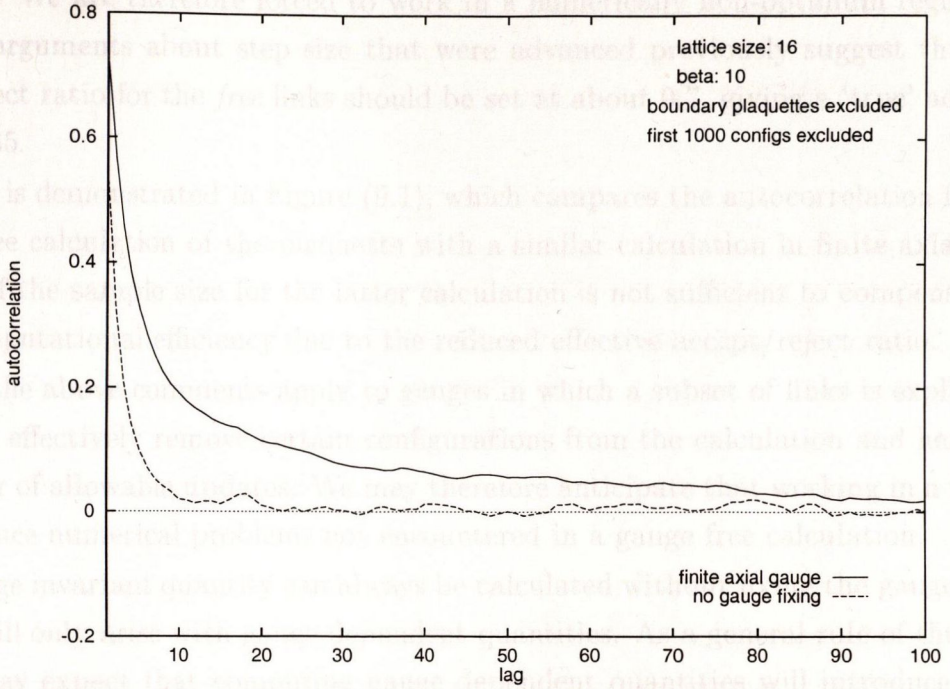

Figure 9.1: : Autocorrelation functions for the plaquette with and without gauge fixing. Sample sizes were 30 000 with no gauge and 60 000 in finite axial gauge (to allow for the fact that approximately half the links are not updated in this gauge). The first 1000 configurations were removed in each case. A Monte Carlo step of 0.35 giving an accept/reject ratio of about 0.7 was used. The behaviour of the autocorrelation function is significantly worse when finite axial gauge is imposed.

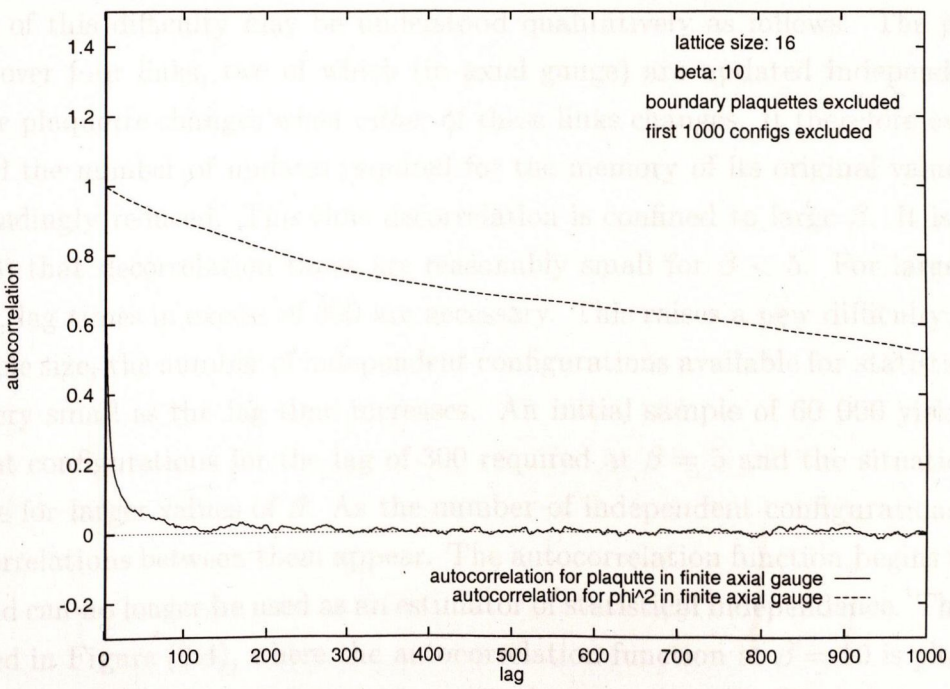

Figure 9.2: : Autocorrelation functions for the plaquette and for $\langle \phi^2 \rangle$ in finite axial gauge. Sample sizes were as in Figure (9.1), with the first 1000 configurations removed. The Monte Carlo step was adjusted so that the accept/reject ratio was 0.7. The $\langle \phi^2 \rangle$ autocorrelation function decays extremely slowly by comparison with the plaquette at for this value of β and is still significant for lag values of 1000

exceed 0.5. We are therefore forced to work in a numerically non-optimum regime. In fact the same arguments about step size that were advanced previously suggest that that the accept/reject ratio for the *free* links should be set at about 0.7, giving a 'true' accept/reject ratio of 0.35.

This effect is demonstrated in Figure (9.1), which compares the autocorrelation function for a gauge free calculation of the plaquette with a similar calculation in finite axial gauge. A doubling of the sample size for the latter calculation is not sufficient to compensate for the loss of computational efficiency due to the reduced effective accept/reject ratio.

Although the above comments apply to gauges in which a subset of links is explicitly fixed, *all* gauges effectively remove certain configurations from the calculation and hence restrict the number of allowable updates. We may therefore anticipate that working in a fixed gauge will introduce numerical problems not encountered in a gauge free calculation.

Now a gauge invariant quantity can always be calculated without fixing the gauge, hence the problem will only arise with gauge dependent quantities. As a general rule of thumb, therefore, we may expect that computing gauge dependent quantities will introduce difficulties not present in the calculation of gauge invariant quantities.

Figure (9.2) illustrates a further difficulty that arises for large β when a computation of the SSL is attempted; the decorrelation time is increased dramatically as compared with that for the plaquette.

The origin of this difficulty may be understood qualitatively as follows. The plaquette is a product over four links, two of which (in axial gauge) are updated independently. The value of the plaquette changes when *either* of these links changes. It therefore evolves more quickly and the number of updates required for the memory of its original value to be lost is correspondingly reduced. This slow decorrelation is confined to large β. It is clear from Figure (9.3) that decorrelation times are reasonably small for $\beta < 5$. For larger values of β, however, lag times in excess of 300 are necessary. This raises a new difficulty; for a fixed initial sample size, the number of independent configurations available for statistical analysis becomes very small as the lag time increases. An initial sample of 60 000 yields only 200 independent configurations for the lag of 300 required at $\beta = 5$ and the situation becomes much worse for larger values of β. As the number of independent configurations decreases, spurious correlations between them appear. The autocorrelation function begins to fluctuate strongly and can no longer be used as an estimator of statistical independence. This situation is illustrated in Figure (9.4), where the autocorrelation function at $\beta = 10$ is plotted out to lag values of 15000 for three different Monte Carlo step sizes. The figure also shows that, as expected, the best performance is obtained for a step size of 0.35 corresponding to an accept/reject ratio of about 0.7.

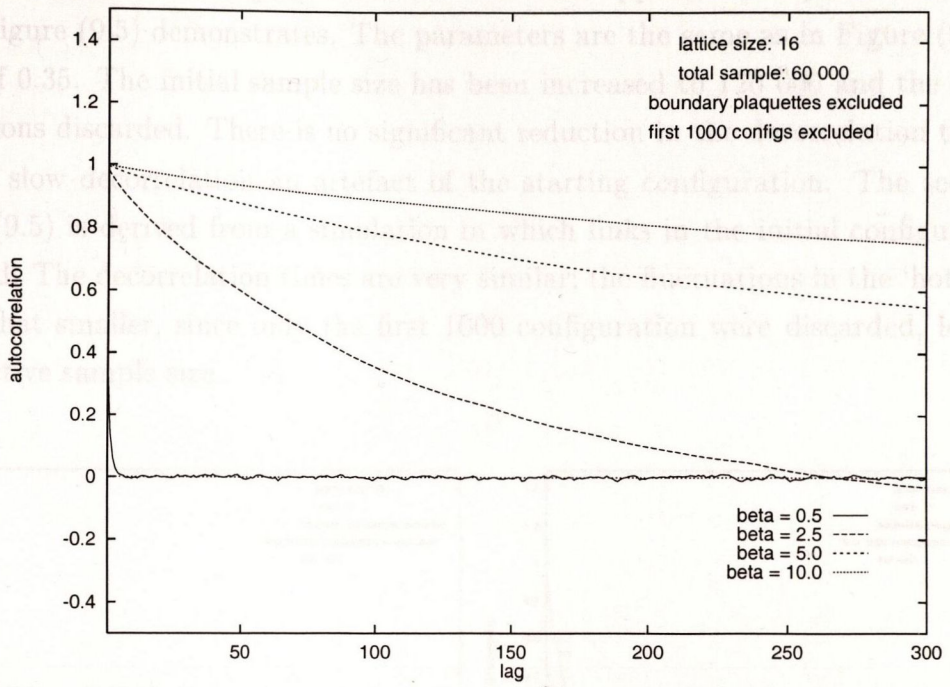

Figure 9.3: : Autocorrelation functions for $\langle \phi^2 \rangle$ at different β in finite axial gauge. Sample sizes were 60 000 with in each case, with the first 1000 configurations removed. The Monte Carlo step was adjusted so that the accept/reject ratio was 0.7. The decorrelation time increases dramatically with β.

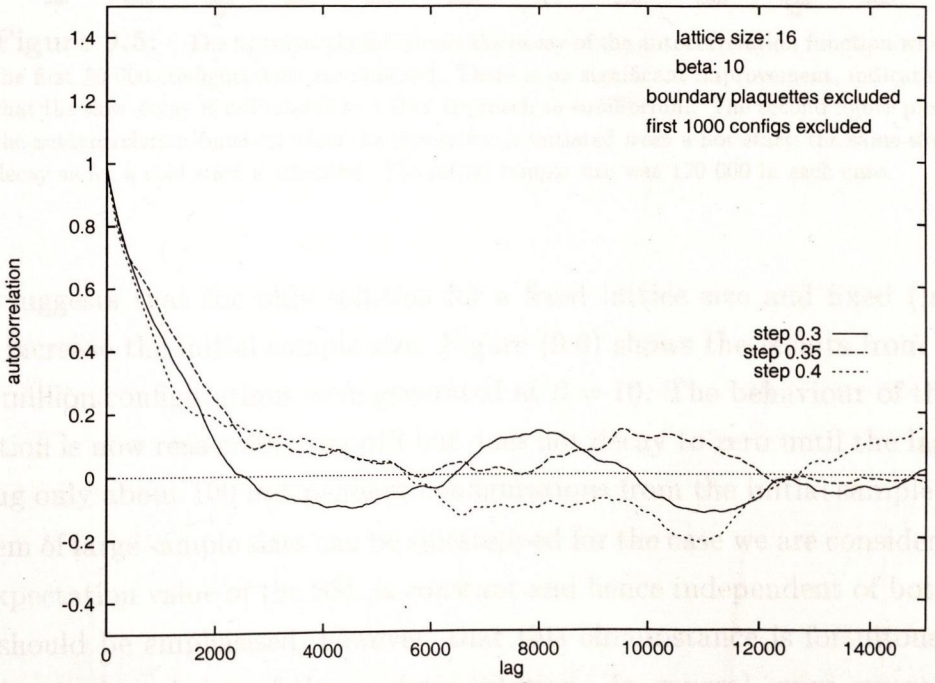

Figure 9.4: : Autocorrelation functions for $\langle \phi^2 \rangle$ at different step sizes. The sample size was 60 000 and lag values were computed up to 5000. The standard step size of 0.35 gives the best performance but fluctuations due to the small effective sample size set in before the autocorrelation function has decayed sufficiently.

The slow decorrelation at large β is not due to a slow approach to equilibrium, as the first graph in Figure (9.5) demonstrates. The parameters are the same as in Figure (9.4), with a step size of 0.35. The initial sample size has been increased to 120 000 and the first 50 000 configurations discarded. There is no significant reduction in the decorrelation time.
Nor is the slow decorrelation an artefact of the starting configuration. The second graph in Figure (9.5) is derived from a simulation in which links in the initial configuration were randomised. The decorrelation times are very similar; the fluctuations in the 'hot start' case are somewhat smaller, since only the first 1000 configuration were discarded, leading to a larger effective sample size.

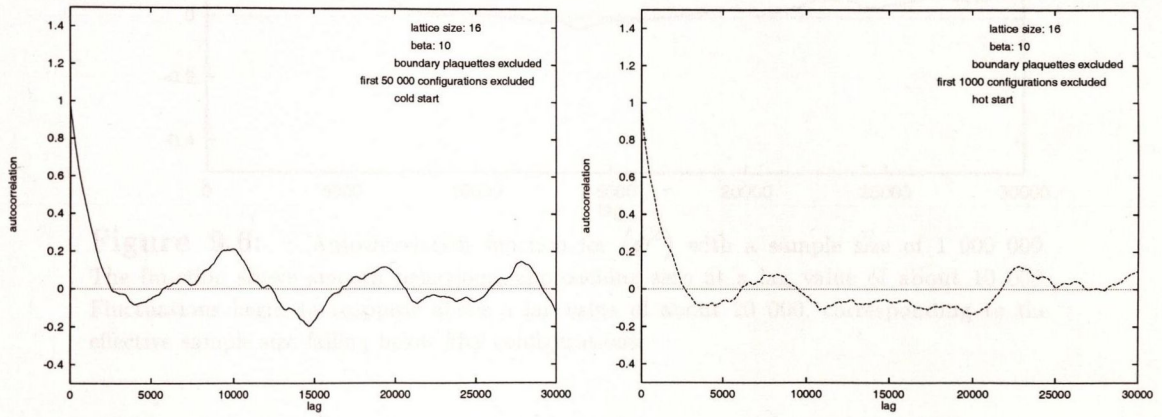

Figure 9.5: : The figure on the left shows the decay of the autocorrelation function when the first 50 000 configurations are removed. There is no significant improvement, indicating that the slow decay is not related to a slow approach to equilibrium. The second figure plots the autocorrelation function when the simulation is initiated from a hot start; the same slow decay as for a cold start is observed. The initial sample size was 120 000 in each case.

All of this suggests that the only solution for a fixed lattice size and fixed (large) β is to drastically increase the initial sample size. Figure (9.6) shows the results from a simulation in which a million configurations were generated at $\beta = 10$. The behaviour of the autocorrelation function is now reasonably smooth but does not decay to zero until the lag is about 10 000, yielding only about 100 independent configurations from the initial sample of a million. This problem of large sample sizes can be sidestepped for the case we are considering, since by (9.1) the expectation value of the SSL is constant and hence independent of both lattice size and β. It should be emphasised, however, that this circumstance is fortuitous and results from an advance knowledge of the analytic solution. In general, pure gauge expectation values will be functions of both lattice size and β and a complete analysis of such expectation values will require simulations on large lattices at large values of β.
Let us for the moment take advantage of out advance knowledge. The gauge free analysis

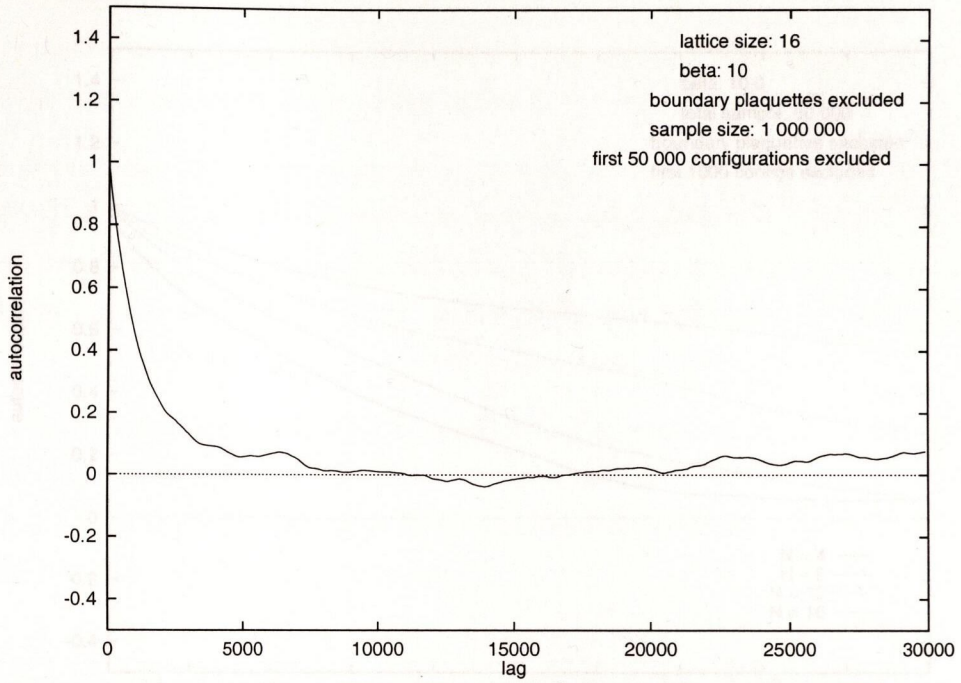

Figure 9.6: : Autocorrelation function for $\langle \phi^2 \rangle$ with a sample size of 1 000 000. The function shows smooth behaviour, approaching zero at a lag value of about 10 000. Fluctuations begin to reappear above a lag value of about 20 000, corresponding to the effective sample size falling below fifty configurations.

of the plaquette in Section ((42)) suggests that decorrelation occurs more quickly on smaller lattices. Figure (9.7) confirms this picture in the present case; from the point of view of rapid decorrelation it is clearly advantageous to work on the smallest possible lattice. If the sample size is fixed, of course, then reducing the size of the lattice increases the errors due to statistical fluctuations–the magnitude of these errors can, however be reliably predicted. Figure (9.8) plots the autocorrelation function out to a lag of 5000 on a 4×4 lattice, using a total sample size of 500 000. This should be compared with Figure (9.6) which relates to a 16×16 lattice. The decorrelation length on the small lattice is about a quarter of that on the large one even though the sample size has been reduced by a factor of two. The overall computational work has been reduced by a factor of about thirty.

Let us summarise our conclusions on the numerical evaluation of the expectation value of the SSL in finite axial gauge.

1 Axial gauge simulations may be regarded as gauge free simulations in which configurations which require updates to the fixed links are always rejected. One is therefore forced to work in a non-optimum simulation regime.

2 An immediate consequence is the fact the decorrelation times will be significantly increased

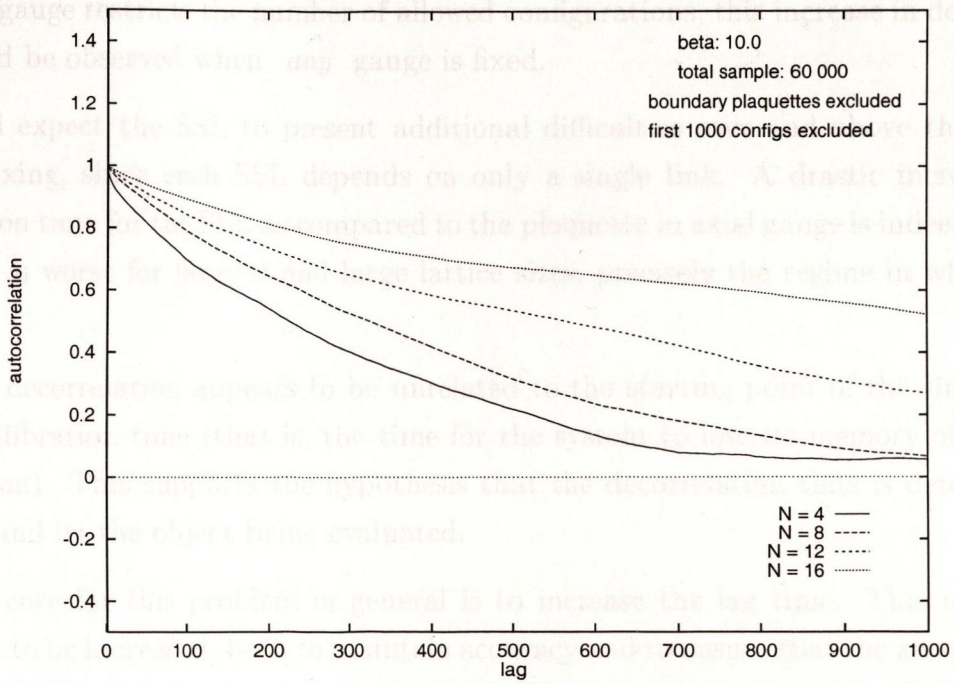

Figure 9.7: : Autocorrelation function for $\langle \phi^2 \rangle$ at different lattice sizes. The sample size was 60 000 in each case. Configurations decorrelate more quickly on smaller lattices.

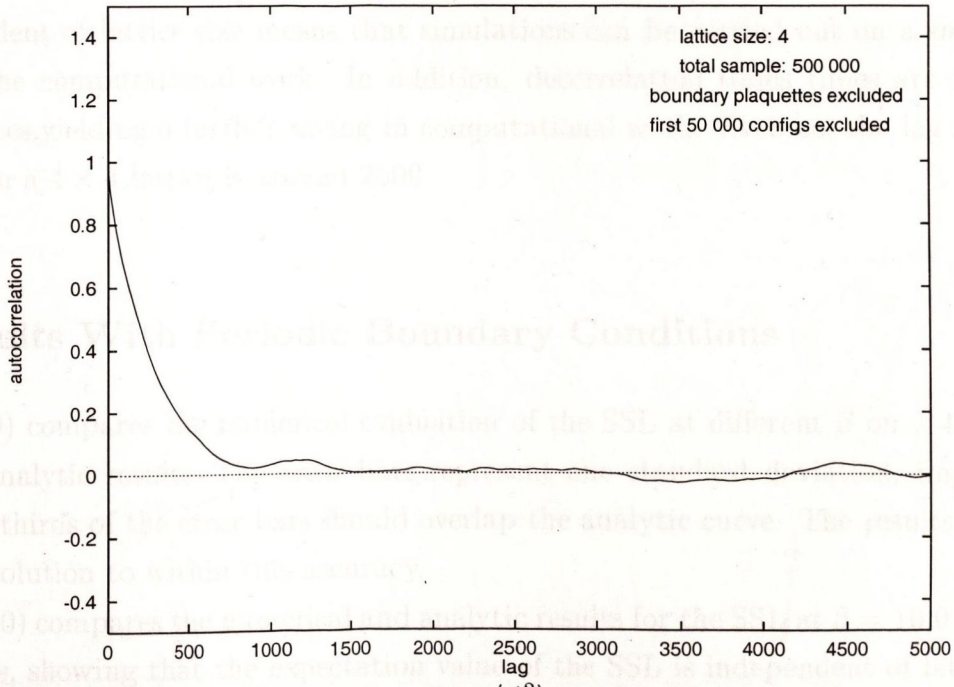

Figure 9.8: : Autocorrelation function for $\langle \phi^2 \rangle$ on a 4×4 lattice. Effective decorrelation has occurred at a lag value of about 2500

by comparison with the gauge free case.

3 Since any gauge restricts the number of allowed configurations, this increase in decorrelation time should be observed when *any* gauge is fixed.

4 We would expect the SSL to present additional difficulties over and above those related to gauge-fixing, since each SSL depends on only a single link. A drastic increase in the decorrelation time for the SSL as compared to the plaquette in axial gauge is indeed observed. This effect is worst for large β and large lattice sizes, precisely the regime in which we are interested.

5 This slow decorrelation appears to be unrelated to the starting point of the simulation or to the equilibration time (that is, the time for the system to lose its memory of the initial configuration). This supports the hypothesis that the decorrelation time is determined by the gauge and by the object being evaluated.

6 The only cure for this problem in general is to increase the lag time. This requires the sample size to be increased, both to maintain accuracy and to ensure that the autocorrelation function remains smooth enough to be a reliable estimator of decorrelation. This solution is potentially very computationally expensive.

7 For the special case of the SSL in axial gauge, the fact that the expectation value of the SSL is independent of lattice size means that simulations can be carried out on a small lattice, reducing the computational work. In addition, decorrelation times times are reduced on small lattices,yielding a further saving in computational work. Even so, the lag required at $\beta = 10.0$ on a 4×4 lattice is around 2500.

45. Results With Periodic Boundary Conditions

Figure (9.9) compares the numerical evaluation of the SSL at different β on a 4×4 lattice with the analytic result. The error bars represent one standard deviation, implying that about two thirds of the error bars should overlap the analytic curve. The results agree with the exact solution to within this accuracy. .

Figure (9.10) compares the numerical and analytic results for the SSL at $\beta = 10.0$ at different lattice sizes, showing that the expectation value of the SSL is independent of lattice size as predicted (at least to within the accuracy of the simulation).

Figures (9.11) and (9.12) show the statistical fluctuations on a small lattice for small and large β. The decorrelation times in the two cases are about 10 and 2500 respectively. This

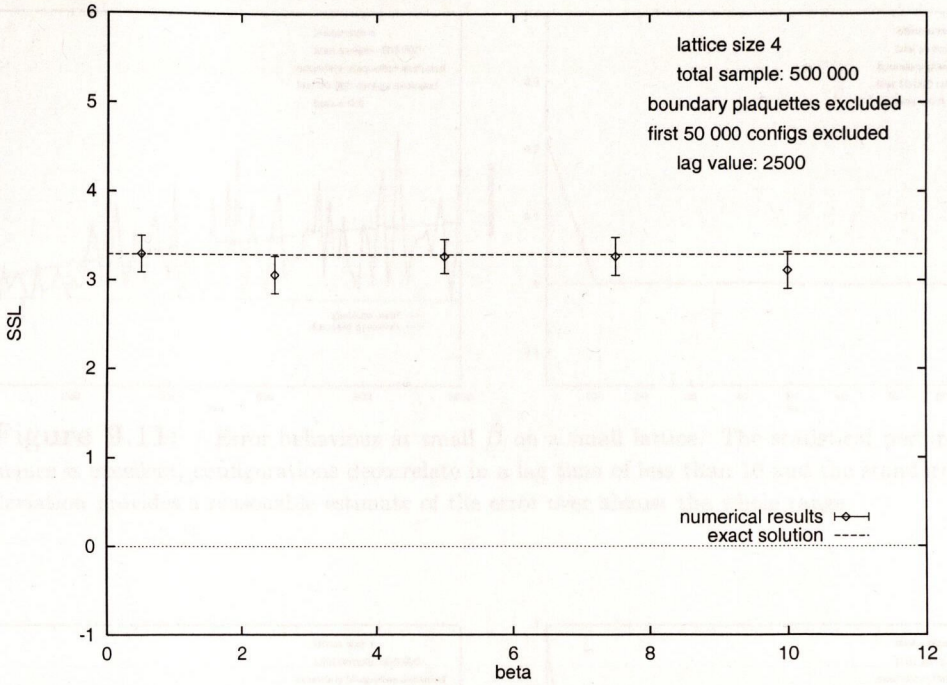

Figure 9.9: : Expectation value of SSL against β. Numerical data supports the prediction that the SSL is independent of β.

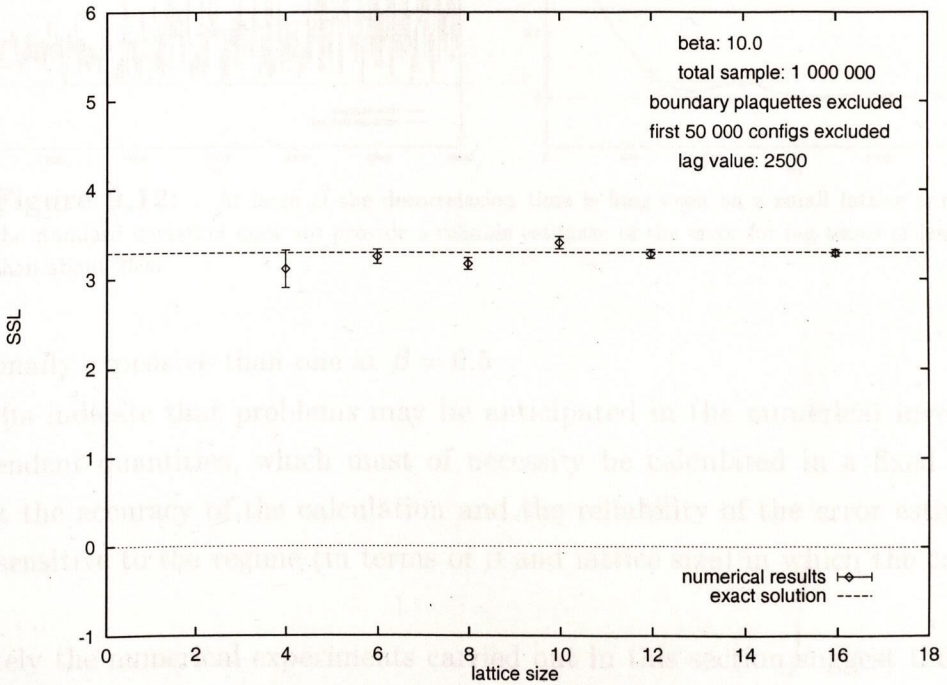

Figure 9.10: : Expectation value of SSL against lattice size. Results are consistent with the prediction that the SSL is independent of lattice size.

means in effect that a calculation of the the SSL at $\beta = 10.0$ is about 250 times more

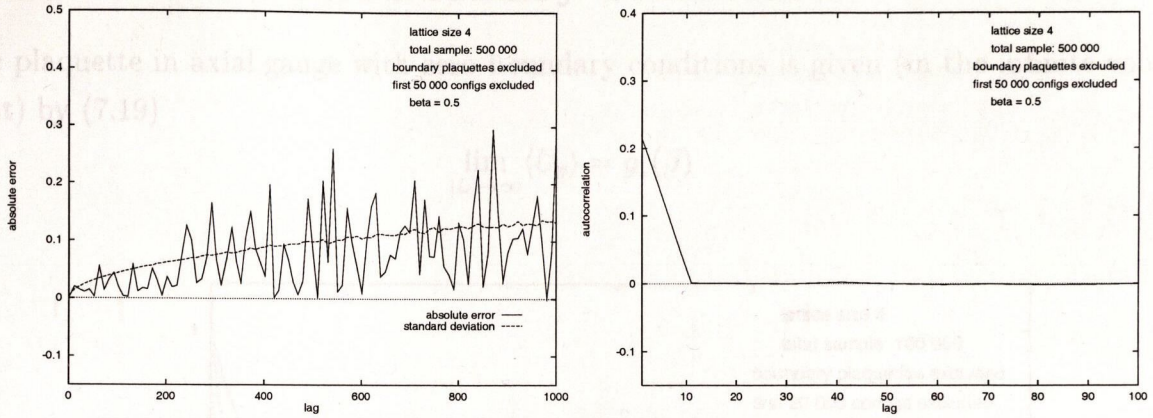

Figure 9.11: : Error behaviour at small β on a small lattice. The statistical performance is excellent; configurations decorrelate in a lag time of less than 10 and the standard deviation provides a reasonable estimate of the error over almost the whole range.

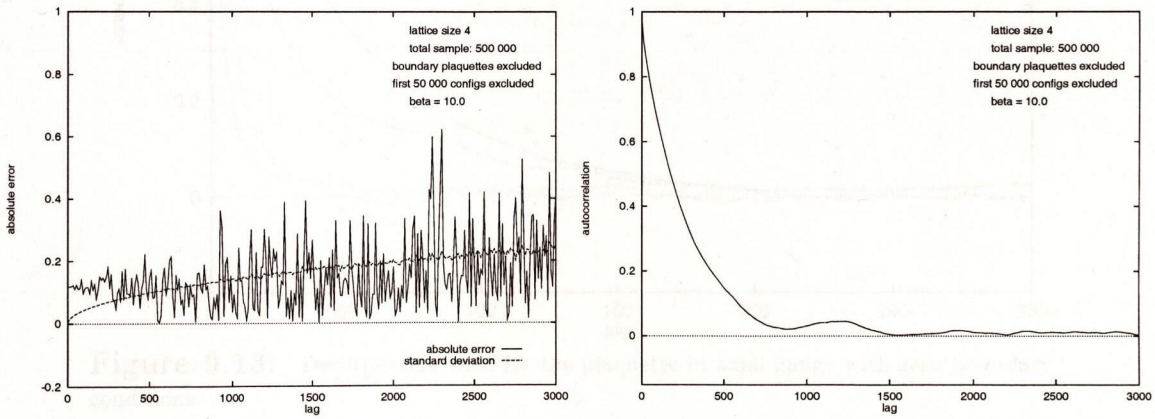

Figure 9.12: : At large β the decorrelation time is long even on a small lattice and the standard deviation does not provide a reliable estimate of the error for lag times of less than about 2500.

computationally expensive than one at $\beta = 0.5$

These results indicate that problems may be anticipated in the numerical investigation of gauge dependent quantities, which must of necessity be calculated in a fixed gauge. We may expect the accuracy of the calculation and the reliability of the error estimates to be extremely sensitive to the regime (in terms of β and lattice size) in which the calculation is performed.

Unfortunately the numerical experiments carried out in this section suggest that the worst results can be expected at large β and large lattice size, which is exactly the regime that we shall be focusing on in subsequent chapters.

46. Results With Zero Boundary Conditions

The plaquette in axial gauge with zero boundary conditions is given (in the infinite volume limit) by (7.19)

$$\lim_{|L|\to\infty} \langle U_p \rangle = g_1(\beta)$$

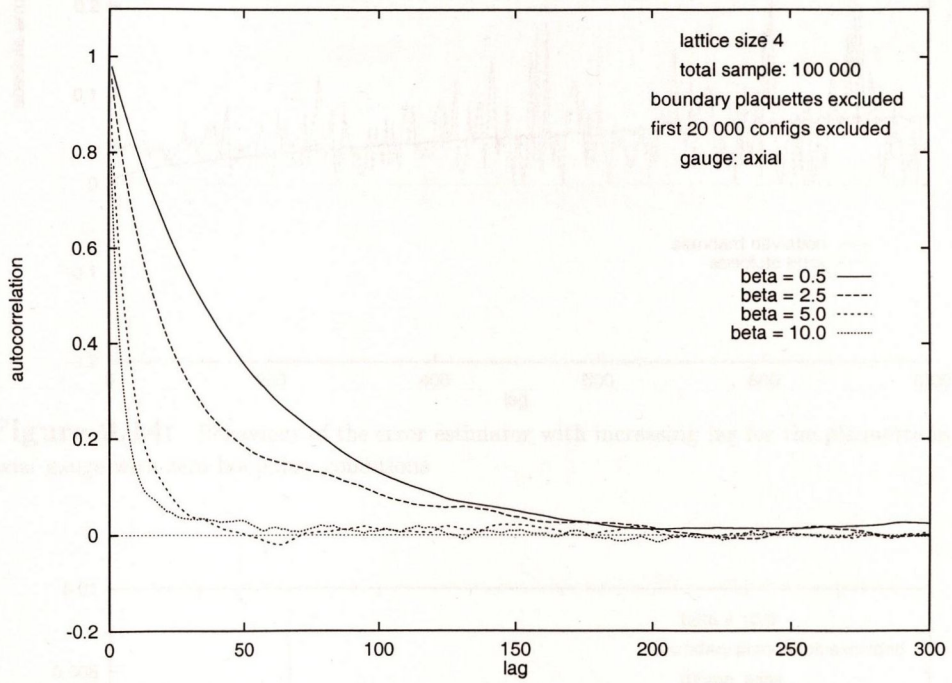

Figure 9.13: Decorrelation time for the plaquette in axial gauge with zero boundary conditions

Figure (9.16) compares this limit with the results from a Monte Carlo computation of the plaquette on a 4×4 lattice with zero boundary conditions imposed. The results are in excellent agreement, despite the small size of the lattice.

The expression for the expectation value of the square of a spacelike link is given by (7.21):

$$\langle {\phi_i}^2 \rangle = \frac{\pi^2}{3} + \lim_{K\to\infty} \frac{4}{1+2\sum_{r=1}^{K} g_r(\beta)^{|L|}} \left\{ \sum_{r=1}^{K} \frac{(-1)^r}{r^2} \left({g_r}^{|S_1|}(\beta) + {g_r}^{|S_2|}(\beta) \right) \right\}$$

$$+ \lim_{K\to\infty} \frac{2}{1+2\sum_{r=1}^{K} g_r(\beta)^{|L|}} \left\{ \sum_{\substack{r'=-K \\ r'\neq 0,\, r}}^{K} \sum_{\substack{r=-K \\ r\neq 0}}^{K} \frac{(-1)^{(r'-r)}}{(r'-r)^2} \, {g_r}^{|S_1|}(\beta) {g_r}^{|S_2|}(\beta) \right\}$$

Since

$$\lim_{r\to\infty} g_r(\beta) = 0$$

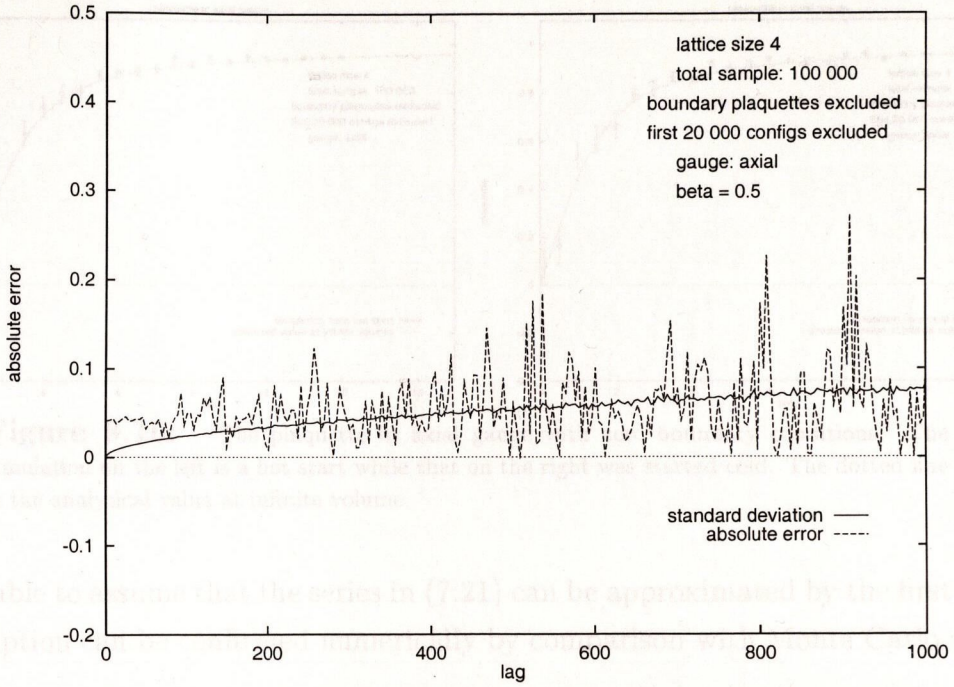

Figure 9.14: Behaviour of the error estimator with increasing lag for the plaquette in axial gauge with zero boundary conditions

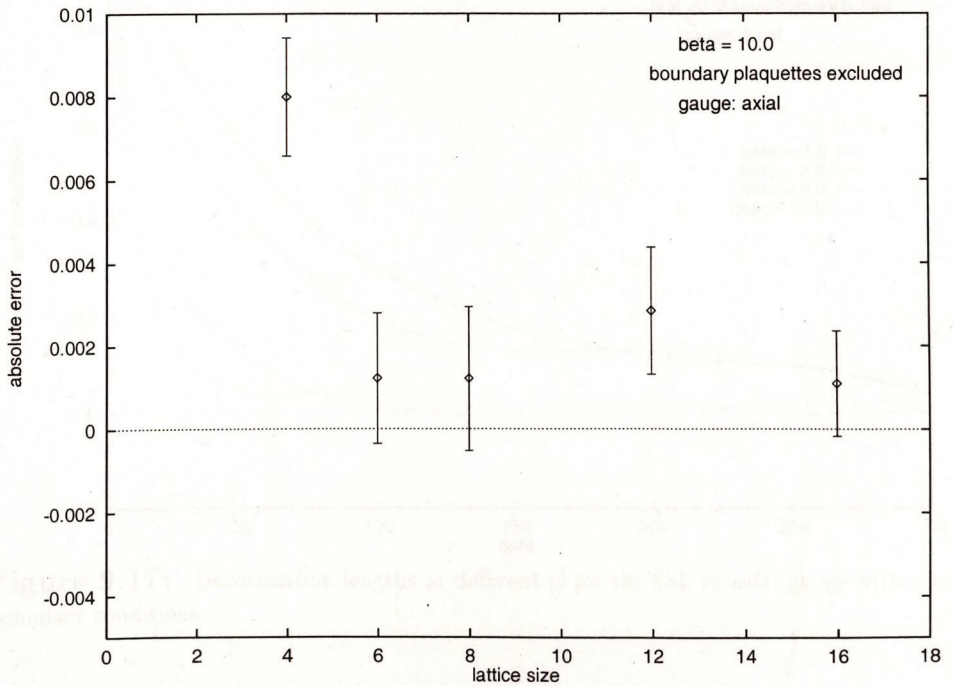

Figure 9.15: Finite size errors for the plaquette in axial gauge with zero boundary conditions. Sample sizes have been normalised to yield comparable accuracies for each lattice size.

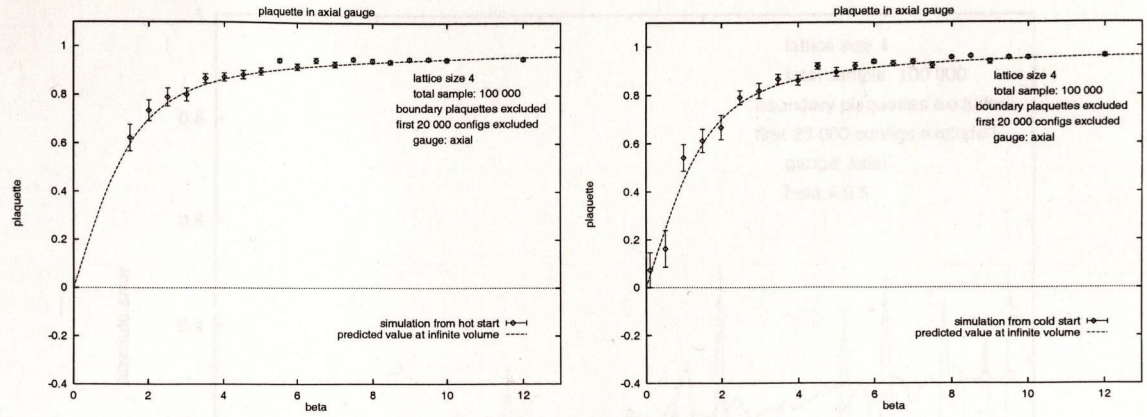

Figure 9.16: The plaquette in axial gauge with zero boundary conditions. The simulation on the left is a hot start while that on the right was started cold. The dotted line is the analytical value at infinite volume.

it is reasonable to assume that the series in (7.21) can be approximated by the first few terms. This assumption can be confirmed numerically by comparison with Monte Carlo simulation.

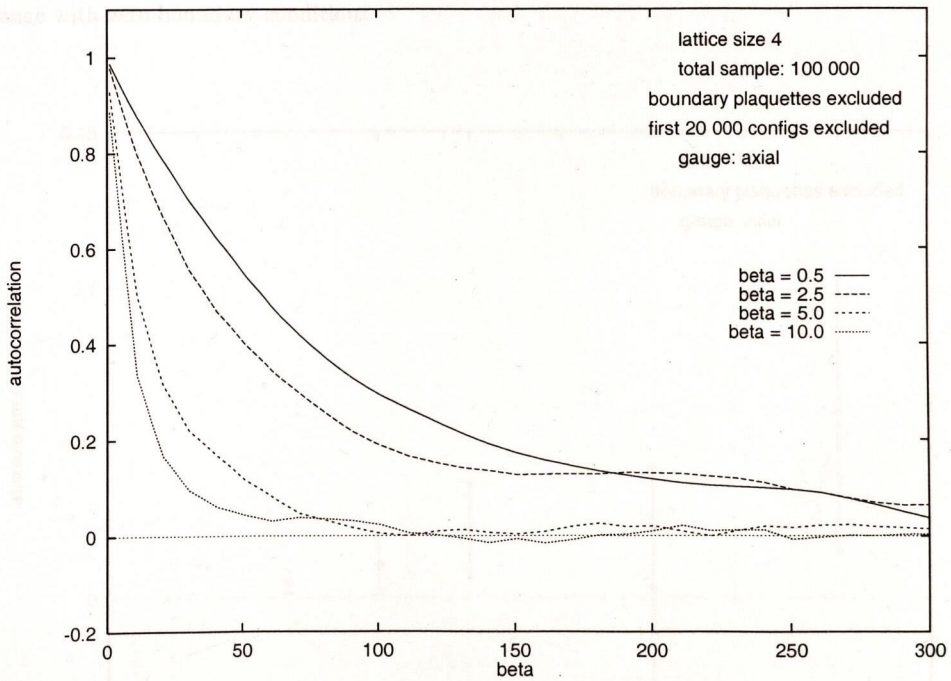

Figure 9.17: Decorrelation lengths at different β for the SSL in axial gauge with zero boundary conditions

Figure (9.20) compares the results of such a simulation, with the analytical value (7.21) where the series have been summed up to $K = 10$

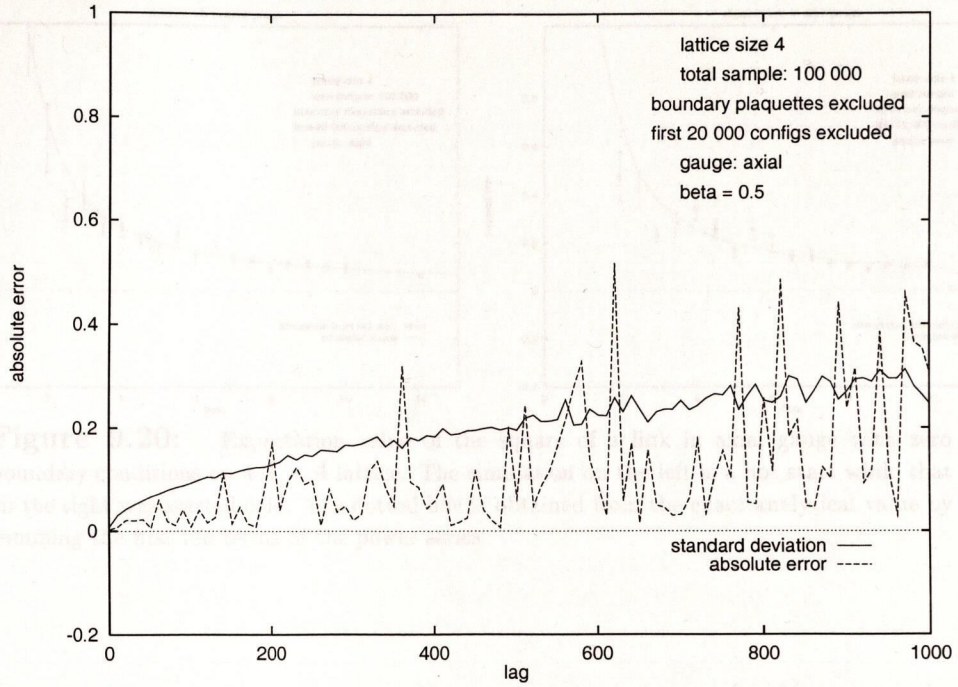

Figure 9.18: Behaviour of the error estimator with increasing lag for the SSL in axial gauge with zero boundary conditions

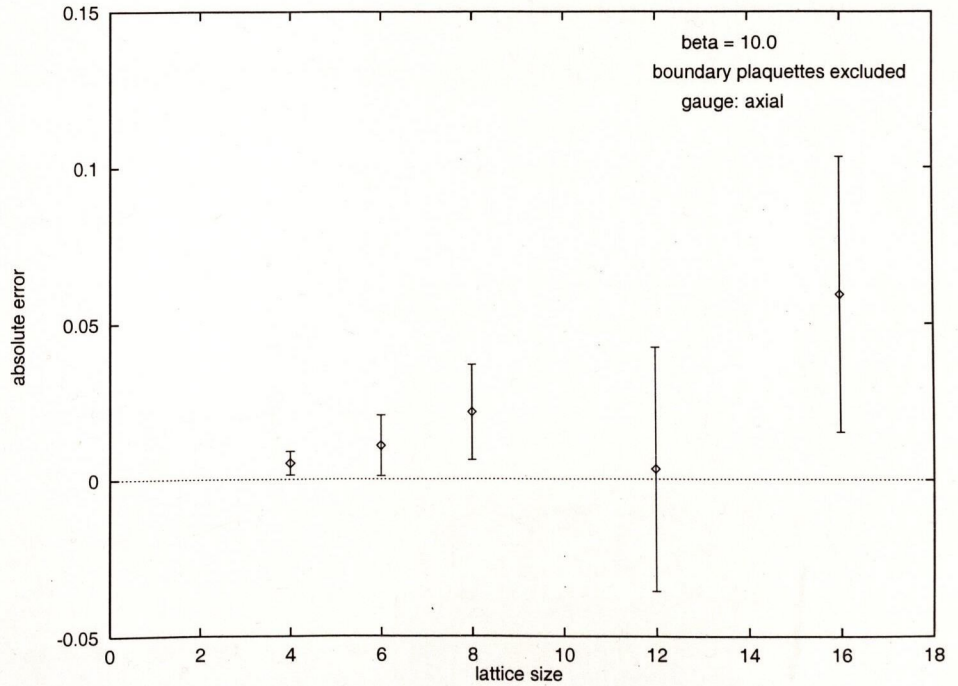

Figure 9.19: Finite size effects for the SSL in axial gauge with zero boundary conditions

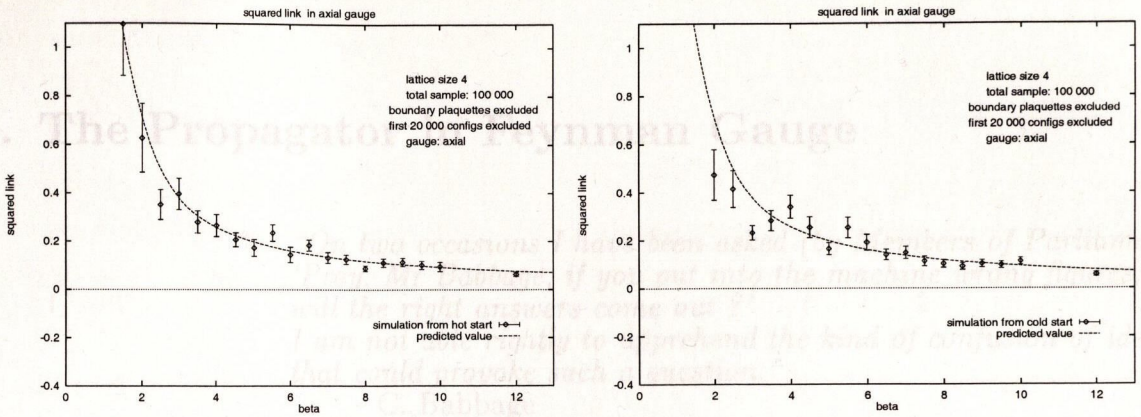

Figure 9.20: Expectation value of the square of a link in axial gauge with zero boundary conditions on a 4×4 lattice. The simulation on the left is a hot start while that on the right was started cold. The dotted line is obtained from the exact analytical value by summing the first ten terms of the power series.

10. The Propagator in Feynman Gauge

"On two occasions I have been asked (by Members of Parliament!)
'Pray, Mr Babbage, if you put into the machine wrong figures,
will the right answers come out ?'
I am not able rightly to apprehend the kind of confusion of ideas
that could provoke such a question."
– C. Babbage

In this Chapter we carry out the numerical calculation of the plaquette and of $\langle {\phi_i}^2 \rangle$ in Feynman gauge. We present evidence that the simulation is not ergodic if periodic boundary conditions are imposed. It is noteworthy that the correct value is nevertheless obtained for the gauge–invariant plaquette. We show that simulation is well–behaved when zero boundary conditions are imposed and that the expectation values obtained are in agreement with the analytic prediction.

47. Implementation of Feynman Gauge

The calculations of the last Chapter may be repeated in Feynman gauge. Of particular interest is the expectation value of the gauge dependent quantity ϕ_i^2. The value of this quantity is not known analytically although an approximate result for large β is available. Feynman gauge is established by adding an extra term to the action (8.8) to give the modified or *gauge–fixed* action:

$$S_F = \sum_{\underline{n}} 1 - \cos\theta(\underline{n}) + \frac{1}{2} \sum_{\underline{n}} \sum_{\mu} (\Delta_\mu^L \phi_\mu(\underline{n}))^2$$

with the left derivative Δ_μ^L being defined by

$$\Delta_\mu^L f(\underline{n}) = \frac{f(\underline{n}) - f(\underline{n} - \underline{\mu})}{a}$$

No links are fixed in this gauge so that all link variables are available for updating.
The update of a link variable $\phi_\mu(\underline{n})$ will affect three sites:

1. site $\underline{n}$ through the plaquette term and the gauge term.
2. site $(\underline{n} - \underline{\nu})$ through the plaquette term.
3. site $(\underline{n} + \underline{\mu})$ through the gauge term.

If we denote the gauge term associated with a site $\underline{n}$ by $g(\underline{n})$ for brevity, the change in the action under the update of $\phi_\mu(\underline{n})$ is given by

$$\Delta S_F = S'_F - S_F = (\cos\theta(\underline{n}) + \cos\theta(\underline{n}-\underline{\nu})) - (\cos\theta'(\underline{n}) + \cos\theta'(\underline{n}-\underline{\nu})) + (g'(\underline{n}) + g'(\underline{n}+\underline{\mu})) - (g(\underline{n}) + g(\underline{n}+\underline{\mu}))$$

With this modification to the definition of ΔS, the generation of a sample set of configurations may in principle proceed as before.

48. Results With Periodic Boundary Conditions

Feynman gauge presents new difficulties not present in axial gauge, however. These are signalled by the appearance of enormously long decorrelation times. Figure (10.1) is the usual plot of autocorrelation against lag for the plaquette. Decorrelation takes place at a lag of about 100 and all appears to be well.

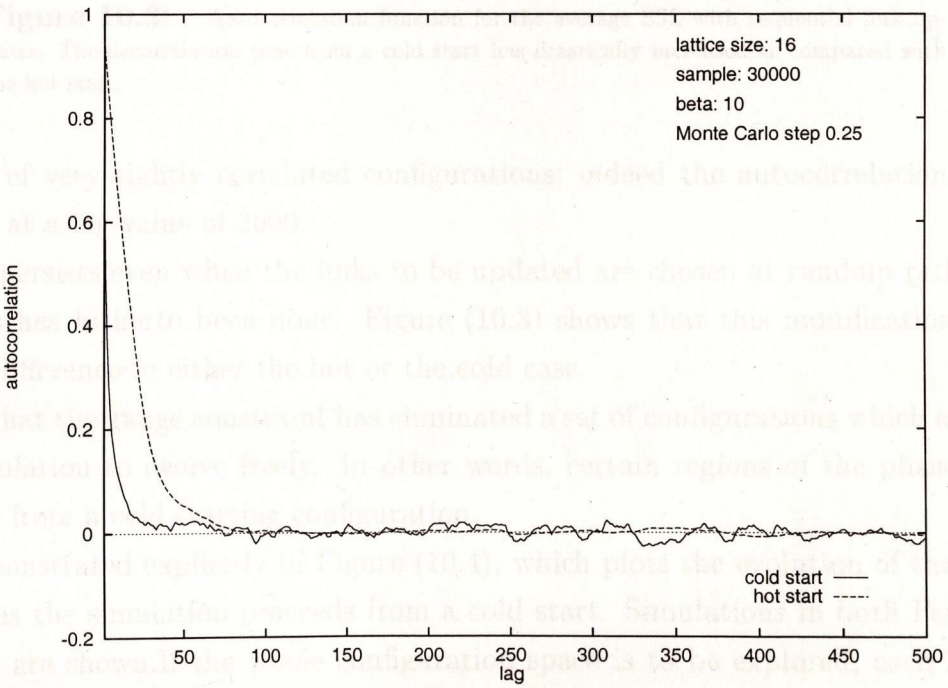

Figure 10.1: : Autocorrelation function for the average plaquette.Effective decorrelation has occurred at a lag value of about 100

The SSL, however, presents a very different picture, as is demonstrated in Figure (10.2). The decorrelation length is strongly dependent on the starting point of the simulation; a randomised initial configuration yields a Markov chain which decorrelates at a rate comparable to that of the plaquette. A cold initial configuration, on the other hand gives rise to

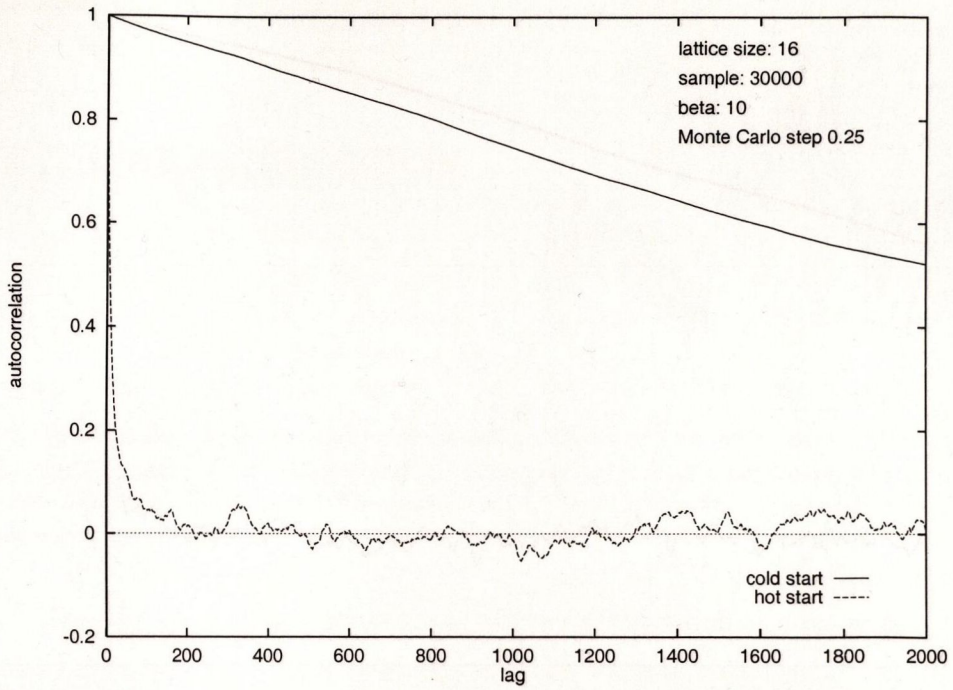

Figure 10.2: : Autocorrelation function for the average SSL with sequential link updates. The decorrelation time from a cold start has drastically increased as compared with the hot start.

a sequence of very tightly correlated configurations; indeed the autocorrelation coefficient exceeds 0.5 at a lag value of 2000.

This effect persists even when the links to be updated are chosen at random rather then in sequence as has hitherto been done. Figure (10.3) shows that this modification makes no significant difference in either the hot or the cold case.

It appears that the gauge constraint has eliminated a set of configurations which are required for the simulation to evolve freely. In other words, certain regions of the phase space are inaccessible from a cold starting configuration.

This is demonstrated explicitly in Figure (10.4), which plots the evolution of the value of a single link as the simulation proceeds from a cold start. Simulations in both Feynman and axial gauge are shown.If the whole configuration space is to be explored, each link should take values over the whole interval $[-\pi, \pi]$. This behaviour is indeed observed in axial gauge; in Feynman gauge, however, the value of the link is confined to a relatively small interval around zero.

These simulations were repeated, this time from a hot start. In view of the fact that the tight correlations observed in the cold start case are absent in the hot case, we might expect that the whole configuration space is being explored. Figure (10.5) shows that this is not in fact the case; link values are again clustered strongly around the starting point.

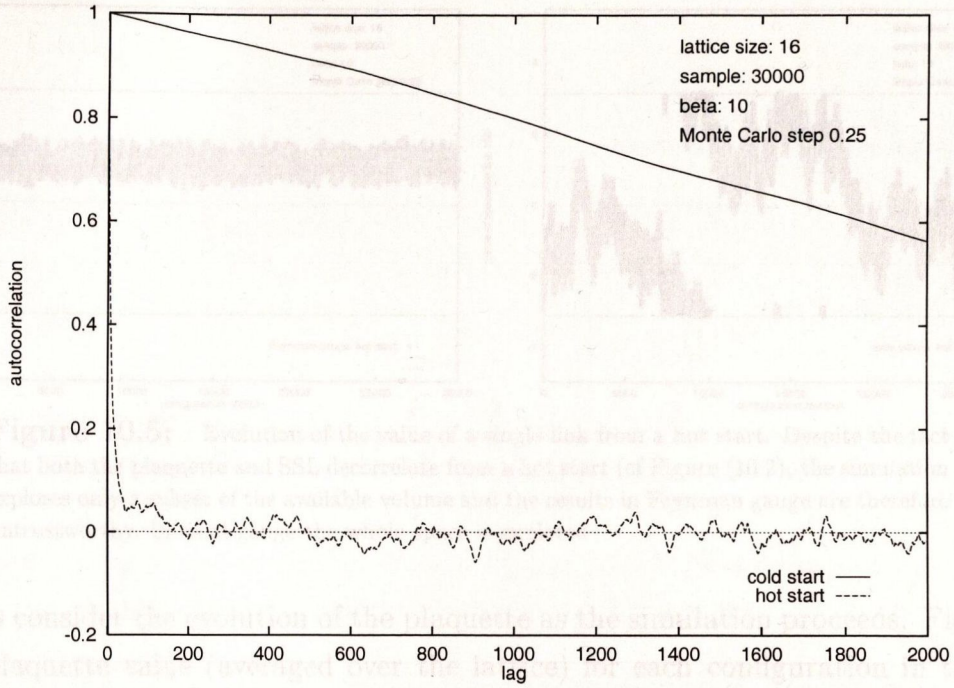

Figure 10.3: : Autocorrelation function for the average SSL with random link updates. Choosing the links to be updated at random has no significant effect on the decorrelation time (cf Figure (10.2))

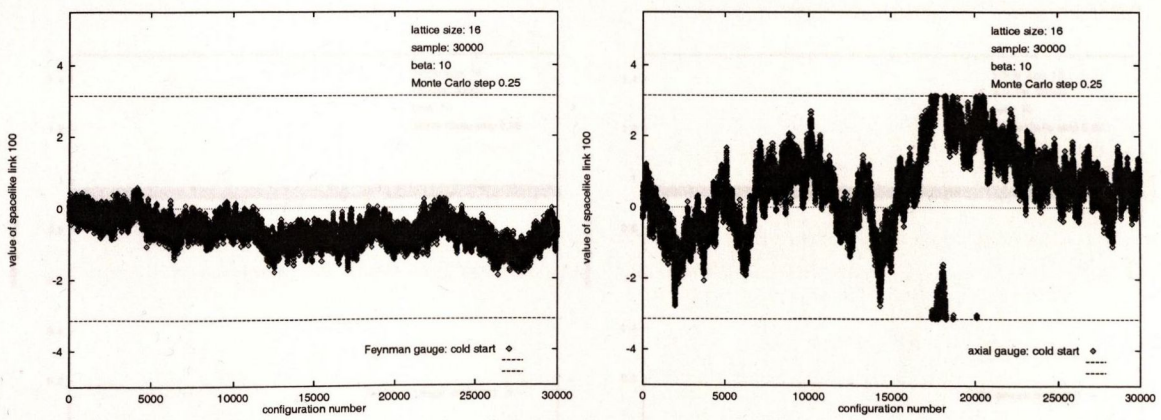

Figure 10.4: : Evolution of the value of a single link from a cold start.This value is confined to a subset of the available values in the case of Feynman gauge. In contrast the whole space of values is explored in axial gauge.

Let us summarise the situation. When Feynman gauge is imposed on the pure U(1) gauge theory in two dimensions we find that the possible values of the link variables are restricted to a small interval arount their starting points under Monte Carlo updates. This restriction persists irrespective of the starting point or the sequence in which the links are updated. The indications from these numerical experiments, therefore, are that the system is not ergodic.

§48. Results With Periodic Boundary Conditions

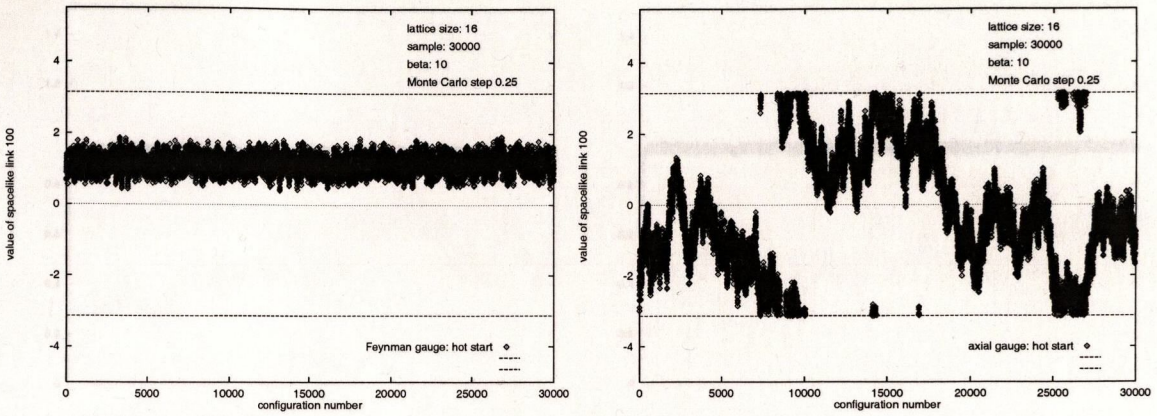

Figure 10.5: : Evolution of the value of a single link from a hot start. Despite the fact that both the plaquette and SSL decorrelate from a hot start (cf Figure (10.2), the simulation explores only a subset of the available volume and the results in Feynman gauge are therefore untrustworthy. In axial gauge the whole space is explored

Next, let us consider the evolution of the plaquette as the simulation proceeds. Figure (10.6) plots the plaquette value (averaged over the lattice) for each configuration in the Markov chain from a cold start simulation in both Feynman and axial gauge. Figure (10.7) shows the equivalent results from a hot start. It is remarkable that all four simulations give identical results for the plaquette even though, in the case of Feynman gauge, only a subset of the configuration space is sampled and indeed, a *different* subset for the hot and cold start cases.

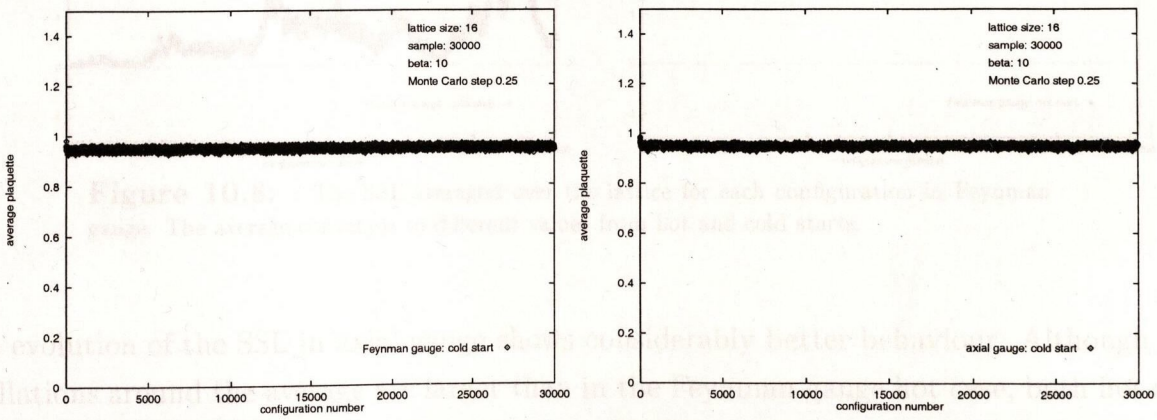

Figure 10.6: : The plaquette averaged over the lattice for each configuration from a cold start. A stable, correct value for this observable is obtained in both Feynman and axial gauge.

Turning next to the SSL, we find a very different situation. Figure (10.8) compares the evolution of the SSL (averaged, as before, over the lattice) from hot and cold start simulations in Feynman gauge. The hot simulation converges to a stable value, though we have no reason to suppose that this value is actually correct. In the case of the cold simulation

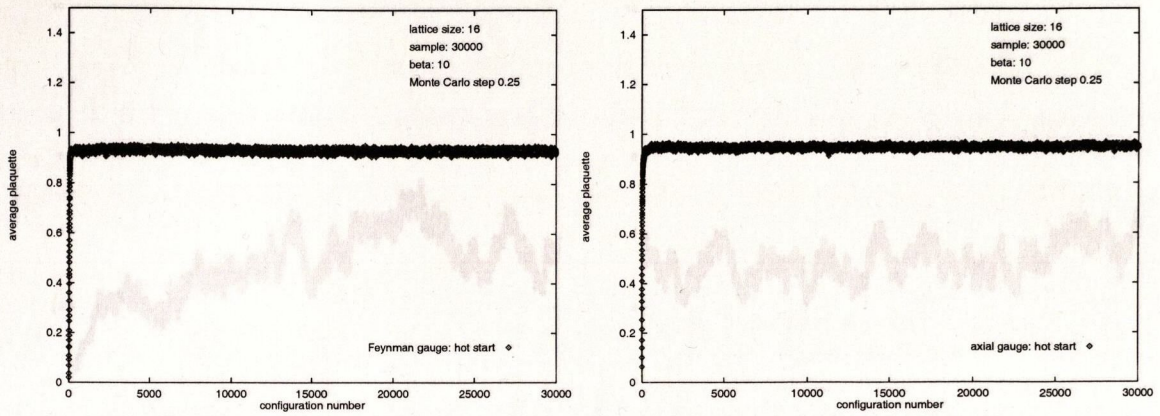

Figure 10.7: : The plaquette averaged over the lattice for each configuration from a hot start. A stable, correct value is obtained in both Feynman and axial gauge.

no convergence is apparent even after 30 000 lattice sweeps.Moreover, the range of values obtained in this case is significantly lower than the result from the hot simulation.

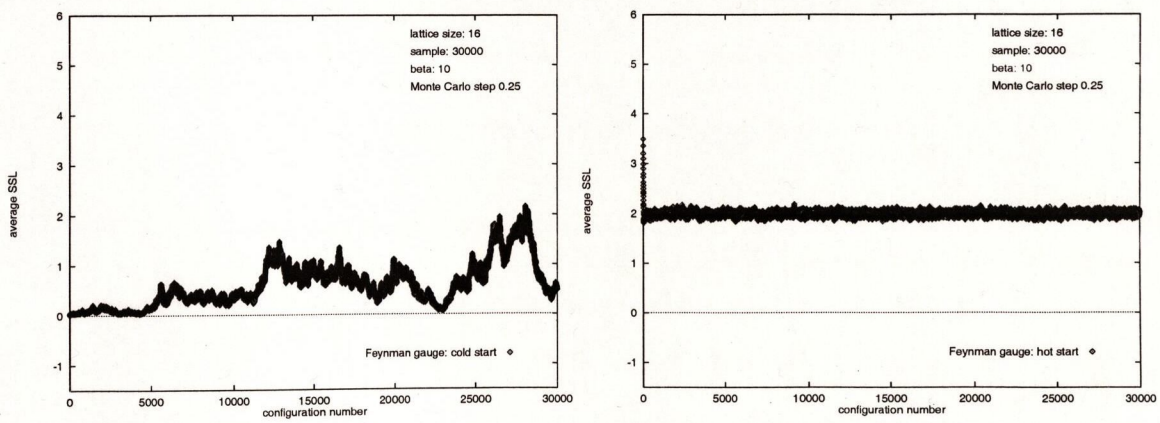

Figure 10.8: : The SSL averaged over the lattice for each configuration in Feynman gauge. The average converges to different values from hot and cold starts.

The evolution of the SSL in axial gauge shows considerably better behaviour. Although the oscillations around the average are larger than in the Feynman gauge hot case, both hot and cold simulations converge to roughly the same value.

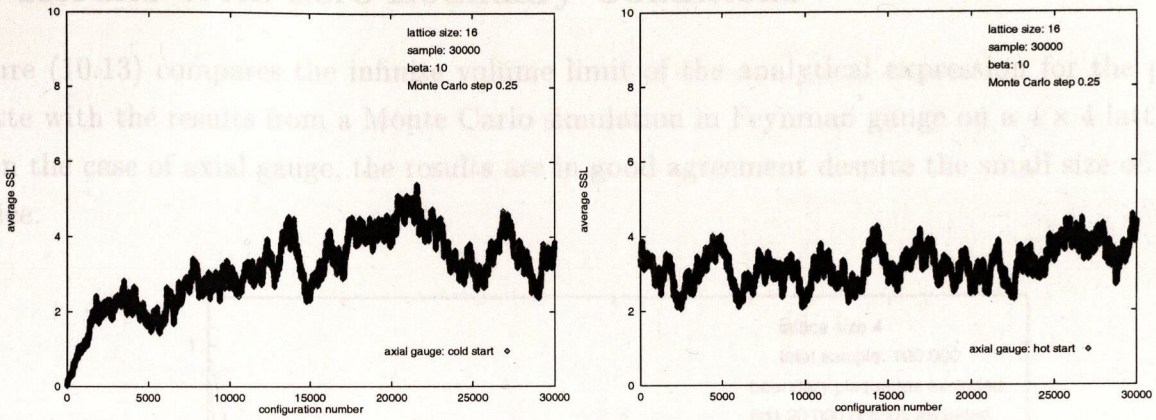

Figure 10.9: : The SSL averaged over the lattice for each configuration in axial gauge. Hot and cold starts converge to the same average.

49. Results With Zero Boundary Conditions

Figure (10.13) compares the infinite volume limit of the analytical expression for the plaquette with the results from a Monte Carlo simulation in Feynman gauge on a 4×4 lattice. As in the case of axial gauge, the results are in good agreement despite the small size of the lattice.

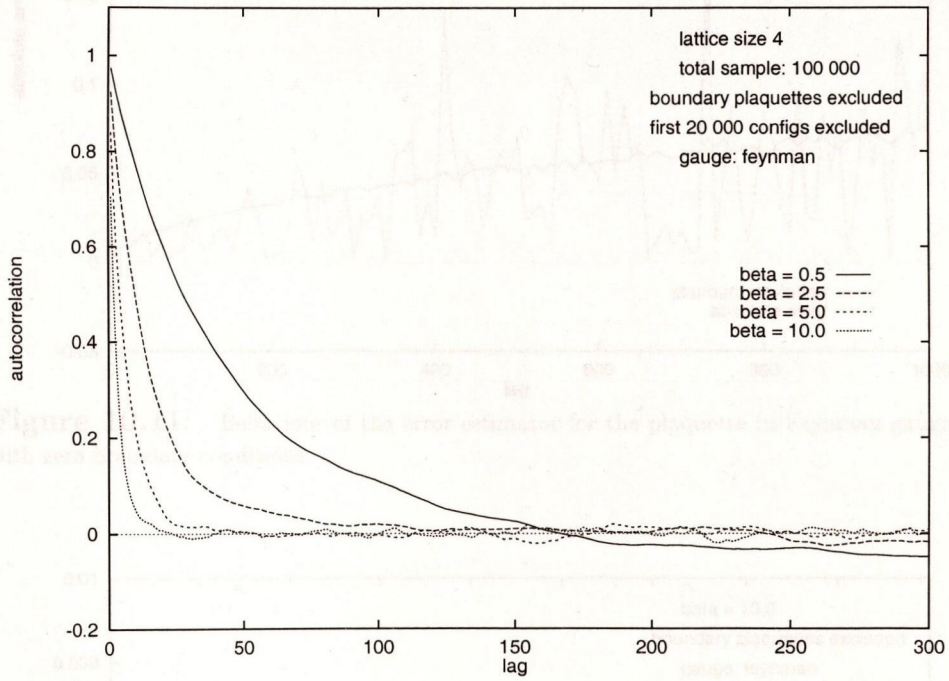

Figure 10.10: Decorrelation lengths for the plaquette in Feynman gauge with zero boundary conditions.

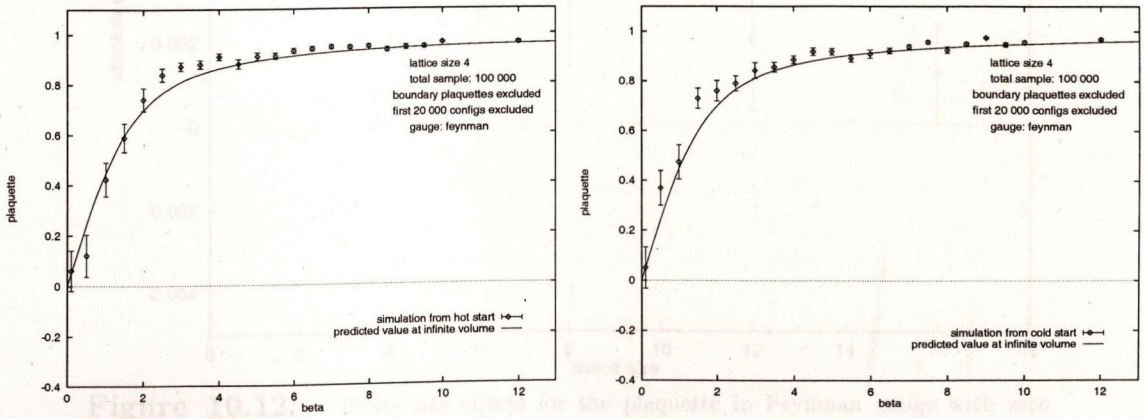

Figure 10.13: The plaquette in Feynman gauge with zero boundary conditions. The simulation on the left is a hot start while that on the right was started cold. The solid line is the analytical value at infinite volume.

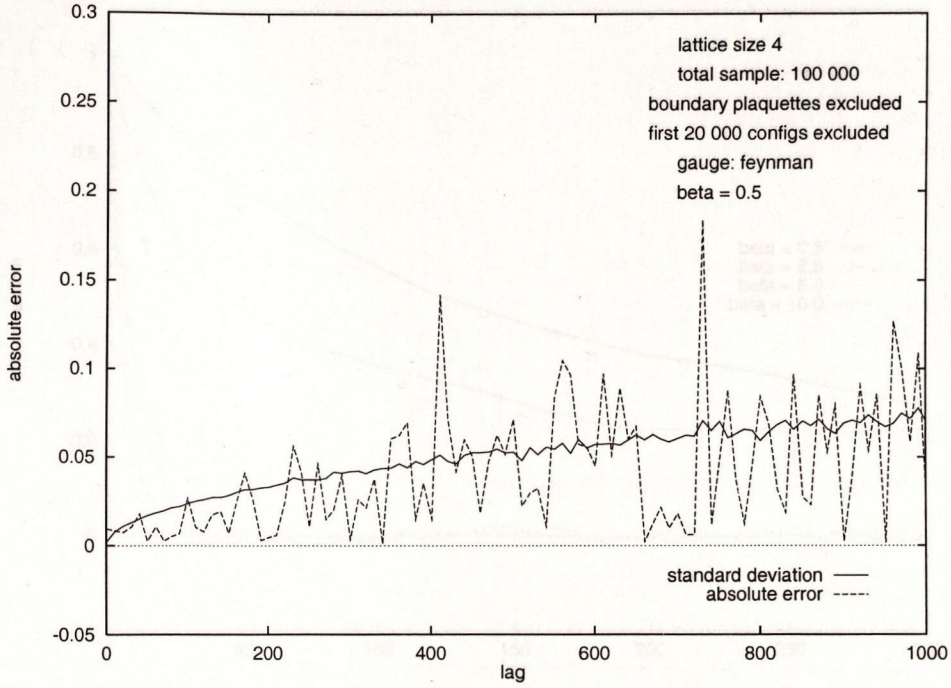

Figure 10.11: Behaviour of the error estimator for the plaquette in Feynman gauge with zero boundary conditions.

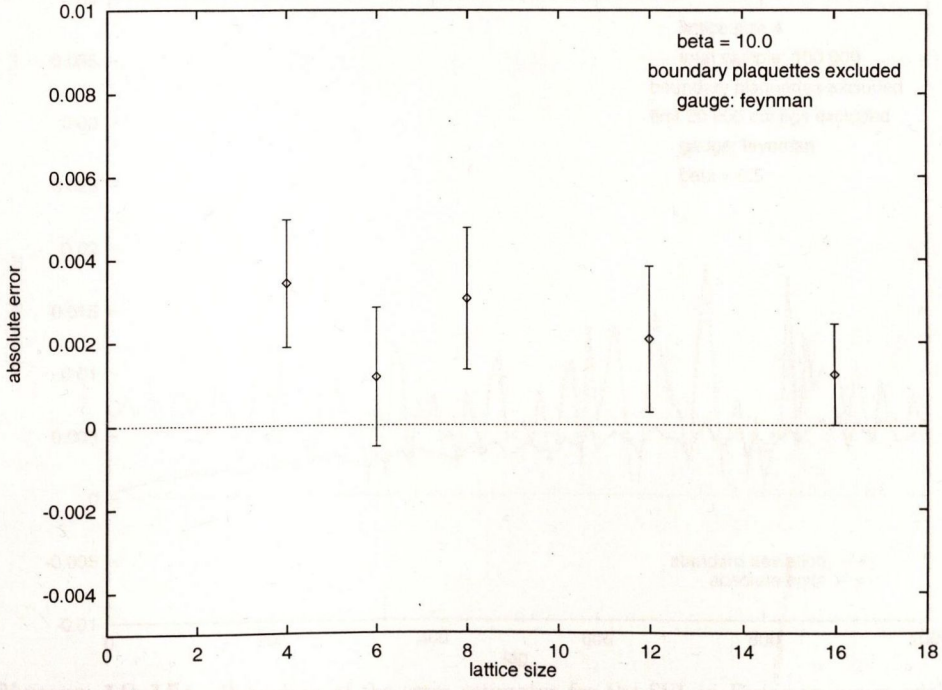

Figure 10.12: Finite size effects for the plaquette in Feynman gauge with zero boundary conditions.

Figure (10.17) compares the results of such a simulation, with the weak coupling approxi-

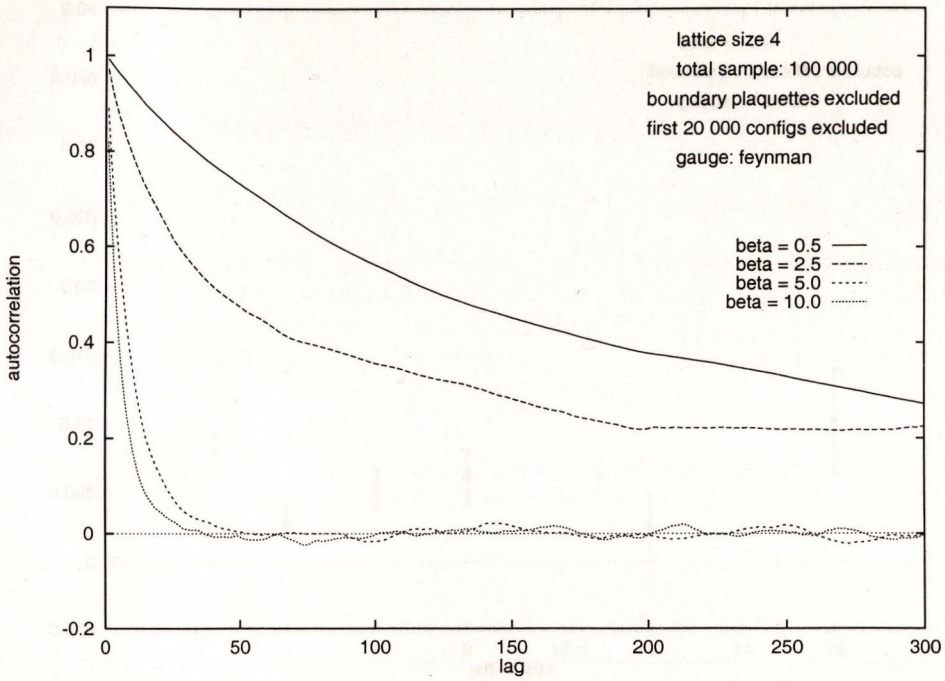

Figure 10.14: Decorrelation lengths for the SSL in Feynman gauge with zero boundary conditions.

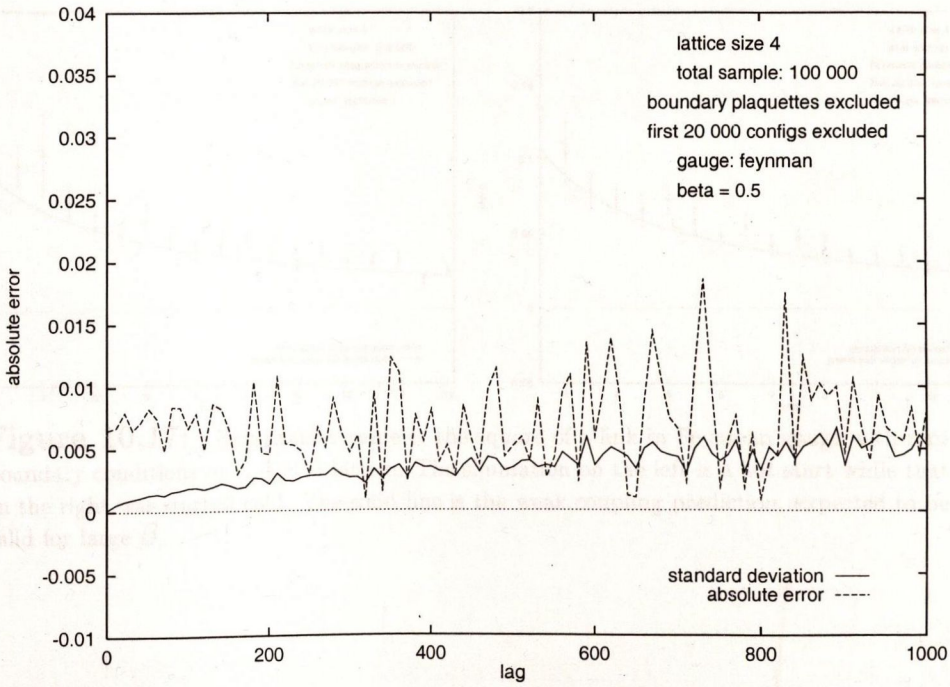

Figure 10.15: Behaviour of the error estimator for the SSL in Feynman gauge with zero boundary conditions.

mation with zero boundary conditions, valid for large values of β.

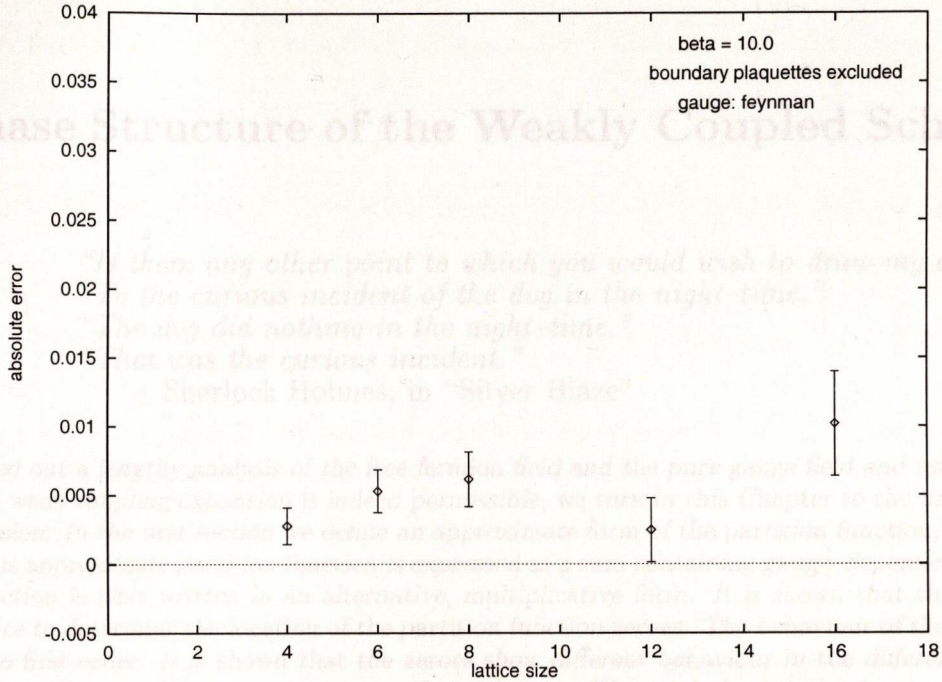

Figure 10.16: Finite size effects for the SSL in Feynman gauge with zero boundary conditions.

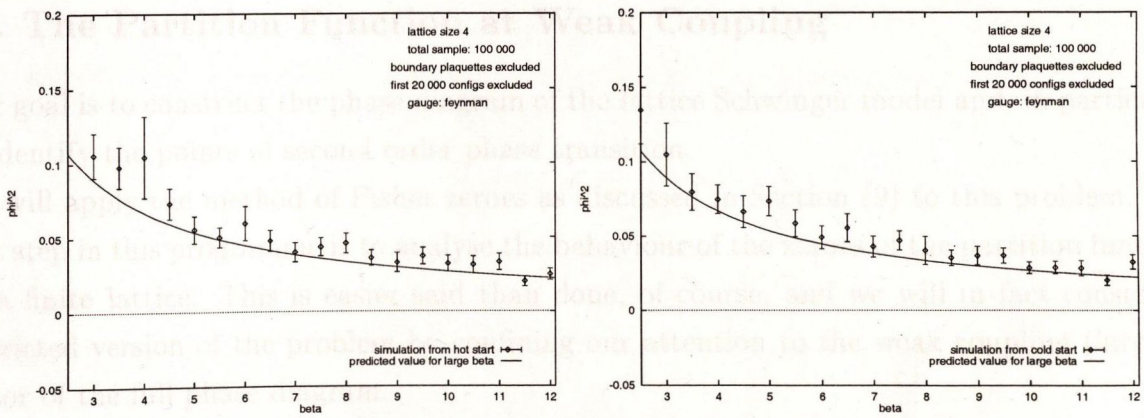

Figure 10.17: Expectation value of the square of a link in Feynman gauge with zero boundary conditions on a 4×4 lattice. The simulation on the left is a hot start while that on the right was started cold. The solid line is the weak coupling prediction, expected to be valid for large β.

11. Phase Structure of the Weakly Coupled Schwinger Model

"Is there any other point to which you would wish to draw my attention ?"
"To the curious incident of the dog in the night–time."
"The dog did nothing in the night–time."
"That was the curious incident."
– Sherlock Holmes, in "Silver Blaze"

Having carried out a lengthy analysis of the free fermion field and the pure gauge field and established that the proposed weak coupling expansion is indeed permissible, we turn in this Chapter to the implementation of this expansion. In the first section we define an approximate form of the partition function, valid at weak coupling. This approximate partition function is expressed as a sum containing gauge–dependent terms. The partition function is next written in an alternative, multiplicative form. It is shown that these two forms together suffice to determine the location of the partition function zeroes. The behaviour of the lowest zeroes is analysed to first order. It is shown that the zeroes show different behaviour in the different momentum regimes, but in all cases fail to converge onto the real axis. We conclude that (at least at this level of approximation) the Schwinger model fails to exhibit a phase transition in the weak coupling sector.

50. The Partition Function at Weak Coupling

Our goal is to construct the phase diagram of the lattice Schwinger model and, in particular, to identify the points of second order phase transition.

We will apply the method of Fisher zeroes as discussed in Section (9) to this problem. The first step in this programme is to analyse the behaviour of the zeroes of the partition function on a finite lattice. This is easier said than done, of course, and we will in fact consider a restricted version of the problem by confining our attention to the weak coupling (large β) sector of the full phase diagram.

The full partition function for lattice QED_2 is given by

$$Z_{QED_2} = \int D[U]D[\bar{\psi}\psi]\, e^{-(S_{FG}+S_G)}$$

The integral over the fermion fields may be carried out to yield a determinant factor, leaving

$$\begin{aligned} Z_{QED_2} &= \int D[U](\det M_{QED_2})\, e^{-S_G} \\ &= Z_G \langle \det M_{QED_2} \rangle_G \end{aligned} \tag{11.1}$$

where Z_G is the pure gauge partition function, $\langle\,\rangle_G$ denotes an expectation value over the gauge field and the operator M_{QED_2} is given by

$$M_{QED_2} = \delta_{\underline{nm}} - \kappa \left\{ (1-\gamma_\mu)\, U_{\underline{\mu}}(\underline{m})\, \delta_{\underline{n}(\underline{m}+\underline{\mu})} + (1+\gamma_\mu)\, U^\dagger{}_{\underline{\mu}}(\underline{m}-\underline{\mu})\, \delta_{\underline{n}(\underline{m}-\underline{\mu})} \right\}$$

It will prove convenient to extract a factor of $\frac{1}{2\kappa}$ and work instead with the operator

$$M_{QED_2} = \frac{1}{2\kappa}\delta_{\underline{nm}} - \frac{1}{2}\left\{ (1-\gamma_\mu)\, U_{\underline{\mu}}(\underline{m})\, \delta_{\underline{n}(\underline{m}+\underline{\mu})} + (1+\gamma_\mu)\, U^\dagger{}_{\underline{\mu}}(\underline{m}-\underline{\mu})\, \delta_{\underline{n}(\underline{m}-\underline{\mu})} \right\} \qquad (11.2)$$

In other words, the partition function is simply proportional to $\langle \det M_{QED_2} \rangle_G$. The zeroes of Z_{QED_2} are therefore fully determined by the zeroes of $\langle \det M_{QED_2} \rangle_G$. This object is a pure gauge expectation value.

Note that Z_{QED_2} and Z_G are both gauge invariant by construction. It follows from (11.1) that $\langle \det M_{QED_2} \rangle_G$ is also gauge invariant.

Our strategy in determining the zeroes of $\langle \det M_{QED_2} \rangle_G$ will be as follows. We will consider only the weak coupling regime. The problem of developing an unambiguous weak coupling approximation for a two–dimensional U(1) gauge field was considered in Chapter 3. It was shown there that a simple restriction of the angular variables ϕ to small values would suffice, provided that a zero boundary condition was imposed on the gauge field. It is therefore permissible to expand perturbatively around the free fermion field in powers of the angular gauge field variables ϕ_i. The shift in the free field zeroes due to the introduction of a weak gauge field may thus be determined (in principle) to any required order in ϕ_i. The nth order shift will then be a function of nth order pure gauge correlation functions $\langle \phi_1 \dots \phi_n \rangle$. In particular, at second order the shifts will be functions of the pure gauge propagator.

Let us therefore define an approximate pure gauge partition function by

$$Z_{WG} = \int D[U]\, e^{-\beta S_W} \qquad (11.3)$$

where

$$\beta = \frac{1}{2g^2}$$

and

$$S_W = \sum_{p,\mu,\nu} (1 - \cos \phi_p(\mu,\nu)) \quad ; \quad -\epsilon < \phi_p(\mu,\nu)) \leq \epsilon$$

The partition function (11.3) is effectively Z_G with the contributions from large-ϕ configurations removed. It may be may be regarded as a family of functions parametrised by the the inverse coupling, β. For large values of β the integral is strongly peaked around $S_W = 0$, the large-ϕ contribution is negligible and we have

$$Z_{WG} \approx Z_G$$

It should be emphasised that two approximations are being made here. Firstly, we make a saddle-point approximation in which the integral is truncated to run only over small values of ϕ. This approximation in turn is valid only if the integral is strongly peaked around such values; we ensure that this is the case by choosing a sufficiently small value for the coupling constant g.

51. Additive Expansion Of The Partition Function

In this section we will develop an additive expansion of $\langle \det M_{QED} \rangle_G$.
It is convenient at this point to write

$$M_{QED_2} = M_0 + \Delta M$$

where M_0 is the free fermion operator (scaled, as above, by a factor of $\frac{1}{2\kappa}$) and ΔM contains the gauge terms in M_{QED}, thus

$$M_0 = \frac{1}{2\kappa}\delta_{\underline{n}\underline{m}} - \frac{1}{2}\left\{(1-\gamma_\mu)\,\delta_{\underline{n}(\underline{m}+\underline{\mu})} + (1+\gamma_\mu)\,\delta_{\underline{n}(\underline{m}-\underline{\mu})}\right\}$$

$$\Delta M = \frac{1}{2}\left\{(1-\gamma_\mu)\,(1-U_{\underline{\mu}}(\underline{m}))\,\delta_{\underline{n}(\underline{m}+\underline{\mu})} + (1+\gamma_\mu)\,(1-U^\dagger{}_{\underline{\mu}}(\underline{m}-\underline{\mu}))\,\delta_{\underline{n}(\underline{m}-\underline{\mu})}\right\} \qquad (11.4)$$

Note that ΔM, which is the gauge dependent part of M_{QED_2} is independent of the hopping parameter κ. Moreover ΔM depends on the gauge field through terms of the form $(1 - U_\mu(\underline{m}))$; that is:

$$\Delta M \propto i\phi - \phi^2 + \ldots$$

Therefore, in carrying out a perturbative expansion to second order in ϕ, it is sufficient to retain only terms up to second order in ΔM.
The eigenvalues of the free field operator M_0 follow from (6.9) and (6.13):

$$\lambda_{\underline{k},\alpha} = \frac{1}{2\kappa} - \sum_\mu \cos k_\mu + (-1)^\alpha i \left(\sin^2 k_\mu\right)^{\frac{1}{2}} \qquad (11.5)$$

It is possible to obtain the eigenvalues of M_{QED_2} from those of M_0 by means of standard perturbation theory (see for example Schiff, 1949) and thereby to determine the zeroes of $\det M_{QED_2}$ to any desired order. This does not suffice, however, to determine the zeroes of the partition function, which is the pure gauge expectation value of $\det M_{QED_2}$
The first stage in the determination of these zeroes is to express the partition function in terms of pure gauge expectation values of ΔM. Let us therefore write

$$
\begin{aligned}
M_{QED_2} &= (M_{QED_2} M_0{}^{-1}) M_0 \qquad (\det M_0 \neq 0) \\
\Rightarrow \det M_{QED_2} &= \det(M_{QED_2} M_0{}^{-1}) \det M_0 \\
\Rightarrow \langle \det M_{QED_2} \rangle_G &= \det M_0 \, \langle \det(M_{QED_2} M_0{}^{-1}) \rangle_G \\
&= \det M_0 \, \langle \det(1 + \Delta M M_0{}^{-1} \rangle_G
\end{aligned}
$$

and hence

$$
\frac{\langle \det M_{QED_2} \rangle_G}{\det M_0} = \langle \det(1 + \Delta M M_0{}^{-1} \rangle_G \qquad (\det M_0 \neq 0)
$$

Now if the matrix $1 + \Delta M M_0{}^{-1}$ is diagonalisable its determinant may be written in the form

$$
\det(1 + \Delta M M_0{}^{-1}) = \exp(\operatorname{tr} \log(1 + \Delta M M_0{}^{-1})) \tag{11.6}
$$

The exponential term in (11.6) may now be evaluated approximately. Since we are working to second order in ϕ we need only retain terms up to this order in ΔM. Thus, to order $(\Delta M)^2$ we have

$$
\operatorname{tr} \log(1 + \Delta M M_0{}^{-1}) = \operatorname{tr}(\Delta M M_0{}^{-1}) - \frac{1}{2} \operatorname{tr}(\Delta M M_0{}^{-1})^2
$$

and

$$
\begin{aligned}
\exp(\operatorname{tr} \log(1 + \Delta M M_0{}^{-1})) &= 1 + \operatorname{tr}(\Delta M M_0{}^{-1}) - \frac{1}{2} \operatorname{tr}(\Delta M M_0{}^{-1})^2 \\
&\quad + \frac{1}{2} \{ \operatorname{tr}(\Delta M M_0{}^{-1}) - \frac{1}{2} \operatorname{tr}(\Delta M M_0{}^{-1})^2 \}^2 \\
&= 1 + \operatorname{tr}(\Delta M M_0{}^{-1}) - \frac{1}{2} \operatorname{tr}(\Delta M M_0{}^{-1})^2 + \frac{1}{2} (\operatorname{tr}(\Delta M M_0{}^{-1}))^2
\end{aligned}
$$

The expression (11.6) for $\langle \det M_{QED_2} \rangle_G$ can therefore be written in the approximate form

$$
\begin{aligned}
\frac{\langle \det M_{QED_2} \rangle_G}{\det M_0} &\approx 1 + \langle \operatorname{tr}(\Delta M M_0{}^{-1}) \rangle_G - \frac{1}{2} \langle \operatorname{tr}(\Delta M M_0{}^{-1})^2 \rangle_G + \frac{1}{2} \langle (\operatorname{tr}(\Delta M M_0{}^{-1}))^2 \rangle_G \\
&= \frac{\langle \det M_W \rangle_G}{\det M_0}
\end{aligned} \tag{11.7}
$$

It is essential to note that gauge invariance has been lost in the process of developing this perturbative expansion. The expectation values appearing in (11.7) are gauge-dependent and will yield a gauge-dependent expression for $\langle \det M_W \rangle_G$. We are guaranteed, however, that for sufficiently weak coupling $\langle \det M_W \rangle_G$ will approach the gauge invariant quantity $\langle \det M_{QED_2} \rangle_G$ (in some gauge-dependent way). Therefore, any convenient gauge may be selected—the choice of gauge will determine the manner in which the approximate solution approaches the true solution, but not the final result.

§51. Additive Expansion Of The Partition Function

In order to write the traces in (11.7) in a more explicit form, consider an orthonormal set of basis vectors satisfying:

$$\langle \chi^a | \chi^b \rangle = \delta_{ab}$$

Now consider

$$\sum_a (\chi_\alpha^a)^* \chi_\beta^a = P_{\alpha\beta} \quad \Rightarrow \sum_a (\chi_\alpha^a)^* \chi_\beta^a \chi_\alpha^b = P_{\alpha\beta}\chi_\alpha^b$$

$$\Rightarrow \sum_a \left((\chi_\alpha^a)^* \chi_\alpha^b\right) \chi_\beta^a = P_{\alpha\beta}\chi_\alpha^b \quad \Rightarrow \sum_a \delta_{ab}\, \chi_\beta^a = P_{\alpha\beta}\chi_\alpha^b$$

$$\Rightarrow \chi_\beta^a = P_{\alpha\beta}\chi_\alpha^b \quad \Rightarrow P_{\alpha\beta} = \delta_{\alpha\beta}$$

Any set of orthornormal basis vectors therefore satisfies the identity

$$\sum_a (\chi_\alpha^a)^* \chi_\beta^a = \delta_{\alpha\beta}$$

Next, for any matrix Q, we have

$$\sum_a \langle \chi^a | Q | \chi^a \rangle = \left(\sum_a (\chi_\alpha^a)^* \chi_\beta^a \right) Q_{\alpha\beta} = \delta_{\alpha\beta} Q_{\alpha\beta} = \operatorname{tr} Q$$

Now it was shown in Section (27) that the eigenvectors of M_0, $|\lambda^a\rangle$ form an orthonormal set. We may therefore write

$$\operatorname{tr}(\Delta M M_0^{-1}) = \sum_a \langle \lambda^a | (\Delta M) M_0^{-1} | \lambda^a \rangle = \sum_a (\lambda_i^a)^* \Delta M_{ij} {M_0^{-1}}_{jk} \lambda_k^a$$

$$= \frac{\sum_a (\lambda_i^a)^* \Delta M_{ij} \lambda_j^a}{\lambda_j} = \frac{\delta_{ij} \Delta M_{ij}}{\lambda_j} = \frac{\Delta M_{ii}}{\lambda_i}$$

Similarly, we find

$$(\operatorname{tr}(\Delta M M_0^{-1}))^2 = \sum_{i \neq j} \frac{\Delta M_{ii}}{\lambda_i} \frac{\Delta M_{jj}}{\lambda_j}$$

$$\operatorname{tr}((\Delta M M_0^{-1})^2) = \sum_{i \neq j} \frac{\Delta M_{ij}}{\lambda_i} \frac{\Delta M_{ji}}{\lambda_j}$$

If we now define the pure gauge expectation values

$$t_i = \langle \Delta M_{ii} \rangle_G$$

$$t_{ij} = \langle \Delta M_{ij} \Delta M_{ji} \rangle_G - \langle \Delta M_{ii} \Delta M_{ii} \rangle_G$$

the additive expansion (11.7) can be written

$$\frac{\langle \det M_{QED_2} \rangle_G}{\det M_0} = 1 + \sum_{i=1}^{2N^2} \frac{t_i}{\lambda_i} - \frac{1}{2} \sum_{i \neq j}^{2N^2} \frac{t_{ij}}{\lambda_i \lambda_j} + \dots \tag{11.8}$$

52. Multiplicative Expansion Of the Partition Function

The partition function of the Schwinger model may also be expanded perturbatively in multiplicative form. To this end, let us rewrite the expression (11.2) for M_{QED_2}:

$$M_{QED_2} = \eta\,\delta_{\underline{nm}} - H_{\underline{nm}}$$

where

$$\eta = \frac{1}{2\kappa}$$

and

$$H_{\underline{nm}} = \frac{1}{2}\left\{(1-\gamma_\mu)\,U_{\underline{\mu}}(\underline{m})\,\delta_{\underline{n}(\underline{m}+\underline{\mu})} + (1+\gamma_\mu)\,U^\dagger{}_{\underline{\mu}}(\underline{m}-\underline{\mu})\,\delta_{\underline{n}(\underline{m}-\underline{\mu})}\right\}$$

Since we are working on a finite lattice, M_{QED_2} is of finite dimension and its determinant may therefore be written as a polynomial in η.

$$\det M_{QED_2} = \sum_{\tau=1}^{2N^2} F_\tau(\phi)\,\eta^\tau$$

The gauge expectation value of $\det M_{QED_2}$ is therefore given by

$$\langle \det M_{QED_2}\rangle_G = \sum_{\tau=1}^{2N^2} \langle F_\tau(\phi)\rangle_G\,\eta^\tau$$

which is again a polynomial in η. It may therefore be written

$$\langle \det M_{QED_2}\rangle_G = \prod_{i=1}^{i=2N^2} (\eta - \eta_i)$$

Here the η_i are the true zeroes of the partition function; note that they are *not* zeroes of the determinant except when the gauge field vanishes. The expression (11.8) may therefore be written in the alternative form

$$\frac{\langle \det M_{QED_2}\rangle_G}{\det M_0} = \prod_{i=1}^{i=2N^2} \frac{(\eta-\eta_i)}{(\lambda_i)} \tag{11.9}$$

The free field eigenvalues λ_i can be written $(\eta - \eta_i^0)$, where, from (11.5) we have

$$\eta = \frac{1}{2\kappa}$$
$$\eta_i^0 = \sum_\mu \cos k_\mu + (-1)^\alpha i \left(\sin^2 k_\mu\right)^{\frac{1}{2}}$$

The η_i^0 are therefore the zeroes of the free fermion partition function, which is now to be regarded as a function of η. The multiplicative expansion (11.9) can now be written in the form

$$\frac{\langle \det M_{QED_2} \rangle_G}{\det M_0} = \prod_{i=1}^{i=2N^2} \left(1 - \frac{\Delta_i}{(\eta - \eta_i^0)}\right) \tag{11.10}$$

Here $\Delta_i = (\eta_i - \eta_i^0)$ represents the shift in the ith zero due to the presence of the gauge field. The expression (11.10) is exact; it is the Δ_i which are to be determined perturbatively.

53. The First Order Shift

The partition function of the Schwinger model has now been expressed in two different ways. An additive expansion was derived in terms of pure gauge expectation values was derived in Section (51). These expectation values are computable; however, the shift in the zeroes cannot be directly derived from them.

An alternative, multiplicative expression was obtained in Section (52). This expression contains the shift in the zeroes explicitly, but in a form which is not amenable to direct calculation.

We therefore require a relation beween the shifts in the zeroes, Δ_i and the calculable pure gauge expectation values t_i and t_{ij}. From (11.8) and (11.10) we have

$$1 + \sum_{i=1}^{2N^2} \frac{t_i}{(\eta - \eta_i^0)} - \frac{1}{2} \sum_{i \neq j}^{2N^2} \frac{t_{ij}}{(\eta - \eta_i^0)(\eta - \eta_j^0)} + \ldots = \prod_{i=1}^{i=2N^2} \left(1 - \frac{\Delta_i}{(\eta - \eta_i^0)}\right) \tag{11.11}$$

where we have used $\lambda_i = (\eta - \eta_i^0)$.

The required relation may be obtained by observing that both sides of (11.11) are analytic in η with poles at η_i^0.

Before proceeding, let us expand t_i, t_{ij} and Δ_i in powers of ϕ (or, equivalently, in powers of the coupling constant, g). Note that $t_i^{(1)}$ is proportional to $\langle \phi \rangle$ which is zero. Moreover t_{ij} depends quadratically on ΔM; therefore $t_{ij}^{(1)}$ is also zero. Therefore, to second order, we have simply

$$\begin{aligned} t_i &= t_i^{(2)} + \ldots \\ t_{ij} &= t_{ij}^{(2)} + \ldots \\ \Delta_i &= \Delta_i^{(1)} + \Delta_i^{(2)} + \ldots \end{aligned} \tag{11.12}$$

The eigenvalues of the free field operator were shown in Section (28) to be either two–fold or four–fold degenerate if antiperiodic boundary conditions are imposed. Consider first the case of two–fold degenerate eigenvalues:

$$\lambda_{m_1} = \lambda_{m_2} = \lambda_m$$

Equating residues of the single pole at $\eta = \eta_m^0$ in (11.11) yields, to second order

$$t_{m_1}^{(2)} + t_{m_2}^{(2)} - \sum_{i \neq m_1, m_2} \frac{t_{im_1} + t_{im_2}}{\eta_m^{(0)} - \eta_i^{(0)}} = -(\Delta_{m_1}^{(1)} + \Delta_{m_1}^{(2)} + \Delta_{m_2}^{(1)} + \Delta_{m_2}^{(2)}) \left(1 - \sum_{i \neq m_1, m_2} \frac{\Delta_i^{(1)} + \Delta_i^{(2)}}{\eta_m^{(0)} - \eta_i^{(0)}} \right)$$

Comparing the first and second order terms respectively on each side gives

$$\begin{aligned} \Delta_{n_1}^{(1)} + \Delta_{n_2}^{(1)} &= 0 \\ \Delta_{n_1}^{(2)} + \Delta_{n_2}^{(2)} &= -t_{m_1}^{(2)} - t_{m_2}^{(2)} + \sum_{i \neq m_1, m_2} \frac{t_{im_1}^{(2)} + t_{im_2}^{(2)}}{\eta_m^{(0)} - \eta_i^{(0)}} \end{aligned} \tag{11.13}$$

An analogous result holds for the four–fold degenerate eigenvalues

$$\sum_{j=1}^{4} \Delta_{m_j}^{(1)} = 0 \quad ; \quad \sum_{j=1}^{4} \Delta_{m_j}^{(2)} = \sum_{j=1}^{4} \left(t_{m_j}^{(2)} + \sum_{i \neq m_j} \frac{t_{im_j}^{(2)}}{\eta_m^{(0)} - \eta_i^{(0)}} \right)$$

The first order shifts $\Delta_i^{(1)}$ may be determined explicitly by expanding the multiplicative expression (11.10) and comparing it with the additive expression (11.8).In the case of the two–fold degenerate eigenvalues this yields the additional condition

$$(\Delta_{m_1}^{(1)})^2 + (\Delta_{m_2}^{(1)})^2 = 2t_{m_1 m_2}^{(2)}$$

This, together with (11.13) yields

$$\begin{aligned} \Delta_{m_1}^{(1)} &= +\sqrt{t_{m_1 m_2}^{(2)}} \\ \Delta_{m_2}^{(1)} &= -\sqrt{t_{m_1 m_2}^{(2)}} \end{aligned} \tag{11.14}$$

54. The Lowest Zeroes

The techniques outlined in the preceding sections have been used by Kenna, Pinto and Sexton (1999) to investigate analytically the behaviour of the zeroes of the partition function of the Schwinger model at weak coupling. They present results up to second order for both two–fold and four–fold degenerate zeroes.

The main features of the analysis can be illustrated by considering the two–fold degenerate zeroes associated with momentum

$$\underline{k} = (2\pi p_1/N\,,\,0) \qquad (-N/2+1/2) \leq p_1 \leq (N/2-1/2)$$

First order effects will dominate for sufficiently large β and the following discussion will be confined to this order.

According to (11.14) the first order shift in a two–fold degenerate zero of the type we are considering is given by

$$\begin{aligned} \eta^{(1)}(p_1,0) &= +\left(\left\langle \Delta M_{\underline{p}(\alpha),-\underline{p}(\alpha)}, \Delta M_{-\underline{p}(\alpha),\underline{p}(\alpha)} \right\rangle\right)^{\frac{1}{2}} \\ \eta^{(1)}(-p_1,0) &= -\left(\left\langle \Delta M_{\underline{p}(\alpha),-\underline{p}(\alpha)}, \Delta M_{-\underline{p}(\alpha),\underline{p}(\alpha)} \right\rangle\right)^{\frac{1}{2}} \end{aligned} \tag{11.15}$$

The two zeroes associated with the degenerate free eigenvalues $\lambda(\pm p_1, 0)$, which coincide in the free case therefore become distinct when the gauge field is turned on.

This behaviour is illustrated in Figure (11.1)

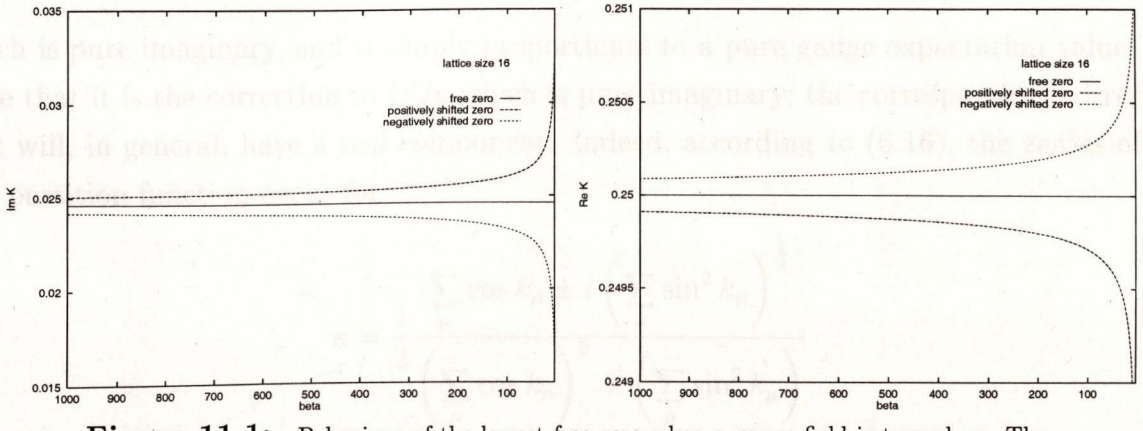

Figure 11.1: Behaviour of the lowest free zero when a gauge field is turned on. The free zero splits into two zeroes, which diverge as the field strength is increased.The figure on the left shows the imaginary part of the free and shifted zeroes, while that on the left shows the real part.

The general expression at first order for expectation values of the type in (11.15) is given

from perturbation theory by

$$\left\langle \Delta M^{(1)}_{\underline{p}(\alpha),\underline{q}(\beta)} \Delta M^{(1)}_{\underline{q}(\beta),\underline{p}(\alpha)} \right\rangle = \frac{1}{2N^4} \sum_{\mu} \left\langle |\phi_\mu(\underline{p}-\underline{q})|^2 \right\rangle$$
$$\times \Bigg\{ -\cos(p_\mu + q_\mu)$$
$$+ \frac{(-1)^{\alpha+\beta}}{\sqrt{PQ}} \Big[\delta_{\mu 1} (\sin p_2 \sin q_2 - \cos(p_1+q_1) \sin p_1 \sin q_1)$$
$$+ \delta_{\mu 2} (\sin p_1 \sin q_1 - \cos(p_2+q_2) \sin p_2 \sin q_2) \Big]$$
$$+ i \left[\frac{(-1)^\alpha}{\sqrt{P}} \sin p_\mu + \frac{(-1)^\beta}{\sqrt{Q}} \sin q_\mu \right] \sin(p_\mu + q_\mu) \Bigg\}$$

where

$$P = \sin^2 p_1 + \sin^2 p_2$$
$$Q = \sin^2 q_1 + \sin^2 q_2$$

This rather formidable looking expression reduces, in the case of the special zeroes we are considering, to

$$\left\langle \Delta M^{(1)}_{\underline{p}(\alpha),-\underline{p}(\alpha)} \Delta M^{(1)}_{-\underline{p}(\alpha),\underline{p}(\alpha)} \right\rangle = -\frac{1}{2N^4} \left\langle |\phi_1(2\underline{p})|^2 \right\rangle$$

where we have taken $\alpha = 2$.

The correction to the free zero is then given by

$$\eta^{(1)}(p_1, 0) = \frac{i}{\sqrt{2}N^2} \left(\left\langle |\phi_1(2\underline{p})|^2 \right\rangle \right)^{\frac{1}{2}}$$

which is pure imaginary, and is simply proportional to a pure gauge expectation value.

Note that it is the correction to $1/2\kappa$ which is pure imaginary; the corresponding correction to κ will, in general, have a real component. Indeed, according to (6.16), the zeroes of the free partition function occur for

$$\kappa = \frac{1}{2} \frac{\sum_\mu \cos k_\mu \pm i \left(\sum_\mu \sin^2 k_\mu \right)^{\frac{1}{2}}}{\left(\sum_\mu \cos k_\mu \right)^2 + \left(\sum_\mu \sin^2 k_\mu \right)}$$

If we consider only momenta of the form $(p_1, 0)$, we may write

$$\kappa = \frac{A \pm iB}{2(A^2 + B^2)}$$

where

$$A = 1 + \cos k_1 \qquad B = \sin k_1$$

We then have

$$\frac{1}{2\kappa} = A \pm iB \longrightarrow \frac{1}{2\kappa'} = A \pm i(B \pm R)$$

where

$$R = \eta^{(1)}(p_1, 0)$$

This gives

$$\kappa' = \frac{A \pm i(B+R)}{2\left(A^2 + (B+R)^2\right)} \tag{11.16}$$

It is clear from this expression that the shifted zero will fail to converge onto the real axis if R remains finite as the lattice size tends to infinity.

55. Partition Function Zeroes in Feynman Gauge

The shifted zeroes (11.16) may be determined explicitly once a gauge has been fixed. In Feynman gauge we have from (7.29)

$$\left\langle |\phi_1((2p)|^2 \right\rangle^{\frac{1}{2}} = \frac{N}{2\sqrt{\beta}} \frac{1}{|\sin \frac{2\pi p_1}{N}|}$$

which gives, in the notation of the preceding section

$$R = \frac{1}{2\sqrt{2\beta}} \frac{1}{N|\sin \frac{2\pi p_1}{N}|}$$

It is the dependence of R on N that determines the behaviour of the zeroes at fixed β
Let us first consider the case where p_1 is small compared with N. Setting $p_1 = 1/2$ we obtain

$$R = \frac{1}{2\sqrt{2\beta}} \frac{1}{N|\sin \frac{\pi}{N}|}$$

In the limit of large N, the N-dependence disappears from R and we have simply

$$\lim_{N\to\infty} R = \frac{1}{2\pi\sqrt{2\beta}}$$
$$\lim_{N\to\infty} A = 2$$
$$\lim_{N\to\infty} B = 0$$

giving, for the shifted zeroes

$$\lim_{N\to\infty} \kappa' = \frac{2 \pm iR}{8 + 2R^2}$$

For large β (small R) the imaginary part of the zero is given approximately by:

$$\lim_{N\to\infty} \mathrm{Im}\ \kappa' \approx \frac{R}{8} = \frac{1}{16\pi\sqrt{2\beta}}$$

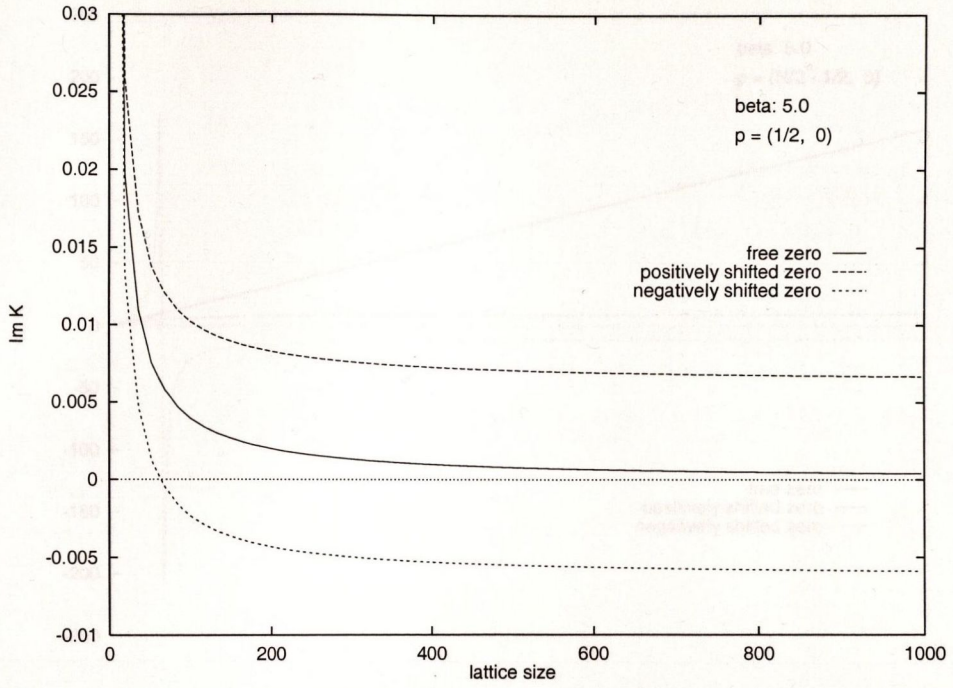

Figure 11.2: Behaviour of the imaginary part of the lowest zero when a weak gauge field is turned on. The free zero splits into two new zeroes. As the lattice size is increased the lower zero crosses the real axis while the higher one tends to a fixed distance above the real axis.

The zero does not therefore converge onto the real axis for finite β.

Figure (11.2) displays the behaviour of the imaginary parts of each of the shifted zeroes with increasing lattice size at $\beta = 5.0$.

Next let us consider the large momentum limit. Setting $p_1 = N/2 - 1/2$ gives

$$R = \frac{1}{2\sqrt{2\beta}} \frac{1}{N|\sin\pi - \frac{\pi}{N}|} = \frac{1}{2\sqrt{2\beta}} \frac{1}{N|\sin\frac{\pi}{N}|}$$

The infinite volume limits are now

$$\lim_{N\to\infty} R = \frac{1}{2\pi\sqrt{2\beta}}$$
$$\lim_{N\to\infty} A = 0$$
$$\lim_{N\to\infty} B = 0$$

and hence

$$\lim_{N\to\infty} \mathrm{Im}\ \kappa' = \frac{1}{2R} = \pi\sqrt{2\beta}$$

Note that this zero moves further away from the real axis with increasing β, indicating that zeroes of this type do not accumulate on the real axis even in the absence of a gauge field. The behaviour of these high momentum zeroes is exhibited in Figure (11.3).

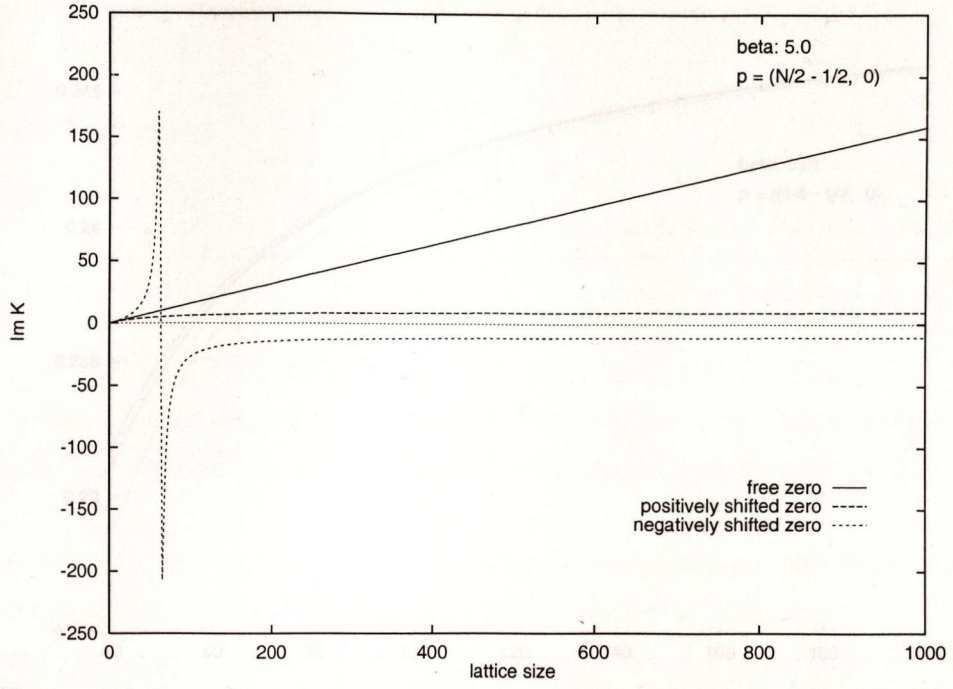

Figure 11.3: Behaviour of high momentum zeros when a gauge field is turned on. The zeroes diverge from the real axis in both the free and interacting cases. Note the sharp spike in the lower zero at $R = -B$

Lastly, let us consider $p_1 = N/4 - 1/2$. Then

$$R = \frac{1}{2\sqrt{2\beta}} \frac{1}{N|\sin\frac{\pi}{2} - \frac{\pi}{N}|}$$

which gives

$$\lim_{N\to\infty} R = 0$$
$$\lim_{N\to\infty} A = 1$$
$$\lim_{N\to\infty} B = 1$$

and this time

$$\lim_{N\to\infty} \mathrm{Im}\ \kappa' = \frac{1}{4}$$

This time the zeroes converge on the free value, the imaginary part of which in this case is 0.25 in the infinite volume limit. This behaviour is illustrated in Figure (11.4)

The zeroes therefore display very different behaviour in the different momentum regimes. At low momenta, the shift in the zeroes decays with increasing β, but is always sufficient to prevent the accumulation on the real axis which occurs in the free case. At moderate momenta the shift disappears altogether for large N, and the behaviour is identical to that of the free zeroes, which do not, however, condense in this regime. At high momenta the

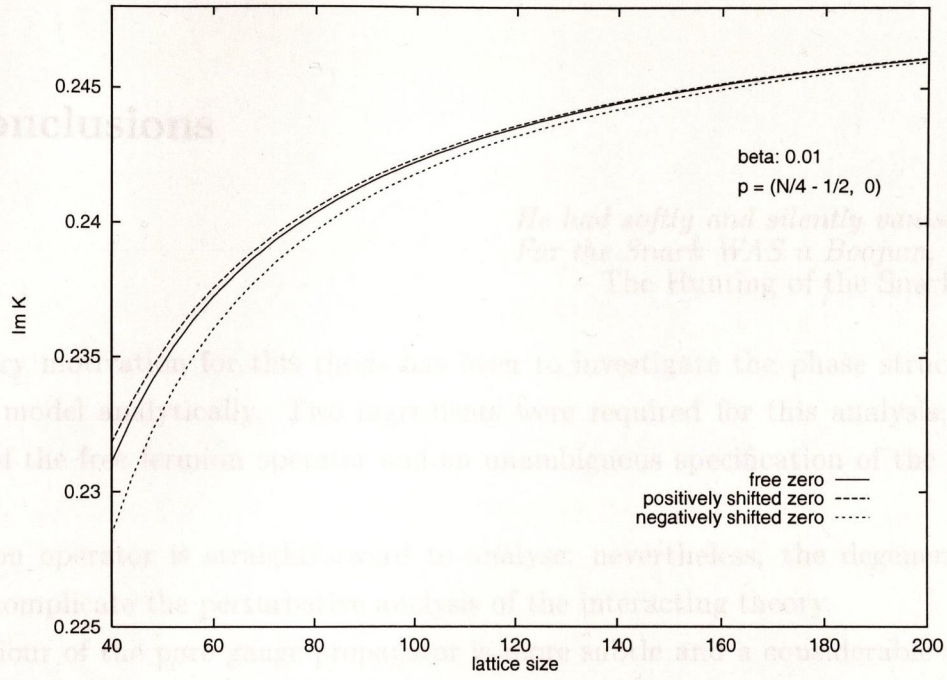

Figure 11.4: Behaviour of intermediate momentum zeros when a gauge field is turned on. The zeroes converge on the free value with increasing lattice size; however the free zeroes do not themselves approach the real axis in this regime. A value of $\beta = 0.01$ was used in order to display the zeroes on a reasonable scale.

shift grows with increasing β, indicating that the free zeroes diverge from the real axis in this regime.

In all cases the zeroes fail to converge onto the real axis, indicating (at least as far as this analysis goes) the absence of a phase transition in the weak coupling regime.

Two further possibilities should be considered, before such a conclusion can be established. Firstly, it is possible that classes of zeroes, other than those we have considered, do accumulate on the real axis and give rise to a phase transition.

Secondly, it is conceivable that higher order terms in the weak coupling expansion are so strongly dependent on N that they dominate the first order term and force an accumulation of zeroes for *any* value of β, however large. This is simply another way of saying that perturbation theory cannot be used for this problem; while this objection is undeniable, it is one which could be levelled against many if not all perturbative calculations.

12. Conclusions

He had softly and silently vanished away—
For the Snark WAS a Boojum, you see
– The Hunting of the Snark

The primary motivation for this thesis has been to investigate the phase structure of the Schwinger model analytically. Two ingredients were required for this analysis; the eigenstructure of the free fermion operator and an unambiguous specification of the pure gauge propagator.

The fermion operator is straightforward to analyse; nevertheless, the degeneracies in its spectrum complicate the perturbative analysis of the interacting theory.

The behaviour of the pure gauge propagator is more subtle and a considerable part of this thesis has been devoted to its study. The investigation focused primarily on the expectation value $\langle \phi^2 \rangle$, or SSL, which is of particular relevance to lowest order perturbation theory.

From the analytic point of view, it was shown that the unusual behaviour of this object was related to the vacuum degeneracy induced by the imposition of periodic boundary conditions on a finite lattice. In the case of Feynman gauge, this manifests itself as an infra–red divergence. In axial gauge the SSL is a constant.

It was shown analytically that these problems can be resolved by the imposition of zero boundary conditions.

These conclusions were confirmed by a detailed numerical study.

With these results in hand, a perturbative analysis of the zeroes of the Schwinger partition function was performed. This analysis, although not completely conclusive, indicates strongly that the phase transition reported by other groups on the basis of numerical studies is in fact absent.

It is planned to extend this work both to higher zeroes of the partition function and to higher orders in perturbation theory. In addition, the novel perturbative scheme introduced is likely to be applicable to other models.

13. References

R. Feynman *Rev. Mod. Phys.* 20, 267 (1949) [4]

R. Rivers, "Path Integral Methods In Quantum Field Theory", (1987) [4]

G. Roepstorff, "Path Integral Approach to Modern Physics", (1994) [4]

M. Peskin and D. Schroeder, "An Introduction To Quantum Field Theory", (1995) [6]

M. Kaku, Quantum Field Theory: A Modern introduction (1993) [6]

C.N.Yang and T.D.Lee, *Phys. Rev* 87, 404 (1952) [19]

M.E. Fisher, in "Lectures In Theoretical Physics", Vol VIIC, (1968) [19]

D ter Haar "Elements of Statistical Mechanics", (1995). [19]

M. Creutz, "Quarks, Gluons and Lattices", 1983 [20]

I. Montvay and G. Munster, "Quantum Fields On A Lattice", 1994 [20]

D. Callaway, *Contemp. Phys.* 26, 23 1985 [20]

D. Callaway, *Contemp. Phys.* 26, 95 1985 [20]

H. Rothe, "Lattice Gauge Theories: An Introduction", 1997 [20]

K. Wilson, *Phys. Rev* D, 10, 45 (1974) [20]

J. Cornwell, "Group Theory In Physics", (1984) [23]

J. Kogut and L. Susskind, *Phys. Rev.* D, 11, 395 (1975) [33]

K.Wilson, in "New Phenomena In Subnuclear Physics" (1975) [33]

I. Montvay and G. Munster, "Quantum Fields On A Lattice", (1994). pp 166–170 [33]

N. Sadooghi and H. Rothe, hep-lat/9610001 (1996) [37]

M. Peskin and D, Schroeder, "An Introduction to Quantum Field Theory", pp 667–672 [44]

S. Aoki, *Nuc. Phys.* B, B314, 79 [44]

Y. Nambu and G. Jona–Lasinio, *Phys. Rev.* 122, 345 (1961) [44]

J. Goldstone *Nuove. Cim* 19, 154 (1961) [44]

J. Schwinger, *Phys. Rev.* 128 (1962) 2425 [45]

J. Zinn–Justin, "Quantum Field Theory And Critical Phenomena", 1993 pp 730–736 [45]

H. Gausterer and C.B.Lang, *Nucl. Phys.* B, 455, 785, (1995) [47]

H. Gausterer, C.B.Lang and M. Salmhofer *Nucl. Phys.* B,388, 275, (1992) [47]

H. Gausterer and C.B.Lang *Phys. Lett.* B 341, 46, (1994) [47]

I. Hip, C.B.Lang and R. Teppner *Nucl. Phys.* B (Proc. Suppl.) 63, 682, (1998) [47]

V. Azcoiti, G. Di Carlo, A. Galante, A.F. Grillo, and V. Laliena *Phys. Rev.* D 53, 5069, (1996) [47]

H. Dosch and V.F Muller, *Fortschritte der Physik* 27, 547 (1979) [69]

Montvay and Munster, "Quantum Fields on a Lattice", 1994 pp 377–378 [91]

Leonard I. Schiff, 'Quantum Mechanics', 1949, pp 244–251 [140]

Kenna, Pinto and Sexton, in preparation, (1999) [145]